UNIVERSITY OF SOUTHAMPTON

FACULTY OF NATURAL AND ENVIRONMENTAL SCIENCES

Ocean and Earth Sciences

Hydrodynamic and Geotechnical Controls of Scour Around Offshore Monopiles

Gregor J. Melling

Thesis for the degree of Doctor of Philosophy

September 2014

Abstract

Marine monopiles can suffer from removal of sediment around their foundations by waves and currents, a process termed scour, which can negatively affect structure stability and integrity of associated infrastructure. Scour is a function of the interaction of local hydrodynamics with the geotechnical properties of the seabed, the feedbacks of which are not well understood. Using the largest prototype scour data base available to date, assembled from field data routinely collected during the consents and design phase of wind farms, this study aims to offer a detailed characterisation of marine monopile scour and conduct critical testing of the current, experimentally-derived, state-of-the-art knowledge and practices. Scour research has been hampered by a dearth of prototype scour observations and much of the existing knowledge is derived from physical and numerical work which has had very little validation with field data. This study addresses the dearth of prototype scour analysis and by adding observations from 281 monopiles more than doubles the size of the currently existing knowledge base on marine monopile scour. Furthermore, the scope, variety and quality of data available in this study have enabled a wider-ranging and more in-depth and problem-focussed analysis of scour to be conducted. The data used in this study comes from a "natural offshore laboratory", consisting of three offshore wind farms in the Outer Thames Estuary, which were strategically chosen to minimise the flow variability within the data set in order to focus on identifying and quantifying the controls on scour exerted by the sea bed substrate. The effect of geotechnical conditions on scour is, so far, little understood as most scour research has focused on unconsolidated sandy sediments. Nevertheless, scour experiments in cohesive substrates have revealed the great complexity of the scour response in such materials. For this reason, quantitatively scrutinizing prototype scour in various substrate types and attempting to establish causal links between geotechnical properties and scour development from real data is important. In order to fulfill the remit of this study, the research is guided by a set of questions, derived from a review of the current scour framework, which pose testable hypotheses and identify knowledge gaps which will be evaluated throughout the course of the analysis. The outcomes of the study include an extensive quantitative description and contextualisation of observed scour with existing prototype observations, a critical validation of current knowledge and methods and an investigation of hydrodynamic and geotechnical controls on scour. Some key findings include improved predictive models for scour depth based on mean water depth as well as secondary relationships for lateral extent and scoured volume. For scour in consolidated and cohesive materials, equations for the estimation of scour-limiting material strength as a function of erosion depth are also proposed. The study concludes with a discussion of temporal, survey resolution and geotechnical issues and recommendations for optimised field data collection and survey strategy, alongside suggestions for additional research to fully resolve some of the findings of this research.

Contents

List of Figures

List of Tables

Declaration

I, *Gregor John Melling*, declare that the thesis entitled

Hydrodynamic and Geotechnical Controls of Scour Around Offshore Monopiles

and the work presented in the thesis are both my own, and have been generated by me as the result of my own original research. I confirm that:

1. This work was done wholly or mainly while in candidature for a research degree at this University;
2. Where any part of this thesis has previously been submitted for a degree or any other qualification at this University or any other institution, this has been clearly stated;
3. Where I have consulted the published work of others, this is always clearly attributed;
4. Where I have quoted from the work of others, the source is always given. With the exception of such quotations, this thesis is entirely my own work;
5. I have acknowledged all main sources of help;
6. Where the thesis is based on work done by myself jointly with others, I have made clear exactly what was done by others and what I have contributed myself.
7. None of this work has been published before submission.

Signed:

Dated:

Acknowledgements

I wish to thank various people for their contribution to this project. First and foremost, I'd like to thank Justin Dix for his guidance and never-ending enthusiasm for the subject which helped me get this far. I am grateful to Richard Whitehouse and John Harris from HR Wallingford who provided expert knowledge and time for hours of discussion. Also my thanks go to Stephen Turnock for his assistance with all things numerical, Carl Amos for his reflections during panel meetings, Mike Clare for his help with geotechnical data interpretation and Amelia for sharing methods.

I would like to express my appreciation to friends and family who provided encouragement, support, some proof reading and much needed distractions. Thanks to Kiki for being a good listener.

The data for this study was kindly provided by London Array Ltd, Dong, Vattenfall and Royal Haskoning. Funding was gratefully received from NERC and HR Wallingford.

Notation

A_S	Scour area
c_s	speed of sound in sediment
c_w	speed of sound in sea water
c_u	undrained shear strength
D	pile diameter
d_{50}	median grain size
f	frequency
g	gravitational acceleration
H	wave height
H_s	significant wave height, defined as 1/3 of wave heights
H_{m0}	significant wave height, calculated from first moment
h	water depth
KC	Keulegan-Carpenter number
L	wave length
M	amplification of bed shear stresses τ/τ_∞
p	pressure
q_c	cone resistance
R_f	friction ratio
Re	Reynolds number
Re_D	pile Reynolds number
S	Scour depth
S_e	Equilibrium scour depth
St	Strouhal number
T	wave period or temperature
t	time
U	flow velocity
U_c	Current velocity
U_s, s	speed of sound in sediment
$U_{s,w}$	speed of sound in water
V	volume
V_S	Scour volume
x	horizontal coordinate
y	horizontal coordinate orthogonal to x
z	vertical coordinate, height above bed
z_{sed}	thickness of granular sediment
α_L	orientation of long axis
β	Scour hole slope angle
δ	boundary-layer thickness
δ_w	wave boundary-layer thickness
ν	kinematic viscosity
ρ	density
τ	wall shear stress
τ_{cr}	critical wall shear stress
τ_∞	ambient wall shear stress

Glossary

BODC British Oceanographic Data Centre, http://www.bodc.ac.uk/
CCO Channel Coastal Observatory, http://www.channelcoast.org
CEFAS Wavenet Governmental wave data collection and monitoring, http://cefas.defra.gov.uk/
GEBCO General Bathymetric Chart of the Oceans, http://www.gebco.net
mMSL Vertical datum, referenced to mean sea level
mLAT Vertical datum, referenced to lowest astronomical tide
Petrel Schlumberger Petrel v2011.2 software package for geophysical data exploration, http://www.software.slb.com/products/platform/Pages/petrel.aspx

Chapter 1

Background

1.1 Introduction

Scour is understood as the removal of sediment from around the base of an object due to the interaction of wave and current-induced flows with the structure and the substrate. Historically, scour has been an engineering problem for the transport industry focussed around the safety of bridge piers. For this reason, much of our present knowledge originates from fluvial scour research, which has been developed overwhelmingly by means of experimentation over a number of decades (e.g. Shen et al., 1965; Breusers et al., 1977; Chiew and Melville, 1987; Melville and Sutherland, 1988; Richardson and Davis, 1995; Melville and Coleman, 2000). This research, which has focussed mainly on the determination of maximum scour depth and scour time development in simplified scenarios (e.g. scaled tests, on simple objects, under uni-directional flows, acting on uni-modal and unconsolidated sediment), have provided the basis for the understanding of the scour process and the development of prediction methods. Notwithstanding the abstractive simplicity of the experiments and scaling issues between physical experiments and prototype (Sheppard et al., 2004; Ettema et al., 2006; De Vos, 2008), these methods are still being employed today in a broad range of physical environments for which they were not necessarily appropriate. Until recently, there was very little validation of this experimentally-derived knowledge against prototype data from the field, resulting in scant appreciation of how accurate the existing framework actually is. Not only is the existing guidance for marine scour based on over-simplified physical model test, it is also relatively old, as exemplified by some of the most popular design equations devised in the 70s and 90s (eg. Breusers et al. (1977); Sumer et al. (1992b)).

Scour in the marine environment is typically more complex than in rivers due to the increased complexity of tidal flows and wave action. Herbich et al. (1984) provided some early investigations into scour around offshore piles and pipelines. At present, the basis for most scour applications are practitioner's guides delivered by authors such as Hoffmans and Verheij (1997); Whitehouse (1998) and Sumer and Fredsoe (2002). These monographs provide reviews of studies undertaken in the foregoing decades, treatments of the scour process and offer a framework of empirical techniques for the prediction of depth and time evolution of scour in granular sediments which are generated on the back of experimental

data. So while the guidance and commonly used prediction equations (eg. Breusers et al., 1977; Sumer et al., 1992b; Melville, 1997; Richardson et al., 2001) have been developed some 10-20 years ago, the experimental data it relies on can be much older. Matutano et al. (2013) have highlighted the uncertainty in the current methods by using a variety of empirical prediction formulae for maximum scour depth, and data from 10 European offshore wind developments, scour was overpredicted in all but two cases. Recognising the limitations of semi-empirical equations for scour prediction, some effort has been directed to developing advanced numerical methods based on detailed hydrodynamic simulation and bed deformation models (eg. Olsen and Melaaen, 1993; Roulund et al., 2005; Zhao and Fernando, 2007; Liu and García, 2008; Escauriaza and Sotiropoulos, 2011). These methods have not matured yet and are also being calibrated against physical model tests, thus also have little validation in the prototype setting. Thus, it is clear that the development of currently available methods has been hampered by the lack of understanding of scour in the context of real physical conditions and more observational data are required to validate and improve current methods (eg. Black, 2013). This dearth of real observations is primarily a result of constraints in the feasibility, quality and cost of acquiring such data which has until recently been a hindrance in the collection of meaningful amounts of field data. With the increase in offshore infrastructure associated with the oil industry and, recently, with the offshore renewables sector, marine scour is becoming ever more relevant. With regards to offshore wind farms, monopiles are the most prevalent structures in terms of number installed offshore. Of all turbine foundations in European developments, 74% are monopiles; in Rounds 1 and 2 of the UK offshore wind farm developments, which are mostly in relatively shallow water, installed foundation types have been almost exclusively monopiles.

At offshore wind farms, scour is particularly hazardous for the stability of the turbine monopile foundation and the integrity of power cables (Whitehouse et al., 2010; Harris and Whitehouse, 2012). Monopiles are typically piled some tens of metres into the ground. Where the seabed is susceptible to erosion, waves and currents will work to excavate a scour hole at the foundation, decreasing the lateral load and bearing capacity. While this has implications for piling depths and structure stability it also increases the effective length of the monopile thus changing its natural frequency of vibration which can result in structure fatigue, particularly when the altered eigenfrequency coincides with excitation frequencies of waves, currents, wind and turbine rotation (Tempel et al., 2004; Offshore Center Danmark, 2006). Excessive vibration can also render the turbine inoperable. Exposure of the high-voltage cables leads to unsupported free spans which increases the mechanical loads on the structure, by own weight and exposure to hydraulic forces. Furthermore, there is a larger risk of snagging and external impact from anchors and fishing equipment and abrasive wear by water-borne constituents (CIGRE, 2009; Worzyk, 2009; Karlsdottir, 2013). Figure 1.1 shows a 9.3m deep scour hole around a wind turbine foundation captured on high-resolution bathymetry; the reflection from the free-spanning cables is clearly visible and measures over 20m in this example. Once the cable is exposed, accelerated flows around the structure can cause scour at the span shoulder and further excavation along the cable route (e.g Cheng et al., 2009). Apart from the aforementioned engineering aspects, scour can also play a role in environmental and heritage considera-

tions with emergence, burial or modification of habitats and historical artefacts (McNinch et al., 2001; Richardson et al., 2001; Trembanis and McNinch, 2003; Inman and Jenkins, 2002; Quinn, 2006; Trembanis et al., 2007). To manage scour it is thus necessary to understand the vertical and lateral extent of scour and their temporal variability, as well as the more conventional properties of maximum scour depth and time development of the scour hole.

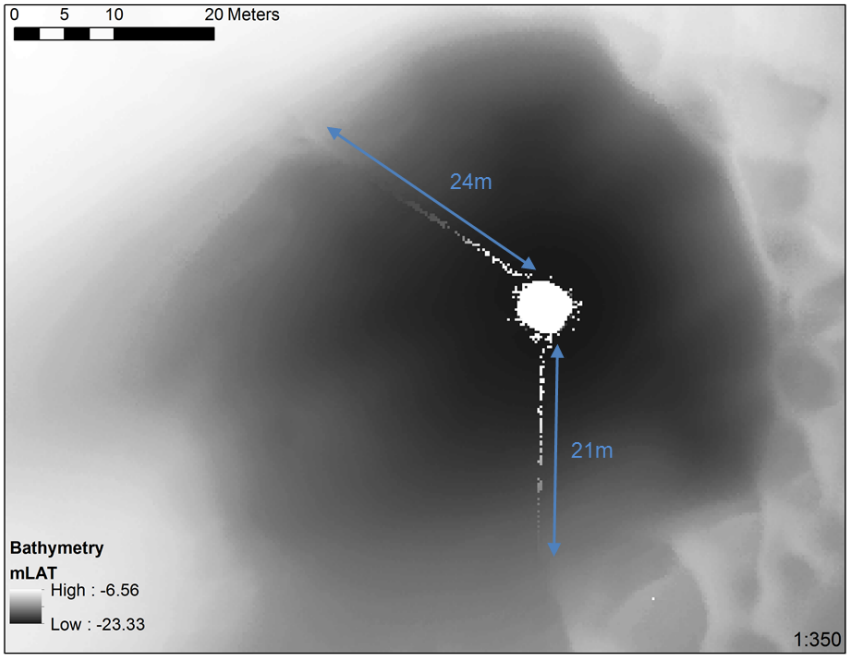

Figure 1.1: Bathymetric survey showing scour hole around turbine foundation and long spans of unsupported cable. From study data set.

Associated with the installation of offshore monopiles, there has been an increase in the amount and range of physical data collected in the field, stemming from the legal requirement to conduct environmental studies in the planning phase and the will to protect against economic losses due to structural damage caused by scour (e.g. Sumer, 2007). Due to the increased design and construction costs associated with offshore infrastructure it has been realised that a sound understanding of expected scour magnitudes can effect cost savings in structure design, installation and provision of scour protection (if required). If one considers that turbine foundations can be responsible for up to 35% of the installed cost (Byrne and Houlsby, 2003) the incentive to manage these costs is clear. The recent availability of these data now provides the opportunity to undertake a large-scale and detailed investigation of scour around monopiles in the prototype setting. So far, some individual observations of monopile scour in the field have been reported (Walker, 1995; Noormets et al., 2003; Harris et al., 2004; Rudolph et al., 2004; Louwersheimer et al., 2009) and larger data sets from offshore wind projects have been collated in DECC (2008); COWRIE (2010); Whitehouse et al. (2010) and Whitehouse et al. (2011). To the author's understanding, the currently available database of unique monopile scour records stands at 183 data points, overwhelmingly of scour depth measurements with some observations of time evolution; little to no information has been gathered on horizontal extents or scour pit shape. The data in the current prototype knowledge base originates from a wide range of hydrodynamic regimes and sea bed types around the UK continental shelf

and the North Sea and the diversity of the physical conditions complicates the interpretation of scour observations as the relative effect of hydrodynamics and geotechnics on scour varies throughout the data set. However, as will be demonstrated in section 1.3 even this relatively minor amount of real observations, small number of recorded parameters and limited (often qualitative) analysis has proven sufficient to cast doubt on the completeness of the current framework, especially in respect to the control on scour development exerted by the engineering properties of the sea bed. Hitherto, it is understood that the composition and physical characteristics of the sea bed can affect the scour development; however as most research has focussed on experiments with cohesionless granular sediments, the erodibility of complex and cohesive substrates, and the engineering factors that affect it, are not well understood.

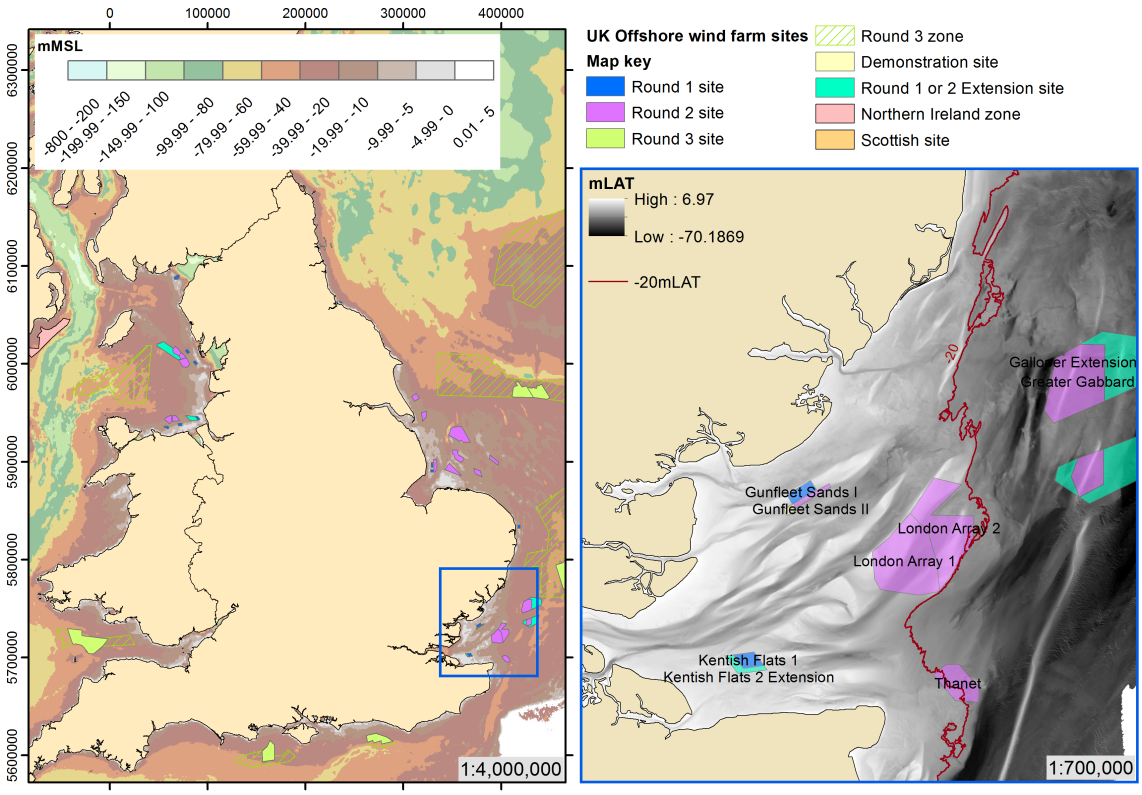

Figure 1.2: Location of study area (left) and inset map of Outer Thames Estuary. Data from Crown Estate, bathymetry from GEBCO_08 Grid (http://www.gebco.net).

The importance of geotechnical effects on scour was already recognised in Herbich et al. (1984) and reiterated in COWRIE (2010), yet still little is known about the feedback between substrate properties and scour. The data in COWRIE (2010) and Whitehouse et al. (2011), where qualitative geotechnical context was given, has shown that scour depths can vary greatly at prototypes and that this variability might be explained by the type and nature of the local sea bed. The body of research that investigates scour in sediments that deviate from simple unconsolidated granular material (e.g Breusers and Raudkivi, 1991; Briaud et al., 1999, 2001; Rambabu, 2003; Debnath and Chaudhuri, 2010; Porter et al., 2012b; Link et al., 2013) suggests the nature of substrate control on scour is increasingly elaborate, diverse, multi-variate and still not well understood, thus, universal prediction methods are not easily defined for this scenario. Annandale (2006) has suggested a method which attempts to account for varying geotechnical properties

and complex substrates for a variety of flow situations. It is based on the quantification of the erosion resistance of the substrate profile and the erosive capacity of the fluid which appears to have potential for complex marine substrates (Harris et al., 2010b) but requires further validation for the marine environment (Whitehouse et al., 2011). A prerequisite for this method is access to appropriate quality and quantity of geotechnical information (e.g particle size distributions, densities, shear strength) throughout, at minimum, the scour-relevant profile, which is not routinely available. Briaud et al. (2001) have suggested an empirical equation for scour in cohesive material that only relies on hydrodynamic parameters. While the experimental evidence, based on artificial sediment mixes, indicates that a complex and non-linear response of the seabed to erosion should be expected in real sediments, more evidence is needed to substantiate current knowledge. It is hoped that with a significantly large amount of data, emerging trends might become visible against the background of scatter and noise which typically obscure correlations between geotechnical parameters and scour (Briaud et al., 2001).

The main aim of this study is to address a series of research questions that will be developed as part of the review of current state of the art scour research in sections 1.3 and 1.4. A summary of these themes is given below. The research themes are designed to test the existing understanding of scour or augment the current knowledge where there are uncertainties or gaps and pertain to three main fields of investigation, the general characterisation of prototype scour, the examination of geotechnical controls on scour and the evaluation of the current scour knowledge against real data.

Overarching research questions:

- What range of prototype scour (dimensions, morphologies, time-evolution) is observed and how do they compare to current understanding of scour from experiments, field data and literature?
- What structural, hydrodynamic, geotechnical and sedimentological controls on the observed scour dimensions and morphologies can be found in the data? How do these effects compare with the state of the art in the current scour framework?
- How do the predictions from empirical equations compare to the prototype data?

This thesis aims to tackle these overarching research questions through the analysis of an extensive set of prototype observations, taken from three offshore wind farm installations, under similar hydrodynamic conditions in the Outer Thames Estuary, effectively providing a "natural laboratory". During the pre-installation phase of offshore wind farm developments, typical field campaigns usually encompass the collection of hydrographic, seismic, hydrodynamic and geotechnical information and these data will be employed to demonstrate that, using appropriate methods (outlined in Chapter 2), these routinely collected data can be used for a comprehensive scour analysis. The composition of this study's data set in the spatial domain has been strategically designed to create the best possible natural laboratory. The data set used in this study encompasses a total of 281 monopiles, thus more than doubling the current number of prototype observations, from wind farm developments in the Outer Thames Estuary (OTE) which is home to a number of Round 1 and 2 offshore wind energy projects (Figure 1.2). Data from three wind

farms (London Array, Gunfleet Sands and Thanet) have been collated in a bid to build a prototype data set that will be, to the author's knowledge, pioneering in terms of spatial clustering and data density. One of the key advantages of this data set is that the hydrodynamic conditions are relatively well constrained over the chosen sites, offering some degree of control over the hydraulic forcing parameter in the scour analysis. On the other hand, the regional morphological, topographical, geological and geotechnical contexts are quite variable offering an opportunity to focus on the surface and sub-surface controls on scour.

The thorough analysis of the described data set in terms of an extensive characterisation of scour forms the basis of all other investigations in this study, while providing a quantitative understanding of the nature of prototype scour. To this day the knowledge of the nature of scour at prototypes is limited to the small number of studies identified above and more field data are required to address this and validate current knowledge. This study will more than double the number of existing field scour observations, while widening greatly the scope of recorded parameters and amount of analysis. The parameters will include not only vertical but also areal and volumetric dimensions of scour holes, while the time-evolution of these scour dimensions will be examined. Alongside this, a number of morphological parameters will be introduced that quantify the lateral extent and shape of a scour hole. All these data will be folded into the existing database to provide context and create a large body of prototype data in diverse physical conditions that will enhance the experimentally-derived understanding of the scour process and benchmarks for scour predictions.

The influence of the substrate on all scour dimensions and scour hole shape will be investigated in some depth. The scour characterisation above will be employed in conjunction with detailed study of the local substrates, by means of seismic and geotechnical data interpretation, to attempt a causal interpretation of scour in various substrates. It is anticipated that this knowledge will help the understanding of the scour process in real sediments, offer a benchmark for scour in various substrates and promote improvement of scour predictions in the future.

On the basis of comparisons between observed and estimated scour depths, the existing field data appear to suggest that the current scour knowledge and prediction methods are not capturing the processes of real scour at prototypes. The engineering equations presently used for scour predictions employ no or over-simplified parameters to represent the hydrodynamic and geotechnical conditions at a particular site, offering relations on scour development based on the pile diameter. With the increased evidence base built during the course of this study, the performance of the predictive methods will be evaluated against field data.

The following short review of the current state of research has been undertaken to, not only set out a baseline understanding of scour, but to inform on gaps in research and to frame the research themes of this study. At first, the nature of the turbulent hydrodynamic flow around monopiles and the generated bed shear stresses will be illustrated in section 1.2 followed by a description of typical scour patterns generated by the monopile flow in part 1.3. The geotechnical parameters that affect the erodibility of a substrate and scour

in complex cohesive substrates are reviewed in section 1.4. At the end of Sections 1.3 and 1.4 a list of detailed research questions, pertaining to the preceding discussion, are collated which are designed to inform the analysis and interpretation of the scour data.

1.2 Hydrodynamics around a slender vertical monopile

1.2.1 Turbulent flow pattern

The flow resulting from the placement of a monopile in uni-directional current has been studied thoroughly in the physical and numerical domain and is generally well understood. The flow around a vertical cylinder is characterised by the presence of two large-scale eddy structures, the horseshoe and the lee-wake vortex (Fig 1.3). Depending on the structure and flow conditions the hydrodynamics can exhibit both, one or none of these transient features (Breusers et al., 1977).

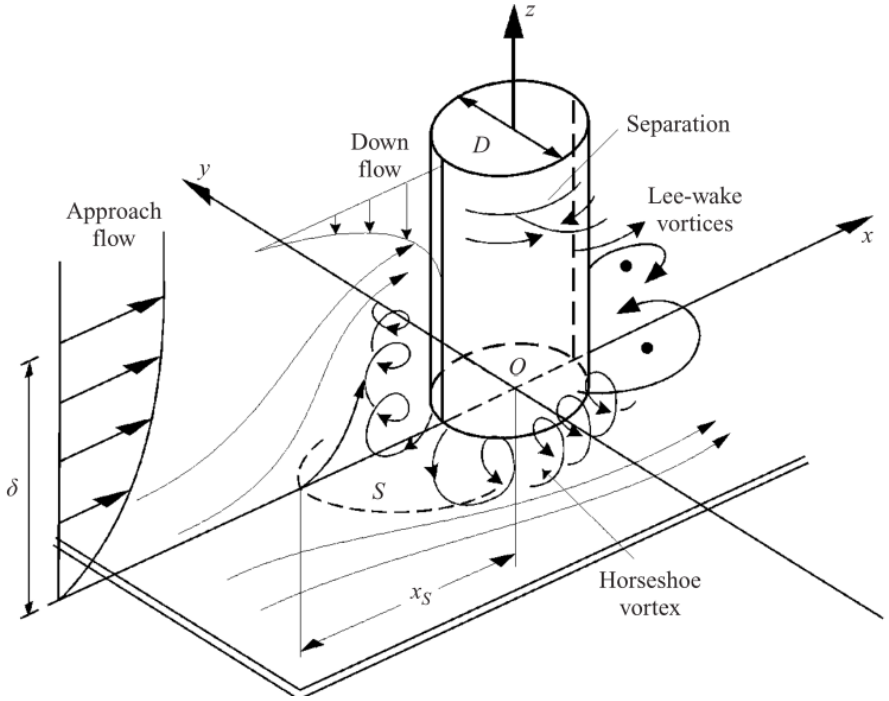

Figure 1.3: Flow features around a slender vertical cylinder in uni-directional current. From Roulund et al. (2005).

1.2.1.1 Horseshoe vortex

This turbulent vortex is a result of the three-dimensional separation of the boundary layer due to the vertical gradient in stagnation pressure towards the bed. A recirculating vortex develops when the down-flow interacts with the seabed. The horseshoe vortex and its downstream limbs are responsible for excavation of sediment at the cylinder-seabed interface creating the main scour pit around the structure. While wake turbulence can cause erosion downstream, it is the horeshoe vortex that controls the deepest scour depth at the structure. The importance of this vortex in the scour process is illustrated in numerical studies (eg. Tseng et al., 2000; Ali and Karim, 2002; Roulund et al., 2005;

Kirkil et al., 2009; Escauriaza and Sotiropoulos, 2011) which have shown that to model scour successfully the horseshoe vortex, its fluctuations in time and space and all associated turbulence scales must be resolved as accurately as possible. The topology of the vortex system reveals that the horseshoe vortex consists of between 4 and 6 individual counter-rotating eddies depending on the nature of the boundary layer separation (for all practical applications this separation is turbulent), the boundary layer thickness (δ) to diameter (D) ratio δ/D, the structure geometry and the pile Reynolds number (Baker, 1979, 1980; Dargahi, 1989, 1990) given as

$$Re_D = \frac{UD}{\nu} \tag{1.1}$$

where D is the pile diameter, U is the flow velocity and ν is the kinematic viscosity of water. The strength of the horseshoe vortex has been found to scale with Re_D (e.g. Shen et al., 1966; Hjorth, 1975). Roulund et al. (2005) has demonstrated the control of δ/D on the position of the boundary layer separation and magnitude of maximum bed shear amplification. Boundary layer separation, a prerequisite for horseshoe vortex formation, is facilitated with large values of $\delta/D > 1$ and can be suppressed entirely for very small values ($\delta/D < 0.01$, Roulund et al. (2005)). In nature, the tidal boundary is commonly considered to be fully developed over the entire depth of the flow (ie. $\delta = h$), so the pre-conditions for the formation of the vortex are met. The bed shear stress amplification is dependent on the strength of the horseshoe vortex hence exhibits a positive relationship to δ/D. For constant δ/D Roulund et al. (2005) show that the point of separation is dependent on Re_D the maximum of both observed $Re_D = 500$, the critical value for the development of primary oscillations in the horseshoe vortex. Typical Re_D numbers for prototype monopile foundations are in the range of 1×10^6 to 1×10^7. Baker (1980) reports the location of the horseshoe vortex between $0.2D$ and $0.3D$ upstream of the cylinder; for smaller δ/D a location closer to the cylinder is observed. Muzzammil and Gangadhariah (2003) reports that as the scour hole develops, the horseshoe vortex lowers into the scour hole and the size becomes proportional to the depth of the scour hole; contrary to findings of Baker (1979) the strength of the vortex is shown to vary throughout the scour process with a peak in the initial stages of scour and decrease of vortex strength in the latter stages.

1.2.1.2 Lee-wake vortex

The lee-wake vortex system is created by consolidation of the shear layers generated by the separation of the flow around the cylinder. The pile acts to concentrate the existing transverse vorticity into a concentrated band of turbulence, that depending on Re_D number can be periodically shedding (Breusers et al., 1977; Williamson, 1996). For very low $Re_D < 5$ numbers the wake vortex system can be stable, i.e. no detachment of vortices occurs. However, for all flows of practical interest, vortex shedding will be observed, either at a certain frequency (von Karman condition) or exhibit chaotic shedding patterns for higher Re_D numbers (Zdravkovich, 1997); for a range of $Re_D = 10^2 - 10^5$, eddies are shed periodically. For higher Re_D numbers, as commonly encountered in nature, the shedding

occurs chaotically.

To the author's knowledge, very little is known about the length of the turbulent lee-wake and no prediction methods exist. Theoretically, a wake will remain until all the turbulence has dissipated. While wakes are often the subject of numerical modelling, the length of a lee-wake is notoriously difficult to simulate since turbulence can often not be sustained due to limitations in the turbulence models, prohibitive computational costs for adequate mesh resolutions and numerical dissipation effects. Nevertheless, an indication of the zone downstream affected by increased turbulent energy is give in Figure 1.4 which shows a LandSat satellite image where the wakes can be identified by the presence of suspended sediment. Fine particles will be held in suspension by the turbulent kinetic energy, even where large scale coherent turbulent structures have dissipated, and thus the downstream zone of influence can be estimated. In the image the wakes generated by the incoming flood tide at Thanet can measure up to 2km in length, equivalent to approximately $450D$, with a width of 30-150m.

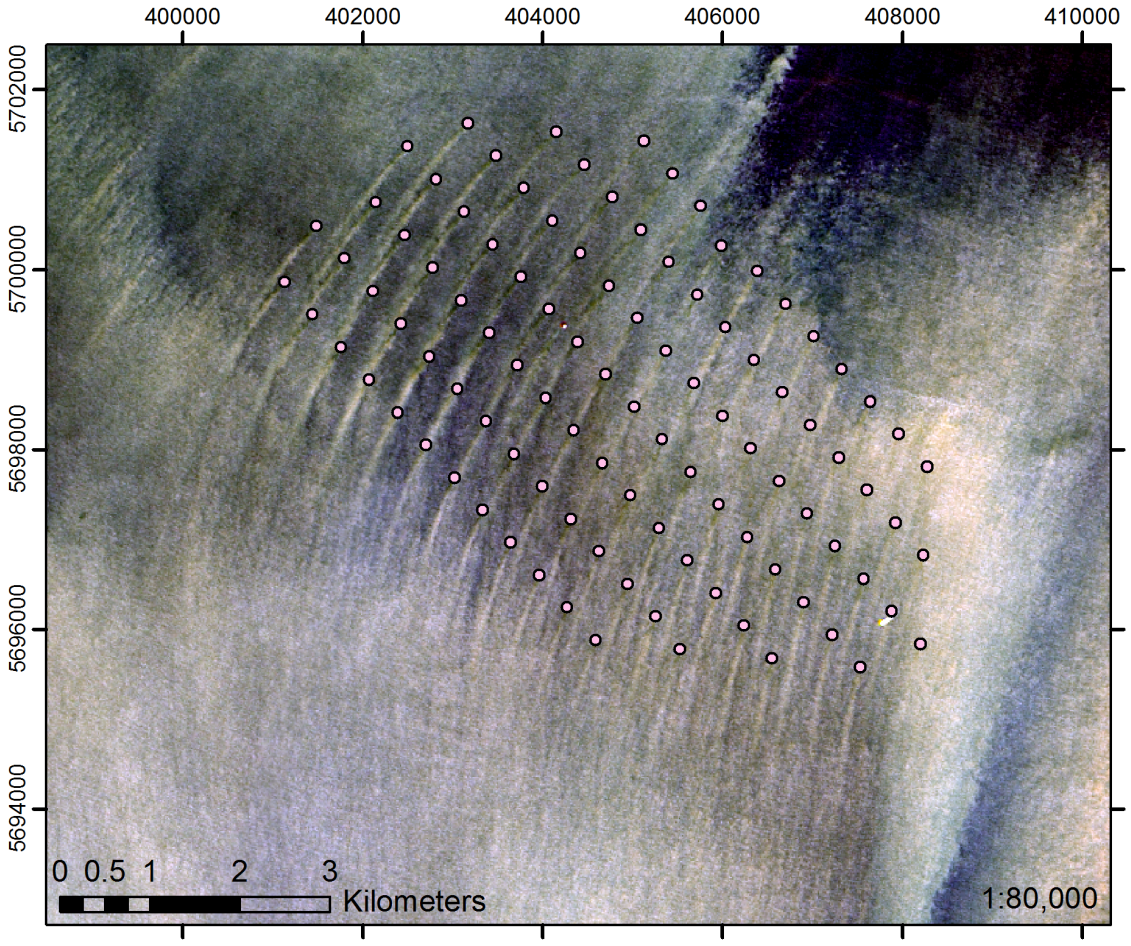

Figure 1.4: Remotely sensed image of Thanet wind farm, recorded on 18/01/2013. Source: NASA

1.2.2 Bed shear stresses

Shear stress amplification The structure-induced amplification of shear stresses is a function of the contraction of streamlines around the flow obstacle and the amplification factor M is defined as the ratio of local (τ) and ambient shear stress (τ_∞) given in Equation 1.2.

$$M = \tau_0/\tau_\infty \tag{1.2}$$

The magnitude of M depends on size, shape and orientation of the structure towards the flow and the horizontal extent of amplification is determined by cylinder diameter and flow strength. In the literature a range of M values between 4 and 12 are given as shown in Table 1.1. The distribution in Figure 1.5 reveals that maximum amplification is found at 45° from the axis of flow which corresponds to the reported location of onset of scour around cylinders by Dargahi (1990) and Whitehouse (1998). It also demonstrates that higher M are observed for the shallower flow depth of $h = 0.1$m, as opposed to $h = 0.2$m. While average bed shear stress distributions can indicate where erosion thresholds are likely to be exceeded, they are not sufficient to explain scour patterns. Numerical tests by Ali and Karim (2002) concluded that instantaneous vorticity, near-bed turbulence and transient boundary layer phenomena play a significant role in the scour process as will be illustrated in the following section.

Table 1.1: Bed shear stress amplification values around cylinders in current.

Source	τ-amplification M
Whitehouse (1998)	≈ 4
Niedoroda and Dalton (1982)	11-12
Sumer et al. (1997)	4 (waves), 10 (current)
Sumer and Fredsoe (2002)	5-11
Hjorth (1975)	5-11

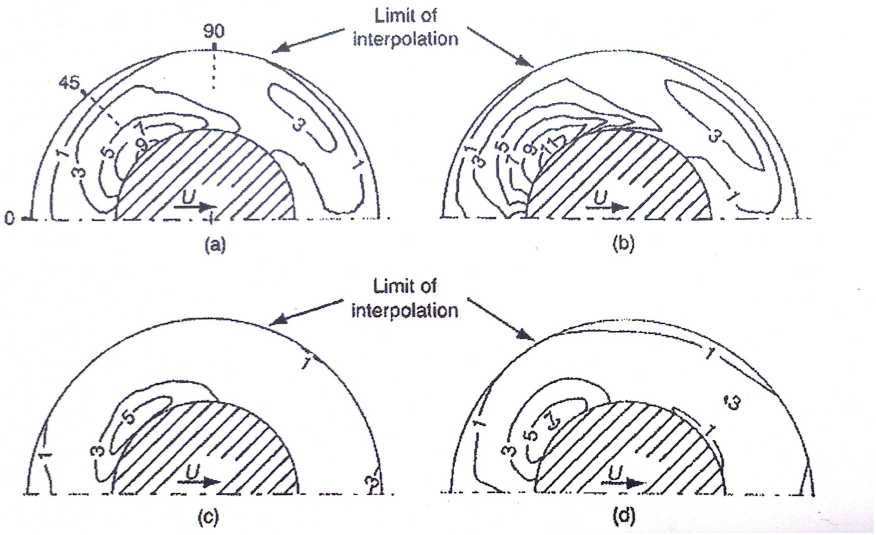

Figure 1.5: Plan view of shear stress amplification M around a cylinder with $D = 0.05$m. Water depth $h = 0.1m$ and (a) $U = 0.15ms^{-1}$ (b) $U = 0.30ms^{-1}$. Water depth $h = 0.2m$ and (c) $U = 0.15ms^{-1}$ and (d) $U = 0.30ms^{-1}$. From Whitehouse (1998) with data from Hjorth (1975).

Effect of near-bed turbulence In addition to increased average bed shear stresses generated by large-scale turbulent structures, instantaneous shear stresses can be generated by small-scale, short-lived events. Sediment can be destabilised by the action of vortex-associated injection of high-momentum fluid into the bed (Dargahi, 1990). Experiments carried out by Sumer et al. (2003) have quantified the significance of turbulence for bed load transport with rates reported to be enhanced by a factor of 2.2-4.4 (of the undis-

turbed value) for a rough bed with turbulence increase of 11% and 56% respectively and 6-fold for a plane bed with 20% increased turbulence. Dargahi's experiments concluded that sediment transport is strongly dependent on the scale of turbulence, which is positively related to the cylinder diameter (*cf.* Re_D) as the dimension of the flow obstruction increases the turbulent energy in the flow. Other factors such as flow velocity, depth and sediment characteristics are of decreased importance, other than for sediments that are prone to armouring. The influence of particle size on local scour depends on their relationship with the boundary layer. Where particles are fully enveloped in the viscous sublayer, the flow remains hydrodynamically smooth; larger grain sizes, protruding through the width of the sublayer increase the roughness of the surface, affect the velocity distribution and turbulent shear stresses in the bottom boundary layer Komar, 1977; Heathershaw, 1988) and even induce vortex shedding (Hardy et al., 2010).

Turbulent kinetic energy can impinge on the bed via the destabilisation of the viscous sublayer (Annandale, 2006). Figure 1.6 shows the viscous sublayer, that forms a thin layer of fluid immediately adjacent to the boundary. For all intents and purposes the velocity distribution dU/dz in the sublayer is linear; however under turbulent flow conditions, which are typically encountered in nature, the thickness and velocity distribution is unstable which gives rise to intermittent, short-duration "bursting" events (e.g. Einstein and Li, 1956; Offen and Kline, 1975). Where the boundary layer Re number is sufficiently large, ie. in turbulent flow, instabilities in the laminar sublayer are not dampened out but grow into vortices and cause pressure gradients within the sublayer. The upward movement of a vortex causes high-velocity water ingress towards the bed from the surrounding fluid, called "sweeps". As the main vortex breaks up, its limbs create negative pressure hoses, so-called "low velocity streaks", exerting lifting action on the bed. Both sweeps and streaks are capable of dislodging particles. These bursts, being the main agent of momentum exchange at the fluid-sediment boundary, have been heavily implicated in the initiation of motion of particles; as much as 50-80% of the total bed shear stress is attributed to this phenomenon in marine boundary layers while it only occurs 20-25% of the flow time (Komar, 1977; Soulsby, 1983).

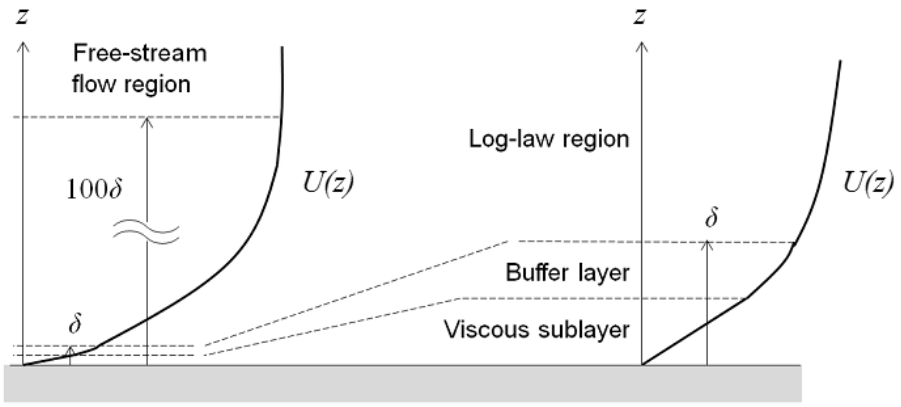

Figure 1.6: Conceptual model of boundary layer flow over smooth boundary. Modified from source [1]

[1] Comsol, 16/09/2013, Which Turbulence Model Should I Choose for my CFD Application?, http://www.comsol.com/blogs/which-turbulence-model-should-choose-cfd-application. Accessed: 16/06/2014.

1.3 Scour around a vertical monopile

The review begins with the description of scour characteristics and prediction methods for the idealised benchmark case of a slender vertical cylinder in steady (constant in time) uni-directional current and, typically, uniform single grain-size fine or medium sand. This will be augmented by a discussion of existing prototype observations. The idealised scour pattern is complicated by deviation of the hydrodynamic and geotechnical parameters from the idealised conditions of the archetype. The effect of increasing complexity of the flow will be discussed in section 1.3.3.

1.3.1 Scour dimensions

1.3.1.1 Scour depth definitions

A number of scour definitions are used, sometimes inconsistently, in the literature and therefore some clarification is required. In physical tests scour depth tends to be reported as equilibrium scour depth S_e, when it is clear that the bed has fully adjusted to the flow. To indicate that scour is caused by the action of uni-directional currents, typically as a reference scour depth for other flows, often S_c is used, where typically $S_c = S_e$. It is difficult to apply these concepts to prototype scour since flow conditions are variable and it is problematic to establish the equilibrium state from a single or small number of post-installation bathymetric surveys. Furthermore, real conditions are dynamic thus the scour hole can undergo change perpetually. In this case, the scour depth is referred to as simply S, ie the deepest depth in the scour hole, at the time of surveying. However, this should not be confused with the maximum expected scour depth S_{max} which is an upper limit derived from physical model tests (eg. Melville and Sutherland, 1988; Sumer et al., 1992b; den Boon et al., 2004). In the results presented as part of this study S_{max} is used as the maximum scour depth observed at a scour hole during the whole observation period. For example, where multiple post-installation surveys exist, the greatest scour depth at any individual foundation with time constitutes S_{max}; where only a single scour survey is available, S_{max} cannot be determined and only S is recorded. It is customary to report the scour depth as a normalised, non-dimensional ratio S/D in order to remove the effect of varying pile sizes as it is generally assumed that S scales with the monopile diameter. The validity of this notion will be tested in Section 5.1.1.1.

1.3.1.2 Scour depth

The most studied parameter in scour research is the scour depth since it has been long considered the decisive factor for engineering safety. For a slender cylinder (where water depth $h > 2D$) the scour process commences at 45° either side of the cylinder centreline (Whitehouse, 1998) where the amplification of bed shear stresses τ is greatest (Fig 1.5). With scour progression, the initial depressions join to form a conical hole around the pile; two scour depressions are formed with sediment deposited in the shadow zone between these (Fig 1.7). The equilibrium scour depth in experiments has been found to scale with diameter D (e.g. Carstens, 1966; Breusers, 1972; Breusers et al., 1977; Sumer et al., 1992b)

and lie between $1.0D$ and $2.3D$ for uni-directional flow under clear-water conditions (bed not actively moving under ambient flow conditions - Clark, 1982); when the current is strong enough to cause sediment transport over the entire bed (live-bed scour) a value of $S_e = 1.3D$ is suggested (Sumer et al., 1992b).

Figure 1.7: Uni-directional scour pattern with two-limbed wake. From Whitehouse (2004)

Only a relatively small amount of data exist from field observations at marine monopiles (eg. Walker, 1995; Noormets et al., 2003; Harris et al., 2004; Rudolph et al., 2004; DECC, 2008; Louwersheimer et al., 2009). The largest amount of scour depth information is compiled in COWRIE (2010) and Whitehouse et al. (2011), including data from the previously listed studies, from a number of, primarily, wind farms from different location around the UK. COWRIE (2010) provides 105 scour depth assessments from 5 wind farm sites, while Whitehouse et al. (2011) report 92; the data overlap between the two reports is believed to be 14, thus resulting in 183 scour depth records from unique locations. Inevitably, the data include a variety of hydrodynamic and geological conditions and brief descriptions of the environmental conditions encountered at the sites in the datasets are presented in Table 1.2. All of the data are plotted in Figure 1.8 and conveys the notion that a wide range of scour depths can be observed in the field. There are locations that have not scoured (e.g North Hoyle and Barrow), while the largest scour recorded in the field is $S/D = 1.77$ at Robin Rigg. Whitehouse et al. (2011), while not reflecting much on the relationship between h/D and S/D, proposed a limiting depth curve as shown in Figure 1.8 which is calculated after Breusers et al. (1977), with $\alpha = 1.75$. The curve reflects assumption about the scour reduction in shallow water and a maximum scour depth of 1.75. The plot does not suggest a strong relationship between water depth and scour depth as similar range of scour is observed over h/D. However, the question of water depth will be revisited in Section 5.1.1.2 where the plot is populated with additional data from this study.

The deepest erosion appears to have developed in non-cohesive sandy sediments as

the largest scour magnitudes are associated with Robin Rigg and Scroby Sands offshore wind farms, Otzumer Balje pile and Destin bridge pier. Scour at the Princess Amalia wind farm illustrates the importance of the geotechnical stratigraphy as although the top sediment is loose sand the scour depth appears to have been limited by clays near the surface resulting in the data clustering between $0.4 - 0.7D$, equivalent to approximately 1.5-3.0m of scour. Other sites that are either directly influenced by clay or are underlain by it typically display lower scour magnitudes; where the substrate is heterogeneous, large ranges of values can be observed, e.g. Barrow. At Barrow, Whitehouse et al. (2011) have suggested that the depth level of erosion-resistant materials in the sea bed profile are responsible for the distribution of scour depths witnessed here and scour depths are a function of the thickness of loose surface sediment package. At clay sites very small magnitudes of up to $0.1D$ are found, whereas for limited packages of sand over glacial till typical depths are S/D=0.2-0.8 and in thicker sand deposits values up to $1.21D$ are reported. The authors also reported that the erosion into glacial till occurred more slowly than in the sandy sediments, but no quantification was made. At Kentish Flats and North Hoyle the surface sediments are underlain by clay (London Clay at Kentish Flats) and similarly show subdued scour, $S/D < 0.5$ and $S/D < 0.2$ respectively, which is again attributed to the more erosion-resistant substrate at depth, although it is also noted that the last three mentioned sites show somewhat lower current speeds and wave energy exposure. For relative water depths of $h/D < 2$ it is expected, according to guidance, that scour will be reduced (see section 1.3.3). However the prototype data do not show such a pattern as the range of scour depths either side of $h/D = 2$ is quite similar. In Figure 1.8 the largest recorded scour values are in shallow water.

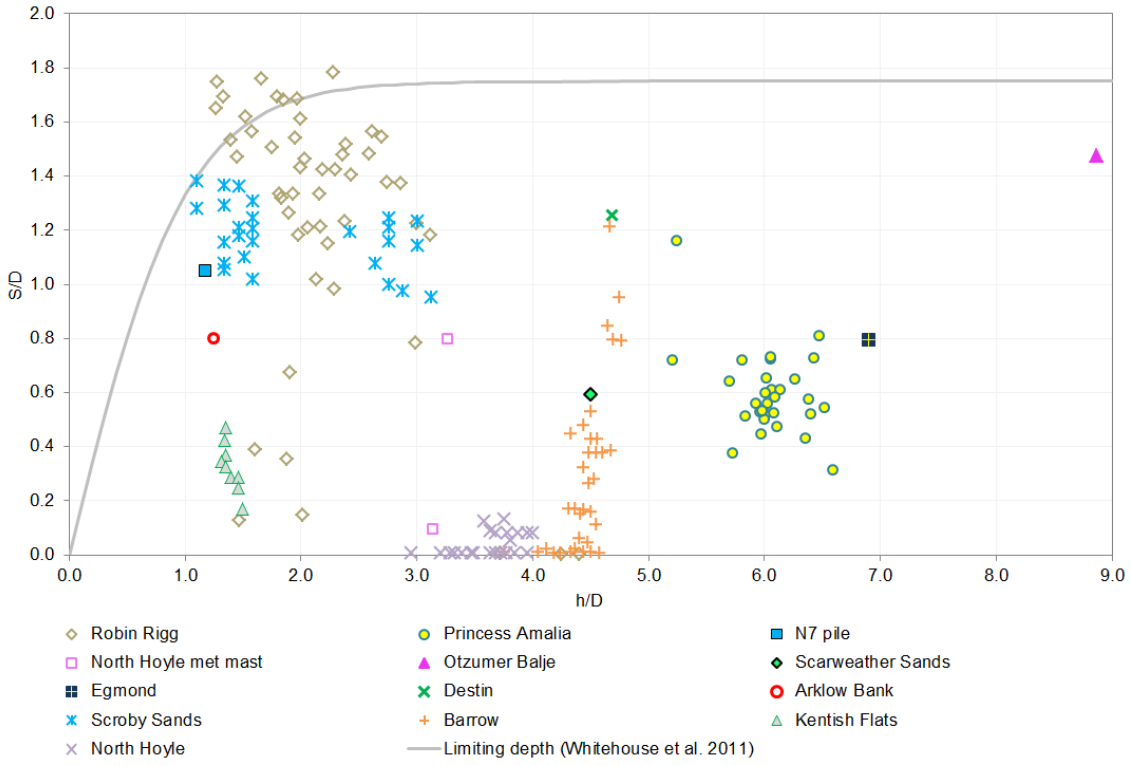

Figure 1.8: Non-dimensionalised plot of mean water depth h/D against scour depth S/D for marine monopiles. Data from COWRIE (2010) and Whitehouse et al. (2011).

Based on the experimental findings of scour around a monopile a variety of predictive

Table 1.2: Environmental conditions for prototype data. Compiled from COWRIE (2010) and Whitehouse et al. (2011).

Site	D [m]	h [m]	Sediments	Hydrodynamics
Robin Rigg	4.3	0-12	On sand bank, loose superficial deposit with compact core. Fine to medium sand (medium dense to very dense) interbedded with silts and clays and sandy muds overlying glacial tills.	$\overline{U_c}$ = 1m/s, peak $\overline{U_c}$ = 2m/s, tidal range 3-8m. Waves can be significant (no data given)
Princess Amalia	4.0	19-24	On sand bank. Poorly sorted fine to medium, loose to medium dense sands, up to 3m thick. Underlain by soft to firm clay and silty sands. Below this, thick package of Pleistocene fine to medium, dense to very dense sands	tidally dominated, peak $\overline{U_c}$ = 1.4m/s, no wave data given
Barrow	4.75	18-24	medium dense to very dense muddy fine sands and sandy gravels (0-10m thick), overlying tillite and stiff clay, exposed clay in places.	peak $\overline{U_c}$ = 0.3-0.8m/s, tidal range 4.1-8.2m, typical $H <$ 0.5m, 1:1 H_s= 4.9m
Kentish Flats	4.3	6-9	fine to coarse shelly sand, underlain by soft to firm clays, on top of London Clay	$\overline{U_c}$ = 0.7-0.9m/s, tidal range 2.9-4.7m, 1:1 H_s= 3.3 (depth-limited at low water)
North Hoyle	4.0	11-17	fine to medium, poorly sorted, highly heterogeneous, muddy sands and gravels (0-10m thickness), overlying Permo-Triassic bedrock or glacial tills	$\overline{U_c}$ = 0.75-1.0m/s, peak $\overline{U_c}$ = 1.2m/s, tidal range 4.1-6.1m, 1:1 H_s= 4.9m
Arklow Bank	5.0	3-7	On sand bank, loose to medium dense sand and sandy gravel	peak $\overline{U_c}$ = 2m/s, tidal range 1-2m, 1:1 H_s= 5.6m (breaking)
Scroby Sands	4.2	5-14	On sandbank, fine to medium sands, some gravel, overlying clays	peak $\overline{U_c}$ = 1.65m/s, tidal range 1.1-1.9m, 1:1 H_s= 1-3.5m (breaking)
N7 pile	6.0	7	medium dense fine sand	mean tidal range 2.6m, peak $\overline{U_c}$ = 0.25 - 0.75m/s, 1:1 H_s= 1.1m
Scarweather Sands	2.2	11	on sand bank, medium to fine shelly sands	peak $\overline{U_c}$ = 1.1m/s, tidal range 4.2-8.9m, 1:1 H_s= 2.8m
Otzumer Balje Inlet	1.5	13	in tidal inlet, medium sand	mean tidal range 2.6m, peak $\overline{U_c}$ = 1.4m/s, sheltered from waves.
Egmond aan Zee	2.9	17		peak $\overline{U_c}$ = 1.1m/s
Destin Inlet	0.86[a]	4	in tidal inlet, fine to medium sand	mean tidal range 0.2m, peak $\overline{U_c}$ = 0.6m/s, sheltered from waves

[a] square pile of 0.61m side lengths, $D = 0.86$ is cross-sectional length from corner to corner.

equations for scour depth are available in the literature. Although most of the equations have been developed for bridge scour they are routinely applied in marine scour applications. Some of the commonly used equations for scour in non-cohesive sediments will be presented below. The most basic prediction equation for scour in the marine environment was derived by Sumer et al. (1992b) and is generally accepted to be industry standard (Det Norske Veritas, 2007, 2010), but is technically only valid for a monopile in uni-directional current on clean, abiotic, uni-modal sand (Black, 2013). The expected equilibrium scour depth is given as in Equation 1.3. Sumer et al. (1992b) calculated the statistical distribution of scour depths aggregated in Breusers et al. (1977) and determined the standard deviation $\sigma_{S/D}$. Thus, the maximum expected scour S_{max} can be given as in Equation 1.4. den Boon et al. (2004) assume $S_{max} = 1.75D$ while, for comparison, Melville and Sutherland (1988) quote, based on experimental data, the greatest possible scour depth as $S_{max}/D = 2.4$ for fluvial bridge pier scour.

$$S = 1.3D; \text{ with } \sigma_{S/D} = 0.7D \tag{1.3}$$

$$S_{max} = 1.3D + \sigma_{S/D} = 2.0; \text{ or } S_{max} = 1.3D + 2\sigma_{S/D} = 2.7 \tag{1.4}$$

For a circular cylinder in steady current, Breusers et al. (1977) gives equation 1.5, developed for bridge pier scour, that accounts for the limiting effect of water depth.

$$S/D = \alpha \tanh\left(\frac{h}{D}\right) \tag{1.5}$$

Values for α are usually between 1.3 and 1.3+$\sigma_{S/D}$=2.0 with 1.3 and 1.75 commonly used; α=1.75 (used in Figure 1.8) and α=2.0 are recommended as conservative design values; however values of up to α=2.7 have been put forward (den Boon et al., 2004; Offshore Center Danmark, 2006). In deep water $h/D > 2-3$, $\tanh\left(\frac{h}{D}\right) \rightarrow 1$ and the equation will equal that of Sumer et al. (1992b) if $\alpha = 1.3$.

Another equation from fluvial scour that has been used in marine scour prediction is that of Richardson et al. (2001). This equation includes flow conditions and sediment and bed form correctors. The non-dimensionalised scour depth S/D is given as

$$S/D = 2.0K_1K_2K_3K_4\left(\frac{h}{D}\right)^{0.35} Fr^{0.43} \tag{1.6}$$

where the Froude number Fr is defined as

$$Fr = \frac{U}{(gh)^{0.5}} \tag{1.7}$$

For circular piers $K_1 = K_2 = 1$, K_3 is dependent on type of bed forms present and is 1.1 in most conditions, 1.2 for dunes between 3 and 9m height and 1.3 for bed features greater than 9m height. The appropriate value for K_3 can be derived from a quantitative assessment of the type of bed features at a site using the method described in Section 2.2.4.2.

A similar equation which includes factors for flow and sediment type is provided by Melville (1997) where the scour depth is calculated as

$$S = K_{\gamma D} K_I K_d K_S K_\alpha K_G \tag{1.8}$$

where $K_s = K_\alpha = 1$ for circular piles and K_G is unity for marine applications and $K_{\gamma D}$ accounts for relative flow depth, K_I for clear-water and live-bed scour and K_d for relative sediment size as shown in the equations below.

$$K_{\gamma D} = \begin{cases} 2.4D & \text{for} \quad D/h < 0.7 \\ 2\sqrt{hD} & \text{for} \quad 0.7 < D/h < 5.0 \\ 4.5h & \text{for} \quad D/h > 5.0 \end{cases} \tag{1.9}$$

$$K_I = \begin{cases} U_c/U_{cr} & \text{for} \quad U_c/U_{cr} < 1 \\ 1 & \text{for} \quad U_c/U_{cr} > 1 \end{cases} \tag{1.10}$$

$$K_d = \begin{cases} 0.57 \log\left(2.24 \frac{D}{d_{50}}\right) & \text{for} \quad D/d_{50} < 25 \\ 1 & \text{for} \quad D/d_{50} > 25 \end{cases} \tag{1.11}$$

The above discussion has highlighted the variability of scour depths observed at marine monopiles. Scour depths can be considerably smaller and larger than the experimentally derived value for live-bed scour of $1.3D$. A number of the most common prediction methods are introduced, which rely on presumed scaling between S and D to offer scour depth estimates. Although some methods include parameters for gross hydrodynamics, water depth and bed mobility, sediment properties, if considered at all, are limited to median grain size, implying possible shortcomings of these equations for all but unconsolidated granular materials.

1.3.1.3 Horizontal scour extent and scour pit slope angles

Hitherto, no scour areas have been reported in literature. Existing research has focussed on measures of the lateral extent along the long and short axis. The latter is assumed to be controlled by the slope angles in the scour pit, hence these parameters are discussed together here. The expected lateral extent of scour is important since it provides a design estimate for the dimensioning of scour protection as discussed in Matutano et al. (2013).

Scour hole width The lateral extent of the scour pit measured from the cylinder wall x_s is thought to be a function of the angle of repose of the sediment ϕ (e.g. Yanmaz, 1991; Whitehouse, 1998) but scales with the cylinder diameter D as the magnitude of flow interference increases. Current guidance by Det Norske Veritas (2013) suggests the required width of scour protection is a function of the internal friction angle and maximum expected scour depth as given in Equation 1.12.

$$x_s = \frac{D}{2} + \frac{S_{max}}{\tan \phi} \tag{1.12}$$

From this relationship the concept of scour hole width is developed. Assuming a circular scour pit of $1.3D$ depth and sand with a typical $\phi = 30°$, the width W of the scour hole will be approximately $5.5D$ (Whitehouse, 1998) after Equation 1.13.

$$W = 2\left(\frac{S}{\tan\left(c\phi\right)}\right) + D \tag{1.13}$$

where c is a slope angle modifier based on considerations about the typical angles assumed by unconsolidated sediments in scour pits relative to ϕ. Commonly, c is assumed equal to unity (Whitehouse, 1998), implying scour pit slope angles are equal to the internal friction angle. Harris et al. (2011) have proposed side slope angles less than ϕ and give $c = 5/6$; again others advocate angles can be steeper than ϕ, within a range of $c = 1-1.15$ (Link et al., 2013). Furthermore, Harris et al. (2011) also noted that prototype data can display wider scour pits than would be expected from the ϕ-relationship. This was explained by the observation of slope angles in the main scour pit that can be significantly less than the repose angle (eg. circa 10°) in areas of strong morphological activity, irrespective of sediment properties. Thus, evidence appears inconclusive as to what slope angles are witnessed in scour holes. Further, the correct choice of internal friction angle is somewhat ambiguous and often varies over a site or even within a scour pit. Peck et al. (1974) and Carter and Bentley (1991) suggest a range of internal friction angles between $30° < \phi < 40°$ for sands and sandy sediments, while a greater range of $26° < \phi < 45°$ is put forward by Hoffmans and Verheij (1997). Based on this latter range and $S = 1.3D$, predicted values using Equation 1.13 vary between $3.05 \leq W/D \leq 7.54$ (see Table 1.3) using the previously suggested slope angle modifiers c. From existing field observations at prototype monopiles in sandy beds, Whitehouse et al. (2011) report the lateral extent to be circa 4-5D (it is not clear whether this measurement represents W, L or both), which lies in the range of forecast widths. Recommendations on lateral extension of scour protection, as measured from the cylinder wall, compiled by Matutano et al. (2013) shows a range from $2 - 4.5D$, suggesting the width of riprap including the cylinder diameter of between $5 - 10D$.

Table 1.3: Predicted non-dimensionalised scour pit width W/D based on Equation 1.13 for $S = 1.3D$ and a range of ϕ and c.

ϕ [°]	$c = 1$	$c = 0.833$	$c = 1.15$
26	6.33	7.54	5.52
30	5.50	6.58	4.78
35	4.71	5.66	4.07
40	4.10	4.95	3.51
45	3.60	4.39	3.05

Scour hole length and orientation of long axis In steady, directionally dominant flow, the upstream slope β_u and downstream slope β_d will not be equal, thus the length $L \neq W$. While β_u is considered to be controlled by ϕ, β_d is given as $\phi/2$ (Hoffmans and Verheij, 1997) or $\phi/2 \pm 2°$ (Harris et al., 2010a), thus predicting a longer extension in the downstream direction. The modifier c is given as unity for the flow-aligned slope angles. The length of scour hole can hence be approximated as

$$L = \frac{S}{\tan\phi} + \frac{S}{\tan(\phi/2)} + D \tag{1.14}$$

Using the same range of ϕ as in Table 1.3 and assuming $S = 1.3D$, the predicted dimensionless scour pit length lies in a range of $5.44 \leq L/D \leq 9.30$. In asymmetric flows, the orientation of the long axis α_L, reported in $^\circ N$ is expect to align itself with the axis of flow, due to the downstream extension of the wake scour. The importance of the lee-wake for the scour process is discussed in Cantwell and Coles (1983). The vortices contain large amounts of turbulent energy and associated with them is an upward spiral of flow which acts to entrain sediment. The "vacuuming" action of the lee-wake vortices has been confirmed numerically using Lagrangian particle tracking and turbulence-resolving Large Eddy Simulation (Pasiok and Stilger-Szydlo, 2010). As wake vortices travel in the direction of flow they can effect sediment movement a long distance downstream, creating a characteristic scour pattern in the wake. Downstream scour occurs in close vicinity along the symmetry plane of the cylinder, with flow instabilities impinging on the bed and sediment being transported downstream. The primary wake vortices continue to dislodge sediment while a small recirculation zone at the base of the cylinder piles sediment against the cylinder Dargahi (1990). Figure 1.7 shows this scour pattern exemplified around a caisson structure. The effect of shedding lee-wake vortices is appreciable as they have created two elongated scour depressions with a narrow ridge separating them. Not much information on the downstream zone of scour is available but Whitehouse (1998) quantifies the realm of influence of wake vortices downstream of the structure as $8D$. In field observations from Scroby Sands wind farm, Whitehouse et al. (2011) report scour wakes of up to $100D$ as a result of secondary edge scour around the scour protection. Rudolph et al. (2004) describe a scour extent of 200m for the N7 monopile, equivalent to approximately $33D$, although it is not known how this dimension was defined. The wake erosion shown in Figure 1.9 was recorded downstream of a wind turbine foundation. Not all of the wake was captured in the survey but a wake length of approximately 125m is visible, which corresponds to over $26D$. It is clear that monopiles can cause flow perturbations many diameters downstream. These can potentially impact the sea bed morphology and nature of heritage sites, raising planning concerns.

The discussion above reveals that there is considerable uncertainty about the horizontal scour dimensions at marine monopiles only a very small, insignificant number of observations are available in the literature. The notion that the internal friction angle of sediment controls the lateral dimensions and slope angles in scour holes will be investigated.

1.3.2 Time-evolution of scour

In terms of time development, scour is seen to progress rapidly upon initiation of the process, then steadily approach the equilibrium condition (e.g. Breusers, 1972; Yanmaz, 1991; Whitehouse, 1998). Sumer et al. (1992a) suggest an asymptotic relationship between scour depth and time for both wave and current scour and found that the rate of change dS/dt, and thus the time required to reach equilibrium condition S_e, depends on intensity of hydraulic forcing, sediment properties and non-dimensionalised boundary

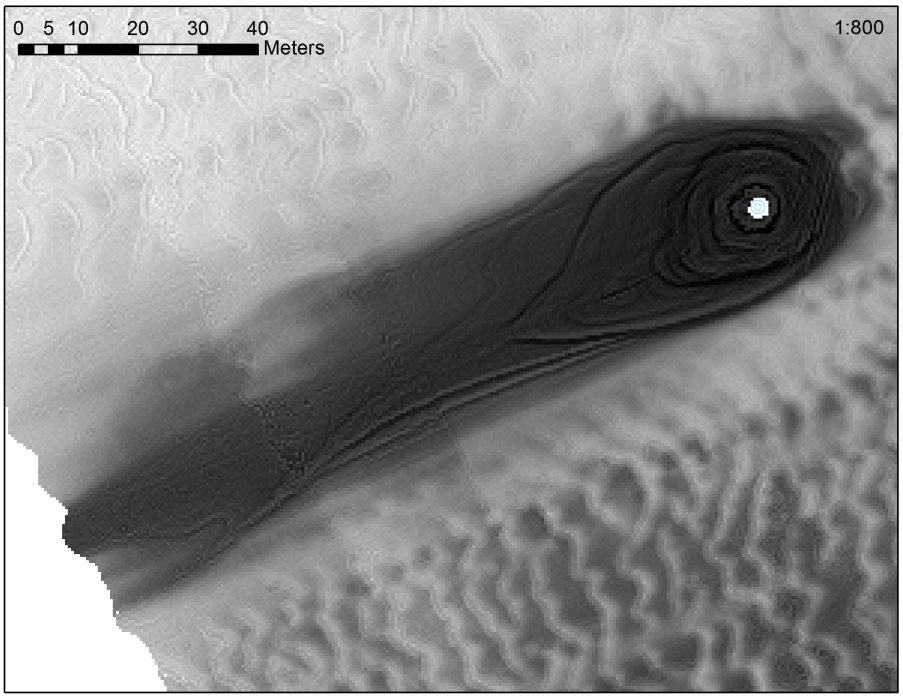

Figure 1.9: Downstream wake scour of wind turbine foundation at Gunfleet Sands wind farm. From study data set.

layer thickness δ/D. Scour development occurs more rapidly with increased flow velocity, hence S_e is reached in less time in live-bed conditions, and in finer sands, whereas the pile diameter was not found to influence the time evolution (Shen et al., 1965, 1966; Sumer et al., 1992a). An experimentally derived scour time function for a pile in steady current or wave flow is suggested by Sumer et al. (1992a) as

$$S(T) = S_e \left[1 - e^{\left(-\frac{T}{T_s}\right)^p}\right] \tag{1.15}$$

where T is the elapsed time, T_s is characteristic scour time scale, defined as the time to achieve 63% of the equilibrium scour value S_e and p is a curve-fitting coefficient. It has been noted that the scour process at prototypes begins immediately after installation and can be appreciably developed in the short period of a few tidal cycles between piling and placing of scour protection, although no exact numbers are given (den Boon et al., 2004; Whitehouse et al., 2006). Harris et al. (2004) explain that the average scour depth around a recently installed monopile diminished by $0.3D$ in the 6 hour period between low and high water. This illustrates just how dynamic scour hole development can be. Unfortunately, this detail is often lost as post-installation surveys are rarely repeated at a temporal resolution that would allow this rapid change to be captured. Walker (1995) recorded a scour depth of 0.9m ($S/D = 1.05$) around a square pier after 8 days or 13 tidal cycles in the sandy sediments of Destin inlet, Florida; partial infilling was observed during the ebb tide; however this did not counteract the net loss of sediment. Notwithstanding the rapid onset of scour, evidence has emerged that appears to indicate that scour can continue developing in sandy sediment for a number of years. Repeat surveys at the N7 pile in the North Sea (see Figure 1.8) shows that between 1.7 and 4.7 years after installation scour had increased by 2.3m equivalent to $0.38D$ and is potentially developing further

(Rudolph et al., 2004). Conversely, Whitehouse et al. (2010) and Harris et al. (2010b) have noted that infilling can gradually reduce the scour depth by some $0.2 - 1.3D$ over some 1-2 years.

The discussed nature of temporal scour development illustrates that the scour process operates on various time scales. The gross time-development is expected to follow an exponential relationship. However, considerable short-term (minute-hour scale) fluctuations are revealed as scour holes adjust to cyclical or extraordinary changes in hydrodynamic forcing. Conversely, long-term observations suggest that the achievement of the "final" scour depth can take several years; however more field data are required to corroborate existing knowledge.

1.3.3 Effect of hydrodynamics

1.3.3.1 Bi-directional, reversing flow

McGovern and Ilic (2014) conducted a flume experiment with a scaled offshore wind monopile foundation in reversing flow. A flow pattern, mimicking tidal conditions, developed three scour regimes of clear water, transitional and live-bed conditions. The resulting scour hole was reported to be shallower and develop less rapidly than under uni-directional flow, which was attributed primarily to the variable intensity of scour action during the three regimes but also to a degree of infilling upon reversal of the flow direction. Escarameia and May (1999) tested both square and circular vertical cylinders in reversing flow and also reported smaller scour depths compared to the uni-directional case. The authors reported that live-bed conditions created the largest scour depths in bi-directional flow, whereas in uni-directional current the clear-water scenario creates the maximum erosion as no infilling occurs. Similarly, Offshore Center Danmark (2006) reported slightly greater scour depths under tidal flow compared to uni-directional current in live-bed conditions. Scour patterning with scour depressions in both flow directions are reported in the bi-directional case.

Escarameia and May (1999) offer a prediction method in equation 1.16 for clear-water equilibrium scour depths under tidal flows. The equilibrium scour depth in equivalent uni-directional flow is

$$\frac{S_c}{D} = 1.32 \left(\frac{h}{D}\right)^{0.6} \left[1 - 3.66 \left(1 - \frac{U}{U_{cr}}\right)^{1.76}\right]$$

The scour depth after one tidal half-cycle reads

$$S_{D_T} = \frac{S_c}{2} \left(\frac{D_T}{T_{50}}\right)^{\alpha}$$

where $D_T = 3600 \times 6 \times (2/\pi)$ and $\alpha = 0.327$ for a circular pile and the time factor T_{50} is calculated as

$$T_{50} = \frac{5500D}{\beta U - U_{cr}}$$

where $\beta = 1.92$ for circular piers. The equilibrium scour depth in tidal flow conditions is given as

$$S_{e,t} = \begin{cases} \left(1.80 - 0.24\frac{D_T}{T_{50}}\right) S_{D_T} & 0.55 \leq \frac{D_T}{T_{50}} \leq 2.5 \\ 1.20 S_{D_T} & \frac{D_T}{T_{50}} > 2.5 \end{cases} \tag{1.16}$$

Although marine prototypes are commonly subject to tidal flows, the above review has shown that only a small number of experimental studies have examined the effect of reversing flows and the results have been ambiguous as to the relative magnitude of scour depths under symmetric and uni-directional flow. So far, this question has not been addressed in relation to prototype data.

1.3.3.2 Oscillatory flow

Sumer et al. (1992b) present the findings of an experimental study into the scour around a vertical pile caused by regular waves. Similar to the steady current case the horseshoe vortex and turbulent lee wake are found to be the main drivers of erosion. The occurrence of these flow features and the onset of scour is controlled by the amplitude of the orbital velocity as expressed by the Keulegan-Carpenter number KC, given as

$$KC = \frac{U_m T}{D} \tag{1.17}$$

where U_m is the maximum oscillatory flow velocity and T is the wave period. The threshold for the emergence of the horseshoe vortex, lee-wake eddy shedding and onset of scour is $KC > 6$ (Sumer et al., 1992b; Zanke et al., 2011). Scour increases with KC until the scour depth under steady current $S_c = 1.3D$ is reached at KC values above 100. The permanence of the horseshoe vortex during the oscillatory flow cycle shows a positive relationship with KC and the wave boundary layer thickness δ_w. For large KC the horseshoe vortex is reported to behave similarly as in steady current. Unsurprisingly, amplification of bed shear stresses M shows strong dependence on KC but a maximum value of 3-4 is given located at the sides of the cylinder, compared with 11 for uni-directional flow (Sumer et al., 1997). The nature of the wake vortices in oscillatory flow and the downstream zone of influence are a function of KC. As KC controls the occurrence of unsteady flow features, the bed shear stress both upstream and downstream of the cylinder is found to be related to the parameter. Sumer et al. (1993) report an equilibrium scour depth of $2.0D$ for square piles under waves. Offshore Center Danmark (2006) found that bed shear stress distributions and scour depths were slightly larger in regular waves compared to irregular breaking waves; both hydraulic forcings only produced small scour holes $S/D < 0.3$. Zanke et al. (2011) has posited that the scour depth under oscillatory flow depends on the relative dimensions of the near-bed displacement x_o during a half wave period and the diameter of the pile. When $x_o \geq D$, achieved for $KC > 100$, the oscillations are so long-periodic as to act like current flow, confirming findings by Sumer et al. (1992b), that wave scour approaches the uni-directional scour value. Prototype observations that qualify as being in an exclusively wave-driven hydraulic forcing regime are not known to the author as most marine locations are at least partly influenced by currents.

1.3.3.3 Combined flow

The effect of combined wave and current action remains ambiguous. Some studies have suggested a decrease in equilibrium scour depth for non-breaking waves (Abou-Seida, 1963; Bijker and de Bruyn, 1988) or at least no exceedance of current-only scour depths (Clark and Novak, 1984). Other studies indicate that the rate of scour is enhanced under combined flow (Armbrust, 1982; Chow and Herbich, 1978; Machemel and Abad, 1975; Clark and Novak, 1984). More recently, numerical investigations carried out by Stahlmann and Schlurmann (2012) suggest that average bed shear stresses around a tripod foundation were largest in combined flow and smallest in steady current, implying that scour might be greatest in waves and currents. On the other hand, for irregular breaking waves in uni-directional current, the Offshore Center Danmark (2006) reports an increase over the wave-only case but a reduction in scour depth compared to the current-only case. Harris et al. (2010a) employed currently available theory for scour time development and showed that waves act to suppress scour development and lead to shallower scour depths. However, it has been noted that waves can act as a catalyst for scour where the current alone is insufficient to initiate scour (Kroezen et al., 1982). The diverging observations could be explained by the dynamics of the horseshoe vortex under combined flow which can vary depending on the relative dominance of current or oscillatory flow (Sumer and Fredsoe, 1992; Sumer et al., 1997). For current-dominated flow the horseshoe vortex is likely to be present permanently, owing to the maintenance of the adverse pressure gradient on the stagnation line and boundary layer separation. The strength of the vortex will be augmented periodically in a positive or negative manner by the oscillatory flow component. In wave-dominated flow the horseshoe vortex might only be weak, exist only periodically or not at all. The scour pattern in co-linear combined flow is assumed to be very similar to the uni-directional case, whereas some modification of the shape of the scour hole is expected for wave and current flows at an angle (Whitehouse, 1998).

Sumer et al. (1992b) offer a method for scour estimation of monopiles in waves and combined flow. In wave flow, for Keulegan-Carpenter numbers (Eq 1.17) $KC \geq 6$, scour is given by Equation 1.18 and for combined wave and currents the scour depth is calculated by Equation 1.19.

$$S/D = \frac{S_c}{D}\left[1 - \exp\{-0.03(KC - 6)\}\right]; \text{ for } KC \geq 6 \tag{1.18}$$

$$S/D = \frac{S_c}{D}\left[1 - \exp\{-A(KC - B)\}\right]; \text{ for } KC \geq B \tag{1.19}$$

where S_c/D is the scour under currents (i.e. typically 1.3) and factors A and B are calculated as

$$A = 0.03 + \frac{3}{4}U_{cw}^{2.6}$$
$$B = 6\exp(-4.7U_{cw})$$

where U_c is the current velocity, U_m is the maximum orbital velocity at the sea bed and the combined flow velocity is determined from

$$U_{cw} = U_c/(U_c + U_m)$$

In case of waves that do not cause the erosion threshold given by B to be exceeded, the scour will tend towards the current-only value of $S/D = 1.3$. Zanke et al. (2011) developed a method for scour prediction under current and wave flow from experiments. The author demonstrates that his method results in very similar predictions of S/D and equal scour threshold KC as in Sumer et al. (1992b)'s method. For this reason, and since it is still the most used equation for wave and combined flow scour, only the latter is applied here.

1.3.3.4 Water depth

The foregoing discussion was concerned with monopiles in deep water where the water depth h does not influence the resulting scour depth. In relative water depths of $h/D < 2$, structures are no longer considered slender and flow-structure interaction and scour tends to deviate from the patterns outlined in section 1.3 (Whitehouse, 1998). For wind turbine foundations with typical diameters of 4-6m, monopiles will behave as large structures where $h < 8 - 12m$, which is common in many offshore wind farm installations built on major sand banks. Hence, it is important to understand the nature of scour in shallow water. Empirical prediction formulae suggest a limiting effect of water depth on scour for $h/D < 2 - 5$ (Hoffmans and Verheij, 1997; Whitehouse, 1998; Sumer and Fredsoe, 2002; Whitehouse et al., 2011), while Breusers et al. (1977) and May and Willoughby (1990) suggest the transition at $h/D < 2.7$ as the impact of water depth is controlled by the factor $\tanh(h/D)$. The effect of water depth on scour depth at the study locations is subsequently investigated in Section 5.1.1.2. Whitehouse (1998) observed that with increasing pile diameter, wave diffraction and reflection effects become more important and the horseshoe and wake vortices have lesser impact. As such, scour and deposition can occur simultaneously around the cylinder. Based on the scour depths quoted in literature it appears that scour at a large structure tends to be significantly smaller than in the slender case. Physical model tests by Rance (1980) showed scour depths of $0.032D$ for waves and $0.064D$ for co-linear waves and currents; however it was noted that for wave flow around large cylinders scour is likely to occur below the slender pile threshold value of $KC > 6$ and that scour in combined wave-current flow is enhanced over the current-only case. Torsethaugen (1975) reports scour depths in the range of $0.2 - 1D$ in live-bed tests at $h/D = 0.66$. The factors influencing scour depths in shallow water are the relative water depth h/D and pile diameter, although the scour does not scale with D in the same way as at slender structures (Torsethaugen, 1975; May and Willoughby, 1990). Escarameia and May (1999) quote a scour depth of just under $1D$ for a circular cylinder in coarse sand and $h/D = 1$. May and Willoughby (1990) found that scour is reduced in relative water depths between $0.1 < h/D \leq 2.7$. To account for reduced scour depths at large structures May and Willoughby have proposed a modified prediction equation for clear water scour

around a circular pier in uniform sediment in Eq 1.20.

$$\frac{S_e}{D} = 2.4A\left[1 - 3.66\left(1 - \frac{U}{U_{cr}}\right)^{1.76}\right] \tag{1.20}$$

where

$$A = \begin{cases} 1 & \frac{h}{D} > 2.71 \\ 0.55\left(\frac{h}{D}\right)^{0.60} & \frac{h}{D} \leq 2.71 \end{cases}$$

and threshold velocity for sediment transport U_{cr} can be calculated after Hancu (1971) as

$$U_{cr} = a\left[g\left(\frac{\rho_s}{\rho_w} - 1\right)d_{50}\right]^{0.5}(h/d_{50})^{0.2}$$

where a=1.0 for $d_{50} > 0.7$mm and a=1.2-1.4 for $d_{50} < 0.7$mm, ρ_s and ρ_w are the density of the particle and water and g is gravitational acceleration. The method is not valid for live-bed conditions in deep water. For live-bed conditions ($U/U_{cr} < 1$) in shallow water ($h/D \leq 2.71$) the scour depth is calculated as

$$\frac{S_e}{D} = 1.32\,(h/D)^{0.60} \tag{1.21}$$

Scour depths in shallow water have been reported by Bishop (1980) who offers field observations from the base of Christchurch Bay Tower ($D = 10.5$m) in $h/D = 0.86$ which show local scour depths between $S = 0.05 - 0.1D$. These scour depths are significantly smaller than in deep water. In bi-directional flows, scour depths are expected to be diminished further as Escarameia (1998) report that scour depths around large structures are less than under uni-directional flow since the reversal of flow causes some backfilling of the scour hole. Similarly, May and Escarameia (2002) have demonstrated experimentally that under clear-water conditions, tidal scour will be significantly reduced compared to the uni-directional case while in the live-bed situation little difference between uni-directional and tidal current is expected. For purely oscillatory flow around large structures, the interaction between the reflected and diffracted wave fields sets up phase-resolved flow and steady streaming as described by Sumer and Fredsoe (2001). Both processes work together to induce scour at the foundation of a large pile. The equilibrium scour depth is controlled by the KC number and a diffraction parameter described by the ratio of cylinder diameter to wave length and a positive correlation is observed.

This section has shown that the modified fluid-structure interaction in shallow water is expected to cause a reduction in scour depths, which seems to be corroborated by individual prototype observations. The exact depth at which scour behaviour changes is subject to debate and more real data are required to examine the validity of the experimental results.

1.3.4 Effect of pile array configuration

Offshore wind farm layouts are designed to maximise the energy yield by avoiding flow interactions between individual wind energy generators. The wake flow of a turbine and blades is characterised by lower velocities and higher turbulence (see Fig 1.10) and siting other wind energy generators in this turbulent wake is bad practice (e.g. Kaminsky et al., 1987; Saravanan et al., 2011). To minimise flow interactions wind turbines are generally placed on the order of several 100s of metres apart, thus the horizontal distance between foundations G to diameter D ratio is typically $G/D \gg 100$ which means that there is no interaction between horseshoe vortices of individual foundations which is considered to occur below $G/D < O(2)$ (Sumer and Fredsoe, 2002) and scour holes develop independently from one another. Despite the remarkably long turbulent lee-wakes that can develop at monopiles (see Fig. 1.4), long enough to have some influence on the flow at a downstream monopile, it seems unlikely that this will have a major impact on the scour patterning of downstream structures as the wake flow interference is temporally limited to a certain current direction and inter-pile spacings should have allowed the significant amounts of the turbulent kinetic energy to dissipate, ie. there should be no large-scale coherent turbulence. Nevertheless, corroboration for the array-independent scour development should be confirmed in the prototype data from various wind farms.

Figure 1.10: Turbulent wakes visualised by "mixing fog" (Emeis, 2010) in the lee of wind energy generators at Horns Rev wind farm, Denmark. Source [1]

1.3.5 Effect of biofouling

The effect of marine growth on the foundation is to effectively increase the diameter and to roughen the structure surface, influencing the intricacies of the fluid-structure boundary layer and potentially increasing scour. In latitudes between 56-59°N, for mean water depths of 2-40m, biofouling is expected to account for an increase in turbine diameter by 0.2m over 25 years (Det Norske Veritas, 2007, 2010). In the southern North Sea, growth

[1] The Guardian, 11/03/2010, The beauty of wind power, http://www.theguardian.com/environment/gallery/2010/mar/11/beauty-of-wind-power. Accessed: 27/06/2014.

can be even more vigorous in shallow waters (up to -10mLAT) and diametral increase of 0.3m is suggested over the same time period. For the same region, Oldfield (1980) proposes even more conservative numbers of up to 0.2m of growth (+0.4m ⌀) within 15 years of structure installation. However, marine growth was not considered in the predictions calculated in this study as it is deemed negligible for the time scale of interest; the time elapsed between monopile installation and subsequent hydrographic survey used for scour assessment is between tens of days to two years, hence it is assumed limited biofouling will have occurred.

1.3.6 Research questions

From this literature review, it is clear that there is still a significant dearth of full prototype investigations of scour from the marine environment. The currently outstanding issues can be summarised as a series of questions. While all questions will be compiled here, the available data might not be suitable to investigate all but the majority will be addressed in the field data analysis in later chapters:

Scour dimensions:

- What is the range and statistical characteristics of observed prototype scour dimensions and how do they compare to existing field data and literature?
  - What is controlling the observed pattern of scour dimensions? Does the data distribution reflect:
    - differences in flow type (symmetric, uni-directional, combined wave and currents)?
    - scaling of scour with diameter D? How sound is the scientific basis for non-dimensionalisation of scour depths as S/D?
    - scaling of scour with water depth h? Are scour depths in shallow water influenced by the proposed depth threshold of $h/D < 2$?
- How does natural morphological activity affect the observed scour dimensions? Is scour greater in areas of high bed mobility as suggested by current knowledge?
- How does the prototype data compare to forecasts using the empirical prediction methods?

Scour morphology:

- What is the range and statistical characteristics of prototype scour horizontal extents and slope angles and how do they compare to existing field data and literature? Are these measures controlled by the internal friction angle of the sediment?
- What range of scour hole morphologies are observed? Is the scour shape controlled by differences in flow type such as symmetric tidal, uni-directional, and combined flow?
- How does natural morphological activity affect scour hole slopes?

Scour time development:

- What is the nature of the scour time development at prototype monopiles? Does it follow the suggested exponential relationship?
- Is there a relationship between scour dimensions and scour hole age?

1.4 Substrate controls on scour

As outlined previously, the majority of the work to date has focussed on experimental examination of uni-directional hydrodynamics operating on unconsolidated, typically uni-modal sandy beds. The sea bed of the continental shelf is far more complex and shows the full complement of sediments from clays to gravels, heterogeneous mixtures thereof, and in many areas exposed bed rock, while the vertical distribution of sediments can be equally as diverse, depending on the stratigraphic history of the area. Sea bed sediments can exhibit varying degrees of internal friction, compaction, cohesion and lithification and, consequently, the sea bed will display a wide range of erosion resistance depending on the physical, chemical and mechanical properties of the substrate as will be discussed in some detail below.

Whitehouse (2006) developed a conceptual model for scour development in different substrate type (see Figure 1.11). Based on this model, scour depth is expected to be greatest in sand and diminishes in coarser grain sizes. Muds show large scour depths which diminish with increasing fraction of sand. Clays can exhibit a large range of scour depths whereas stiff, compacted clays are expected to develop little scour. The time frame of scour development is suggested to increase both with the cohesion of the sediment, ie. larger proportion of fines in the substrate, and the grain size of the dominant particle fraction.

1.4.1 Non-cohesive sediments

Non-cohesive sediments typically consist of grain sizes ($d_{50} > 0.063$mm) and the internal strength originates from frictional contact of individual particles. In the offshore geological context unconsolidated materials are typically modern sediments (Quaternary in age <2Ma, and, more typically from sedimentation over the Holocene marine transgresseion < 11.7ka before present) that has not undergone any lithification, although compaction is possible. It forms surface layers of sediments that can be mobile in sufficiently energetic environments. The resistance to erosion of a cohesionless material is a function of the specific weight of the sediment constituents, gravity, the friction between particles and porosity of the sediment, which will determine the bulk density. The higher the individual particle densities, the greater the force required to initiate erosion. Generally, the more heterogeneous the substrate the lower the erodibility (eg. Nicollet and Ramette, 1971); low porosity sediments will have an increased erosion resistance as small particles occupy the interstitial spaces created by the contact of larger particles, ie. uni-modal sands will erode more easily than mixed sediments, e.g. gravel-sand mixtures. Poorly sorted sediments, show increased packing density, lower porosity and increase the number of frictional

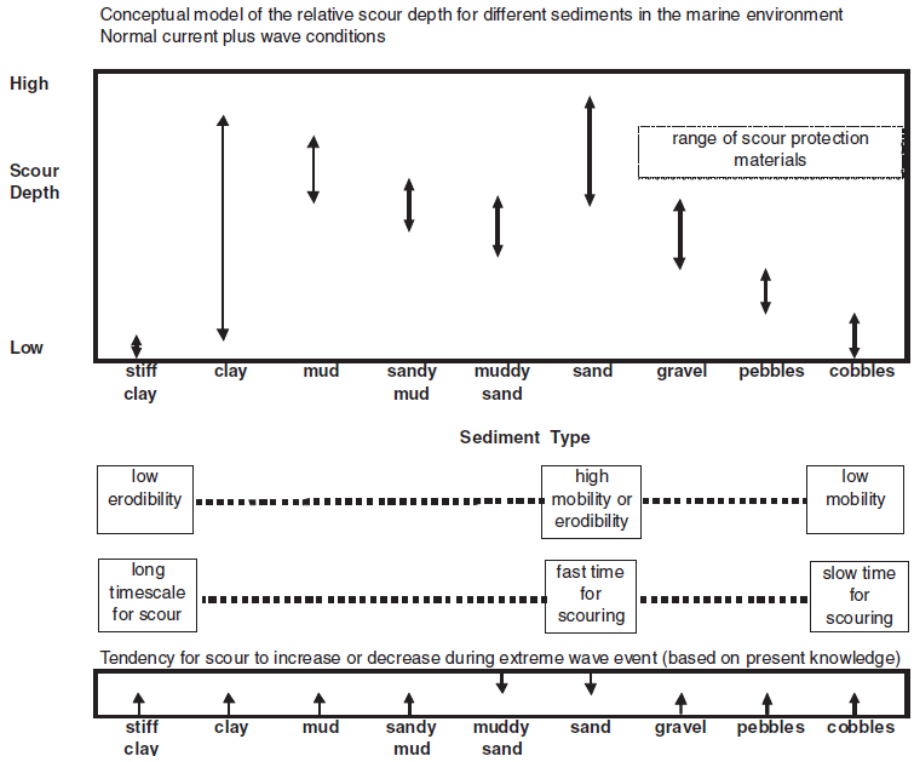

Figure 1.11: Conceptual model for scour in various substrates. From Whitehouse (2006).

contacts between grains (Annandale, 2006). For unconsolidated deposits of single grain size, sands and gravels show porosities between 25-40% and 25-50% respectively whereas once the two constituents are mixed porosity drops to 20-35% (Freeze and Cherry, 1979). Granular materials generally erode on a particle-by-particle basis by sliding, rolling or suspension (Briaud et al., 2001) and the threshold of motion of a particle can be determined by traditional sediment transport theory as described in Soulsby (1997) for example. A modified Shields diagram is plotted in Figure 1.12 which allows the critical shear stress (given as Shields parameter θ_{cr}) for a certain non-dimensionalised grain diameter d_* to be determined.

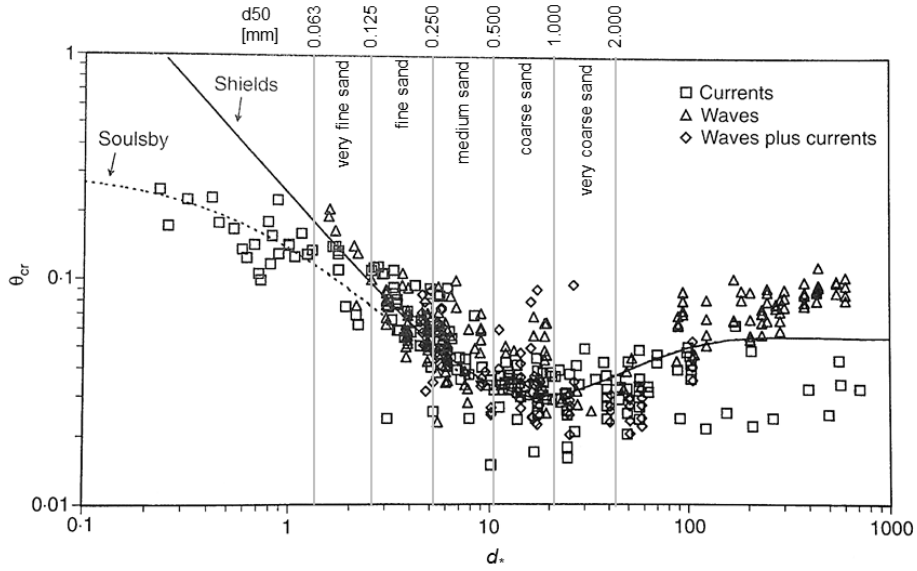

Figure 1.12: Threshold of motion of sediments on a flat horizontal bed. From Soulsby (1997). Limits of sand grain sizes given with equivalent d_{50} for $\rho_w = 1000\text{kg/m}^3$, $\rho_s = 2650\text{kg/m}^3$ and $\nu = 1.36 \times 10^{-6}$.

The Shields parameter is a non-dimensionalised shear stress given as

$$\theta_{cr} = \frac{\tau_{cr}}{g(\rho_s - \rho_w)d} \tag{1.22}$$

and the non-dimensionalised grain size can be calculated as

$$d_* = \left[\frac{g\left(\frac{\rho_s}{\rho_w} - 1\right)}{\nu^2}\right]^{1/3} d \tag{1.23}$$

where ρ_s and ρ_w are the density of the particle and water, g is gravitational acceleration and ν is the kinematic viscosity of water.

According to the diagram the erosion threshold is lowest for medium sands and increases for finer and coarser particles. Once the threshold of motion has been breached, erosion generally occur very rapidly as frictional forces can be overcome instantaneously. The threshold of motion governs the distinction between clear-water and live-bed scour. In the former, the flow is not strong enough to initiate motion other than where bed shear stress amplification (section 1.2.2)occurs around the structure; this also means that no sediment is fed into the scour area from upstream. In the live-bed regime, sediment is in movement across the entire bed.

Breusers and Raudkivi (1991) found that grain size effects become negligible once the characteristic dimension of the structure is significantly larger than the median grain size $D > 50d_{50}$. Conversely, Sheppard et al. (2004) tested relative grain sizes D/d_{50} as large as 4,155 and have shown that scour depths are reduced for values either side of $D/d_{50} = 50$, albeit the dependence of S/D on the relative grain size reduces for $D/d_{50} > 50$, suggesting erosion might be limited where the sediment becomes very small or very large in relation to the structure and also implying issues related to the scaling of physical experiments which operate on much smaller D/d_{50} than prototypes. For prototypes with D=4-6m in fine to coarse sand, D/d_{50} is on the order of 2,000-50,000 implying that scour depths at prototypes could be considerably less than those predicted in physical tests (Melville, 2008).

Under certain circumstances armouring of the bed can occur by means of preferential erosion of the finer material. This leaves a lag deposit of coarser immobile sediment behind that protects the underlying substrate from erosion. Chiew and Melville (1989) found that scour in mixed sediments is less pronounced than in uni-modal sediment, which in their experiments was attributed to formation of an armour layer. It was found that armouring occurs only where a sufficient spread in grain size fractions exists as the ratio d_{84}/d_{50} must exceed 2 in order for protection to be effective. Once created, the armour can however be broken up with increasing flow speed so that at high velocities, the live-bed scour depths in homogeneous and mixed sediments are similar. Similar observations were made by Raudkivi and Ettema (1985); however they found that upon breaching of the armour layer, the scour depth could be greater than when no armour layer is present. Nicollet and Ramette (1971) evaluated scour around a circular pile in a tri-modal mixed sediment and reported the resulting scour depth to be 25% less than depths observed in

uni-modal beds of the same three grain size fractions. Porter et al. (2012a) explain that, for a cylinder in steady current in layered sediments of coarse and fine sand, scour occurs more rapidly, compared to uniform sediment bed of equal depth, in a configuration where coarse sand underlies fine sand and more slowly where fine material is beneath a layer of coarse sand. The latter is explained by armouring effects as it was shown that significant mixing can occur between fractions in the scour hole, but also due to the slower rate of scour in the coarse layer which controls scour evolution in the bottom layer. These results have highlighted that scour in layered deposits is not a straight-forward function of erosion in uniform sediments with corresponding grain sizes. In a mixed bi-modal sandy sediment Porter et al. (2012b) reported shallower scour than for uni-modal sediments of equal d_{50}s. The time evolution of the scour hole was also found to be different with the scour proceeding at a linear rate, after the initial scouring phase, rather than the expected asymptotic trajectory. This suggests that scour in real loose mixed sediments might deviate from what is expected under experimental conditions.

The discussion has shown that, generally, the erosion in unconsolidated particulate sediments is well understood. Complications arise with increasing complexity of the granular sediment composition, eg. mixed multi-modal sediments or layered sediments. The impact of these configurations and their secondary effects such as armouring are not easily quantified in terms of scour depths.

1.4.2 Cohesive substrates

Cohesive materials, or "chemical gels" (Annandale, 2006) contain a significant fraction of fine grain sizes ($d < 0.063$mm) and bonds between particles are maintained by cohesion, which has its origin in physio-chemical attraction forces, and cementation between grains which can further increase the coherence of the substrate. The forces creating cohesion between particles include van der Waals forces, hydrogen bonds, cation bonds and repulsive double-layer forces (Ansari et al., 2002; Debnath and Chaudhuri, 2010). The complexity and non-linearity of the erosion response of cohesive materials is illustrated by Briaud et al. (2001) who have compiled a list of factors affecting the critical shear stress τ_{cr} and rate of erosion $\dot{z}$ for a cohesive material. Generally, τ_{cr} of a cohesive material increases when: sediment unit weight γ increases, plasticity increases, shear strength c_u increases, clay content increases, void ratio e decreases and sediment and water temperature decrease. Further factors with less easily quantifiable effects are type of clay mineral, cation exchange capacity, water content and grain size. The erosion rate $\dot{z}$ will speed up with increasing shear stress τ and sediment and water temperature and decreasing clay content. The term "cohesive substrate" is used here as an umbrella term for sediments that include a minimum significant proportion of silts and/or clays, large enough to affect the engineering properties of the sediment. The presence of fines in a granular matrix can create cohesion in the mixed substrate thus decreasing the erodibility of the bed (Annandale, 2006) and slowing the rate of scour (Briaud et al., 1999). The threshold clay percentage at which sediments display cohesion and a degree of plasticity is ambiguous and can depend on the type and nature of clay mineral present (Molinas, 2003; Link et al., 2013). Typically, the substrate will show altered engineering properties once the proportion of fines

exceeds 10% by weight (Hosny, 1995; Whitehouse, 1998). However, Debnath and Chaudhuri (2010) define a transition zone between 3-20% clay content, while Ansari et al. (2002) noticed plastic behaviour of the material once 20% clay fraction was exceeded and Dey et al. (2011) could not pinpoint a single threshold value for transition to plastic behaviour but reported that, in terms of scour under waves, a sandy sediment with 30% clay behaves like a clay-only bed. In these mixed sediments the erosion resistance will depend on the compound shear strength which is a function of the respective influence of internal friction between particles (as in cohesionless sediments) and cohesion forces originating from the presence of fine-grained material. In experiments by Vallejo and Mawby (2000) the shear strength of a mixture of particulates and clay was equal to that of the granular material alone if the proportion of clay was less than 25% by weight. Similarly, when the clay content by weight exceeded 40% the shear strength was comparable to that of just clay. In more equitable mixes, the shear strength is attributed partly to friction in the granular medium and partly to cohesion in the clay matrix. Generally, the addition of granular material to clay or vice versa will increase erosion resistance of the material (as suggested in Fig. 1.11); the maximum strength is reached at a specific content of clay which will vary with water content and mineralogy (Debnath and Chaudhuri, 2010). Briaud et al. point out that although geotechnical properties influence the erodibility of a sediment, statistically significant correlations between individual engineering properties and erodibility have been very difficult to substantiate and in reality trends are often very weak. This is due to the multitude of non-linear geotechnical relationships and feedbacks which govern the erosion resistance of a mixed cohesive substrate. For this reason, establishing a causal correlation between the observed scour and geotechnical parameters is not likely to be straightforward and has to date not been achieved (Whitehouse et al., 2011). This will be further illustrated in the discussion below.

The nature of scour in cohesive substrates is somewhat ambiguous due to the diversity of substrate type and the complexity of the constituent material properties. While experimental evidence unanimously suggests that scour evolution proceeds at a much slower rate than in sand (e.g. Hosny, 1995; Briaud et al., 1999), even thousands of times slower (Briaud et al., 2001), the results have proved dubious as to whether the equilibrium scour depth S_e in cohesive sediments is less than (e.g. Hosny, 1995; Molinas and Hosny, 1999; Molinas, 2003; Link et al., 2013), similar to (e.g. Briaud et al., 1999; Ting et al., 2001), or even greater than (Ansari et al., 2002) that observed in sand under the same experimental conditions. Nevertheless, it has been witnessed that scour in cohesive substrates can be significant as Jiang et al. (2004) report a scour depth of 5m in firm clay in estuarine flow. Molinas (2003) demonstrated in physical tests that a sand-clay mixture with 12% montmorillonitic clay experiences half the scour depth compared to plain sand. Molinas and Hosny (1999) report a decrease in S_e and rate of scour with increased clay fraction (between 0.05-0.4) in a sand-clay mixture. The greater the compaction of the cohesive material the less pronounced the scour was found to be, while it was observed to increase for greater initial water content. Hosny (1995) reported that the presence of 10-40% montmorillonitic clay by weight in sand resulted in the scour depth being reduced compared to plain sand and slows the scour pit development; compaction further enhances the erosion resistance, but greater initial water contents can have the opposite effect. According to

Briaud et al. (1999) and Ting et al. (2001) clay beds (kaolinite and montmorillonite clay) can exhibit similarly deep equilibrium scour as sandy sediments, while the development of the scour hole proceeds at a much slower rate. Ansari et al. (2002) examine scour in mixed sediments consisting of sand and illite clay (10-60% by weight) and reported that scour in those sediments could be either greater or smaller than for sand, depending on the initial water content. For clay-sand mixtures in oscillatory flow Dey et al. (2011) documented smaller S_e around a cylinder than for the benchmark case of uni-directional current and loose sand. The reduction in scour depth is proportional to the increase in clay fraction up until the proportion of clay reaches 30% by weight, after which the bed responds to erosion like a clay-only bed. Debnath and Chaudhuri (2010) examined scour in sand-clay mixtures with clay (kaolinite and natural river clays) content by weight between 20-100%. Water contents by weight varied from 20-46%. The authors findings are represented conceptually in Figure 1.13. For initial water content below 24% the scour depths decrease with increased clay content. For water content greater than 27% the same trend can be observed up to a minimum that lies between 50-70% clay content by weight but is a function of the water content. Beyond that the equilibrium scour increases again somewhat.

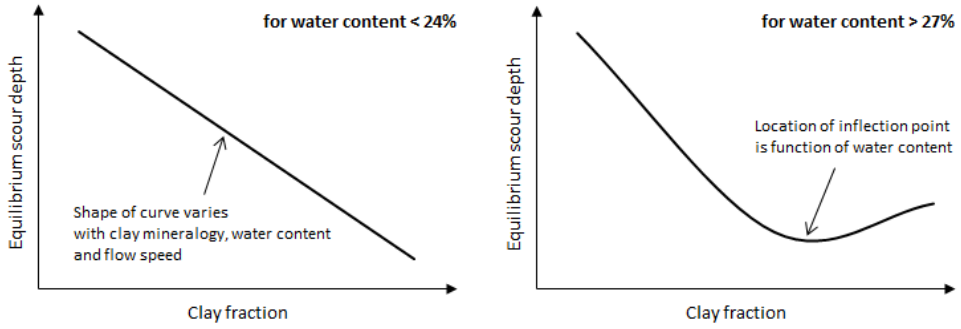

Figure 1.13: Conceptual relationships between clay content and equilibrium scour depth in cohesive substrates for initial water content $< 24\%_{weight}$ (left) and $> 27\%_{weight}$ (right). Based on data from Debnath and Chaudhuri (2010).

Similarly, an minimum was also found in the relationship between scour depth and initial water content by Link et al. (2013) who conducted experiments with a natural sandy silt and kaolinite mixture compacted to various degrees. For a given compaction, the minimum scour depth was found at an intermediate water content and increased with lower and greater water contents (see Figure 1.14). Compaction of the sediment caused an increase in erosion resistance as long as the water content remained below the critical value above which the clay fluidises and internal strength is diminished. The range of scour depths for the mixed sediments with various water contents and degrees of compaction ranged between 10-58% of the benchmark sand case. It was found that the mechanism of erosion changed with the sedimentary water content, from "chunks of aggregates" at lower water contents, over "aggregate by aggregate", to "particle by particle" at high water content. Rambabu (2003) demonstrated that for a natural medium-plasticity silty clay scour depth scales positively with Re_D and decreases with greater average undrained shear strength c_u (Figure 1.15). The scour mechanism was reportedly changing throughout the experiments; at first loose particles were eroded, followed by aggregates and chunks as the substrate surface integrity deteriorated.

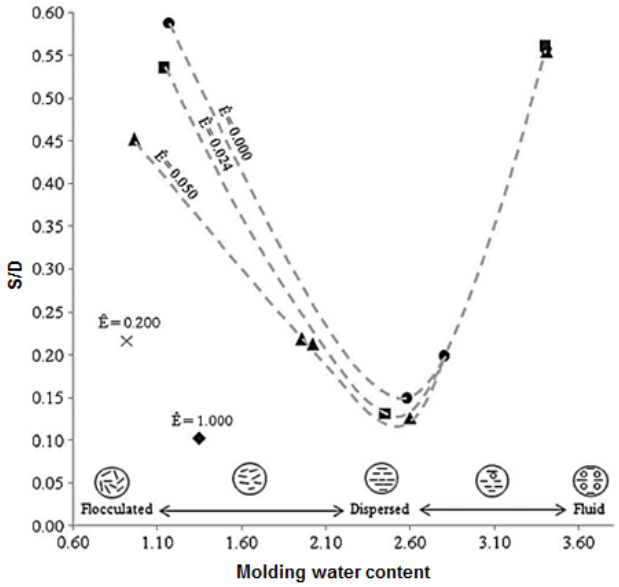

Figure 1.14: Relationship between dimensionless water content, dimensionless compaction energy $\hat{E}$ and dimensionless scour S/D. Modified from Link et al. (2013).

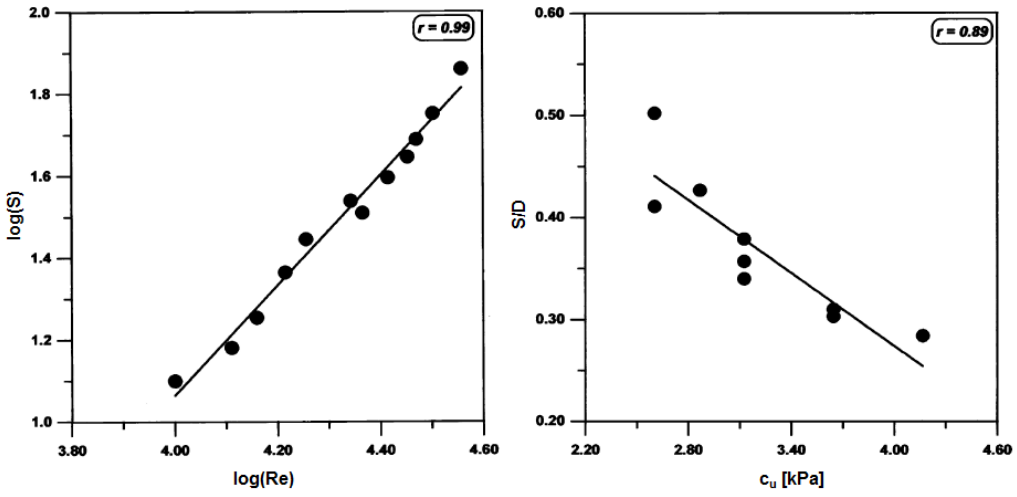

Figure 1.15: Relationship between Reynolds number Re and scour depth S (left) and undrained shear strength c_u and non-dimensionalised scour depth S/D (right) in physical tests. Modified from Rambabu (2003).

A number of authors have reported that the morphology of the scour hole in cohesive substrate is significantly different to the typical non-cohesive pattern. Firstly, slope angles can surpass the natural angles of repose simply by way of presence of fine material (Hosny, 1995; Whitehouse, 1998 but also by way of compaction of cohesive material (Molinas and Hosny, 1999). Link et al. (2013) claim that cohesive materials can support vertical slopes. For high clay fractions ($\geq 50\%$) and saturated mixes Ansari et al. (2002) observed the most pronounced scour at the sides of the pile, whereas for lower clay contents or undersaturated substrates it was more similar to the non-cohesive pattern and located upstream of the pile. Both Ting et al. (2001) and Debnath and Chaudhuri (2010) report that at high clay contents (25-35%) the scour was more pronounced downstream of the pile rather than upstream, especially at high Re numbers. Where less clay is present in the mixture the scour was similar around the pile (Ting et al., 2001) or deeper upstream of the pier (Debnath and Chaudhuri, 2010). Link et al. (2013) also noted the location of maximum scour depth in the wake of the structure, rather than in the vicinity of the pile; however the shape was similar to the non-cohesive case at low and high water contents. Those same sediments also displayed the steepest slopes. Nevertheless, the discussion shows that the primary agent of erosion can change between horseshoe and lee-wake vortices depending on the geotechnical properties of the sediment.

In cohesive substrates, the response to external forcing is characterised by bending, brittle fracture and fatigue failure (Annandale, 2006). The erosive process will typically catch on at surface discontinuities such as fractures, fissures and weathered zones and the exploitation of surface faults allows water to penetrate and influence strength of chemical bonds. Some cohesive materials, such as clay change their physical properties upon contact with water, e.g. the rate of erosion of clay slows with water salinity (Fredsoe, 1990). The clay scour process begins as washing off of individual clay particles, followed by removal of clods of material called "plucking" (Annandale, 2006).

Briaud et al. (1999) developed an equation for scour prediction under uni-directional current in cohesive materials based on physical scour tests in porcelain clay. The maximum expected scour depth is calculated as

$$S_{max} = 1.8 \times 10^{-4} Re_D^{0.635} \tag{1.24}$$

where 1.8×10^{-4}m was the maximum scour observed in Briaud et al.'s experiments upon which the Re_D scaling relationship was developed. As material bonds are affected by the contact with saline water, Equation 1.24, developed for fluvial freshwater scour is likely to overestimate the maximum scour depth.

The above section illustrates the complexity of erosion in cohesive sediments. Although, individual studies have managed to link scour depths to certain substrate engineering properties under certain experimental conditions, the difficulty of deriving universal relationships about scour in cohesive materials is illustrated by the variable results presented in the experimental studies. The non-linearity of feedback between geotechnical factors and the many degrees of freedom, given by number of potentially influencing parameters and the vast number of magnitude combinations of these, mean that a lot

more work is needed to understand the scour process in these substrates. As reviewed in Section 1.3.1.2 cohesive sediments are understood to act as erosion barriers as illustrated eg. at Princess Amalia wind farm or North Hoyle in Figure 1.8. However, it is unknown how much scour the clay layer experienced.

1.4.3 Rock

Lithified material generally makes up the bed rock which is typically much older in age than the unconsolidated material (>20Ma). Bed rock can be buried under a package of unconsolidated sediment or be outcropping at the surface. According to Annandale (2006), rock can be classed as either a chemical or a physical gel depending on the relative scale of the characteristic dimensions of the turbulence and the rock. Where the exposed surface of rock is jointed, fractured and weakened by weathering, and the scale of these weaknesses are small relative to the scale of turbulence, blocks of rock can be removed in a similar manner to erosion of a physical gel. Rock can be classed as behaving like a chemical gel when it is intact or where joints and fractures are on a much larger scale than the turbulence in the flow. In this case the erosion resistance will depend on the degree of lithification of the rock. Under conditions encountered at the seabed, intact rock is very unlikely to erode if it is well lithified. However, it is not inconceivable that poorly lithified material might be erodible in a manner similar to cohesion-less sediments. The strength of the rock, which is said to be related to the unconfined compressive strength of the material (Annandale, 2006) will also play a role. Softer rocks such as chalks can display behaviour very similar to soft to very stiff clays in terms of geotechnical parameters, as suggested by CPT records in these substrates. The existing observations of scour in bed rock areas have been reviewed in Section 1.3.1.2 for London Clay at Kentish Flats and glacial till at Barrow wind farm. Scour has been limited by the presence of bed rock, yet it is also reported that these materials have experienced a certain degree of erosion.

1.4.4 Secondary factors and post-erosive processes

In addition to the basic erosion process based on the material properties discussed above, a number of further circumstances have been identified that can affect scour during and after the scour process and might play a role in the explanation of observed scour patterns. Processes that can mitigate scour are backfilling and infilling of the scour hole. Generally, a suitably large sediment supply is required and currents that are strong enough to create live-bed conditions. The migration of bed forms can also contribute to infilling of scour holes. Infilling can also occur by means of simple slope failure and this process is reversible by renewed erosion. As mentioned above, seabed armouring with coarse sediments, precluding the removal of finer sediments beneath, can work to reduce the final scour depth (eg. Raudkivi and Ettema, 1977; Chiew and Melville, 1989; Raudkivi and Ettema, 1985; Porter et al., 2012a). Along with processes that reduce scour, there are mechanisms that can overcome the natural erosion resistance of a material. Abrasion by water-borne sand can exacerbate scour in resistant materials and quarrying of bedrock along lines of weakness in the rock are examples of such mechanisms. The latter process

can exploit joints and faults in rock and hydraulic lift forces can remove blocks of rock (Annandale, 2006). Abrasive erosion, effected by the rasping action of sand particles in the flow in contact with cohesive or poorly lithified material, as suggested by Whitehouse et al. (2011), depends on the hardness differential of the two materials, the amount of time where conditions are suitable for abrasion to occur and the sediment loading of the flow (Wohl, 2014). Processes that can either enhance or reduce scour include the response of the scour to the wider morphological evolution of the area, eg. regional morphological sea bed changes and migration of large-scale bed forms such as sand banks. To the author's knowledge, the change in geotechnical strength of a marine substrate or bedrock after the piling operation has not been investigated. For a cohesive material, it seems possible that the internal strength might be reduced due to increased bending, shearing, faulting and introduction of weaknesses at the surface and throughout the profile. However, equally, it is not inconceivable that for a clay-rich substrate local compression and compaction due to downward force applied during piling might increase the material strength. For lithified materials, brittle fracturing can be envisaged which could lead to an increase in erodibility.

1.4.5 Research questions

From the review of substrate-related scour knowledge, it is clear that while scour in simple granular sediments are relatively well understood, much less is known in respect to scour development in mixed granular sediments or complex, cohesive and consolidated sediments. The currently outstanding issues can be summarised as a series of questions. While all questions will be compiled here, the available data are not suitable to investigate all of them but the majority will be addressed in the field data analysis in later chapters:

- How does prototype scour in various substrates compare to the conceptual scour model by Whitehouse (2006)?
- Does the thickness of surface sediment control the observed scour depths?
- Do geotechnical properties of the sea bed control the pattern of observed scour depths?
  - What is the nature of prototype scour in cohesive substrates and is it less than, equal to, or larger than in unconsolidated sediment?
  - What is the nature of prototype scour in consolidated materials such as bed rock?
  - Which engineering properties of cohesive or consolidated substrates can be identified that influence observed scour depths?
  - Is scour in heterogeneous unconsolidated sediment less than in uniform granular sediment?
  - Is there any evidence of existence and nature of armouring in prototypes and how does it compare to experimental data?
  - Is there an effect of relative grain size D/d_{50} on scour?

- Does the nature of the sea bed substrate affect the observed scour hole morphologies or slope angles?
- How does the prototype data compare to the scour equation for cohesive substrates?

Chapter 2

Methods

This chapter introduces the concepts and techniques used in this study. The first section deals with the design and characteristics of the study area, while section 2.2 discusses the techniques employed in the analysis of the various types of data. This is followed by the evaluation of methods to enable an automatic recognition of the scour hole in Section 2.3, while parameters to quantify scour dimensions and shape are defined in Section 2.4.

2.1 "Natural laboratory"

This section discusses the Outer Thames Estuary (OTE), where all three wind farm sites under investigation are located, in respect to its characteristics as a prototype natural laboratory. Thus, the similarities and differences in the regional physical environment, the wider hydrodynamic regime and geological characteristics of the OTE are established. The study zone was purposefully designed to constrain, as far as possible, the natural hydrodynamic variability thus allowing an emphasis to be placed on the investigation of substrate controls on scour. Figure 1.2 shows the location of the study area and a map of wind farms in the wider study region. A more detailed map of the region is given in Figure 2.1 with the main topographical features in the area and the seaward limit of the OTE drawn approximately at the -20mCD contour as suggested by Burningham and French (2011). Seaward of which the hydrodynamic, morphological and depositional environment changes from estuarial to more shelf sea-like.

2.1.1 Hydrodynamic regime of the Outer Thames Estuary

Information on tidal flow patterns has been compiled from field measurements and tidal diamond data and the information is summarised in Figure 2.2. The 11 current measurements covering the area, available in the public domain from BODC, were taken between 1972-1979; however the most recent measurement is from 1998. The individual record lengths cover at least a single neap-spring-tidal cycle, although most are longer, commonly 1-2 months and were recorded with impeller current meters. The current roses show that in general the flow pattern is dominated by two flow directions, one in the NNE-ENE sector and the other in the SSW-WSW sector. The tidal current is understood to flow

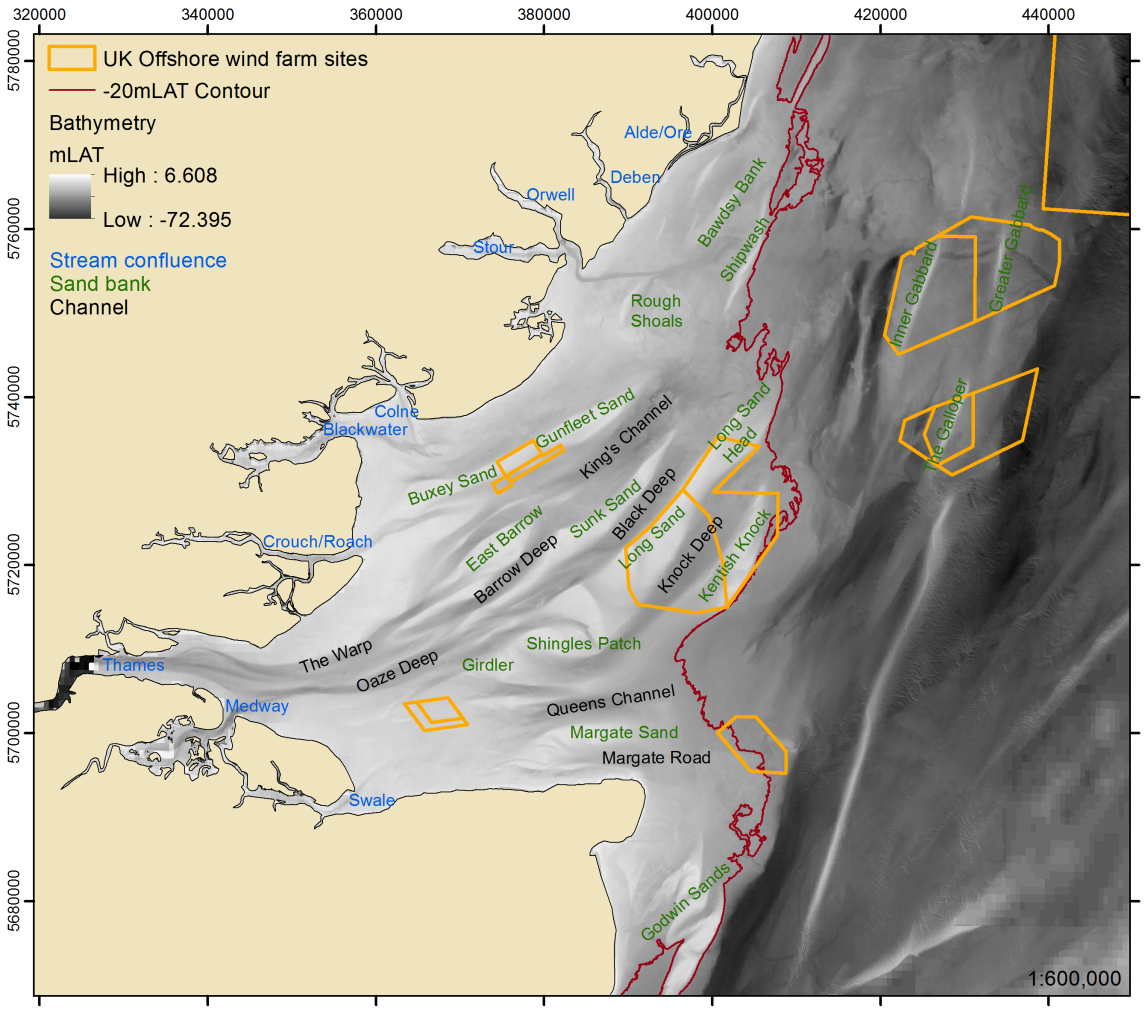

Figure 2.1: Map and bathymetry of Outer Thames Estuary. After Burningham and French (2011).

in a south-westerly direction and the ebb in the opposing direction, creating a bi-modal flow pattern, except for where some flow complexity is introduced by topographic features such as the Kent headland or around Long Sand Head. For London Array and Gunfleet Sands, the flood tide is generally in a south-westerly direction and the ebb in a north-easterly direction while at Thanet the flood travels due south and the ebb due north. The major sand banks are tidally aligned and flows are confined to the intervening channels as preferential flow pathways. Analysis of the current speed measurements in Figure 2.2 show that flows generally do not exceed 1.2ms^{-1}, except on the ebb at Long Sand Head and most commonly lie in the range of 0.6-1.0ms^{-1}. The current rose data suggest slight dominance of the incoming flood tide in the depicted area, but tidal dominance is seen to vary throughout the estuary and the ebb tide can be stronger on the northern side of the banks (Kenyon and Cooper, 2005), as illustrated by the rose at Long Sands Head or to the north-east of Gunfleet Sands. In the wind farm areas, the tidal diamonds show that flows are generally fastest on the incoming tide and diamonds 3,4 and 5 in Knock Deep and Black Deep (see Fig 2.1) exhibit the highest flow speeds between 1.1-1.3ms^{-1} but peak current speeds during neap tides are some 0.4ms^{-1} less. The time duration of ebb and flow is similar and the transition around high water slack generally occurs quite rapidly but is markedly more gradual around the coastline of Kent (tidal diamonds 1 and 2). From measured data, the tidal range over the three wind farm sites is between $2.2 - 2.5$m on neaps and $3.9 - 4.1$m on springs. Numerical modelling results of average metocean conditions in the OTE by ABPmer (2008) are displayed in Figure 2.3. The mean spring tidal range is shown to increase from NE to SW, which is a result of the controlling amphidromic point to the north-east of the region, some 80km offshore of eastern Norfolk (Sturt et al., 2009). The simulated conditions (Fig 2.3) suggest that mean spring tidal range is 4.0m at Gunfleet Sands and London Array and 4.1m at Thanet with average spring tidal currents of 0.7-1.0^{-1} suggested over the sites which compares well with measurements.

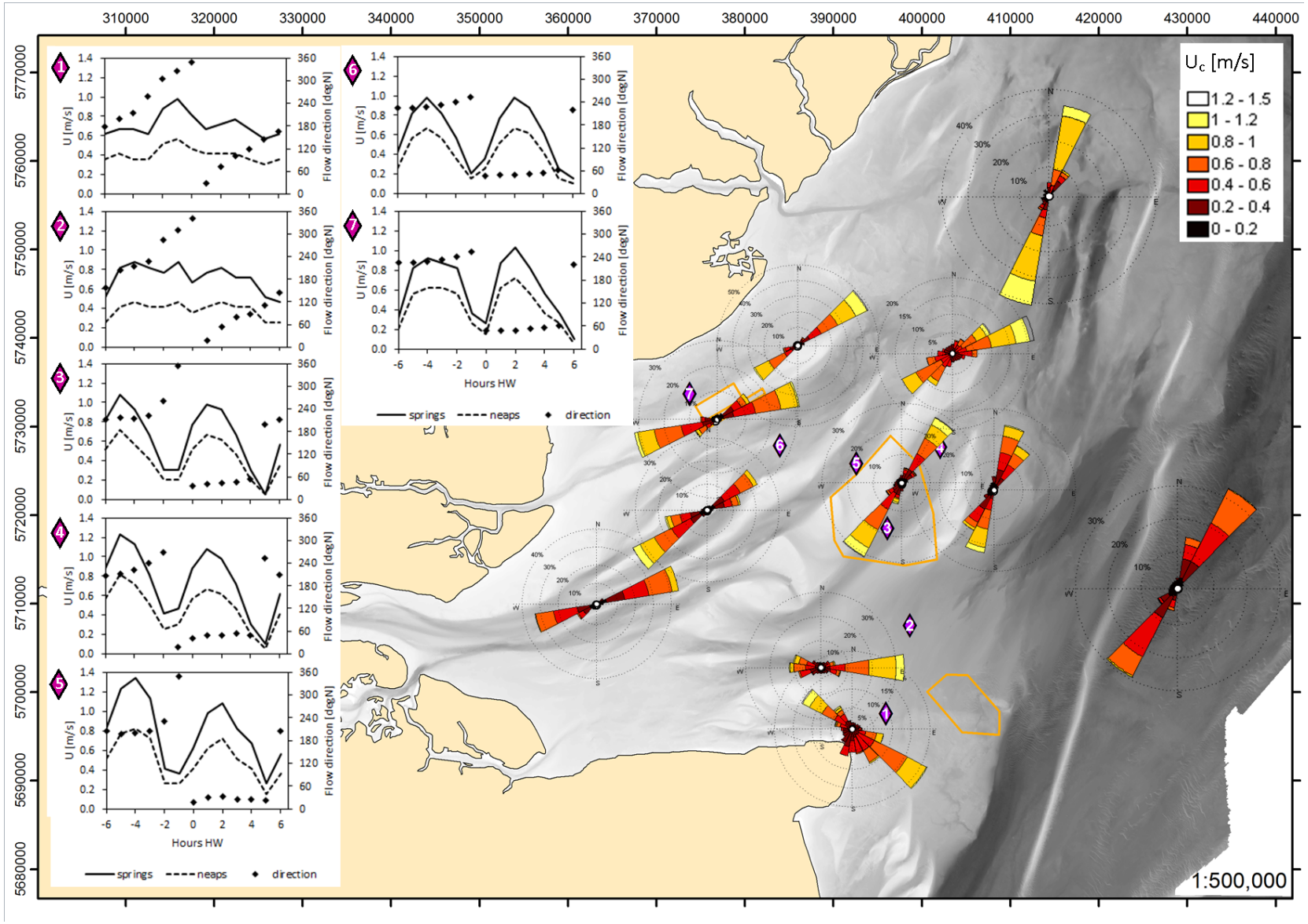

Figure 2.2: Current roses and tidal diamond information for the Outer Thames Estuary. Data from BODC and UKHO Admiralty charts.

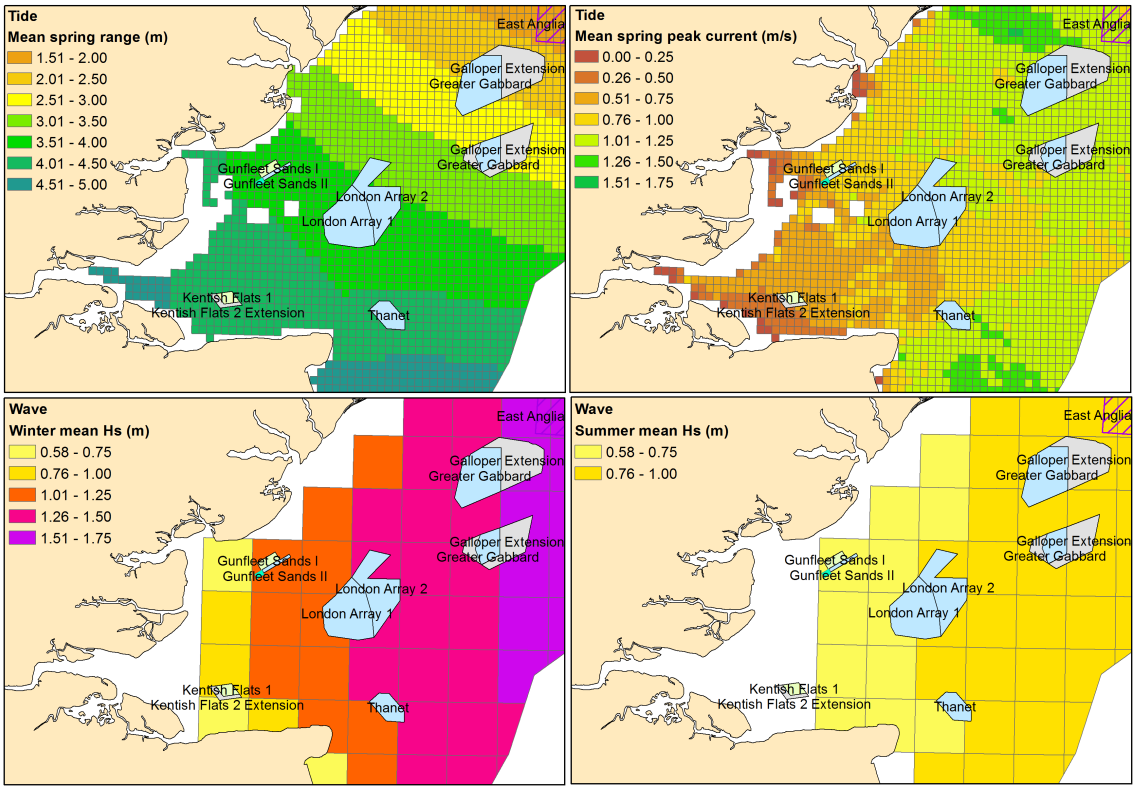

Figure 2.3: Average metocean conditions in the Outer Thames Estuary after numerical modelling by ABPmer (2008). Mean spring tidal range (top left), mean spring peak current (top right), winter mean significant wave height (bottom left) and summer mean significant wave height (bottom right).

A number of wave buoy records are accessible in the public domain (CEFAS Wavenet, CCO, BODC). These data are plotted in Figure 2.4 and provided some insight into the wave climate in the Outer Thames. The gross pattern suggests that the wave energy received at any one location is a function of exposure. Wave energy is greater in the east and diminishes towards the inner estuary with increasing shelter of the land mass, shallowing water depths and the breaking of waves on the sand banks. Even in exposed locations wave heights are relatively moderate and very rarely exceed 2.5m and peak periods are typically less than 10s. Unsurprisingly, the largest waves arrive from north-easterly to easterly directions, having been generated in long fetch conditions in the southern North Sea. In the more sheltered western part of the OTE and in the nearshore areas typical wave conditions are H_s <1.5m, T_p < 6s; the average zero-crossing wave period is T_z < 4s. The further inshore, the greater the influence of locally generated waves owing to the fact that waves from the easterly sectors tend to be limited over the sand banks. Analysis of the wave record on Kentish Knock (south-eastern corner of London Array wind farm) has revealed that over 7.5 years of measurements, 90% of observations of H_s are below 1.5m and a peak wave period of 6s is only exceeded 20% of the time. The larger wave heights, when they occur, are typically associated with short-duration winter storms. Astley et al. (2014) undertook an analysis of extreme events using wave data from a buoy in the Outer Thames Estuary. It was found that between 2002-2012 there was no storm that breached the 1:5 year threshold and typically a single 1:1 year event occurred annually, which suggests that the occurrence of storm events has been limited. Numerical simulation of waves by ABPmer (2008) in Figure 2.3 suggests that wave conditions are more benign in the summer and the approximate difference between winter and summer H_s is 0.25-

0.5m. Summer average wave heights are given in a range of 0.6-0.8m and 1-1.4 in winter. Calculation of winter (taken as November-April) and summer (May-October) average H_s from the measured wave records is in the same range as the previously suggested values.

In summary it can be said that under typical conditions, sea bed processes in the study area will be dominated by the action of tidal currents which are more than capable of moving sand-sized particles (see Section 1.4.1). On a spring tide, the maximum moveable grain size in the area of the offshore wind farms was estimated to be 4mm by HR Wallingford (2002a). In the same study a net tidal residual sediment flux for sand of $d_{50} = 0.1$mm on the order of 100-10,000 kg/m/tide at Thanet and London Array and an order of magnitude less for Gunfleet Sands is predicted. For $d_{50} = 0.4$mm the tidal sediment flux range is an order of magnitude lower again over all sites. At the sites under investigation the median grain size is overwhelmingly in the fine to medium sand range, thus the former estimate is likely to be closer to reality. The numbers indicate vigorous sediment transport potential at all the sites and the likely predominance of live-bed scour conditions. For gravel, very low flux of 0-10 kg/m/tide is suggested at Thanet which is in agreement with the observation that the gravel bed forms do not show any movement (see Section 4.3.2). The wave conditions are quite benign in respect to the typical water depths encountered, other than on shallow areas of the banks, where wave action can play a greater role in sediment transport processes. If it is assumed that wave-induced oscillatory motions can be transferred to the seabed from a depth shallower than the deep-water wave length, then for average wave conditions, water depths less than 10-15 metres might be influenced by waves. Examining the comprehensive map (Figure 2.3) of meto-cean parameters, the data sources of which have been calibrated against measurements by ABPmer (2008) and validated against synthesized historic data here, illustrates that the gross-scale flow regime over the three wind farms is remarkably similar. The implication for the scour assessment is that the variability in the observed scour between sites will to a lesser degree be a result of differences in flow conditions. A little more detail and some local variations to the described flow patterns will be discussed in Chapters 3 and 4, respectively.

2.1.2 Geology and morphology of the Outer Thames Estuary

2.1.2.1 Stratigraphy of the Outer Thames Estuary

The description of the stratigraphic sequence for the OTE is based on an analysis of collected geotechnical and geophysical field data (as illustrated in Section 2.2.2), data from British Geological Survey mapping, complemented with information compiled in Cameron et al. (1992); Sturt et al. (2009) and Entwisle et al. (2013). The bedrock geology is mapped from BGS 1:250,000 data in Figure 2.6 and the relevant stratigraphic sequence, discussed below, is tabulated in Figure 2.5. Tectonically part of the London-Brabant-Massif, the relevant geological history of this region begins in the Mesozoic era with the precipitation of thick layers of chalk during the Late Cretaceous period onto the Palaeozoic basement. In the OTE the Upper Chalk is some 200m thick (Cameron et al., 1992). Although they underpin the majority of the OTE, it does not represent the solid geology

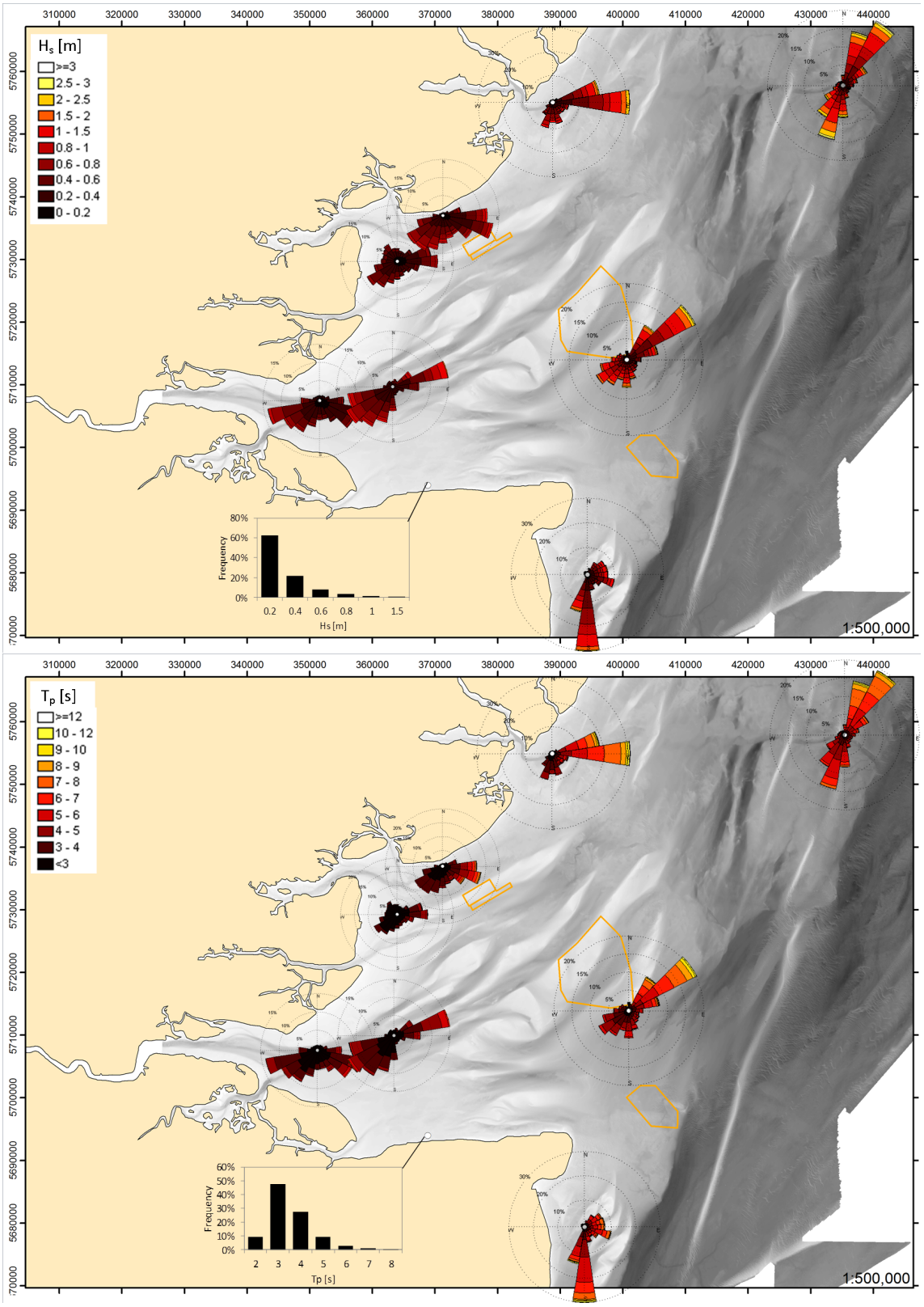

Figure 2.4: Wave direction and significant wave height H_{m0} (top) and peak wave period T_p (bottom) in the Outer Thames Estuary. Data from Cefas Wavenet.

of the seabed, other than in the very south, within the Thanet wind farm area, where the Upper Chalk are only veiled by a thin veneer of gravelly sands (see Fig 2.6). After a depositional hiatus, caused by crustal uplift and marine regression, the early Palaeocene saw the sedimentation of some 10-30m of Thanet Sand Formation on top of the erosional chalk surface. The elevation of the land area created shallow-marine conditions which resulted in a decalcification of sediments and a predominance of siliciclastic deposits laid down during shelf sea-like and coastal conditions. These glauconitic sands represent the first of three cycles of deposition in the Thanetian stage (Cameron et al., 1992). The second cycle produced the highly variable rocks of the Lambeth Group, which consists of the marine Woolwich Formation and the terrestrial Reading Formation. During this cycle more variable and marginal environments of deposition prevailed that have produced a wide variety of mixed and chaotic facies with strongly varying engineering properties. The rest of the solid geology in the OTE is dominated by London Clay, which was deposited during the Lower Eocene some 50 million years ago. Fully marine conditions and warm temperatures prevailed during the Ypresian creating conditions for the accumulation of 100-150m of mud and clay-rich sediments in the Thames Estuary. The genesis, nature and engineering properties of London Clay will be discussed in more detail in Section 3.2.1 while those of Upper Chalk, Thanet Sand Formation and Lambeth group are illustrated in Section 4.2.1.

Era	Period	Epoch	Stage Age	Formation
Cenozoic (65 Ma - present)	Quaternary (2.5 Ma - present)	Holocene (11.7 ka - present)	Holocene	
		Pleistocene (2.5 Ma - 11.7 ka)		
	Neogene (23-2.5 Ma)	Pliocene (5-2.5Ma)	Plio-Pleistocene	Red Crag
			Mid-Pliocene	Coralline Crag
		Miocene (23-5 Ma)		
	Palaeogene (65-23 Ma)	Oligocene (34-23 Ma)		
		Eocene (56-34 Ma)	Ypresian	London Clay
				Harwich Formation
		Palaeocene (65-56 Ma)	Upper Thanetian	Lambeth Group
			Thanetian	Thanet Sand
Mesozoic (251-65 Ma)	Cretaceous (145-65 Ma)	Upper (100-65 Ma)		Upper Chalk
		Lower (145-100 Ma)		

Figure 2.5: Geological stratigraphy of the OTE. Modified from Sturt et al. (2009).

The stratigraphy is truncated at the Eocene. Lying unconformably over the bedrock are Quaternary and recent marine deposits, the presence of which has contributed to the morphological configuration of the estuary as witnessed today. The present-day topography of the OTE is a result of the reforming of the Pleistocene landscape by processes associated with the post-glacial rise and fall in sea-levels (D'Olier, 1972). A network of fossil channel systems can be found at both Thanet and London Array which have been created over the past circa 1 Million years and have been subsequently in-filled and re-worked over multiple transgressive and regressive phases. However, the formation of the sand banks, in their present-day configurations are related to the most recent Holocene transgressive event. The sediments in the OTE consist primarily of sands and gravels with varying degrees of mud. However, over the entire estuary deposits can display significant

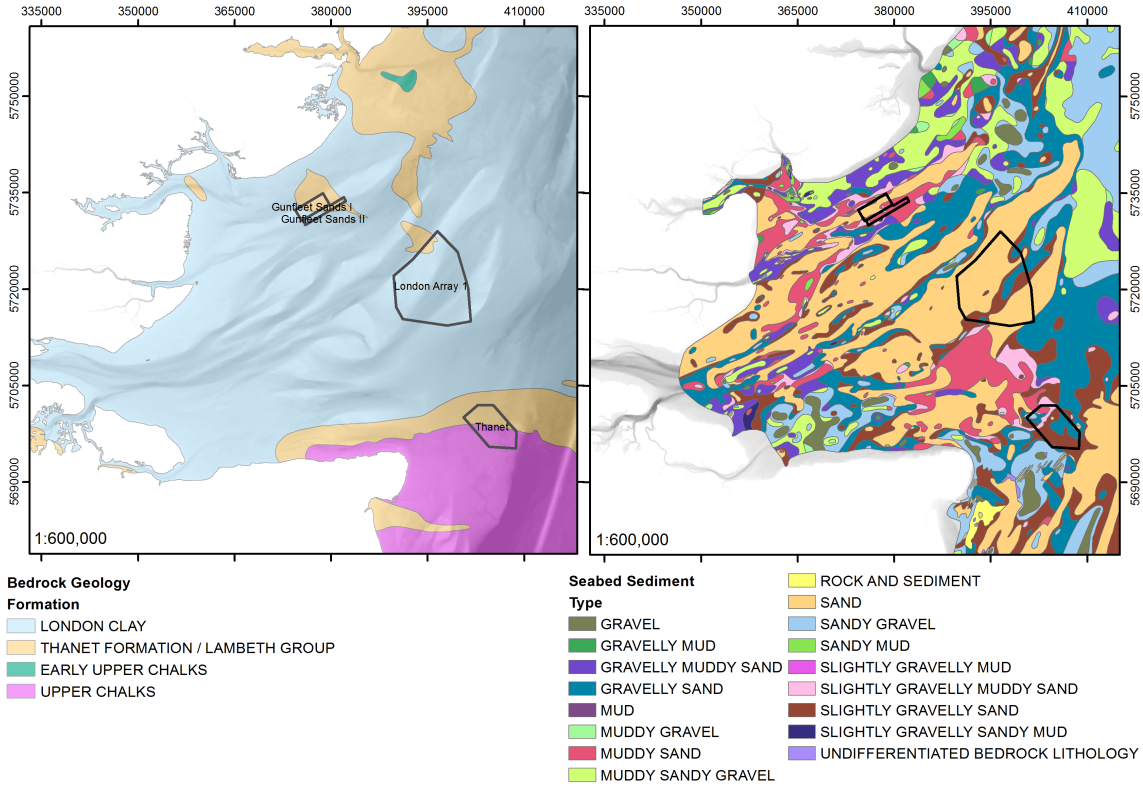

Figure 2.6: Bedrock geology (left) and seabed sediments (right) from 1:250k BGS data.

heterogeneity owing to their lithological and geographical origins; sediment sources include glacially and fluvially-derived sediments, eroded and redistributed around the OTE during the Holocene, material supplied by way of coastal erosion during the transgression and continuing in the present day and to a lesser extent fluvial input of fines through rivers flowing into the OTE as shown in Figure 2.1 (Cameron et al., 1992). Gravels, consisting predominantly of flint, are considered to be largely non-mobile relics of historical glacial, fluvial and coastal erosion processes, while sands are mainly derived from the disintegration of the Norfolk and Suffolk cliffs and are deposited offshore along complex transport pathways (Sturt et al., 2009). A large proportion of the fine sediment fraction is transported into the region from the English Channel, large fluvial inputs are attributed to the Thames, Rhine, Scheldt and Humber, as well as atmospheric dust and coastal erosion (Sturt et al., 2009).

Figure 2.6 (right) demonstrates that a degree of sediment cover exists virtually over the entire OTE. The mobile sediment depth ranges from veneers of tens of centimetres to covers a few metres thick (Cameron et al., 1992; Sturt et al., 2009). In the region shown, sands and gravel/sand mixtures account for over 80% of the sea bed deposits by area. Most of the remaining area is covered with mixed trimodal sandy, gravely and muddy sediments or gravel lag. The proportion of mud tends to increase with proximity to the coastline and the inner estuary (Sturt et al., 2009). The presence of mobile granular sediments facilitates the formation of bed forms. Typical bed features encountered in the OTE are transverse features like megaripples and sand waves and tidally aligned sand banks and ribbons. These features are formed of thick deposits of more homogeneous typically moderately to well sorted fine- to medium sands while coarser sands and gravelly

sands make up the sand ribbons in deeper waters to the east (Cameron et al., 1992). The sand banks are considered to have evolved during the early Holocene transgression with offshore sand banks considered older than the estuarine banks (Cameron et al., 1992). The distribution and size of sand waves varies (Cameron et al., 1992; Sturt et al., 2009); in the deeper waters they are typically found on the crest of sand banks, while within the estuary they are present on the lower flanks of sand banks which is confirmed at London Array, where sand waves are found on the eastern flank of Long Sands. The dimensions range from sub-metre scale to several metres in height with wave lengths of 5 to greater than 100m (Sturt et al., 2009). Megaripples are encountered throughout the OTE either parasitically on lee-slopes of sand waves or as the main bed forms on sand banks or flat areas with sufficient mobile sediment supply. More detail on the bed form composition for each site will be given in the individual wind farm chapters based on the recent time lapse swath bathymetry.

2.1.2.2 Morphological evolution of the Outer Thames Estuary

The significance of the historical perspective is to understand the natural trends of large-scale medium- to long-term seabed developments that might affect the wind farms throughout their design life. Morphologically, the OTE is characterised by tidally-aligned ridge and channel topography (see Fig 2.1). Sand bank dimensions are typically 1-5km across and 5-30km long with inter-bank channels some 1-5km wide. The depth difference between ridge and channel is usually quite pronounced on the order of 15-20m. Some high areas of the sandbanks can experience drying at low tide. Seaward of the -20mCD contour, the OTE is bordered by a deeper plateau exhibiting a generally flatter topography with a small number of isolated but well-defined elongated sand ridges, e.g. Inner and Greater Gabbard and The Galloper banks. Within the OTE the sandbanks and channels are orientated along the predominant tidal flow axis of north-east/south-west. It has been posited that the network of channels witnessed in the Outer Thames are indicative of mutually evasive tidal flow routes (Harris, 1988). While most of the channels are attributed to the incoming south-westerly flood tide, the inner estuary deeps (The Warp and Oaze Deep) are dominated by the north-east flowing ebb. Furthermore, sand wave asymmetry suggests that the flood tide exercises control on the seaward southern side of the sand waves while the outgoing tide dominates on the northern flanks (Kenyon and Cooper, 2005). The orientation and asymmetry of seabed features are evidence of a net sediment transport pathway towards the south-south-west as suggested by Stride (1963). These patterns of tidal flow within the OTE have remained largely similar over the period of 180 years examined in Burningham and French (2011). Similarly, the general morphological make up of the estuary as outlined above has not changed much over the last 100-200 years (Burningham and French, 2011). That said, bank-scale processes are causing some variability in the position and shape of the sand banks and thus, locally, significant bed level changes can be observed, most prolifically in the central estuary at Long Sands, Kentish Knock and Sunk Sand. These developments are typically driven by erosion and progradation of bank margins, the redistribution of sediment and associated with that, on a longer time scale, the offshore or onshore migration or change in plan form of individual

banks. Notwithstanding changes in shape, the crest heights of the banks have been shown, based on transects in Burningham and French (2011), to have remained within ±2-3 metres of the present day, except at Shingles Patch and the area between Buxey Sand and East Barrow which have exhibited considerable lateral and vertical variations over the last 200 years, owed to the growth, evolution and decline of small cross-bank channels (swatch-ways) in these areas. Most major banks are considered to have reached their vertical potential and any significant growth will only occur laterally (Harris, 1988). Harris (1988) has suggested the morphology of the OTE is characteristic of a mature estuary in the final stage of infilling with sediments from the North Sea. Hence modern-day and future sediment deposition is controlled by the balance of available sediment supply, creation of further accommodation space due to sea-level rise and redistribution of sediments within the estuary system (Harris, 1988; Burningham and French, 2011). In fact sediment redistribution is considerable in this area based on the modelled residual sediment fluxes discussed previously in Section 2.1.1. This study is concerned specifically with London Array, Thanet and Gunfleet Sands wind farms; more details relating to morphological trends relevant to the scour development at these sites will be discussed in chapters 3 and 4, respectively, drawing on more recently collected data. From the above discussion, it is clear that London Array has been constructed on what is a relatively active area within the OTE and the main issue has been the migratory potential of Long Sands and southern Kentish Knock. Gunfleet Sands is considered largely stable. No specific historic information is available at the location of Thanet wind farm in the literature. In chapter 4 it will be demonstrated that over the past 10 years very little sea bed elevation change has been witnessed other than associated with transient sediment supply from offshore by means of sand wave migration. The range of natural morphological change has positive implications for the scour analysis in this outdoor laboratory, as it allows the effect of large-scale morphological changes and smaller-scale variability, related to sediment availability and mobility, to be assessed.

2.2 Data analysis

One of the complexities of this study is the handling, visualisation and manipulation of large amounts of different types of data. To conduct a meaningful scour assessment, the available data which includes qualitative, quantitative, discrete, continuous, image and spatial data in four dimensions, must be synthesized in a way that facilitates analysis and interpretation by the user. The bulk of the data are acquired for pre-installation consents and engineering design purposes and is so far not commonly used for scour assessment. Additionally, classic post-installation scour monitoring by means of swath bathymetry is available. The types of data used and appropriate means and methods for the visualisation and manipulation of it will be discussed below.

The data pertaining to London Array offshore wind farm are owned by and provided by London Array Ltd. For Thanet wind farm the ownership lies with Vattenfall and the data were provided via Royal Haskoning. Both data sets were acquired under agreements that grant confidentiality to the wind farm owner. A considerable amount of data for

Gunfleet Sands is available in the public domain from the Crown Estate; further data were provided by Dong Energy.

2.2.1 Bathymetric data

Hydrographic sounding data form one of the important datasets. It provides records of sea bed levels before and after monopile installation, thus the quantification of scour is based solely on these data. The bathymetric surveys were provided either as ascii xyz files or ESRI grid rasters and are in mLAT unless otherwise stated. The manipulation of three-dimensional spatial data and the scour analysis was primarily carried out in a GIS. The surveys used in this study were recorded in a range of resolutions as listed in Table 2.1. From the survey reports, the horizontal and vertical precision for individual bathymetric surveys is given as ±0.1m and ±0.2m respectively. To corroborate the consistency between surveys the sounded depths from every survey at a minimum of 5 stable reference locations are compared. Where possible bed rock locations were used; in the absence of immovable substrates, areas that show very little bed level change on subsequent surveys are used. The vertical precision for London Array was determined to be ±0.12m which lies within the stated survey precision. The vertical precision at Thanet between 2007 and 2012 surveys is ±0.05m. These data sets had to be subsampled to be used with coarse-resolution 2005 survey. For Gunfleet Sands the precision was found to be ±0.13m. These values give an idea of the precision in the scour measurements.

Ideally, the resolution should be appropriate for the relative size of features to be captured. At Thanet for example, scour holes are typically shallow and confined and the hydrographic survey at 1m resolution removes too much detail, hampers the accurate delineation of the scour pit (as will be shown later) and also negatively affects any bathymetry-derived measurements, eg. slope angle. Conversely, high-resolution surveys capture substantial amounts of detail, which facilitates accurate scour analysis, but also tend to contain more artefacts. These surveys typically require more pre-processing to remove unwanted detail, such as reflections from free-spanning cables, J-tubes and the monopile. When comparing two surveys of different resolution, it is advised to re-sample the higher-resolution survey to match the other.

Table 2.1: Type, year and resolution of bathymetric surveys used in this study.

Site	Type	Date	Resolution [m]
Thanet	pre	2005	25
	pre	2007	1
	post	2012	1
London Array	pre	2007	1
	pre	2010	0.5
	post	2012	0.25
	post	2013	0.25
Gunfleet Sands	pre	2005	5
	post	2011	0.5

2.2.2 Sub-surface data

The access to sub-surface data is essential for the aim of this study. A good understanding of the vertical geotechnical profile at foundation locations enables an investigation into how scour responds to physical variabilities in the seabed soil. Three sources of subsurface data were available to this study: borehole logs, cone penetration tests (CPTs) and seismic reflection data. Information from various geotechnical lab tests (e.g. particle size distributions and shear strength tests) undertaken on borehole samples are also available; the coverage and type of investigations is not uniform, between surveys and locations. Often it is helpful to aggregate the sub-surface data to enable concurrent visualisation and interpretation of the qualitative visual descriptions (boreholes), pressure measurements (CPTs) and acoustic reflection data (seismic profiles). Each of these data can provide different insights into the character of the seabed. Schlumberger Petrel v2011.2 is a software package designed for petroleum exploration and production and provides tools for working with sub-surface data. This programme was used to create a three-dimensional ground model of the offshore wind farm areas, which synthesized bathymetric, geotechnical and seismic data into a single interpretative model.

Seismic data Where necessary, the seismic data were pre-processed in Coda GeoSurvey to apply horizontal location corrections or convert the file format. The vertical dimension in the seismic data is typically recorded in milliseconds of two-way-time TWT, the time for the acoustic signal to travel from source to reflector and back. The geotechnical data is recorded in metres. In order to reconcile the two measurements, a velocity model is applied to convert two-way-time into vertical depth. The depth conversion follows is calculated as $z = (ct)/2$ where z is the depth in metres, c is the speed of sound in the respective medium and t is the two-way time. Since there is no detailed information on the down-hole acoustic velocities, a basic two-layer velocity model was employed. In this model, two constant velocities are applied, one for speed of sound in water, one for the speed of sound in the seabed. For sea water with salinity of 30 ppt and temperature of 12°C, the speed of sound is given as 1490ms^{-1} (Mackenzie, 1981; Coppens, 1981). The propagation speed of a sound wave in a seabed soil is typically in a range of 1480-1780ms^{-1} (Richardson and Briggs, 1993; Robb, 2004) but can vary with the geotechnical property of the soil. Estimates of c_s can be derived from empirical relationships that relate substrate properties to velocity, such as those give by Richardson and Briggs (1993). Equation 2.1 relates velocity to the median grain size of the material given in dimensionless ϕ units and 2.2 offers a relationship for bulk density.

$$c_s = c_w \left(1.18 - 0.034 d_\phi + 0.0013 d_\phi^2\right); R^2 = 0.82 \tag{2.1}$$

$$c_s = c_w \left(1.623 - 0.936 \rho + 0.3417 \rho^2\right); R^2 = 0.944 \tag{2.2}$$

where c_w is the acoustic velocity in water and R^2 is the correlation coefficient. The relationships are plotted in Figure 2.7 for the respective validity ranges of the equations.

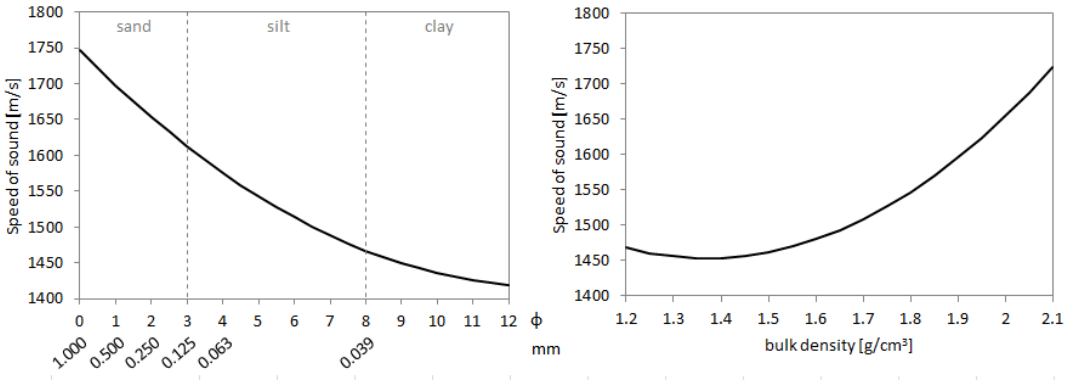

Figure 2.7: Relationships between speed of sound and particle size (left, Eq. 2.1) and bulk density (right, Eq. 2.2).

From the laboratory analysis of the sediments present at the study sites the typical soil characteristics were determined as bulk densities of 1.8-1.95g/cm^3 for London Clay, 1.9-2.0g/cm^3 for Chalks and between 1.7-2.2g/cm^3 for the mixed sandy deposits. Median grain size of the sandy deposits is overwhelmingly in the fine and very fine sand fraction (0.063mm$< d_{50} <$ 0.250mm). Using the equations above and the values for bulk density and grain size, Table 2.2 shows values for c_s. Quite a large range of values are observed.

Table 2.2: Calculated speed of sound in sediment for typical bulk densities (left) and grain sizes (right).

ρ [g/cm^3]	c_s [ms^{-1}]	$d_{50,mm}$	$d_{50,\phi}$	c_s [ms^{-1}]
1.7	1509	0.002	9	1450
1.8	1547	0.063	4	1576
1.9	1596	0.125	3	1613
2.0	1654	0.250	2	1653
2.1	1723	0.500	1	1698

A sensitivity analysis was undertaken to understand the effect of c_s choice on resulting vertical depth. A range of sediment sound velocities were tested and borehole data was used to calibrate the seismic data with the soil profile. This was done at multiple locations throughout the study site to ensure an appropriate c_s value was found. Figure 2.8 shows an example outcome for three different velocities 1550, 1625 and 1700ms^{-1}. Three strong reflectors have been highlighted to illustrate the effect of varying c_s. In all seismic sections, the sea bed is located at -22mLAT as the same c_w was used in all depth conversions. As can be appreciated, the impact of sediment sound speed increases with longer travel times, ie. the variance in depth z resulting from different c_s is small near the sea bed surface and increases with depth. The figures are annotated with depths of the illustrated strata boundaries; for a deviation in $\Delta c_s = \pm 75$ms^{-1}, Δz for the three boundaries is $\pm$0.2m, $\pm$0.3m and $\pm$1.0m, respectively from shallow to deep. This means, that in the zone of interest for scour applications (top 10m of the soil profile) the depth conversion is less sensitive to c_s and introduced errors should be acknowledged but can be tolerated in the context of other sources of uncertainty such as the horizontal distance between core or CPT location and seismic profile and user interpretation of boundaries and their depths on the borehole core, thus justifying an approach based on average substrate properties. A good fit between boreholes, CPTs and seismics throughout the study sites was generally found with $c_s = 1625$ms^{-1}.

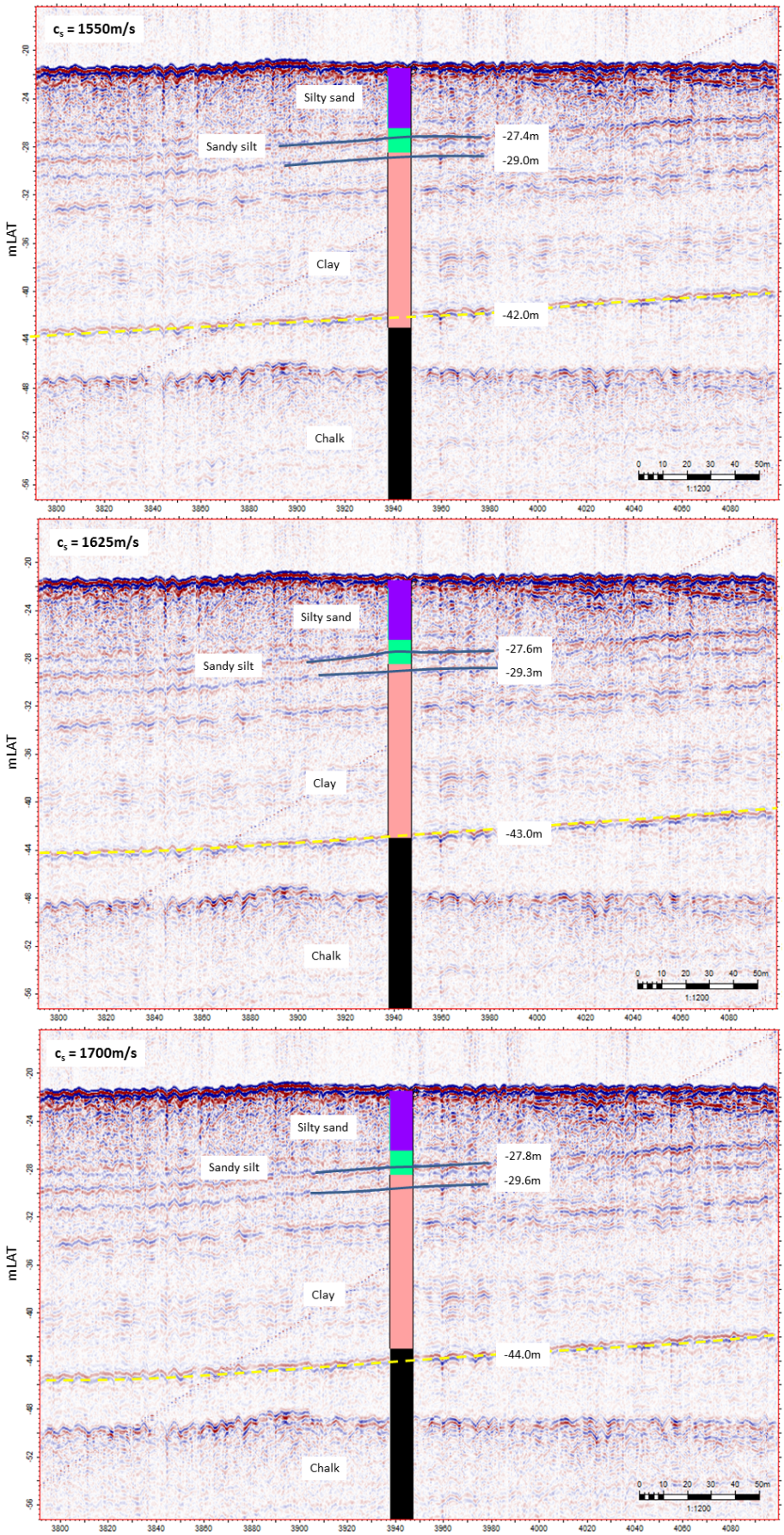

Figure 2.8: Seismic depth conversion from two-way time to depth with two-layer velocity model. c_s = 1550ms^{-1} (top), c_s = 1625ms^{-1} (mid), c_s = 1700ms^{-1} (top). Borehole record for validation.

Geotechnical data The core logs and CPTs were supplied as pdf records and ascii files, respectively. The core data provide a record of the lithological facies with depth and is typically derived from rotary borehole explorations around the site. The core information is imported into the ground model as discrete category data, describing the type of sediment encountered at depth. The CPT data, which contain pressure measurements at various locations of the cone, was reformatted and missing parameters were calculated where necessary for import into the model. Due to the temporal discrepancies between the recording of various data, minor vertical positional adjustments had to be carried out.

2.2.3 Interpreting geotechnical data

Borehole logs provide visual descriptions of the full sediment stratigraphy. It should be noted that a degree of subjectivity is inherent in the interpretation of a core by the field geotechnical engineer. In addition, samples are taken from the cores at various depths and subject to lab tests to determine engineering characteristics such as index properties (liquid index LI, plasticity index PI), densities (dry, wet and bulk), shear strength tests and particle size distributions. This information is added to the borehole log. Since boreholes are more costly and time-consuming than CPTs, the data sets usually contain a limited number of cores and CPT records are much more prolific (see Table 2.3). Boreholes are used to understand and calibrate the CPT records, which can then be used to fill data gaps between core locations.

Table 2.3: Inventory of boreholes and CPT investigations at the wind farms.

	BH	CPT
London Array	25	192
Thanet	46	123
Gunfleet Sands	15	30

Numbers include duplicates.

In this study, the CPTs primary purpose was for geo-stratigraphic interpretation. Although not always straight-forward to interpret, cone penetration tests offer more objective measures of vertical soil profile than boreholes as they provide a continuous vertical record with significantly more detail than simple visual assessment with user bias. Typically, three main parameters are measured during the procedure (Fugro Engineering Services, 2004): cone resistance q_c, sleeve friction f_s and pore pressure u_2. Cone resistance provides a measurement of pressure required to drive the cone through a certain soil and is hence a proxy for the strength and stiffness of the material encountered. The "stickiness" of a soil is quantified by the sleeve friction and pore pressure provides an assessment of how fast soil water dissipates through the surrounding sediment, ie. gives an indication of the permeability characteristics of the soil which in turn are a function of grain size distribution and sediment matrix properties. Pore pressure measurements can be taken at various locations around the penetration cone; the index in u_2 indicates that the data provided for this study have originated from pore pressure measurement just behind the cone shoulder. Further parameters can be derived mathematically from the measurements; table 2.4 presents equations for the most common derived factors.

For granular materials, the parameters of q_c, D_r, ϕ' and the blow count for the standard

Table 2.4: Derived CPT parameters after Robertson and Cabal (2010).

Parameter	Equation	Comments
Total cone resistance q_t	$q_t = q_c + u_2(1-a)$	Cone resistance corrected for pore water effects, a is a constant based on cone geometry
Net cone resistance q_{net}	$q_{net} = q_t - \sigma_{vo}$	σ_{vo} is the vertical overburden stress
Friction ratio R_f	$R_f = f_s/q_t$	Ratio of sleeve friction to cone resistance. Typically given as %.
Pore pressure ratio B_q	$B_q = \Delta u/q_{net}$	Excess pore pressure $\Delta u = u_2 - u_0$, where u_2 is the measured and u_0 si the in-situ equilibrium pore pressure.
Undrained shear strength c_u	$c_u = (q_t - \sigma_{vo})/N_k$	N_k is an empirical cone factor, typically between 15-20 Lunne et al. (1997). Used for strength of cohesive materials.
Peak secant friction angle ϕ'	$\tan\phi' = \frac{1}{2.68}\left[\log\left(\frac{q_c}{\sigma'_{vo}}\right) + 0.29\right]$	σ'_{vo} is effective vertical overburden stress. Used for shear strength of cohesionless granular soils. Other formulae available.
Relative density D_r	$D_r = \frac{1}{C_2}\ln\left(\frac{q_c}{C_o(\sigma')^{C_1}}\right)$	C_o, C_1 and C_2 are soil constants, σ' is effective stress. Used for granular deposits. Other formulae available.

penetration test (SPT) can be related to the compaction state of the substrate as shown in Table 2.5. Generally speaking the erosion resistance of a granular soil will be enhanced with increased compaction, thus the listed geotechnical parameters can be used as proxies. The strength and consistency of cohesive soils can be judged from the undrained shear strength c_u according to Table 2.6.

Table 2.5: Relationship between q_c, D_r and ϕ'. From Fugro Engineering Services (2004).

Compaction	q_c [MPa]	SPT (N)	D_r [%]	ϕ' [°]
very loose	< 2	< 4	< 20	< 30
loose	2-4	4-10	20-40	30-35
medium dense	4-12	10-30	40-60	35-40
dense	12-20	30-50	60-80	40-45
very dense	> 20	> 50	80-100	> 45

Table 2.6: Consistency and strength of material based on undrained shear strength. From British Standard (2010).

Consistency	Strength	c_u [kPa]
very soft	extremely low	< 10
	very low	$10 - 20$
soft	low	$20 - 40$
firm	medium	$40 - 75$
stiff	high	$75 - 150$
very stiff	very high	$150 - 300$
hard	extremely high	$300 - 600$

The CPT data can also be used to determine the soil behaviour type. Robertson et al. (1986) developed soil behaviour classifications based on the ratio of B_q or R_f with cone resistance q_t and charts can used to derive the soil type (see Fig 2.9). Another classification system was developed by Schmertmann (1978) and modified by Tumay (1985) which is shown in Figure 2.10. Both methods have been implemented in software by Abu-Farsakh et al. (2008) allowing continuous soil type profiles to be generated fairly rapidly.

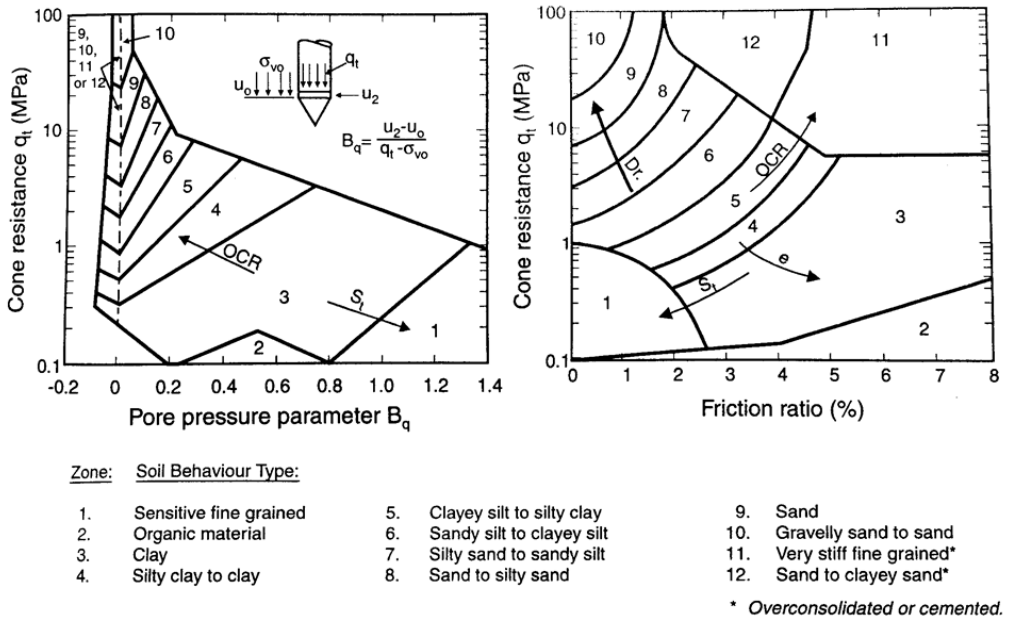

Figure 2.9: Soil behaviour classification chart based on pore pressure ratio B_q and net cone resistance q_t. After Robertson et al. (1986).

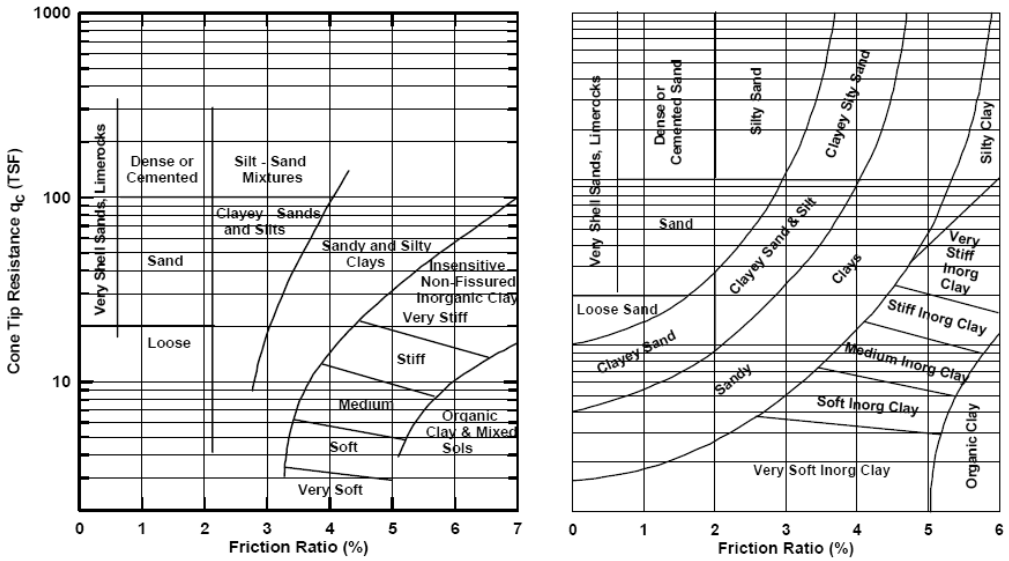

Figure 2.10: Original Schmertmann (1978) soil behaviour chart (left) and modified version by Tumay (1985).

To maximise the scope of interpretation, the data sets are best visualised in parallel in Petrel. Thus, the seismic data can be cross-correlated with borehole information, CPT raw and derived parameters and soil behaviour types. Due to limitations in visualisation options in the software it is not possible to plot all data sources in parallel without overloading the user and obscuring data; however Figures 2.11 and 2.12 are examples of how different types of data can be visualised side-by-side. The software allows the user to explore data in 3D thus the scoured bathymetry can be related to the geotechnical record and the seismic reflection data as shown in Figure 2.13.

2.2.4 Assessing natural bed mobility

Understanding the natural dynamics of the sea bed is important in scour assessment since it can influence the process, nature and dimensions of scour (Whitehouse et al., 2010). Scour can occur in both mobile and non-mobile pre-installation bed conditions. Where the ambient bed, under average flow conditions, is not mobile, clear-water scour can still develop once the monopile is installed due to the shear stress amplification at the structure. In this case sediment transport is only observed in the locality of the structure while the ambient bed remains stable. In live-bed conditions, the critical shear stress for initiation of motion is exceeded under natural conditions and the bed is naturally mobile. The scour becomes a function of local erosion and material arriving at the site from upstream which can cause back- or infilling of the scour hole. One way to inform on the scour regime (clear-water or live-bed scour) at the study site is to examine the bathymetric surveys for evidence of mobile bed features and, if present, rates of migration. Large-scale bed level dynamics can also influence the development and time-evolution of scour holes. The investigations below will illustrate how a comprehensive awareness of bed dynamics can be achieved.

2.2.4.1 Visual assessment

Smaller-scale bed changes In the first instance, the nature of the sea bed as recorded during individual surveys is appraised visually, identifying either presence or absence of bed features and their dimension (wave height H and length λ, crest orientation and asymmetry) and travel direction can be inferred from simple measurements of object geometry (eg. Van Landeghem et al., 2012). This exercise fosters familiarisation with the morphological make-up, large and small, of the seabed, type and size of features present and areas of the site are likely to experience natural bed level variations. Where individual feature crests are distinguishable and trackable over subsequent surveys, the migration rates of individual crests and changes in crest orientation can be established as shown in Figure 2.14. The figure also shows the visual assessment and measurement of feature height and wave length along a representative cross-section.

Large-scale bed changes While the previous paragraph deals with movement of features on the ripple to small sand wave scale, large morphological changes can be associated with active sand banks or large, widely-spaced sand waves. The behaviour of these mor-

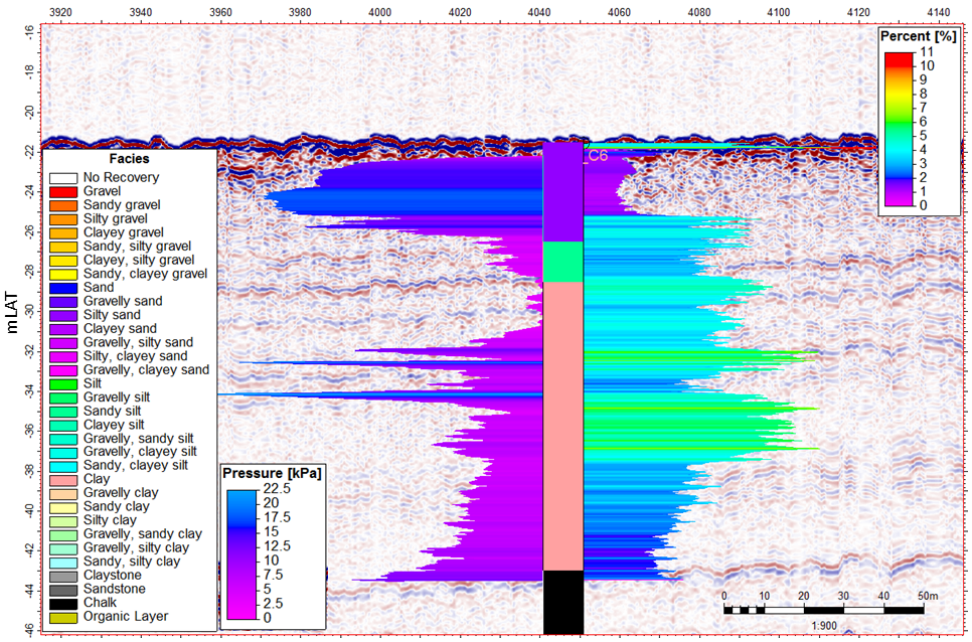

Figure 2.11: Seismic profile, borehole record, cone resistance and friction ratio.

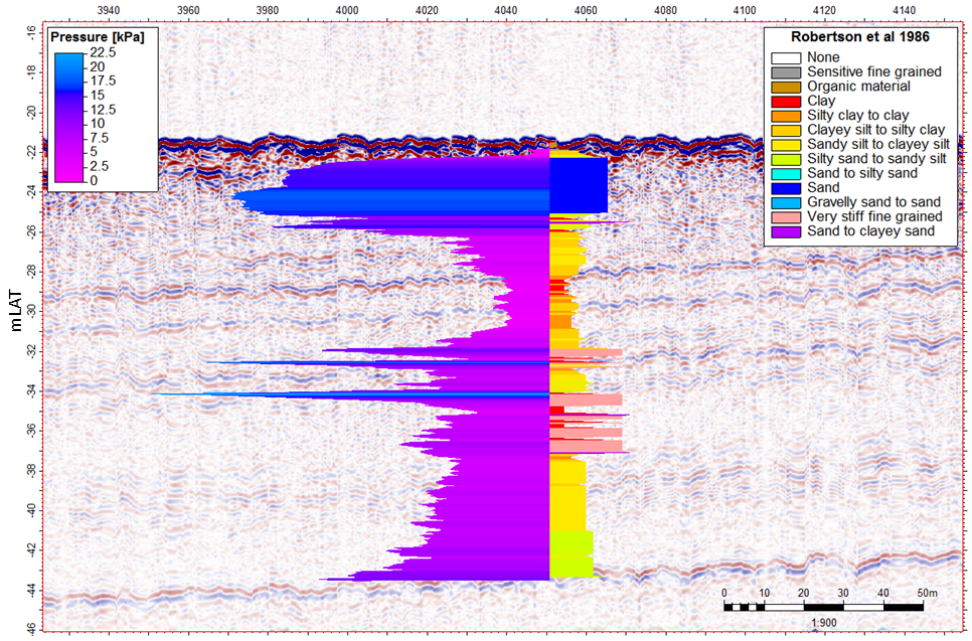

Figure 2.12: Seismic profile, cone resistance and soil behaviour type after Robertson et al. (1986).

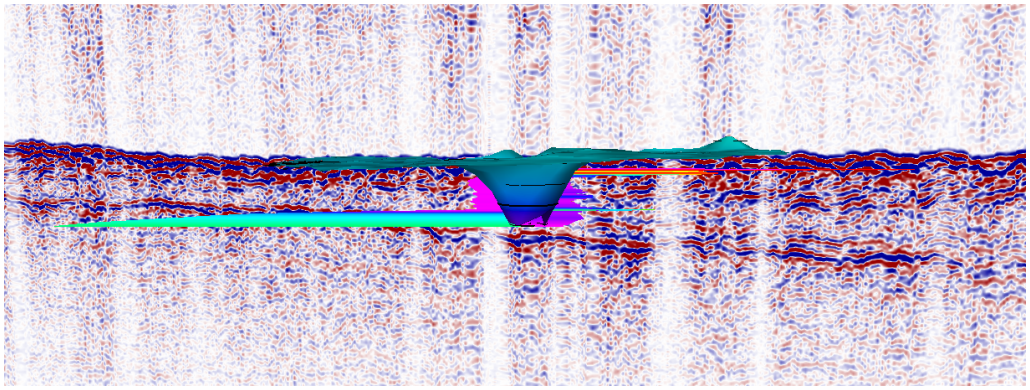

Figure 2.13: Seismic profile, 3D bathymetry and CPT records (cone resistance and friction ratio).

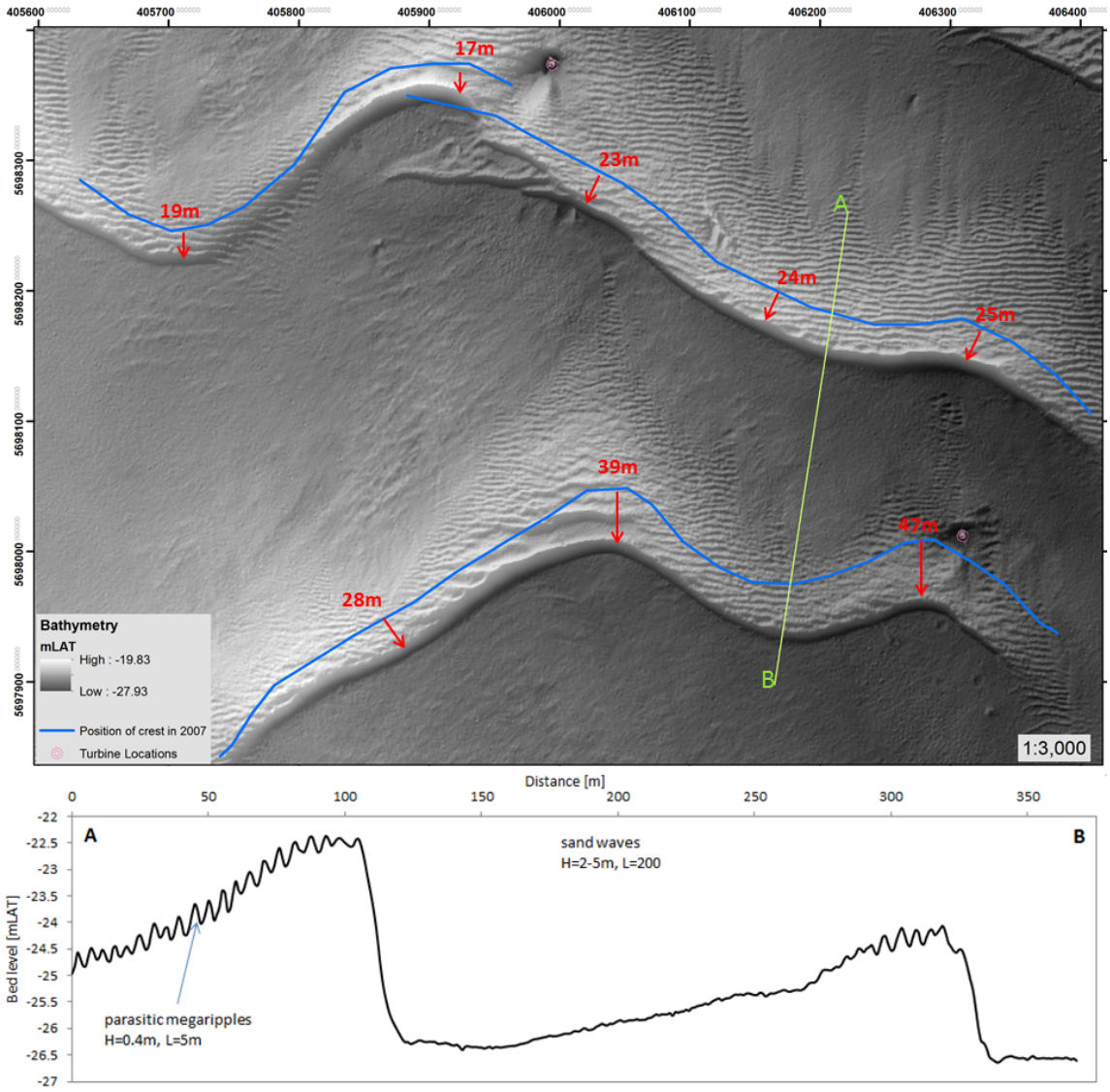

Figure 2.14: Sand wave crest movement between repeat surveys (2007 and 2012) and characterisation of bed forms in cross-section.

phologies are best captured on difference plots between subsequent hydrographic surveys. Figure 2.15 demonstrates the use of difference plots to highlight dynamic areas. In the plots, any vertical bed movement within ±0.5m is transparent, thus highlighting areas of greater change. In Figure 2.15 (top) the south-ward movement of features in a sand wave field is clearly discernible; bank-scale morphological change is shown in Figure 2.15 (bottom) where the red area indicates progradation of a large area of the sand bank over a period of time. This plot also reveals the migration of bed features in the megaripple to sand wave size. Difference plots allow the area and volume of change to be appreciated indicating the scale of mobility. Both large-scale and smaller scale bed level changes can have an impact on scour and thus the natural bed dynamics need to be understood.

2.2.4.2 Quantitative bed form analysis

Once areas of bed forms have been visually identified on the pre-installation surveys an automated method to determine quantitative measures for size and shape of the bed forms developed by Cazenave et al. (2013) was employed. This analytical method applies a fast fourier transform to the bed level data with the aim of extracting recurring patterns. The accuracy of the algorithm is understood to depend on the dimensional homogeneity of the bed forms in a chosen data segment and the appropriate dimensioning of the segment in respect to the features to be captured. The more uniform the bed forms in the segment, the better the outcome. Further, the segment needs to include a sufficient number of feature crests and troughs for the pattern to be accurately quantified by the algorithm. The analysis was undertaken on rectangular raster segments of the area around or near a turbine; typical areal dimensions of the supplied rectangle were between $2500m^2$ ($50m \times 50m$) and $22500m^2$ ($150m \times 150m$) depending on the dimension of bed features to be assessed and, in places, the extent of survey available. The algorithm returns statistics on crest orientation, wave length, height and feature asymmetry, from which migration and sediment transport direction can be inferred; the accuracy of the outcome generally also decreases in that order, thus the results were checked against a visual assessment to ensure consistency. For a full description of the algorithm the reader is referred to Cazenave et al. (2013).

2.3 Defining the zone of scour

Initially, it was attempted to define the scour hole outline from contoured difference plots of pre- and post-install surveys where the zero-metre contour indicates the "no change" iso-line. However, it was found that this method is not universally applicable as it showed deficiencies in conditions where significant changes in bed elevation and bed morphology occurred in the time-span between surveys but also where little change happened. Consequently, a method is required that does not rely on level difference plots or cut-fill techniques, but one that allows the definition of scour extents from the post-installation survey alone. Developing such a method brings up the question of how the extent of a scour hole is defined and what objective criteria can be used to delimit its boundary. To the authors knowledge no such definition currently exists, in part because the area of a

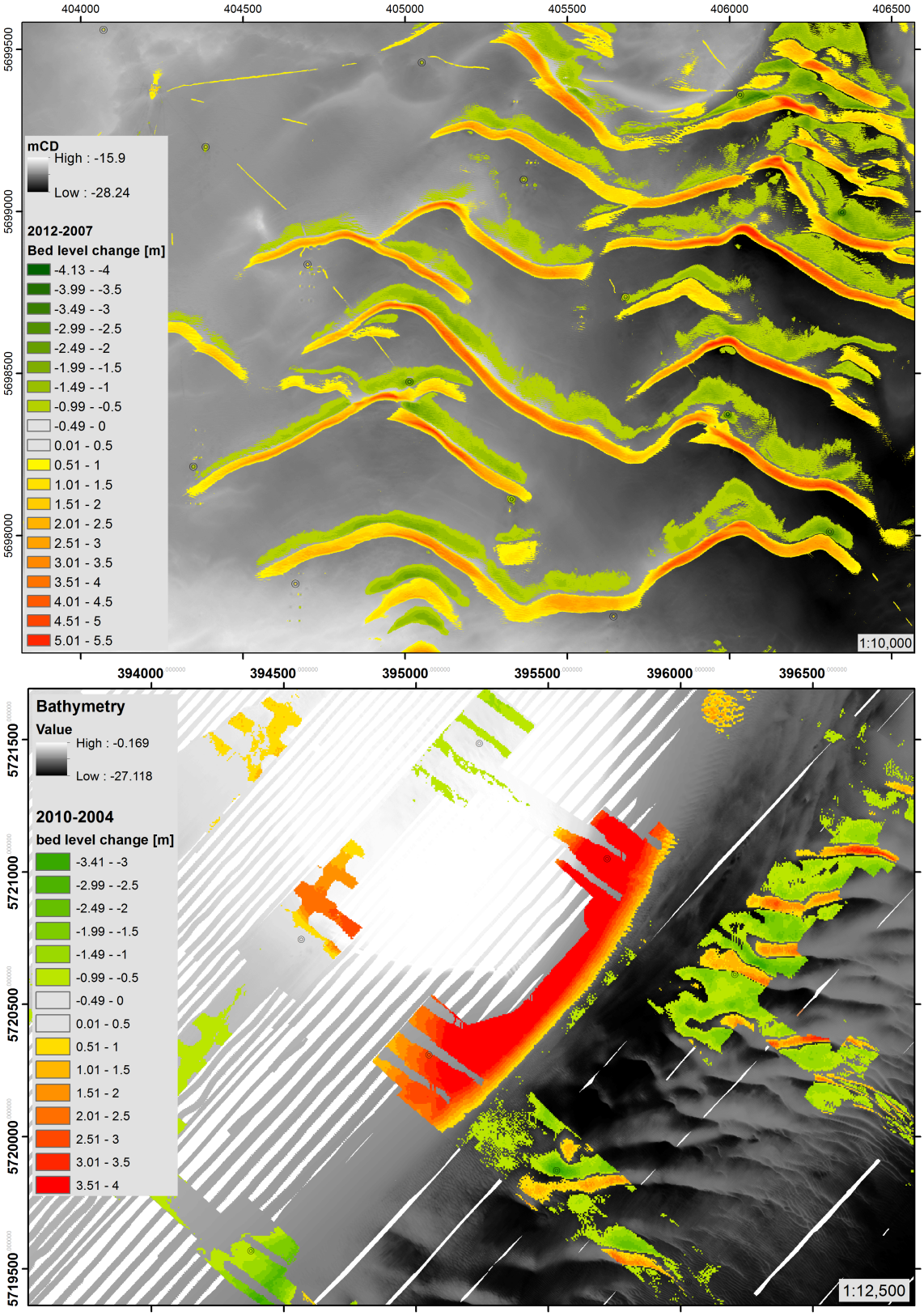

Figure 2.15: Difference plot showing migration of large-scale bed features (top) and progradation of sand bank and migration of megaripples (bottom).

scour hole has hitherto not commonly been under investigation.

For pragmatic reasons and to ensure the scour analysis is consistent over the wind farm datasets, considerable effort was directed to develop an automated method of defining scour extents by manipulating the post-installation survey data using GIS-enabled image analysis and visualisation techniques. Auto-recognition of features has been the subject of investigation in both astronomy, for the definition of impact craters (Barata et al., 2004), and archaeology, for the identification of archeological features from remotely sensed data such as satellite images and LiDAR measurements (e.g. Devereux et al., 2008; Challis et al., 2011). The techniques suggested in these papers encompass various image analysis methods which were evaluated in respect to their suitability to the scour zone identification problem. Amongst the methods investigated are an advanced multi-directional solar illumination technique developed in Kokalj et al. (2011) and Zakšek et al. (2011) and a local relief model after Hesse (2010). In addition, other topographical criteria (e.g. slope angle, curvature) and multi-criteria overlays were examined to determine whether purely morphological characteristics of the scour hole could be used to determine its boundaries. An added complexity in scour analysis is that not only must features be clearly identified, but ideally an automatic, objective delineation of scour holes (e.g. as a specific outline contour) is also possible. The scour hole statistics, such as scour maximum depth, area, volume and shape, are calculated on the basis of the defined boundary. In the following section a number of tested visualisation techniques will be described, illustrated and assessed. Essentially, there are two steps to the automatic scour recognition; the first is visualisation, the second is definition. The first step is to facilitate the identification of the feature by a user or algorithm. In the second step the outline of the scour hole is defined as a line or polygon feature, ideally automatically and unsupervised. Techniques will be demonstrated on a monopile scour pattern with extended down-stream wake feature. The data resolution is 0.5m which provides significant detail to test the methods.

2.3.1 Ramps

Continuous data in raster images can be mapped with both greyscale and coloured ramps. Features can be accentuated by modifying the stretch applied to the data based on various statistical measures, thus allowing larger contrast and feature detail to be uncovered (Challis et al., 2011). Initially, the test bathymetry (Fig 2.16, A) was enhanced by manipulating the colours in the image using a histogram equalization technique. The stretching of the histogram serves to enhance contrast and highlights both dark and light areas (Fig 2.16, B). Consequently, the definition of both the scour hole and the wake deposition zone is improved over the standard bathymetry plot. Sediment accumulation upstream of the turbine is also identified. The redistribution of the histogram over all possible pixel intensities causes a noisier and darker image however the interpretation is not hampered by this, if the feature outline is the subject of examination. This method is judged as an improvement over the standard bathymetry plot (Fig 2.16, A) as the scour hole is more strongly contrasted from the ambient area, particularly in the wake area. Non-linear colour ramps should be avoided as they can lead to mis-interpretation by suggesting topographic breaks where none exist or by over-exaggerating them (Fig 2.16, C and D). Manipulating the

colour ramps does not transform the data stored in the raster, ie. it still consists of bed level readings. Bed elevation is not a suitable metric to define a scour hole, unless ambient bed is flat, since the scour hole edge will not follow a single bathymetric contour, hence colour ramp manipulation is only suitable to facilitate user identification of features.

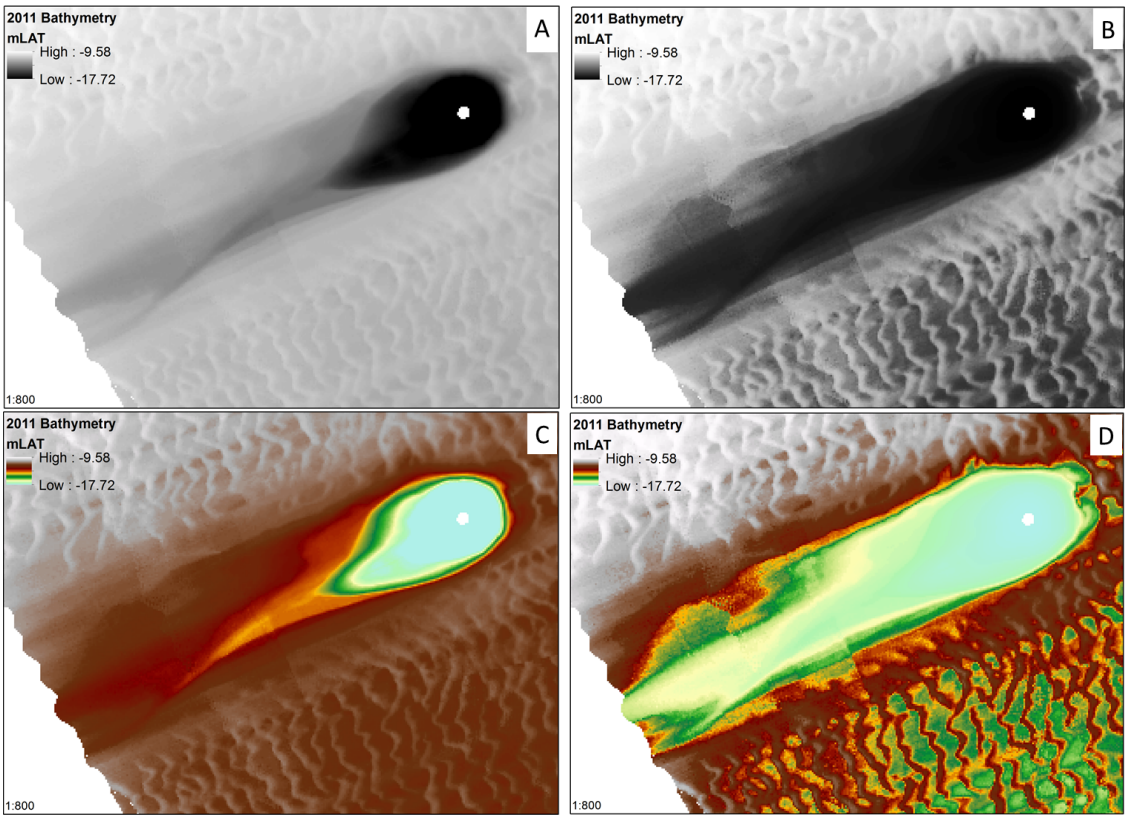

Figure 2.16: Image manipulation using histogram stretch techniques and colour ramps. Greyscale, standard deviation (A) and histogram equalisation stretch (B). Non-linear colour ramp, standard deviation (C) and histogram equalisation stretch (D).

2.3.2 Slope

The slope of a terrain is calculated as a first-order derivative of the bathymetry in a moving window. The results shown in Figure 2.17 (left) suggest that the slope is a good visualisation of prominent features such as the main scour hole, characterised by abrupt changes in slope. Edge features in the wake are also clearly identifiable. An attempt was made to define the scour hole using contours of slope angles as determining factors. It was found that slope angles between 4°-6° (see Figure 2.17, right) showed the "best" agreement with the scour hole extent. The 5° contour described most accurately the main scour hole, while 4° includes some of the ambient bed upstream and 6° omits parts of the downstream scour hole. No slope value captures both local and wake scour and furthermore there is no theoretical basis as to which contour should be appropriate. The method suffers inaccuracies especially where bed forms are present near the scour footprint and in the wake where features are subtle and consequently the breaks in slope are less pronounced and smaller than those around the main pit, thus a single slope contour is unlikely to capture all scour features.

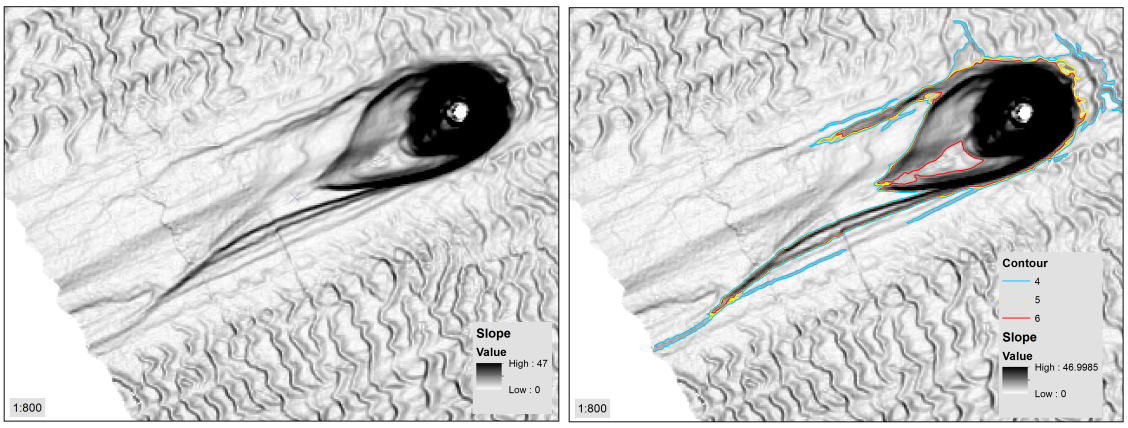

Figure 2.17: Visualisation of scour hole using slope values (left) and slope contours (right).

2.3.3 Hillshade

Hillshade plots are generated by illumination of the elevation model from a certain angle and azimuth and they can be very useful in visualising relief details. The hillshade plot in Figure 2.18 (left) has been illuminated from right angles to the long axis thus the effect is strong and successfully reveals the details of the main scour around the foundation. Improved detail, especially of edge features, in the wake over simple bathymetric plot is observed. As will be demonstrated below (Fig 2.20) hillshades can be used in combination with other visualisations in overlay images to offer improved feature identification. Unfortunately hillshades are unsuitable for contouring of the scour pit since the raster values are representative of illumination strength and features can be delineated as shadows or prominent irradiated features so no single contour can be created. Challis et al. (2011) explain that hillshades suffer from the drawback that features parallel to the illumination direction are not exposed or even hidden (see Figure 2.18, right). Inclination and azimuth of the light source can be varied to illuminate features from different angles however multiple images are not conducive to effective and efficient interpretation, especially for large datasets as encountered in this study.

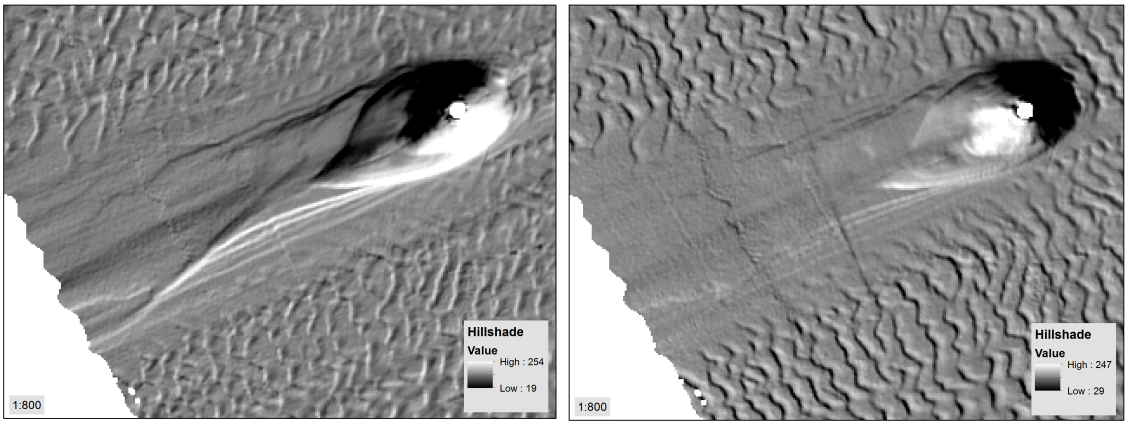

Figure 2.18: Visualisation of scour hole as a hillshade, illuminated from 315° azimuth and 45° inclination (left) and from 50° azimuth and 45° inclination (right).

2.3.4 Principal component analysis

Devereux et al. (2008) have employed principal components analysis (PCA), a branch of multivariate statistics, to construct component images from hillshade sequences created by incrementation of the illumination azimuth by 22.5°, resulting in 16 individual hillshades. Exploiting the highly correlated nature of these images, PCA allows the similarities of the individual shaded images to be summarised into a reduced dataset without much information loss, making interpretation more straightforward. It was found that typically over 95% of information contained in the multi-hillshades can be accessed in just three (high-order) component images, which can be visualised as either a single false colour composite or as three separate greyscale images (Devereux et al., 2008). The PCA image of the test data is illustrated as a RGB false-colour composite of the first three components in Figure 2.19. This visualisation offers an improvement over a simple hillshade and overcomes its drawbacks. Significant detail is revealed both in the main scour pit and also in the wake where subtle flow-parallel ridges are clearly identified. Observers can experience the optical illusion of relief inversion caused by the illumination of the south-facing slope (Hesse, 2010). The PCA is useful for visual identification; however as above, the result cannot be used to create a scour outline without user interpretation.

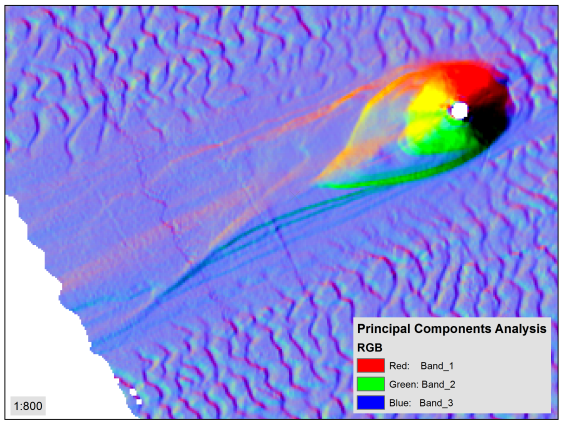

Figure 2.19: RGB false-colour composite of principal components analysis.

2.3.5 Curvature

Kennelly (2008) has proposed using second order derivatives of the topography, plan and profile curvature, to overcome the drawback of hillshade images. Curvature is calculated from elevation data and defines concavity (positive values) or convexity (negative values) of a surface. The curvature plot (Figure 2.20, left) is a product of the planimetric (horizontal, at right angles to the direction of slope) and profile (vertical, in direction of the slope) components. The profile curvature has been found to be particularly suited to defining breaks of slope and edge features (Figure 2.20, right). In the context of scour applications, the accentuation of breaks in slopes and edge features facilitates the definition of the scour hole by the user. Contouring of curvature is problematic, since the contours depend on severity of breaks in slope thus coherent contours are not generally produced and automatic definition of scour pit is not possible. Nevertheless, curvature improves the visual interpretation significantly. Kennelly has suggested plotting curvature as a transparent

overlay on a traditional hillshade and reports the method to be especially successful in highlighting edge features as local contrasts are exaggerated with even minor breaks in slopes of 0.5% revealed. Overlay plots with bathymetry and hillshade are displayed in Figure 2.20 (bottom). Overlaying bathymetry on to the profile curvature (Figure 2.20, bottom right) is an intuitive method of interpretation as the greyscale indicates topographic lows and the breaks are accentuated by the profile curvature. Figure 2.21 suggests that a minimum resolution is required for a meaningful curvature plot, which depends on the relationship between the feature dimension and the resolution. The resolution of the data used to plot this image is 1m and a very small degree of usable information is contained in it. It appears that 0.5m is the minimum resolution to adequately capture edge features in the scour zone.

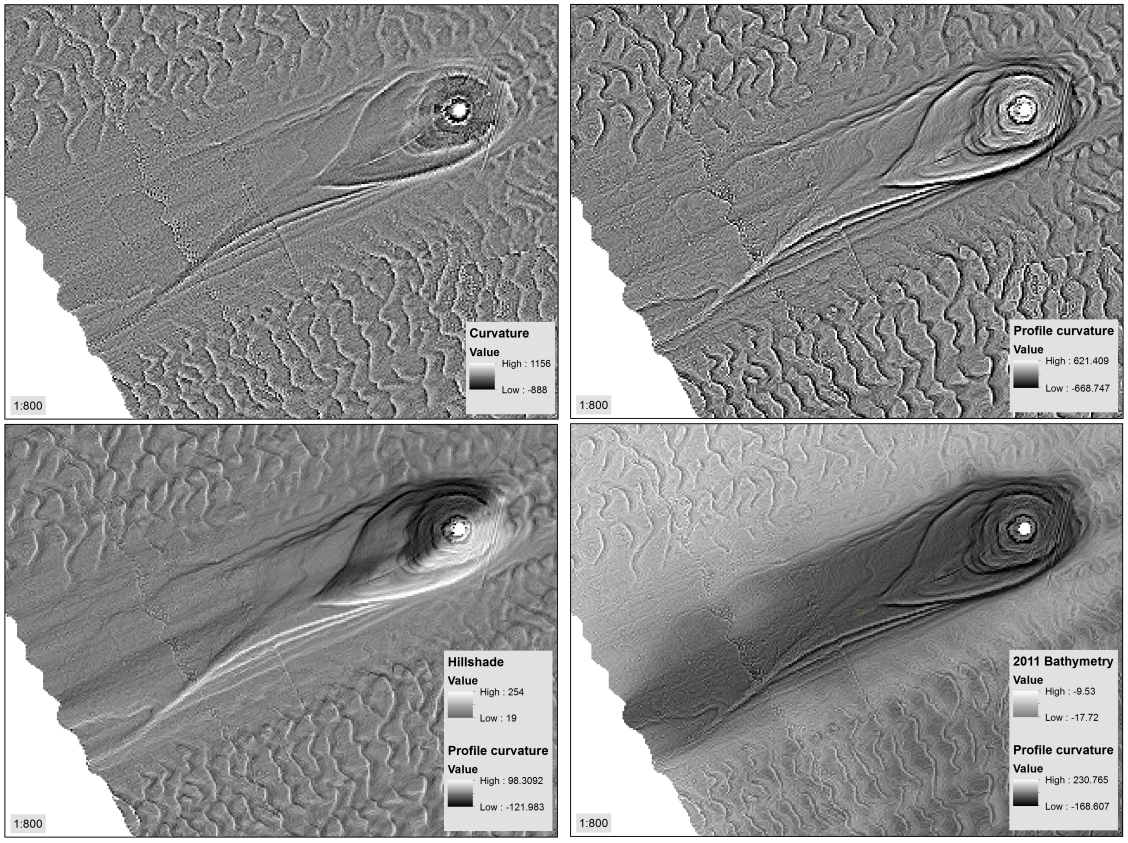

Figure 2.20: Plot of scour hole curvature (top left) and profile curvature (top right). Overlay plots of profile curvature underlying hillshade (bottom left) and bathymetry with histogram equalise stretch (bottom right).

2.3.6 Solar insolation

Solar insolation models are based on the calculation of hemispherical viewshed from any pixel of the digital elevation model (Dubayah and Rich, 1995). The viewshed concept is similar to that of a watershed, in that it describes the amount of solar energy received at any one location which is a function of the amount of "sky" visible and is, thus, influenced by the configuration of the terrain. The terrain can be irradiated with direct radiation from a specific illumination angle, diffuse radiation and reflected radiation. In this study the bathymetry was exposed to diffuse and global (direct and diffuse) irradiation, the results can be seen in Figure 2.22. After solar insolation modelling, the output raster contains

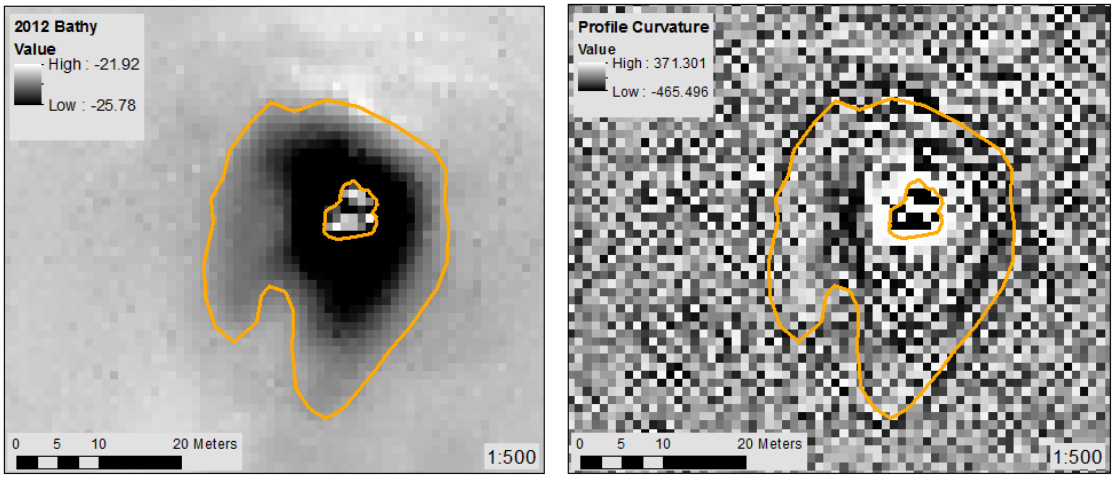

Figure 2.21: 1m-resolution bathymetry of scour hole (left). Calculated profile curvature (right).

values of the amount of radiation received at every pixel location. The primary difference between the diffuse result (Fig. 2.22, left) and global (Fig. 2.22, right) is that the latter has a directional component of the irradiation creating a irregular illumination pattern. While giving a good visual representation of a terrain, similar to a hillshade, this is detrimental to contouring as the irradiation values are determined by the direction of lighting rather than the topography. Diffuse irradiation represents scattered light without directional preference thus is technically suitable for contouring (see Fig. 2.22, left). In the example, two contours were chosen (115,000 and 116,000 J/m^2), that best represented the scour hole. The red contour describes the main scour pit very well but only the more pronounced parts of the wake, while the green contour captures most of the wake but is too generous around the main pit, including large areas of ambient bed. Further tests were undertaken with the solar diffuse model and it was found that the method was most successful for simple scour shapes (ie. no wakes) in flat beds and not universally applicable. Furthermore, the process could not be automated as the "best fit" contour value was different at every site thus requiring user input, contours "spill out" into ambient area where the seabed is complex (eg. presence of bed forms) introducing errors and accurate capturing of the entire scour extent with wake features was generally not possible.

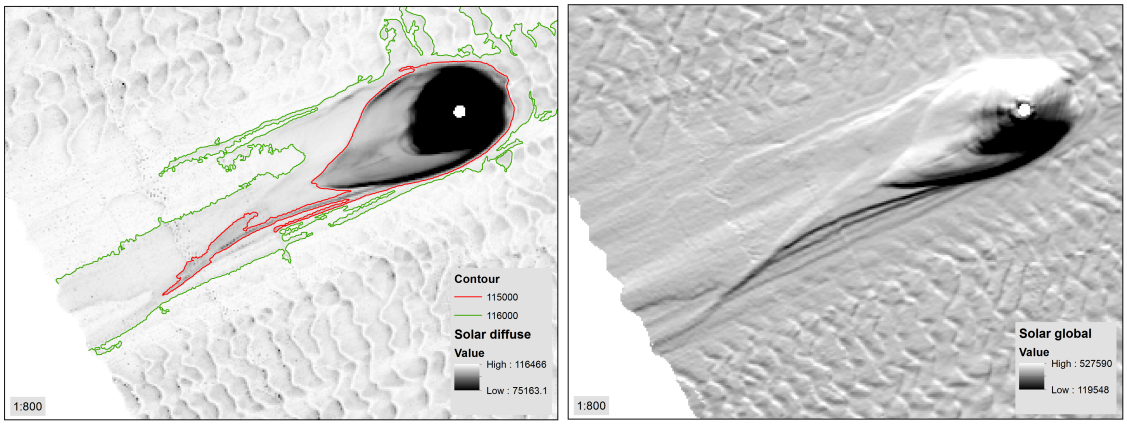

Figure 2.22: Solar insolation modelling using diffuse irradiation (left) and global irradiation (right).

2.3.7 SkyView factor

A method similar to diffuse solar irradiation has been developed by Zakšek et al. (2011) and Kokalj et al. (2011) and is based on the amount of open sky, in an artificial hemisphere, visible from any one location in the DEM. The terrain is illuminated with diffuse light. The amount of irradiation received at any point is proportional to the percentage of visible sky and is calculated as the "sky-view factor" and ranges from 0, no sky visible, to 1, full sky visible. The total amount of sky at every point is determined by the obstruction-free line of sight from the observation point to hemisphere canopy in a specified number of horizon search directions. The size of the hemisphere can be adjusted, thus manipulating the search distance for view-shed obstacles. To calculate the sky-view factor the code provided by Zakšek et al. (2011) and Kokalj et al. (2011) was used. The proportion of open sky at every point was calculated from 16 directions with a hemisphere radius of 4m. A number of other combinations were tested in search for the optimum configuration and it was found that smaller radii provided more detail. The final visualisation is shown with histogram equalisation stretch to increase the contrast and detail discernible (Fig 2.23). Lots of detail is revealed, even in the wake where features are subtle. The output lends itself to contouring since raster values are primarily influenced by shape of terrain. As shown below, the 95% contour showed the best fit to the scour hole, but much of the wake is not captured by this contour.

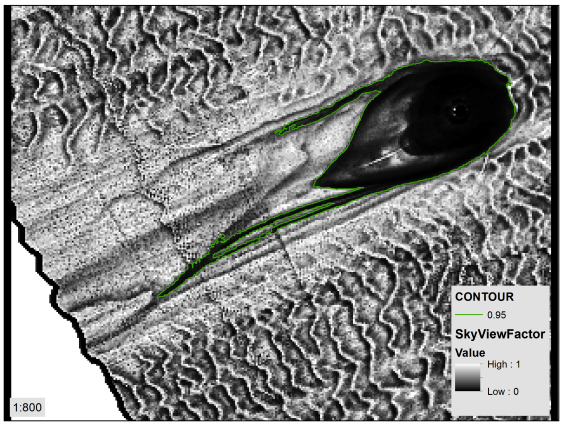

Figure 2.23: SkyView Factor of the bathymetry.

2.3.8 Local relief model

The local relief technique was developed by Hesse (2010). Initially, a low-pass filtered, smoothed surface is subtracted from the original topography, thus producing an image which accentuates positive and negative features. The filtered surface is further purged of detail by extracting original bed levels along the zero-metre contour line of the filtered surface. A new surface is interpolated from these bed levels, thus creating a surface purged of all detail. This feature-less surface is subtracted from the initial terrain model resulting the local relief model (LRM). Figure 2.24 shows the output of the process for the test data set. A diverging colour scheme is used here to distinguish between areas of positive and negative relief. The image contains a surprising amount of information. Much of the edge features have been captured in both the main pit and the wake. Only the most subtle

features in the wake are not visible in the LRM as the difference between the smoothed surface and the features is low. The technique is for feature identification only and does not produce meaningful contours.

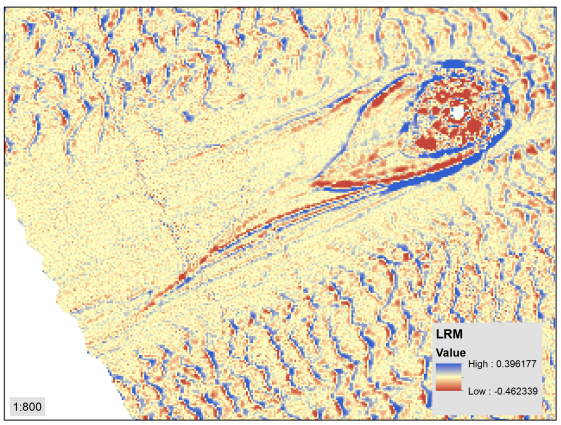

Figure 2.24: Local relief model of the scour hole.

2.3.9 User interpretation

Summarising the above discussion, it has been demonstrated that a number of procedures are available to enhance the visual identification of scour features and, generally, the methods that emphasise edge features have the most merit in facilitating the accurate definition of the scour hole. To produce a scour zone boundary by means of contouring a minimum pre-requisite of the technique is that it produces output raster where the pixel values are a function of the properties of the terrain only (eg. slope, diffuse solar irradiation, skyView factor). Even with these methods the automation of this process is hampered by (i) contours not accurately defining the scour hole, (ii) user input being required to select a "best fit" contour, (iii) contours often not being continuous, and (iv) contours being affected by the morphology of the ambient bed.

Overall, due to the outlined drawbacks of the methods it was decided that user interpretation was the only viable option. It is recognised that this constitutes a weakness in the analysis, as user bias is introduced. Figure 2.25 (left) shows the scour hole outline based on image interpretation using a number of the above techniques. Throughout the course of this study, it was found that compound overlay images using bathymetry, hillshades and curvature in combination provided the most visual enhancement and were judged a sound basis for scour hole definition. Nevertheless, experience has also shown that even with image manipulation it can be difficult to decide on the exact scour extent, especially where the surrounding bed is not flat or where transitions between scour zone and ambient area are subtle, eg. in the wake. Not alone for this reason, user interpretation is also time consuming, considering the number of scour holes under investigation. Nevertheless, it was decided that, compared to the contour-enabled methods above, the degree of error seemed more controllable.

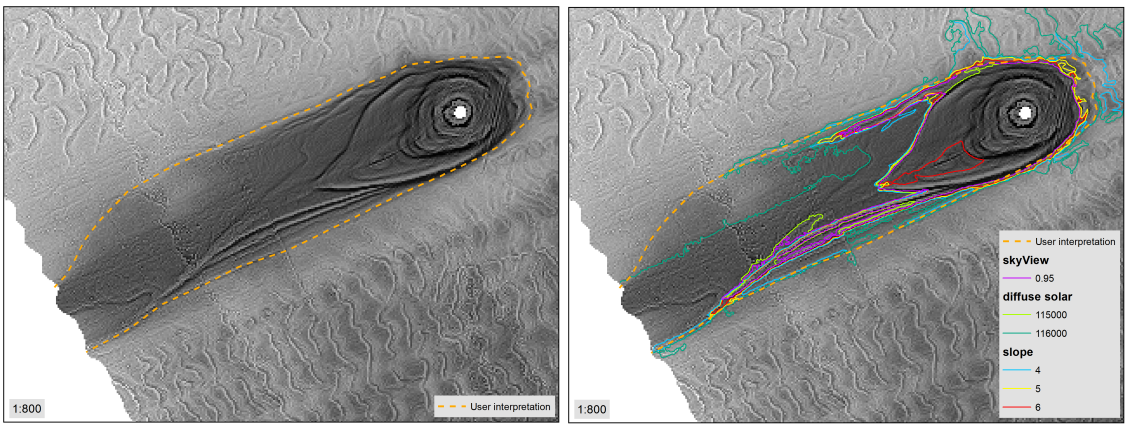

Figure 2.25: Plot showing user interpretation of scour hole (left), and scour polygons from slope, diffuse solar and skyView methods (right).

2.3.10 Methods evaluation

To appreciate the amount of variability between the various contour-enabled methods the slope, diffuse solar irradiation and skyView methods were compared to user interpretation in terms of resulting scour area and volume. This was undertaken for two examples, one is the previously discussed test data set (see Figure 2.25, right) which represents a fairly complex example and the other is a much simpler circular scour hole without wake, surrounded by a flat bed (see Figure 2.26).

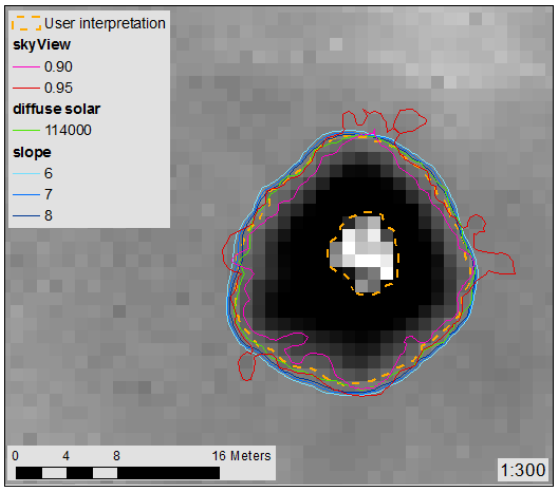

Figure 2.26: User interpretation of scour hole and scour polygons from slope, diffuse solar and skyView methods.

The results are shown in Table 2.7. In the first example there is a striking deviation in area which is typically underestimated by more than 50% compared to the user interpretation, since the wake is not captured adequately. The method that comes closest is the diffuse irradiation; however this is because it includes swathes of upstream sea bed rather than the actual wake. The difference in volume is less, since most of the scoured volume is contained in the main scour pit which is captured in all methods, the discrepancies of approximately 25% are attributable to the missing wake volume. In the second example, visually, there appears to exist better agreement between the contours of individual methods as they exhibit similar dimensions and shapes (Figure 2.26). Nevertheless, the

calculated area is very sensitive to the outline dimension and deviates between 3-19% from the benchmark user interpretation. The volume parameter is much less sensitive to the exact boundary and less than 5% deviation is observed. The results demonstrate that the confidence in the methods is low while the validation effort required to ensure accuracy is similar or potentially greater than conducting a user interpretation.

Table 2.7: Comparison of scour dimensions calculated from various image manipulation methods.

	Method	Contour	Area [m^2]	Δ%	Volume [m^3]	Δ%
	user interpretation		4578		4747	
	slope angle	4°	2243	-51.0	3678	-22.5
		5°	1836	-59.8	3617	-23.8
Fig.2.25		6°	1647	-64.0	3360	-29.2
	diffuse irradiation	115,000	1564	-65.8	3550	-25.2
		116,000	4660	+1.8	4613	-2.8
	skyView factor	0.95	1624	-64.5	3573	-24.7
	User interpretation		234		215	
	slope angle	6°	278	+18.8	222	+3.3
		7°	268	+14.5	221	+2.8
Fig.2.26		8°	258	+10.3	216	+0.5
	diffuse irradiation	114,000	243	+3.8	217	+0.9
	skyView factor	0.90	202	-13.7	206	-4.2
		0.95	272	+16.2	220	+2.3

2.4 Quantifying scour

One of the aims in this study is to quantify scour in both vertical and lateral dimensions and to introduce quantitative measures for the shape of scour holes. To this end, two sets of descriptors are employed.

2.4.1 Scour hole dimensions

Three main quantitative measures are used to define the three-dimensional extents of the scour pits: maximum scour depth (m), area (m^2) and volume (m^3).

Scour depth and area The scour depth around a foundation is determined from bathymetric surveys as the depth difference between the ambient bed level, calculated as the mean elevation in a suitably sized buffer around the turbine (excluding scour zone), and the deepest point within the zone of scour. Where the ambient seabed is variable, eg. sloping, the described method can be inaccurate due to errors in the estimation of the ambient bed level. In these cases the bed level was checked visually and corrected where necessary. The scour depth reported is always the maximum depth at time of survey; it is not possible, without constant surveying, to know whether this constitutes the equilibrium scour value as reported in physical experiments. The scour area is simply determined in GIS from the scour hole outline.

Scour volume Two different techniques were employed to quantify the volume of the scour pit. Both methods are based on difference plots of two surfaces. The preferred method is based on the bed level change between the pre- and post-installation survey; the mean difference is multiplied by the area of the scour pit to generate the volume. However, the nature of the data sets is not always suitable to ensure accuracy of this method. Where ambient bed level change in the time between surveys is high, errors are introduced. In this case an artificial surface can be interpolated from point elevations around the scour hole on the post-installation survey ("fill surface method"). This surface then replaces the pre-installation surface in the previous method. The performance of the two methods will be contrasted in three examples. The first example is used to validate the "fill surface method". Figure 2.27 compares the difference plots created using both methods from a lightly sloping, featureless bed that has experienced very little change in bed elevation thus it is expected that the interpolated surface will match the pre-installation surface well and the volumes calculated from the two methods should be close. The difference plots between pre-installation (artifical and real) and post-installation surface are plotted. The volumes are calculated from these difference plots. As illustrated they show very similar patterns and the calculated volumes are within 1.6% of one another. Figure 2.28 shows an area where significant bed elevation change has occurred between the pre- and post-installation survey, hence this is an area where the artificial fill surface method would be used. The foundation is located on a bank side that is retreating, thus the survey difference plot (right) shows greater differences, by approximately 1m, within the scour zone than the fill surface difference plot (left). Consequently the scoured volume is overestimated and there is a difference of 40% between the calculated volumes. Removing the 1m overestimation in the survey difference plot, the calculated volumes are within 5% of each other. The shape of the contours are quite similar in the two plots which suggests that the influence of bed forms on the volume will be small and likely to account for some of the 5% difference. Figure 2.29 illustrates the deficiency in the fill surface method in an area with bed forms (H=0.6m, λ=15m). Here, the bed level change between pre- and post-installation survey is due to bed form migration. The interpolation procedure cannot recreate the bed features that are present in the pre-installation survey surface, thus the volume is underestimated wherever such features are present. The discrepancy in the volume calculation is 50%, which is volume contained in the bed forms.

Using the default survey difference method, there is a lower limit below which the volume of the scour hole cannot be determined accurately. This limit is determined by the minimum difference between pre- and post-installation surface and the precision of the surveys (see Section 2.2.1). To accurately determine the volume, the mean absolute difference between consecutive surveys must exceed $\approx$ 0.15m, otherwise the uncertainty within the survey is greater than the bed elevation change and these very small volumes cannot be determined with confidence. Where this threshold is not exceeded the volume is calculated as 0.15 times scour area; only a small number of data points in the Thanet data set are affected by this. Quantifying the uncertainty in the fill surface method is difficult. Errors are inevitably introduced by creating an artificial surface; however it is not possible to quantify them. Some uncertainty also lies in the survey accuracy of the post-installation survey which is likely to be negligible compared to the previous source. The uncertainty

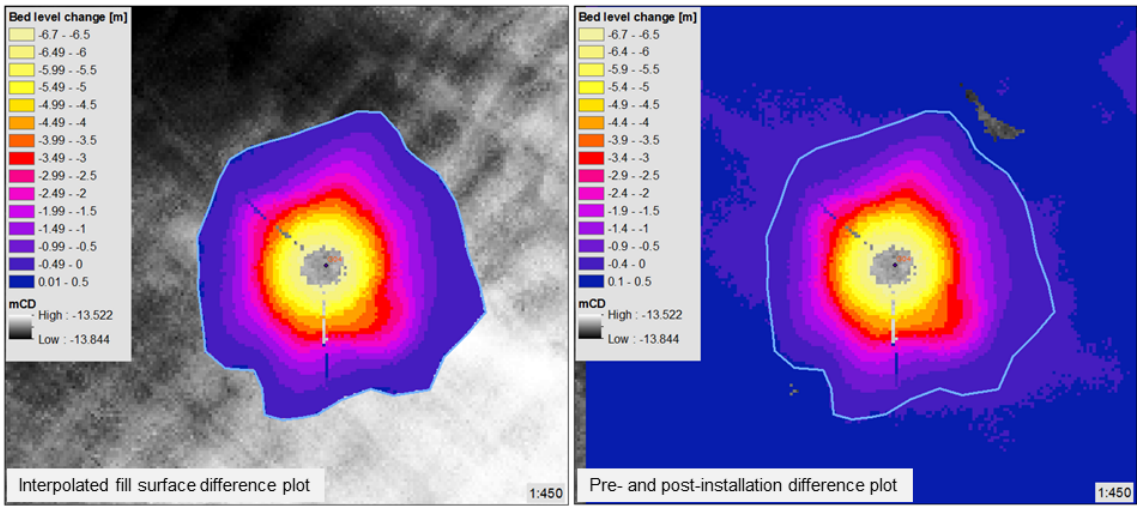

Figure 2.27: Comparison of the two volume calculation methods on a lightly sloping, feature-less bed with little ambient change.

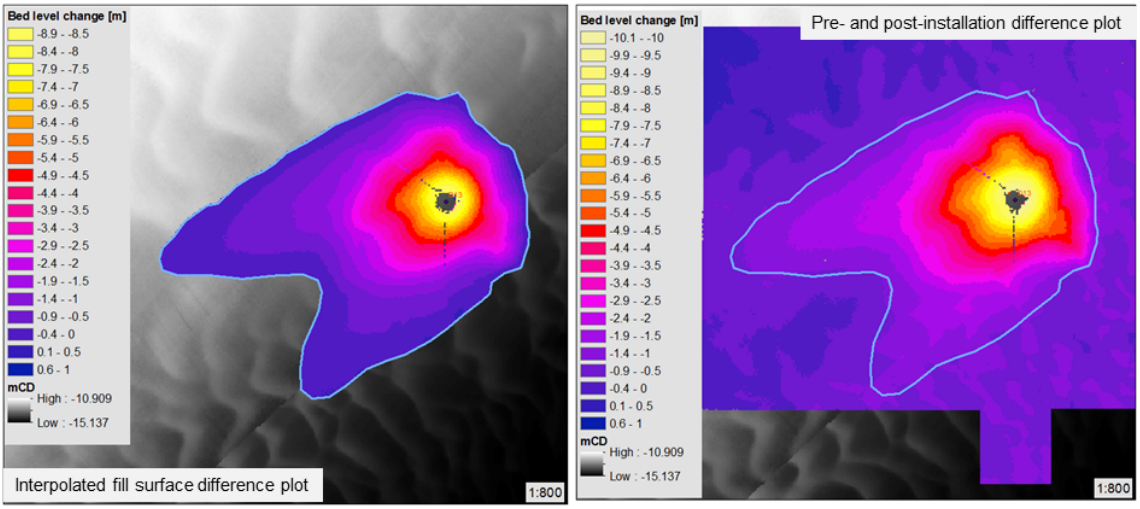

Figure 2.28: Comparison of the two volume calculation methods on a sloping bed with large ambient change.

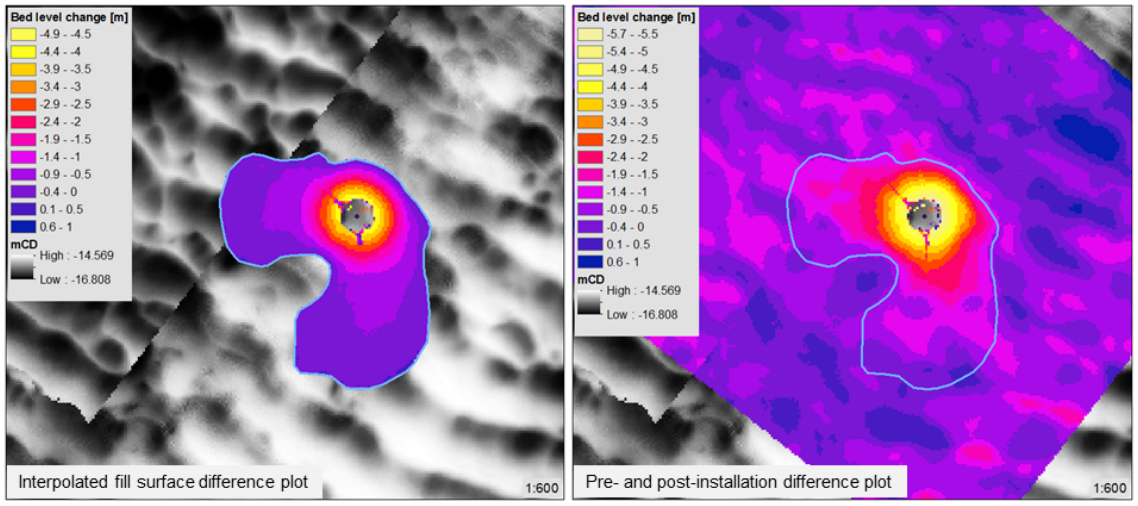

Figure 2.29: Comparison of the two volume calculation methods on a flat bed with migrating bed forms.

associated with the pre- and post-installation survey difference plot method are related to the survey precision.

2.4.2 Scour hole shape

A number of factors were used to quantify the plan shape of scour holes. Lateral extension is reported as the non-dimensionalised short axis W/D and long axis L/D and a ratio of the long and short axis L/W; these parameters are derived from the bounding rectangle as shown in Figure 2.30 (left). The angle of the long axis α_L gives the orientation of the scour hole extension in respect to (°N). The dimensionless isoperimetric quotient (IQ) which is based on the user interpretation of the scour outline represents a measure of how "circular" a scour hole is, expressed as a ratio between the inside area of the scour hole polygon to the area of a circle with equal perimeter p, resulting in

$$IQ = 4\pi A/p^2 \tag{2.3}$$

For shapes of equal circumference a circle gives the maximum possible area thus as $IQ \rightarrow 1$ the scour hole shape approaches a perfect circle. The IQ value diminishes with increasing irregularity of the perimeter (e.g. due to distinct two-limbed wake or irregular, ragged scour hole shape), since this increases the circumference while reducing the encompassed area. A sequence of images that demonstrates the effect of perimeter irregularity on IQ is presented in Figure 2.30 (right).

While the L/W and IQ parameters, in isolation, allow some characterisation of the scour hole shape, their utility is increased when used together. A classification plot has been developed that facilitates the categorization of observed shapes based on these two shape factors (Figure 2.31). This plot was derived from qualitative description of field data in this study and allows approximations of likely scour hole shape; prototypes for each shape are displayed in the plot based on real examples. Being a qualitative method, the charted category boundaries are somewhat fluid and the categories are not necessarily absolute. Where categories are nested, eg. "bi-directional" in "uni-directional, elongated, elliptical", the exact shape has to be confirmed visually. Nevertheless, this chart offers a relatively fast method to achieve an approximate understanding of the type of scour hole shapes present.

Generally, a scour hole consists of a main scour hole, approximately the shape of an upturned conical frustum, with steep side slopes commonly assumed to be controlled by the angle of repose of the sediment. The main scour hole is generated by the excavating action of the junction or horseshoe vortex. Depending on the physical conditions a wider scour pit is formed which is a shallower depression (e.g. wake) around the main scour pit, which has its origin in the erosive action of far-field turbulence and flow acceleration. The three-dimensional shape of the main scour hole is controlled by the slope angles found in the scoured material. To measure this, histograms of the first derivative of the bathymetry data β were calculated for each scour hole with associated statistics: mean, standard deviation σ_β, skewness γ_1 and excess kurtosis γ_2. The kurtosis of a normally distributed variable is 3, thus this is subtracted to determine the excess kurtosis. The

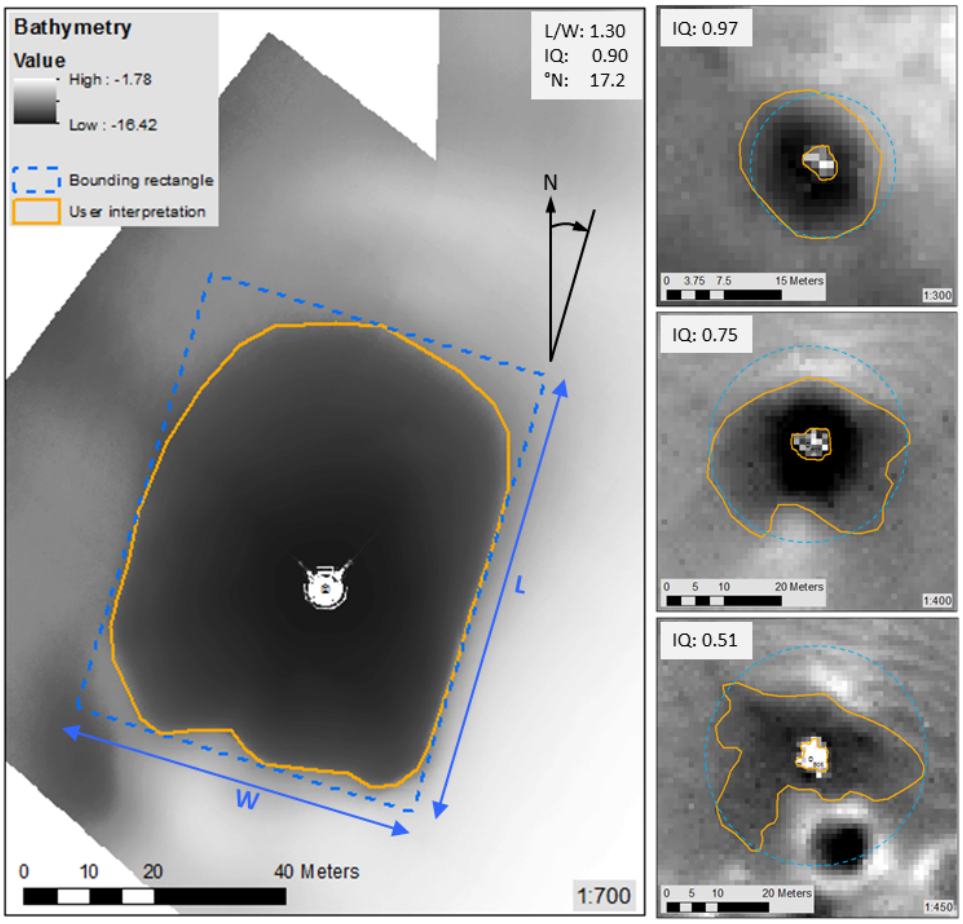

Figure 2.30: Long and short axis dimensions (left) and series showing the effect of scour hole shape on the isoperimetric quotient (right), where blue dashed circle indicates $IQ = 1$.

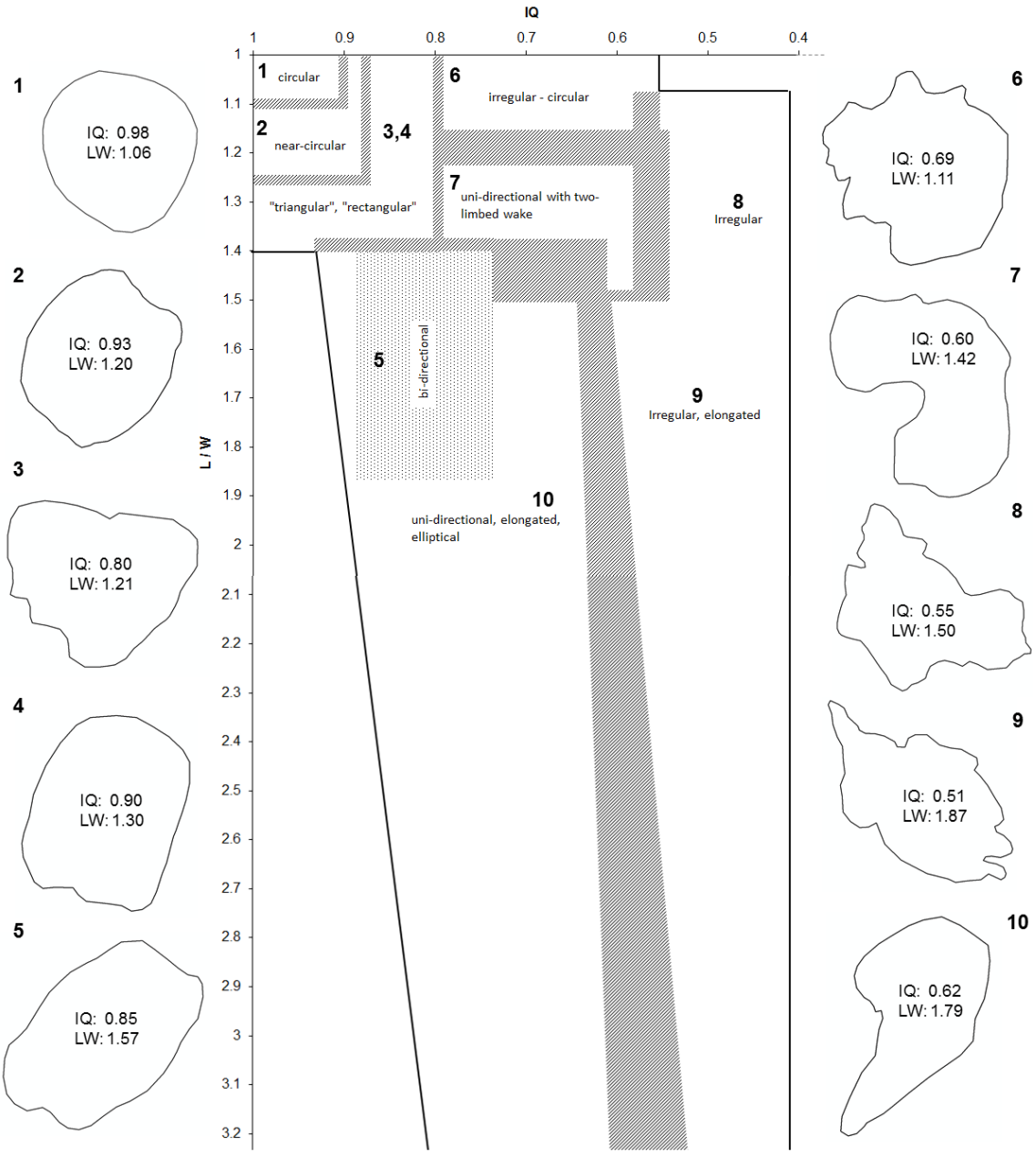

Figure 2.31: Scour hole shape classification chart, based on IQ and L/W. Shape examples no to scale.

skewness and kurtosis are derived using equations 2.4 and 2.5, respectively. In addition, the mean upstream β_u and downstream slope angle β_d was recorded. The upstream portion of the scour hole is defined as the area of the scour hole facing the dominant flow direction, up to the flow-normal through the centre of the monopile (see Figure 2.32). The downstream part stretches from the flow-normal to the end of the wake. The mean slopes are calculated based on the angles encompassed in these areas.

$$\gamma_1 = \frac{\sum_{i=1}^{n} \left(\beta_i - \bar{\beta}\right)^3}{(N-1)\,\sigma^3} \tag{2.4}$$

$$\gamma_2 = \frac{\sum_{i=1}^{n} \left(\beta_i - \bar{\beta}\right)^4}{(N-1)\,\sigma^4} - 3 \tag{2.5}$$

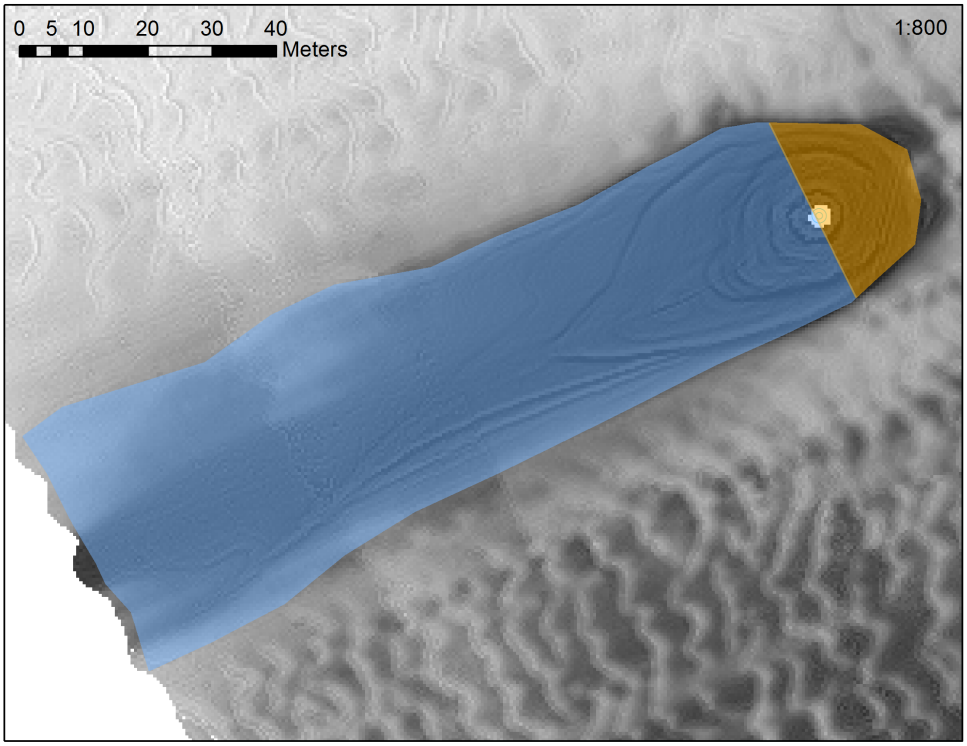

Figure 2.32: Definition of upstream (orange) and downstream (blue) section of scour hole.

2.4.3 Accuracy of models

To objectively measure the performance of the empirical equations introduced in Chapter 1, two statistical measures will be used that evaluate the agreement between the predictions and the field observations. The first measure is the root mean square error RMSE, that is given as:

$$RMSE = \sqrt{\frac{\sum_{i=1}^{n} \left(X_{obs,i} - X_{pred,i}\right)}{n}} \tag{2.6}$$

where $X_{obs,i}$ are the field observations, $X_{pred,i}$ are the predicted values and n is the number of observations.

The Nash-Sutcliffe model efficiency coefficient E (Nash and Sutcliffe, 1970) can be employed to determine the accuracy of model output against observations (see Eq 2.7). The parameter E can take values from $-\infty < E < 1$, where $E = 1$ indicates perfect fit between the model outcome and the observations. When the prediction fits the average of the observations, then $E = 0$. Negative efficiency $-\infty < E < 0$ indicates that the mean of the observations is a better predictor than the model.

$$E = 1 - \frac{\sum_{i=1}^{n} \left(X_{obs,i} - X_{pred,i}\right)^2}{\sum_{i=1}^{n} \left(X_{obs,i} - \overline{X_{obs}}\right)^2} \tag{2.7}$$

where $\overline{X_{obs}}$ is the average of the observations.

Chapter 3

London Array (Phase 1) offshore wind farm

The London Array (Phase 1) offshore wind farm covers an area of 100km^2 in the Outer Thames Estuary, approximately 21km offshore of Margate in east Kent (see Fig 1.2). Phase 1 of the development, completed in late 2012, encompasses 175 Siemens SWT-3.6-120 turbines with an individual capacity of 3.6MW, producing a maximum total of 630MW which is sufficient to provide electricity to half a million homes[1]. The turbines are built on monopile foundations of 4.7 and 5.7m diameter, installed over a 20-month period between March 2011 and October 2012, with approximate spacing of 650m within rows and 1000m between rows. The sea bed topography is dominated by the tidally-aligned sand banks and intervening channels, which is a topographic characteristic of the central Outer Thames Estuary. The three main topographical features over which the development is constructed are two sandbanks (Long Sands, Kentish Knock) and the inter-bank channel of Knock Deep (see Figure 3.1). Consequently, a large range of bed levels observed, from -26mLAT in Knock Deep to very shallow, even drying out at low tide, on parts of the sandbanks.

3.1 Hydrodynamic regime

The general hydrodynamics of the Outer Thames were outlined in Section 2.1.1; however, more detailed data on the specific tidal and wave conditions have been recorded over the last decade which will be discussed here.

Tides The tidal range at the development is given as between 3.9-4.1m on springs and 2.2-2.3 on neaps in London Array Ltd (2005) based on harmonic analysis of field measurements undertaken at the site. The tidal flow axis is aligned in NE-SW direction, where the incoming tide travels south-west and the ebb current in north-easterly direction. Tidal currents can be affected by external influences such as increased river discharge, wind stress, surges and density-driven flows but generally follows the flow pathway created by

[1] LondonArrayLtd, unknown, London Array - Harnessing the power of offshore wind, http://www.LondonArray.com/the-project. Accessed: 02/05/2014

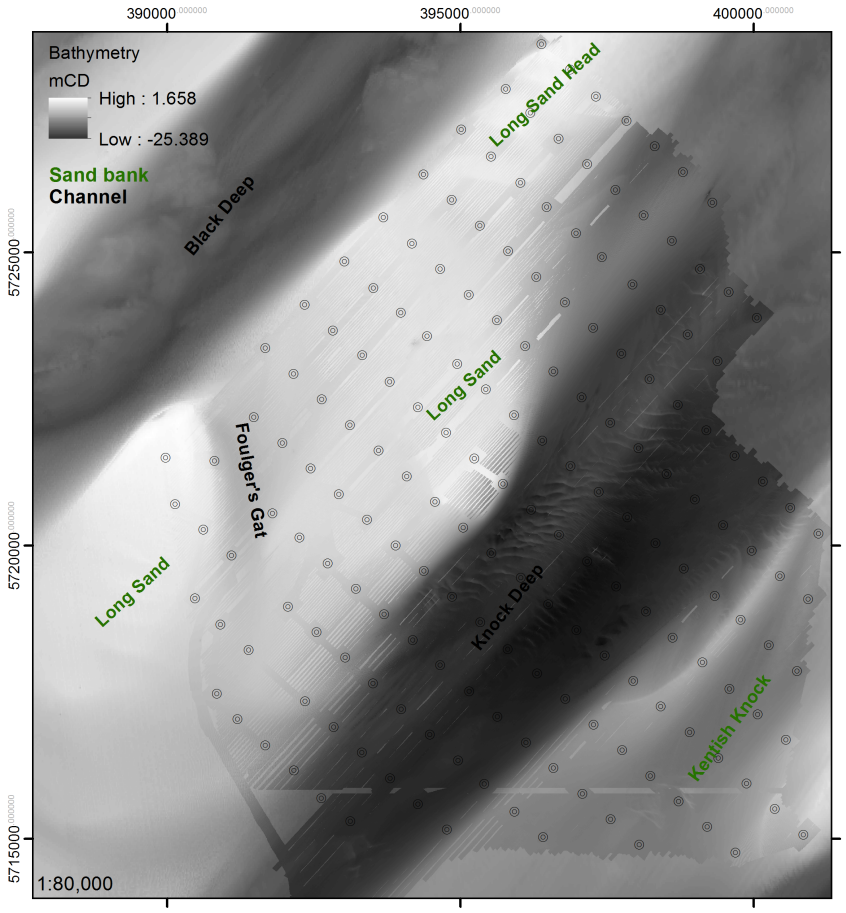

Figure 3.1: Topographical entities at London Array.

the existing topography (London Array Ltd, 2005). The stronger spring tidal current is approximately 0.7ms^{-1} on the sand banks and in the region of 0.8-1.0ms^{-1} in the Deep (ABPmer, 2008). During neaps, the topographical discrepancy of flows is less pronounced with velocities of approximately 0.4-0.6ms^{-1} over the site. Typical ranges of U_c for the three topographical features are also given by HR Wallingford (2008) in Table 3.1 together with mean current speeds, which show that in terms of flow speed the topographical entities show very similar characteristics. The upper limit of $U_c = 1.30 - 1.34$ agrees well with the current measurements at the site shown in Figure 2.2. Overall, the incoming tidal stream is the main agent of sediment transport and morphological change (ABPmer, 2007), a pattern which is confirmed by bed form asymmetry (as will be demonstrated in Section 3.3.2), although the sand banks of Long Sands and Kentish Knock are influenced by the combined action of waves and currents (London Array Ltd, 2005). However, local tidal dominance can vary as the flood tide is deemed to be dominant on the southern flanks of the banks while the ebb tide is more influential on the northern flanks (Kenyon and Cooper, 2005), which is due to the sheltering effect of sand banks that are slightly offset to the alignment of the ebb flow (London Array Ltd, 2005). This effect is especially pronounced at Long Sands.

Waves The predominant wave climate in the Outer Thames is reported as bi-modal, with south-westerly waves dominating with significant contributions from north-easterly storms as shown in Figure 2.4. Histograms and scatter plots of peak wave period T_p

Table 3.1: Metocean parameters for the London Array site. From HR Wallingford (2008).

Parameter	Long Sands	Knock Deep	Kentish Knock
H_s (m)	0.38 - 2.26	0.33 - 2.49	0.47 - 2.57
T_p (s)	2.03 - 9.85	1.63 - 11.64	2.98 - 10.67
h (m)	1.29 - 6.86	17.91 - 22.75	5.62 - 10.62
$\overline{U_c}$ (ms^{-1})	0.13 - 1.34	0.06 - 1.32	0.05 - 1.30
$\overline{U_{c,av}}$ (ms^{-1})	0.70	0.69	0.70

and significant wave height H_s based on recorded data from the closest buoy, the South Knock Wave Rider (location shown in Figure 3.5), is plotted in Figure 3.2 for the 7-year period from October 2006 to February 2014. Typically, wave conditions are benign with $H_s < 1.5$m and $T_p < 6$s. Average conditions as established from the available record are $H_s = 0.83$m, $T_p = 4.7$s and $T_z = 3.6$s while the top 10^{th} percentile of the waves in the record show mean $H_s = 1.86$m, $T_p = 6.2$s and $T_z = 4.6$s. The summer (May-Oct) average wave height determined from the measured record is 0.73m with a peak period of 4.60s, while in winter a slightly higher value of 0.9m is given with $T_p = 4.84$s. The 50-year return period extreme wave reportedly used for monopile foundation design purposes is given as $H_{max} = 9.5$m and $L = 100$m . The water depth required for a wave to break can be estimated as $H_s/h > 0.55$, which means that at London Array waves will only break in very shallow water $h < 2m$ for common wave conditions. It is generally assumed that wave-induced orbital motions can influence bed shear stresses up to a depth of $L_0/2$, where $L_0 \approx 20$m for $T_z = 3.6s$. Soulsby (1997), gives the threshold water depth as $h < 0.1gT^2$ or $h < 10H_s$, suggesting water depth needs to be shallower than 8.3-12.7m for waves to have an effect on the sea bed. Under typical conditions at London Array wave energy is relatively low so that any appreciable impact on scour is expected in the shallow areas of the development (e.g. southern Long Sands); during high-impact events, it is understood that coarse sands and gravels can be moved on the sand banks as described in Section 3.2.2. Further, past severe storm conditions have been deemed to be responsible for significant morphological change of the sand banks, Long Sands in particular as will be illustrated in Section 3.3.1.1. However, during the period between installation and survey no events larger than a 1:1 year event has been witnessed as shown in Figure 3.33 and discussed in Astley et al. (2014).

3.2 Geology

3.2.1 Bed rock

As outlined in Section 2.1.2, Tertiary London Clay forms the bedrock at London Array. The top horizon of this overconsolidated clay lies between -20mLAT and -40mLAT and the thickness of this deposit in the Outer Thames Estuary is approximately 150m (British Geological Survey, 2002). While generally the horizon is found to be gently undulating, a significant south-ward drop of the clay surface by some 15-20m over approximately 180m occurs between turbine rows C and B, the result of the incision of a Quaternary palaeochannel (Section 3.3.1.3). As a result of the bank−inter-bank topography the clay

COWI Ltd, unknown, http://vimeopro.com/cowi/cowi/video/77024713. Accessed: 02/05/2014

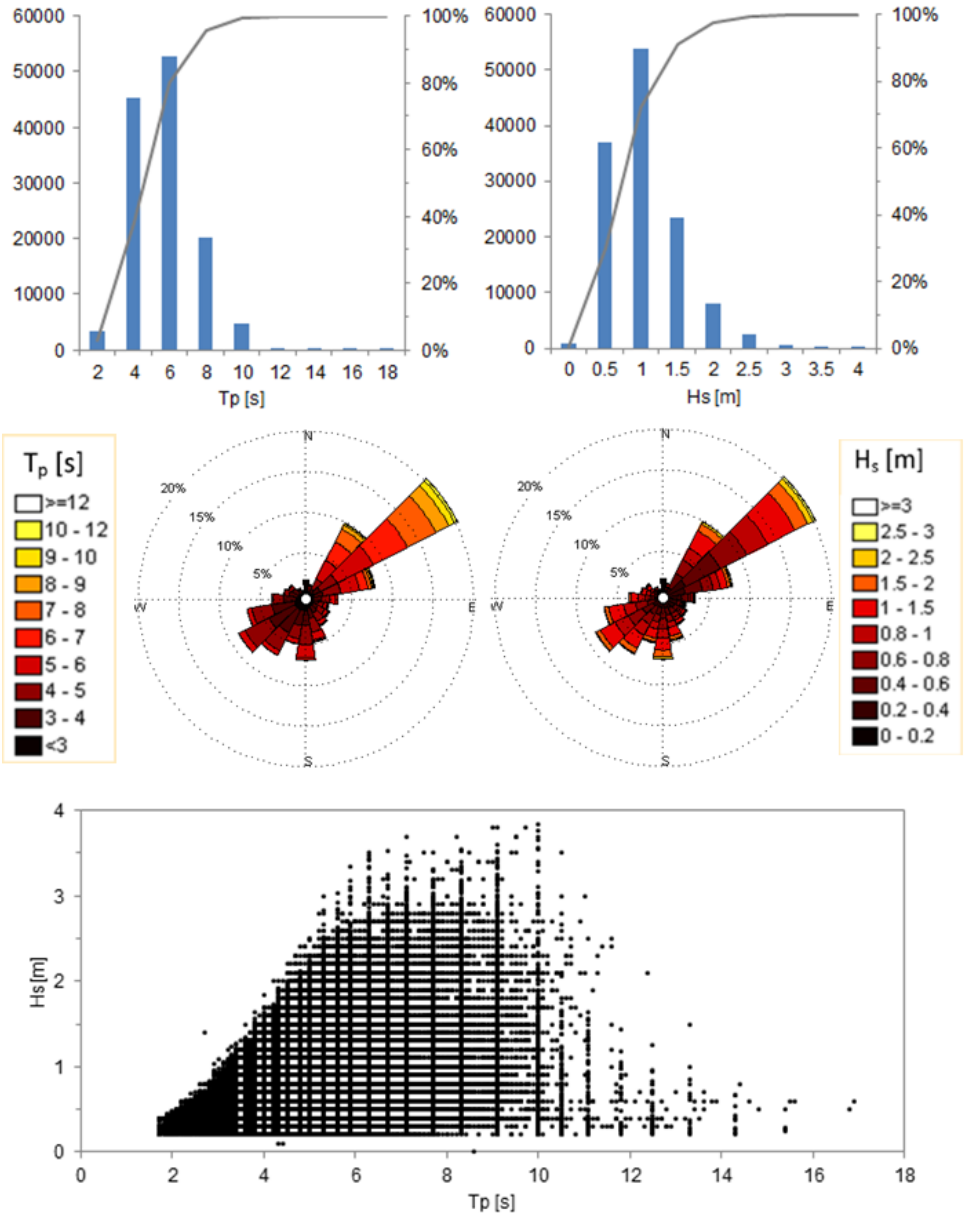

Figure 3.2: Wave data recorded by South Knock wave buoy between October 2006 to February 2014. Data from Cefas WaveNet.

can be within some 2-3m of the seabed surface in central and northern areas of Knock Deep.

The Tertiary clays are firm to stiff, locally very stiff, fissured, variably grey, brown and green grey glauconitic deposits. At the top of the London Clay layer the clay can exhibit a small proportion of sands, silts or gravels likely resulting from mixing with the overlying sediment. Particle size analysis of clay samples from the cores reveals all samples contained a significant amount (50-70%) of particles finer than 0.004mm. In most cases 90% of particles were smaller than very fine sand (0.063mm). Typically less than 5% fraction of sand and gravels was determined, apart from individual samples close to the surface of the clay stratum or individual localised sand deposits within the fine-grained matrix. Moisture content of the clays are typically in the range of 30-40% and the average bulk density is given as 1890kgm^{-3}. Undrained shear strengths c_u from lab-tested samples extracted from boreholes ranged from 33-261kPa, with increasing stiffness with depth (HydroSoil Services, 2005). The average c_u at the top of clay is given as 75kPa, which can be described as "firm" according to British Standard (2010) (see Table 2.6), and this increases to over 200kPa at depth ("very stiff"). The clay is understood to exhibit very high plasticity. The cone resistance is typically less than 5MPa but increases with depth (e.g Figures 3.6 and 3.7).

A typical seismic reflection from London Clay is shown in Figure 3.3. The boundary between London Clay and overlying material is generally marked by a strong acoustic impedance contrast, facilitating the identification of the boundary throughout the site. The internal seismic reflection is weak implying a solid material with little internal structure. However, at depth, the characteristic acoustic signature of London Clay, a set of discontinuous, inclined twin reflectors, can be discerned. Sturt et al. (2009) refer to it as "offset reflector couplet horizons". These small-scale faults are understood to be the manifestation of deformation features in soft sediments that originate from post-depositional compaction during the Ypresian (Cameron et al., 1992). Sturt et al. (2009) understand the features as part of a polygonal fault system and quotes dimensions of the fault throws of less than 3m, with spacings of 12-80m and fault lengths of 15-100m.

At London Array the Tertiary depositional sequence is truncated at the Eocene and as a result Quaternary sediments directly overlie the bedrock.

3.2.2 Quaternary sediments

A distinction between pre- and post-transgressional sediments is difficult at London Array since as Kenyon and Cooper (2005) explains, the bulk of the sand was deposited in the wider estuary before and during the Holocene transgression and has been subject to re-working since. In the post-transgressional period, sandy sediments have been sourced from erosive processes along the surrounding coastline and from offshore. Fossil Pleistocene channels can be found in the northern and southern parts of the site as incisions into the clay bedrock which have been subsequently filled in with sandy silts. Directly overlying the London Clay, CPT records reveal that a layer of firm clay of approximately 1m thickness can be present. Overlying this band of clay is the main package of granular sand deposits. In places, shallow gravel layers mark the interface between the clay and sand deposits

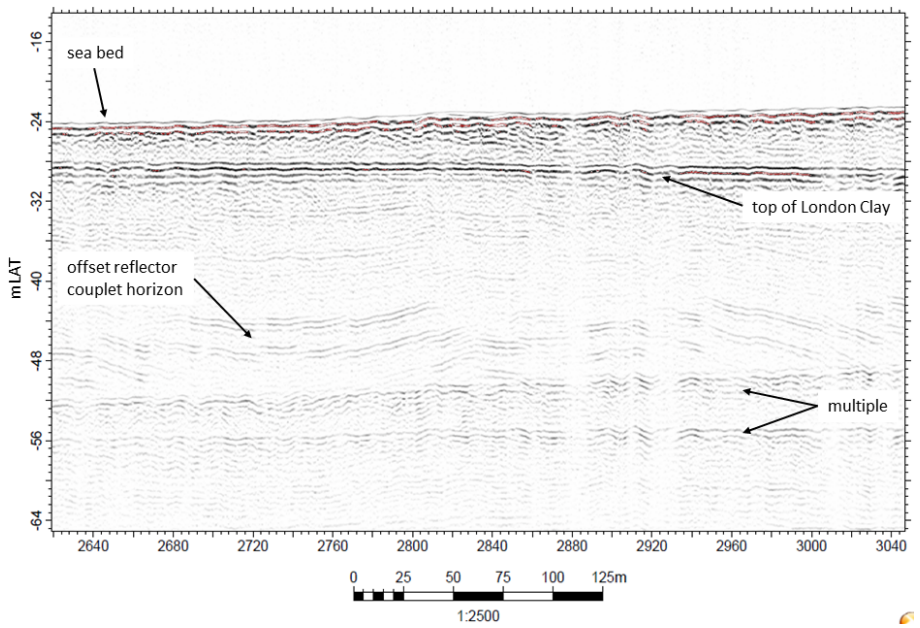

Figure 3.3: Typical seismic reflection of London Clay. Top of clay marked by blue line.

(BH1A and BH07). The thickness of the sand package varies typically between 3-35m. The vertical extent of the sandy sediments was determined from CPT readings taken in 2005 and 2007, cross-referenced against seismic profiles, and a contour plot was interpolated from spot thickness measurements at turbine locations (Figure 3.4). The layer is thickest in the south and south-west is some 20-35m thick with 15-25m typically found on the sand banks. The sediment cover thins to 10-20m at the neck of Long Sand. In Knock Deep depths of granular deposits between 5-10m are representative with slightly shallower veneers of 3-4m in the central and northern part of the channel.

HydroSoil Services (2005) have investigated and summarised the characteristics of the Quaternary sediments. The following section will draw upon that source with some added information from the interpretation of boreholes and CPT records. Throughout the site, the sandy sediments are found to be relatively homogeneous and can be described as green grey to brown, fine to medium sand with a variable component of silt and sand size shell fragments. Geotechnical investigations show that the sand generally becomes more silty with depth. In places, usually associated with thin laminations, a clay component can be present. In terms of the sediment characteristics, the analysis is based on 38 borehole samples from various locations and depths, augmented with 247 surface grab samples. Thus, the change in grain size distributions with depth is not as well understood as the nature of the surface sediment. Nevertheless, from the core samples HydroSoil Services (2005) reports that the sand is well sorted with $d_{50} < 0.2$mm (fine sands) and that medium and coarse sands were generally only found in samples from the top 3m of core length as the sediment tends to become finer with depth. The content of fines in the sandy soil layer was typically less than 15% and gravel and shell content of less than 2%. The average minimum and maximum dry density of sand is given as 1320 kgm^{-3} and 1600 kgm^{-3}, respectively with an average particle density of 2690 kgm^{-3}. Typical cone resistance q_c values for the granular package range from 2-20MPa, which is representative of loose to very dense sand (see Table 2.5). The sediment tends to become more compacted with

Table 3.2: Grain size distributions from seabed sediment samples.

Class	Very fine sand	Fine sand	Medium sand	Coarse sand	Very coarse sand
d [mm]	0.063 - 0.125	0.125 - 0.25	0.25 - 0.5	0.5 - 1.0	1.0 - 2.0
%	0.40%	33.60%	44.13%	17.81%	3.64%

depth reflecting tighter packing, and readings of q_c can exceed 20MPa inside the sand bank core. Analysis of surface grab samples confirms that the median grain size d_{50} of surface sediment is predominantly fine sand in the southern part of the site with medium sands prevailing on the heads of the two major sand banks (see Fig 3.4). Coarser sand on the seabed surface is found predominantly in the central and northern part of Knock Deep and to the north and east of Kentish Knock. Out of 247 surface grab samples, over 75% of grab samples fall in the fine and medium sand class as shown in Table 3.2. Just over half the samples (140 in total, 56.7%) included shell fragments (although exact proportion unknown), 19 included gravel (7.7%) of which 12 included sand and gravel (4.9%). Most of the records containing shells or shell fragments were taken from Knock Deep and Kentish Knock; most samples from Long Sands were shell free. Similarly, all samples with gravel content originated from the slopes and deeps around the head of Kentish Knock. Sediments in Knock Deep are more heterogeneous than samples from the banks, and it is implied by HydroSoil Services (2005) that during extreme events, the combined action of currents and waves is capable of moving large grain size material from the banks into the Deep and large particles and shell fragments deposited in Knock Deep require large energy input to be moved again. This also suggests that storm events can have an influence on scour development on the sand banks.

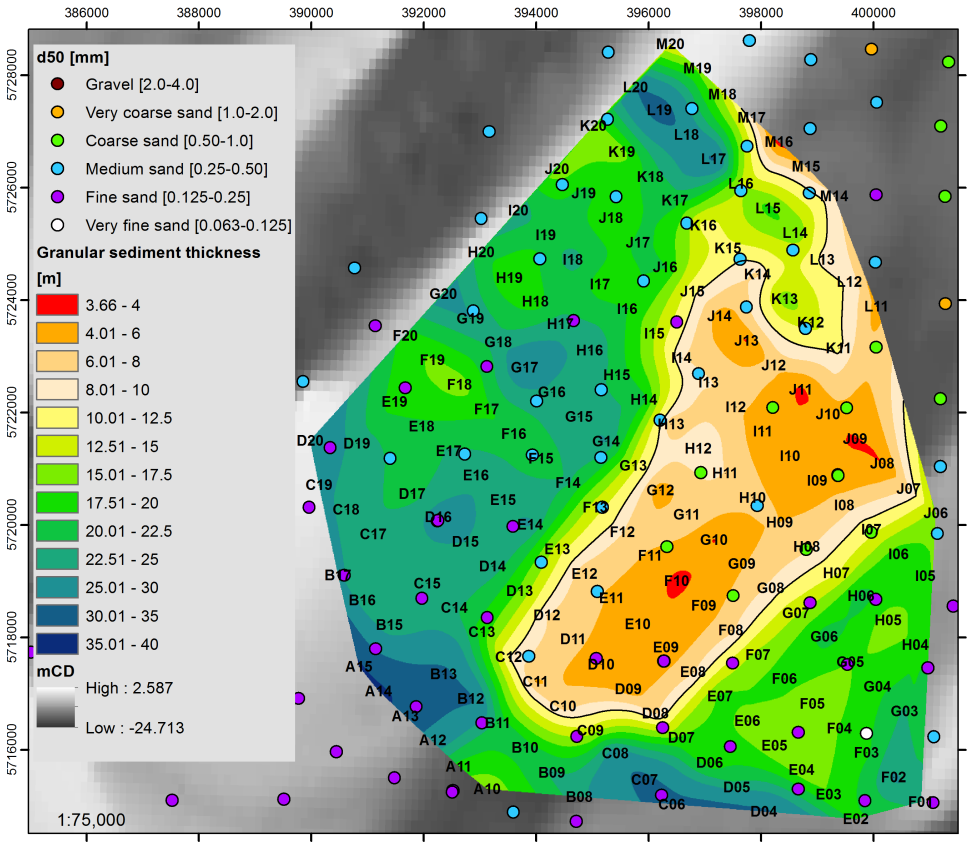

Figure 3.4: Thickness of granular sediment z_{sed} at London Array; $z_{sed} = 10$m contour in black. Median particle size (d_{50}) of surface sediment from grab samples.

3.3 Seabed Morphology

3.3.1 Natural morphological variability

Due to the topography of the site, foundations are located in a wide range of water depths (0-30m). A map of the major topographic features found at London Array is provided in Figure 3.1 for orientation in the subsequent discussion. Long Sands is bordered by Black Deep and Knock Deep in the north and south, respectively. The highest part of Long Sands is south of Foulger's Gat and this area can dry out at low tide. Kentish Knock can also dry at low tide; however drying areas of the bank are not encompassed in Phase I of the London Array development. The channel of Knock Deep is approximately -26mLAT at its deepest. In the following, historical morphological trends described in ABPmer (2005) and ABPmer (2007) are reviewed and supplemented with analysis from recent bathymetric surveys.

3.3.1.1 Long Sands

Examination of historical data by ABPmer (2005) has concluded that Long Sands is stable in terms of its general location and plan position but can vary significantly in profile shape, i.e. large variations in bed elevations. However these bed level changes are chaotic and do not reveal an underlying trend. It is hypothesised by ABPmer (2005) and ABPmer (2007) that this variability in cross-sectional shape of Long Sands is generally the result of storms. Bed level changes of up to 1.5m during relatively common low-return period storm events have been reported ABPmer (2007). Flattening of the bank due to redistribution of sediment, without net loss of material, has also been reported as a mechanism of short-term large-impact topographical change. The legacy of severe storms on the sand bank has been illustrated by ABPmer (2007). Historical bathymetric surveys reveal a large indentation in the southern flank of the Long Sands which has been attributed to the 1953 great storm surge. It has been postulated that the bank has since readjusted towards, what is assumed to be, its pre-storm equilibrium shape over the subsequent 40 years. Nevertheless, if this is the banks response to large storm events, this should be considered in the scour analysis as large movements of the bank slope could potentially uncover several metres of turbine foundation in that area. In the southern part of the bank, the swatchway of Foulgers Gat maintains a shallow channel perpendicular to the general alignment of the bank and channel system. Foulger's Gat has been reported to be rotating in a clockwise direction (ABPmer, 2007) and some crest level readjustment will be associated with this process.

To investigate the natural changes in more recent years, the pre-installation evolution of the area is examined from bathymetric surveys taken between 2004 and 2011. Figure 3.5 shows the changes in bathymetry between 2004 and 2011. Any variation within ±0.5m is plotted transparently, thus removing much of the noise of small scale changes, and highlighting areas where more significant changes occur. Long Sands appears to be the most active area in London Array, and within the bank the neck and the southern flank display the largest variability which agrees well with historical trends suggested by ABPmer (2007) and Burningham and French (2011). While, major areas of the crest

have proven largely stable over the examined period, the southern flank of Long Sands displays significant change, prograding in the central area (F13-G13, Fig 3.5C). Bed levels have increased by 4-8m in this area, representing lateral growth of approximately 120m. Towards the north along the bank margin some progradation of 0.5-1m is observed, likely associated with sea-ward movement of the bank. To the south of this area bed levels have decreased by up to 4m. These changes could be related with bank plan form change and east-ward migration, but would imply that the bank is not moving as a single coherent unit. Much of the crest of Long Sands has reduced in height by some 0.5-1.5m, whereas some localised accretion is found around the eastern slope of Foulger's Gat while the western slope has retreated, which seems to corroborate the directional readjustment of the swatchway as previously suggested. More variable patterns are observed at the neck of Long sands; however the gross changes are consistent with an east-ward movement of this area with net level gains on the east-facing slope. It is not clear what drives the described changes. Astley et al. (2014) have concluded that storm effects over the last 17 years have been ineffective in creating any morphological change at a wreck site in the Outer Thames. In recent times no events larger than 1:1 year return period have been registered and the large bank adjustments are orientated at right angles to the predominant wave (and current) directions, thus it appears unlikely that waves have been a significant agent of morphological change in the area.

In terms of internal sedimentary structure the bank deposits generally show seabed-parallel layering of granular deposits on the ridges. More interesting patterns are revealed on the flanks where inclined reflectors show progradational sequence as shown in Figure 3.6. This pattern of aggradation, in direction of the bank progradation, seems to lie discordantly on a package of granular sediment that makes up the sand deposit of Knock Deep. The layering seen on the seismic reflection appears to manifest itself as subtle changes in cone resistance of $1 - 2$MPa, as seen on the CPT. This discordance to the underlying sediment package is characterised by an increase in density of the sediment.

3.3.1.2 Kentish Knock

Kentish Knock is bordered by Knock Deep to the north-west and in the south-east drops off to -60mLAT. In the topographical context of this area, the bank acts as a refraction point to easterly and north-easterly waves which focusses waves onto the prominent indentation on the southern flank of Long Sands. Thus, during storm conditions, waves tend to induce the most change in that area as previously mentioned in section 3.3.1.1. Morphologically, the bank is understood largely stable but has been shifting slowly eastwards over time causing a widening of Knock Deep (ABPmer, 2007). Figure 3.5 shows that Kentish Knock has remained largely unchanged in recent years. The bank shows signs that are consistent with a slow east-ward migration; bed levels along the central and northern stretch of the channel-facing slope have reduced by some 1-2m. Overall crest level appear to have dropped by between 0.5-1m, but localised accretion is revealed on the ridge in the far south-east of the Knock.

As illustrated in Figure 3.7, the internal organisation of the sand banks is quite similar to the observations made for Long Sands. Orderly, parallel reflector patterns are typical,

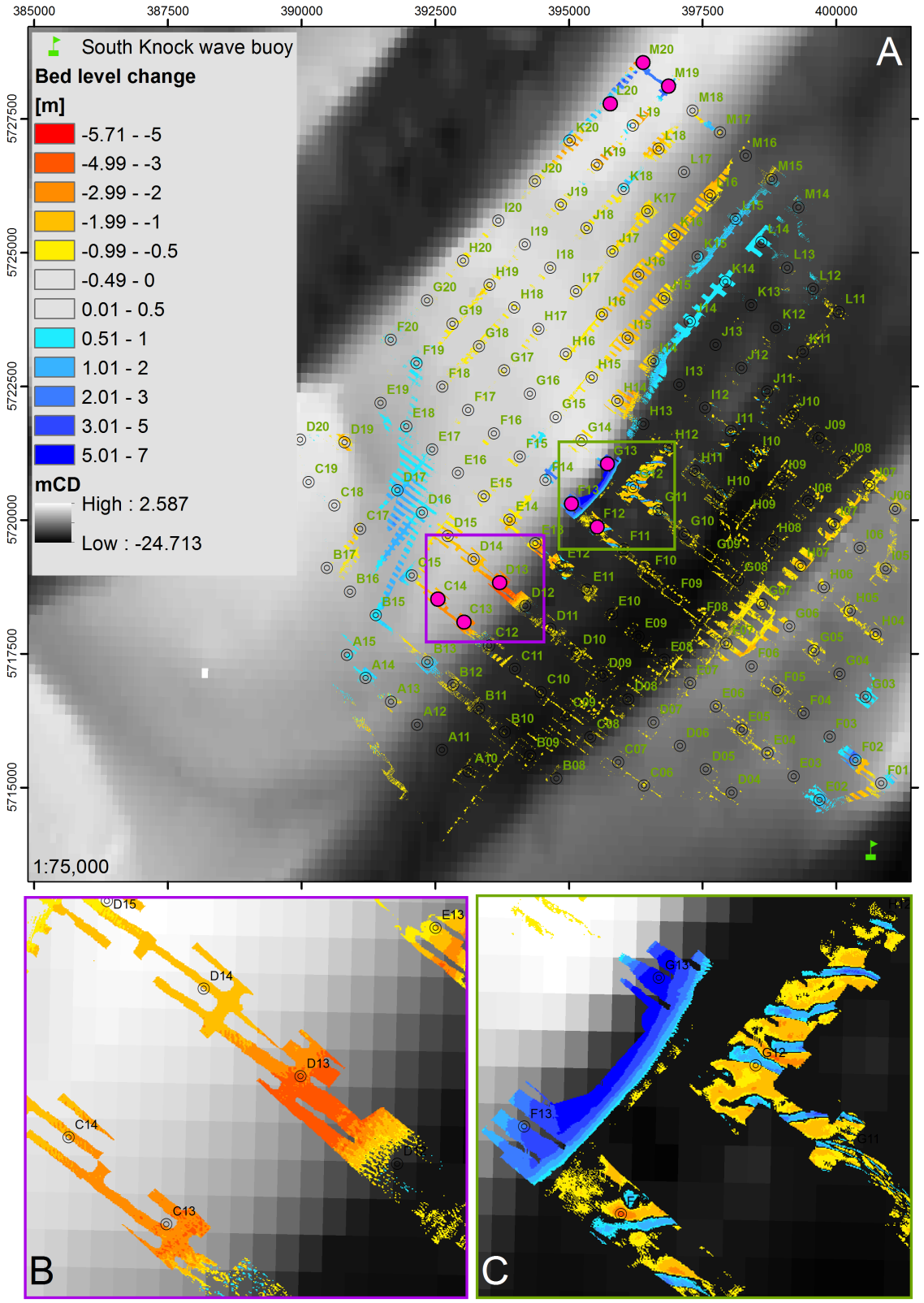

Figure 3.5: Natural change in sea bed levels between 2004 and 2011. Turbine locations with net bed level change greater than ±2m (see Table 3.3) highlighted in purple. Zoomed inset maps of areas of high change in panels B and C.

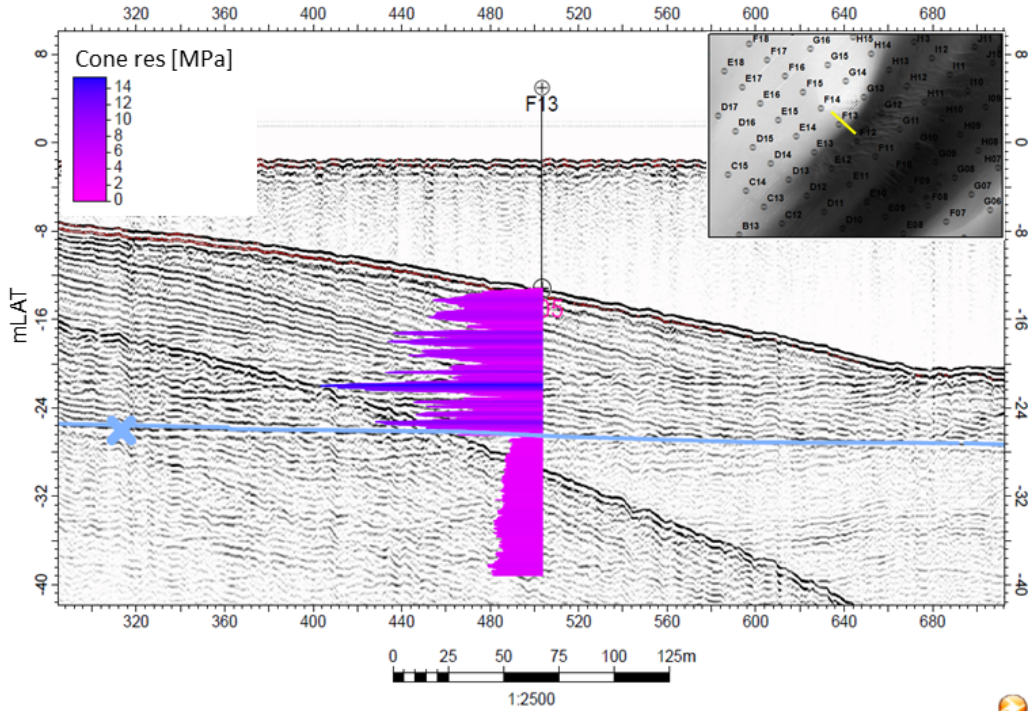

Figure 3.6: Progradational deposition patterns on southern slope of Long Sands, near turbine F13. Inset map shows location of seismic profile. Top of London Clay in blue. CPT record of cone resistance q_c in MPa.

even on the slopes. The progradational pattern described above, although locally present, is not so prolific on the northern slope of Kentish Knock, possibly because the topographical transition is more gradual. Again, the top layer of sediment lies unconformably on a more dense granular layer, which is clearly picked out as a package with higher cone resistance between 25-30MPa (very dense sediment) on the CPT record, while the top layer is generally loose to medium dense with q_c between $2 - 12$MPa.

3.3.1.3 Knock Deep

Knock Deep, while widening due to the east-ward migration of Kentish Knock, has retained fairly constant bed levels over time (ABPmer, 2007). In recent years, little variability of bed levels has been witnessed in Knock Deep although the general trend appears to be a deepening of the channel. Significant changes are limited to the northern side of the channel, particularly in the central area, where larger sand waves are passing through causing temporary bed elevation changes up to 2-3m as shown in Figure 3.5C.

A seismic profile from southern Knock Deep is shown in Figure 3.8. The top of London Clay is indicated in blue. Generally, the London Clay horizon is undulating but fairly constant over the study area. In the southern section however, between foundation rows B and C, the seismics show the top of London Clay dipping fairly rapidly by some 20m towards the south-west. The depth of clay on both sides of the dip has been corroborated in CPT records as exemplified by the plotted record of friction ratio R_f, which increases by a factor of circa 5 in the London Clay. This slope can be followed across the site in an NW-SE direction and is assumed to be the bank of a 1.5km wide palaeochannel the location of which is shown in the inset map in Figure 3.8. The seismic signal in the

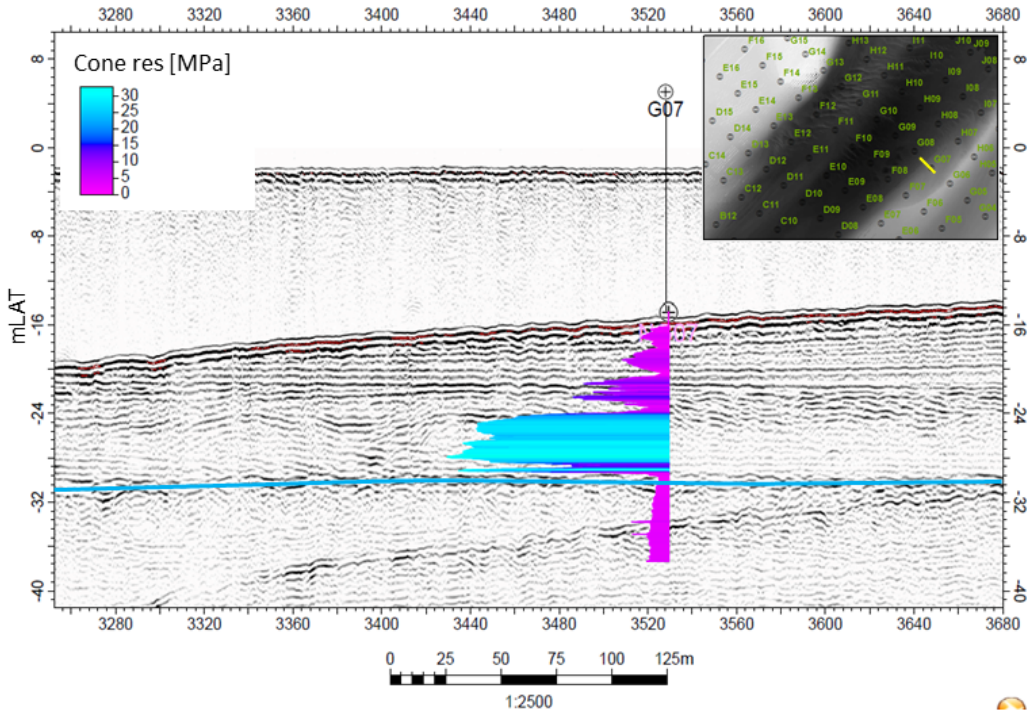

Figure 3.7: Seismic profile on northwest-facing slope of Kentish Knock near turbine G07. Top of London Clay in blue. CPT record of cone resistance q_c in MPa.

granular zone is generally seabed-parallel reflectors suggesting layering of deposits but no particular internal organisation or structure of the granular deposits is observed and this is generally the case for seismic profiles in Knock Deep.

3.3.1.4 Bed level change at foundation locations

Due to the considerable natural morphological activity of the site, especially at Long Sands, it is important to understand which turbine foundations are located in active areas and where scour might be enhanced or abated by ambient morphological change in the long term. The bathymetric variation at each turbine location was calculated for the bathymetric surveys of 2004, 2007, 2010 and 2011. Table 3.3 identifies the foundations with net bed level changes greater than ±2m between 2004 and 2011. Unsurprisingly, the data in Table 3.3 effectively cluster around the neck and eastern flank of Long Sands. Three areas can be identified (Fig 3.5A). Prograding sites at F13, G13 and to a lesser extent L20, M19 and M20; eroding sites at C13, C14, D13 and sites where morphological change is driven by bed form migration (F12, G12). Repeating the analysis to calculate the *cumulative* bed level change instead of *net* change points to the same areas as the most morphologically active.

3.3.2 Bed forms and sediment mobility

The bed forms in the vicinity of turbine foundations were evaluated using a quantitative bed form analysis technique (Section 2.2.4.2). The height, wave length and orientation of crest normal of the seabed features in the area of each turbine foundation is plotted in Figure 3.9. The sediment transport direction has been inferred from the asymmetry of bed

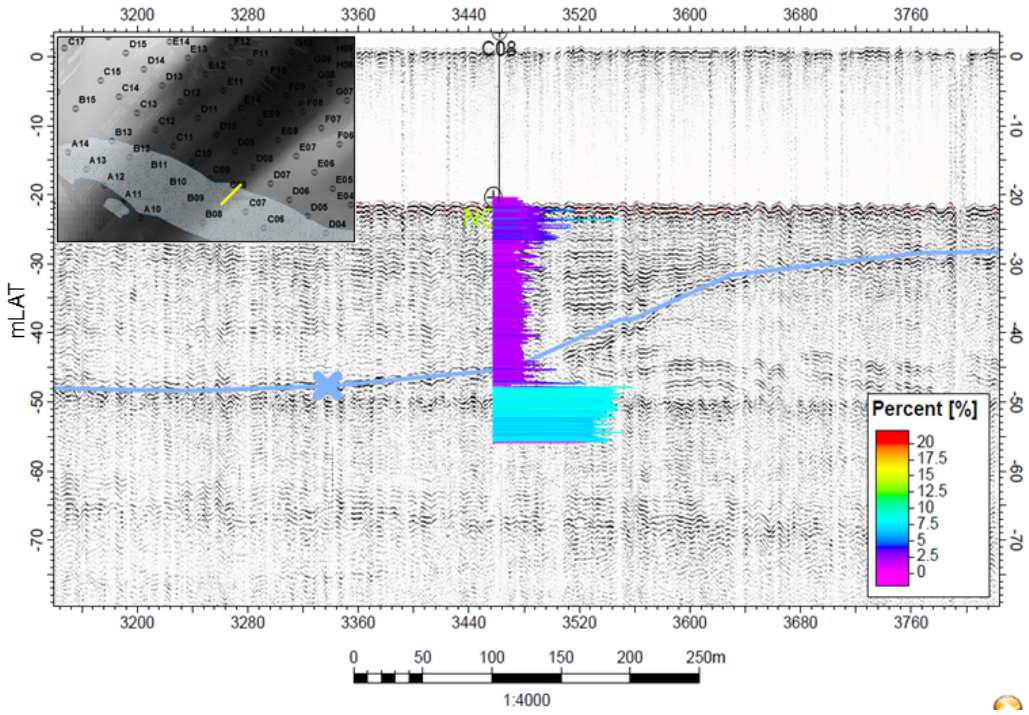

Figure 3.8: Seismic profile in Knock Deep near turbine C08. Top of London Clay (blue) dipping away in southern Knock Deep where the palaeochannel incised. CPT record of friction ratio R_f in [%]. Location of palaeochannel is shown on inset map.

Table 3.3: Monopile locations with largest net bed level changes from 2004 to 2011

ID	Trend	Magnitude [m]	Location
G13	△	+6.42	South flank of Long Sands
D13	▽	−3.28	South flank of Long Sands
F12	▽	−3.24	Knock Deep
M20	▽	−2.98	Neck of Long Sands/Western flank of Long Sands
M19	△	+2.94	Neck of Long Sands
F13	△	+2.69	South flank of Long Sands
C13	▽	−2.55	South flank of Long Sands
L20	▽	−2.40	Neck of Long Sands
C14	▽	−2.30	South flank of Long Sands

forms and the proposed residual tidal sediment transport from numerical simulation (Carrizales, 2010) is shown for comparison. A summary schematic of the sediment transport patterns is shown in Figure 3.10 which includes bed level change, sediment and flow information. The classification system of Ashley (1990) is used to standardise nomenclature and describe bed forms.

Knock Deep Transport directions inferred from the QBA suggest a fairly simple pattern of uniform south-westerly migration of sediment in Knock Deep. Transverse bed forms in the flood-dominated channel range from small megaripples that occur parasitically on the upstream side of large sand waves, or as bed forms in their own right to large sandwaves. The megaripples typically show 3-10m wave lengths and on the order of tens of cms high. Bathymetric surveys are temporally too far apart to confidently identify the position of these smaller bed form crests on consecutive surveys thus the migration rate of these features is uncertain. Large sand waves in central Knock Deep show vertical dimensions of 1-2m and wave lengths $\lambda = 30 - 40$m; however can reach up to 3m height

with irregular $\lambda = 100 - 300$m. These large sand waves appear to be migrating at a rate of approximately 3-10m/year based on the movement of wave crests on consecutive surveys. The only deviation from the south-westerly transport trend is observed along the northern flank of Kentish Knock where megaripple crests suggests north-westerly transport. This could be explained due to the local dominance of the ebb tide as described in Section 3.1.

Sand banks More complicated patterns are observed with the bed forms on the sand banks. Although obscured by significant scatter, a clockwise pattern of sediment transport is discernible on the sand banks (see Figure 3.10). This is understood to be the result of highly variable, multi-directional flows (Sturt et al., 2009) and flow re-circulation on the sand bank as illustrated by the change in bed feature crest orientation in Figure 3.9. This clock-wise pattern is also observed with the tidal residuals suggesting that even in shallow water the tide is the main effector of sediment movement. At Kentish Knock, bed form asymmetry indicates a south-westerly migration in the southern part of the Knock and a north-west to north-north-easterly direction in the northern area. The orientation of crest normals shows good agreement with the pattern suggested by the tidal residuals. Bed features on the Knock are mainly megaripples. Comparison of crest orientations from bathymetric surveys have revealed that the crest orientations are not constant. Bed forms become less pronounced and less well-defined as one moves south-east on the Knock. In the southern part of the Knock, where turbines will be situated in Phase 1, the seabed formations are about 0.5-1.0m high with $\lambda = 10 - 30$m.

The bed forms on Long Sands are mostly confined to megaripples and small sand waves. Megaripples are found on the crest of the sand bank. The height of the bed forms is between $H = 0.2 - 0.5$m with $\lambda = 10 - 35$m. Somewhat larger features are observed locally across the northern part of the bank with heights of 0.6-0.8m. On the southern flank sand waves with crest heights of up to 1.5m and $\lambda = 40 - 60$m are found. While the crest normals of these megaripples show more intricate patterns, ie. south-westerly in the northern bank and clock-wise rotating in the southern bank, the sand waves conform to the overall south-westerly transport pattern, possibly because they are in deeper water. In the northern area of Long Sands and along the western margins, the sediment transport directions inferred from the asymmetry of bed forms shows some deviation from the pattern suggested by the numerical tidal residuals. An increase in the effect of north-easterly waves on sediment movement is a likely explanation of this observation. As shown in Figure 3.5 significant bed changes are witnessed in the area of Foulger's Gat and the south-east-facing flank of Long Sands. The latter does not appear to be related to bed form dynamics as along a line from C13 to G13, the area is devoid of any bed forms. Although related to the offshore migration of the banks, the exact driver of this wholesale morphological change in cross-tidal direction is unknown. There appears to be a conflict between ambient sediment transport direction, gross bank changes and the wave and tidal flows. Similarly, the bed level fluctuations at the neck of Long Sands do not appear to be related to bed forms. At Foulger's Gat bed levels have increase by up to 2m which could be a result of the re-circulation of sediment and deposition in the deeper areas of the Gat.

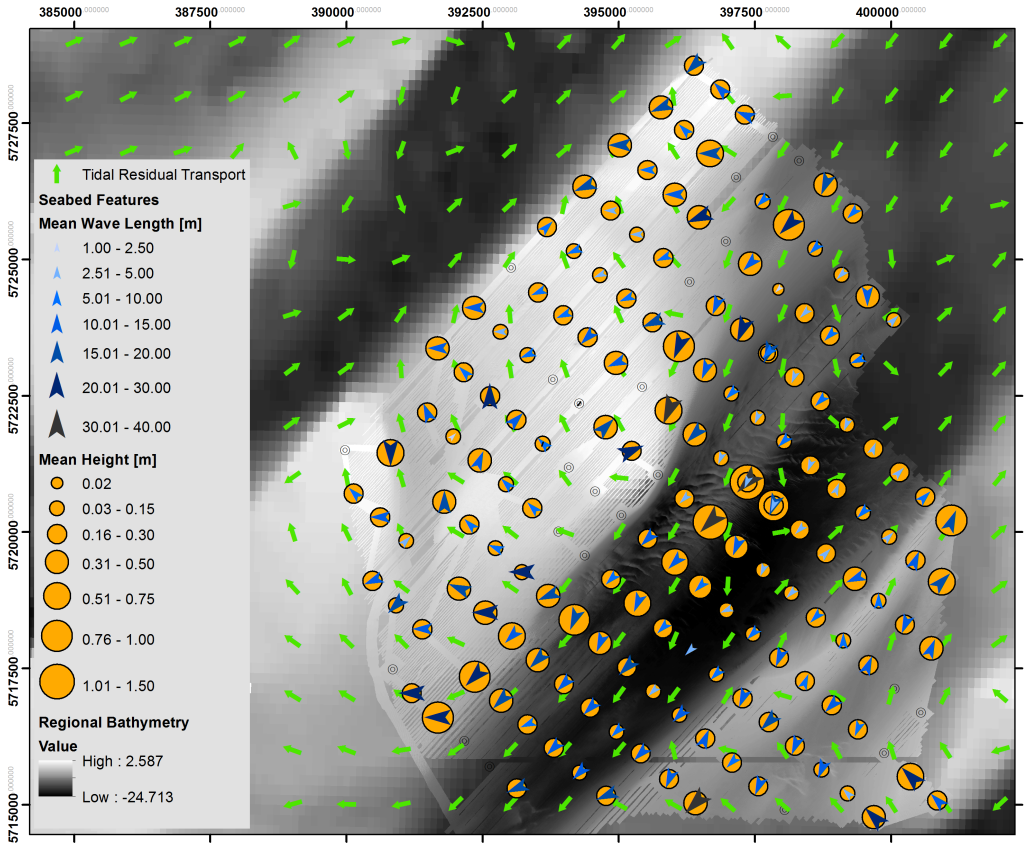

Figure 3.9: Results of quantitative bed form analysis showing mean wave length λ and height H. Sediment transport directions inferred from bed form asymmetry.

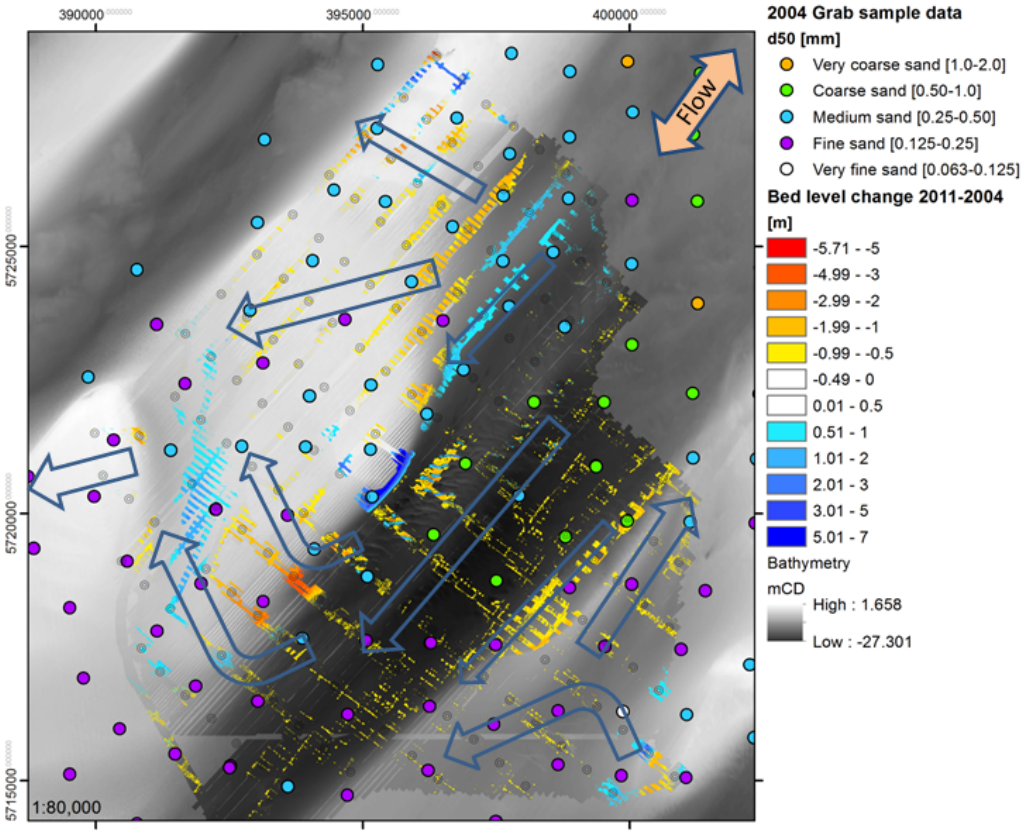

Figure 3.10: Schematic representation of sediment transport direction inferred from the bed form asymmetry (blue arrows), natural bed level change between 2004 and 2011 and surface sediment median grain size. Tidal flow direction marked by orange arrow.

Table 3.4: Statistics of scour dimensional parameters by topographical entity at London Array wind farm.

		S/D	A_S/D^2	V_S/D^3	S [m]	A_S [m^2]	V_S [m^3]
All	Min	0.21	7.9	0.6	1.20	256	119
	Max	2.02	196.1	77.7	9.50	5013	8590
	Mean	1.22	48.0	15.4	6.21	1376	2287
	σ	0.44	38.4	16.4	1.92	952	1927
Long Sands	Min	1.03	19.9	4.8	4.97	439	703
	Max	2.02	154.3	77.6	9.50	5013	8590
	Mean	1.53	77.7	28.3	7.38	2034	3849
	σ	0.20	38.4	19.5	0.92	1119	2595
Knock Deep	Min	0.21	7.9	0.6	1.20	256	119
	Max	1.43	88.4	25.7	8.14	2874	4760
	Mean	0.77	28.5	7.4	4.37	926	1378
	σ	0.30	18.2	6.0	1.72	593	1115
Kentish Knock	Min	0.80	14.9	3.1	4.56	485	575
	Max	1.92	196.1	77.7	9.04	4332	8067
	Mean	1.37	74.8	25.8	7.09	2007	3428
	σ	0.29	44.3	19.4	1.07	923	1724

3.4 Scour at London Array offshore wind farm

The following section discusses the scour observed from prototype monopile foundations at London Array. For the scour analysis, data from two post-installation surveys were available, one dating from 2012 and another from 2013. The 2012 survey covers all foundation sites and connecting cable routes and survey areas often overlap at foundations so that usually two surveys per foundation are available. The time between these overlapping surveys can vary greatly from the same day to more than 250 days apart, although the elapsed time is not always known or reliable due to missing or uncertain survey dates. Furthermore, the spatial extent of surveys at individual turbines does not always encompass the entire scour at the foundations, which made areas of the survey unusable for parts of the analysis where full coverage of the scour pit is required (eg. area, volume, shape). In 2013, a sub-set of 57 monopiles, primarily in Knock Deep, was surveyed with a more generous spatial coverage per turbine. Again, some foundations were surveyed twice with intervals of mostly 0-1 days. Although large parts of the 2012 data are not suitable for a full scour analysis (ie. calculation of all 7 scour hole descriptors as outlined in Section 2.4) due to restricted extents of the surveys, the coverage of the near-foundation area allowed a maximum scour depth value to be determined for every foundation at London Array. Between the 2012 and 2013 survey, the deepest scour at each foundation was determined which generally, but not always, coincided with the most recent survey, ie. 2013. To complete the analysis and determine the remaining six descriptors a suitable subset of data was employed which consists of data that covered the entire scour extent, regardless of survey year. The reduced "full coverage" data set consists of a total of 80 locations, of which 12 are located on Long Sands, 21 on Kentish Knock and 47 in Knock Deep. The reporting of scour depths follows the definitions given in Section 1.3.1.

3.4.1 Scour dimensions

The distribution of scour depths, area and volume is illustrated in Figure 3.11 and dimensional statistics are shown in Table 3.4 for the entire site and for the three main

topographical features Long Sands, Knock Deep and Kentish Knock. Separating the data by topographical entity aims to tease out the effect of varying substrates, if existing, in the interpretation of the scour data. The scour dimensions are given in absolute magnitudes to give the reader an appreciation of real magnitudes and in non-dimensionalised form to facilitate comparison with existing data. The distribution of scour depths reveals a distinct pattern, suggesting that scour depth varies by topographical entity, with considerably larger scour on the sand banks compared to the intervening channel. This is confirmed when the scour dimensions are plotted against relative water depth h/D in Figures 3.12 to 3.14, especially for scour depth S/D. Also, there appears to be a tendency for scour to increase from north-east to south-west, particularly in the channel. A large range of scour depths is observed over the wind farm site, with the smallest $S/D = 0.21$ (S=1.20m) in northern Knock Deep and the largest $S/D = 2.02$ (S=9.50m) on southern Long Sands. The observed values are both significantly deeper and shallower than what is expected using current standard theory ($S = 1.3D$) recommended by Det Norske Veritas (2013) and implies that not enough is known about scour in the prototype setting. The notion of the distinctly different character of scour between the sand banks and the channel is supported by the average scour depths for the three topographies which reveal that scour is greatest on Long Sands $S/D = 1.53$, closely followed by Kentish Knock $S/D = 1.37$ and Knock Deep $S/D = 0.77$. A very similar pattern is observed for scour area and volume. While the mean dimensionless area and volume are of similar magnitude on the sand banks with A_S/D^2 of 77.7 and 74.8 on Long Sands and Kentish Knock, respectively, and V_S/D^3 of 28.3 and 25.8 (see Table 3.4), the two parameters are smaller in the channel by a factor of 2.5 for area and 3.5 for volume. Interestingly, although displaying greatly varying scour dimensions, over the entire site there is strong correlation between S/D and area A_S/D^2 (Figure 3.15, left) and volume V_S/D^3 (Figure 3.15, right). This logarithmic relationship seems to suggest that in smaller scour holes the area and volume are dominated by the main scour hole, typically characterised by the idealised shape of an upturned conical frustum, whereas in larger scour holes, the area and volume grows without as much vertical erosion.

3.4.2 Scour morphology

The dimensionless length and width of the scour holes is plotted in Figure 3.16. This plot also reveals the orientations, relative to °N, of the long and short axis. Unsurprisingly, the pattern for these measures is similar to that of the scour area, with more confined scour holes in the channel. The width of the scour holes W can vary between $3 - 14D$ (approximately 18-70m) over the site, with an average of $6.7D$ (see Table 3.5). The widest scour pits are found on the sand banks with average $W/D = 8.64$ for Kentish Knock and $W/D = 8.67$ for Long Sands, whereas in the Deep they are considerably smaller with $W/D = 5.31$. Over the site the scour hole length L ranges between $3.5 - 19D$ (approximately 20-105m). The longest scour holes are again found on the sand banks. The lower end of the observed W agrees very well with the predictions based on assumed S and ϕ carried out in Section 1.3.1.3, which resulted in a spread of values between $3.05 - 7.54D$. Clearly, more laterally extensive scour holes than the largest forecast W have been observed

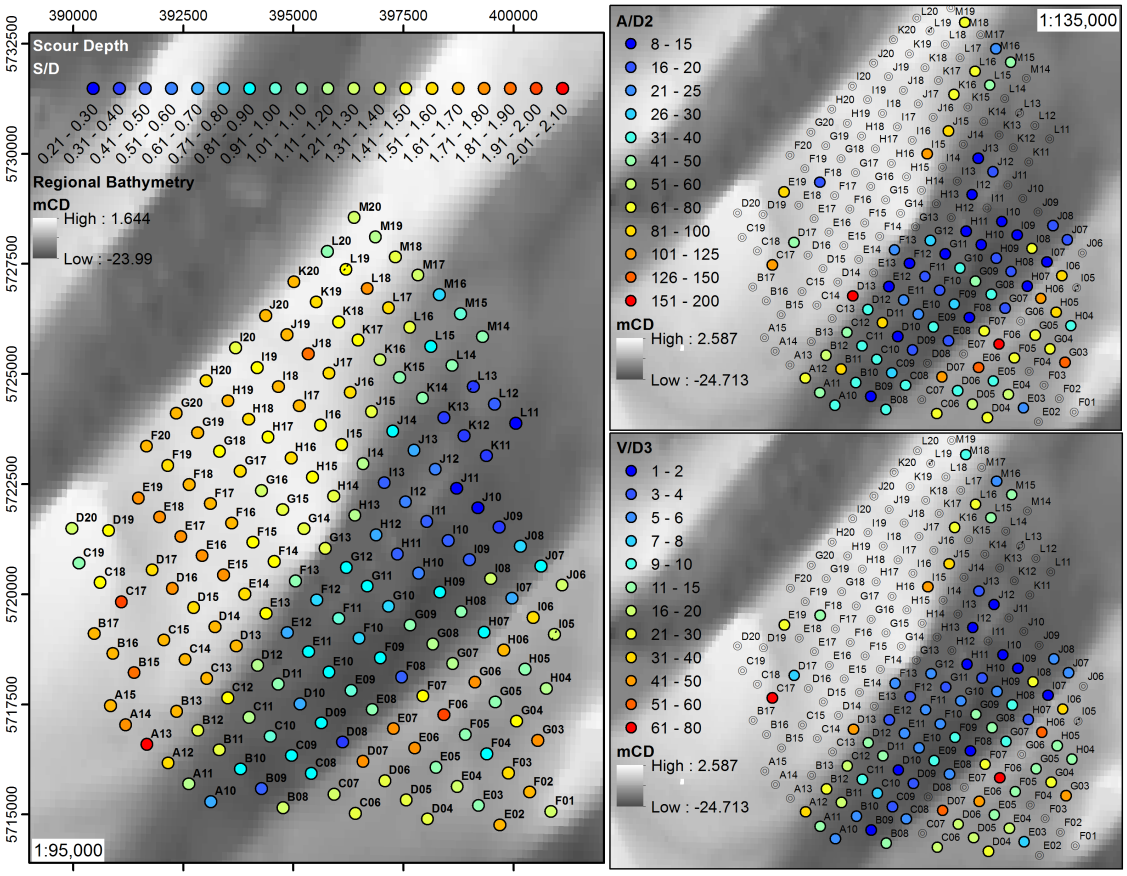

Figure 3.11: Distribution of scour depths S/D (left), areas A_S/D^2 (top right) and volumes V_S/D^3 (bottom right) at London Array wind farm.

at London Array. The mean observed W here exceeds the previous observation of $4-5D$ from wind farm turbines in sandy beds suggested by Whitehouse et al. (2011). The scour hole lengths at London Array are both more confined and extensive than the predicted $5.44-9.30D$ in Section 1.3.1.3, indicating the horizontal scour dimensions might evolve independent of sediment properties (eg. angle of repose ϕ), a notion previously advocated by Harris et al. (2011) in morphologically active areas.

The orientation of the long axis α_L (as defined in Section 1.3.1.3) reveals an interesting picture in Figure 3.16. From experimental knowledge, it would be expected that the long axis would be aligned with the predominant flow direction, ie. north-east to south-west. For foundations on the sand banks, the long axis appears to be aligned with the general flow axis, bearing in mind the somewhat more chaotic flow pattern on the banks as illustrated in Figure 3.9. Where the lee-wake scour is pronounced, resulting in larger $L/D > 14$, the long axis is aligned N-S on the banks as illustrated at foundations F06 and C17 in Figure 3.17C and 3.17D. That said, particularly on Long Sands too few data points are available to make generalised statements. In Knock Deep, the long axis is found to be predominantly transverse to the tidal flow axis. There seem to be two main reasons for this observation. The high-voltage inter-array cables are generally aligned in a flow-transverse manner in Knock Deep and scour has caused the cables to be free-spanning near the foundations which has facilitated scour along the free span shoulder some distance along the cable, thus creating a scour hole that is elongated in a flow-transverse direction (see A10, Fig 3.17A). The constriction of scour holes by bed forms can also cause the long axis

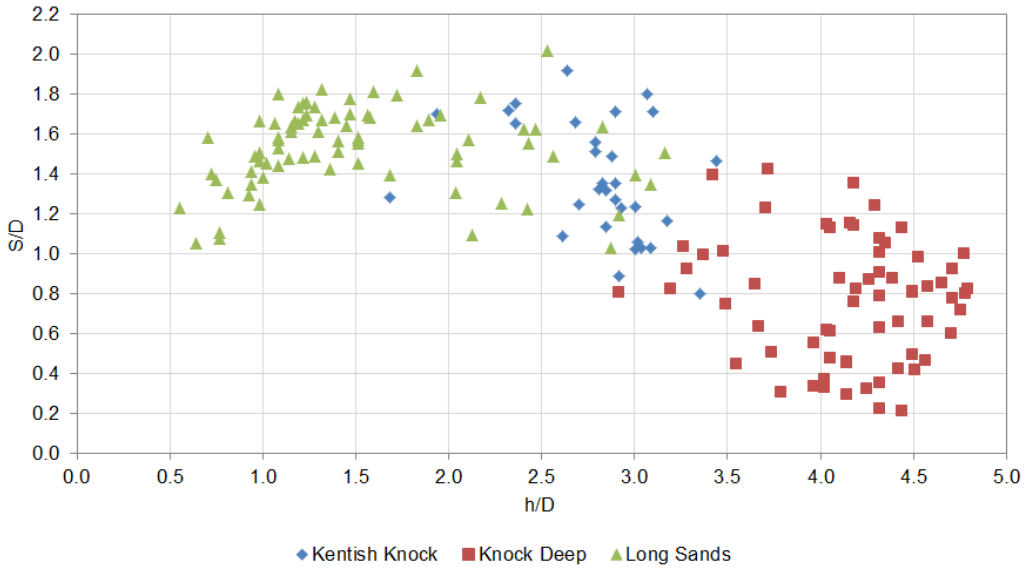

Figure 3.12: Observed scour depth S/D as a function of mean relative water depth h/D at the topographical entities at London Array.

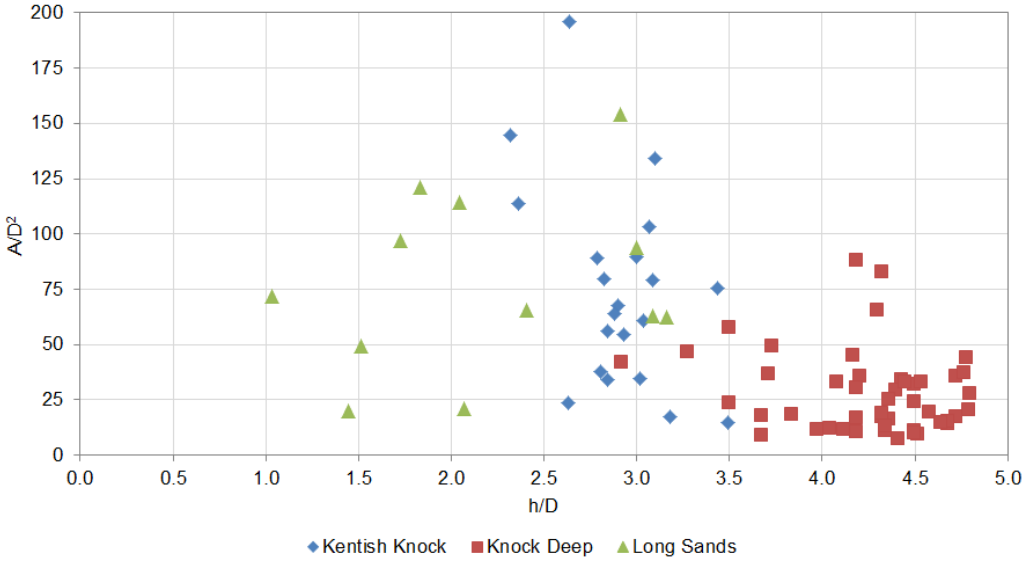

Figure 3.13: Observed scour depth A/D^2 as a function of mean relative water depth h/D at the topographical entities at London Array.

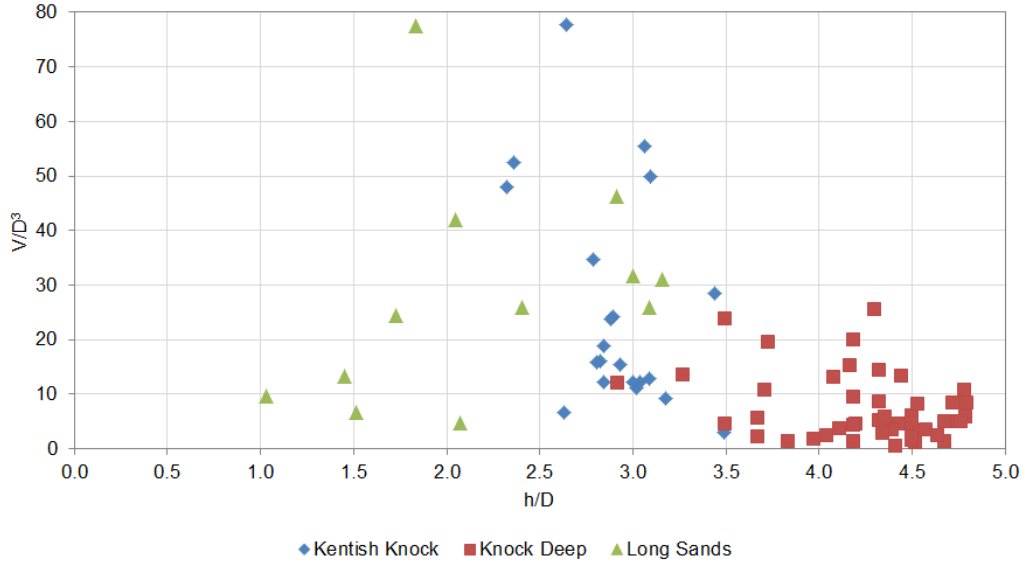

Figure 3.14: Observed scour depth V/D^3 as a function of mean relative water depth h/D at the topographical entities at London Array.

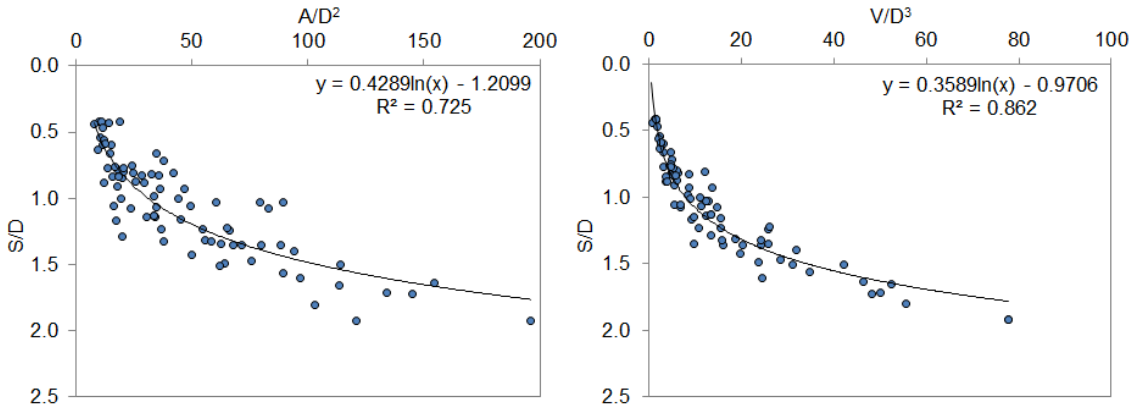

Figure 3.15: Relationship between scour depth S/D and area A_S/D^2 (left) and scour depth and volume V_S/D^3 (right).

Table 3.5: Statistics of morphological scour parameters by topography at London Array wind farm.

		W [m]	W/D	L [m]	L/D	L/W	IQ	α_L	β_{av}
All	Min	18.13	3.18	20.39	3.58	1.02	0.51	-89.1	7.5
	Max	67.32	13.92	104.29	18.85	1.97	0.98	84.0	30.8
	Mean	36.39	6.69	46.81	8.61	1.29	0.81	-9.5	16.1
	σ	12.50	2.57	17.32	3.54	0.20	0.12	47.0	5.3
Long Sands	Min	23.56	4.84	24.97	5.31	1.06	0.51	-89.10	8.84
	Max	67.32	11.81	104.29	18.30	1.66	0.92	79.0	30.8
	Mean	44.27	8.67	59.76	11.70	1.32	0.79	2.6	15.3
	σ	11.08	2.06	20.25	3.81	0.17	0.10	43.9	5.2
Knock Deep	Min	18.13	3.18	20.39	3.58	1.02	0.51	-89.10	8.84
	Max	60.83	10.67	71.60	12.56	1.87	0.98	84.03	28.63
	Mean	30.29	5.31	39.45	6.92	1.30	0.80	-21.72	17.00
	σ	9.31	1.63	13.20	2.32	0.20	0.12	46.42	5.32
Kentish Knock	Min	18.59	3.26	32.97	5.78	1.02	0.54	-78.93	7.47
	Max	65.41	13.92	88.60	18.85	1.97	0.95	79.55	7.47
	Mean	45.54	8.64	55.91	10.62	1.25	0.84	10.78	14.40
	σ	11.35	2.55	14.79	3.41	0.21	0.12	40.92	4.83

to align itself parallel to the bed form crests which themselves are oriented at right angles to the flow. Due to the configuration of bed forms and cables in parallel both processes can occur simultaneously at a single foundation (D11, Fig 3.17B). Additionally, the scour holes in Knock Deep are relatively confined, thus the length of the long and short axis are very similar and a small asymmetry can result in flow-transverse alignment of the long axis. Examples of elongation at right angles to the predominant flow are shown in Figure 3.17A and B.

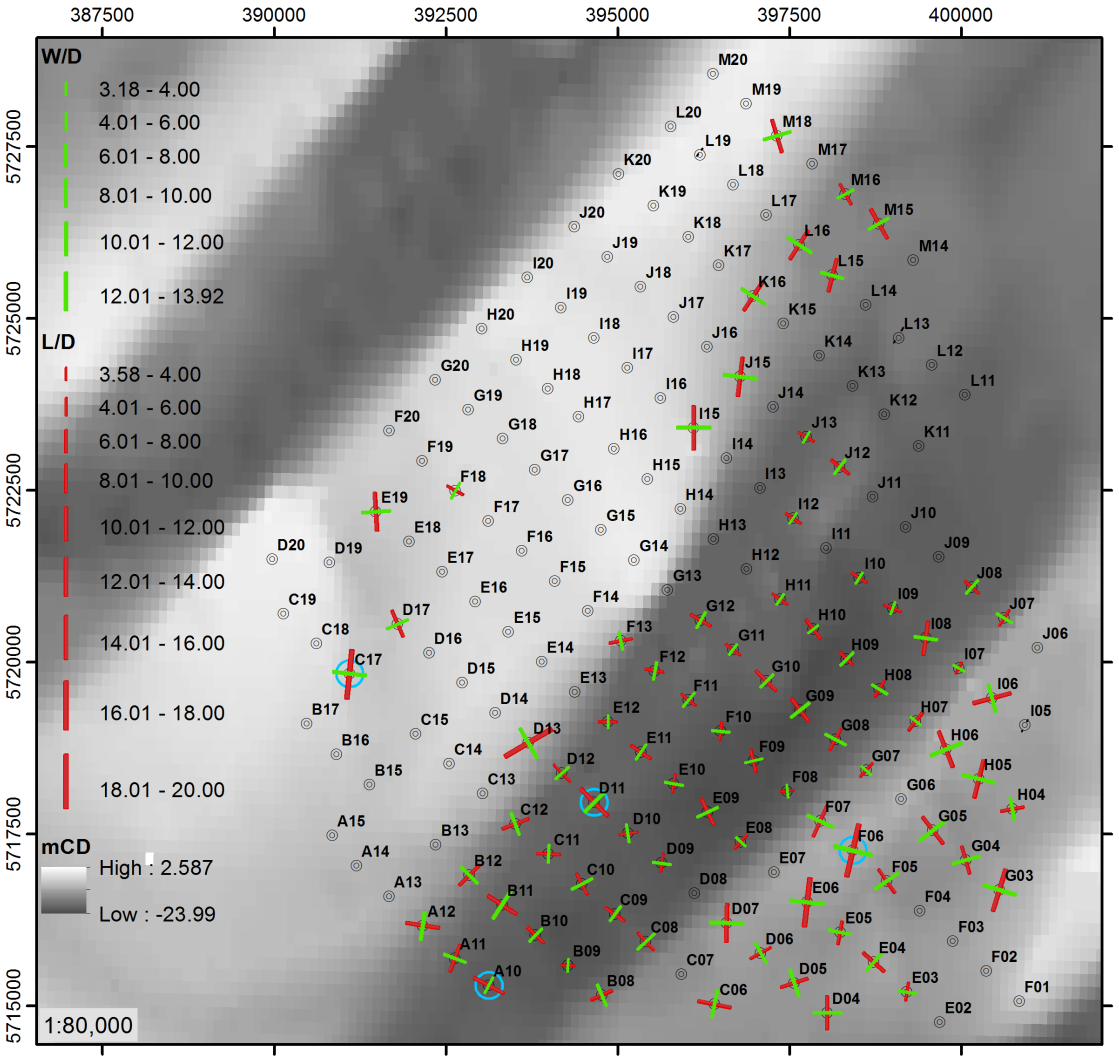

Figure 3.16: Scour hole length L/D and width W/D and orientation of long and short axes. Location of examples in Figure 3.17 marked as blue circles.

The distribution of morphological descriptors IQ and L/W around the site is plotted in Figure 3.18. In contrast to the pattern of scour dimensions, no particular discrimination relating to topography can be established. The statistics for the shape parameters are similar over all three topographical areas (see Table 3.5). The plots show that typically, the circularity of scour pits is $IQ \geq 0.8$, indicating less than 20% deviation from a perfect circle. Similarly, the average ratio $L/W = 1.29$ ($\sigma = \pm 0.2$) which suggests that the dimensions of long and short axis are fairly similar over the whole development. Nevertheless, the plots reveal that scour hole morphology can vary strongly, over short distances. The maximum deviation from the circular shape is found on Kentish Knock. Using the morphological characterisation plot based on IQ and L/W, the approximate shapes of scour pits present

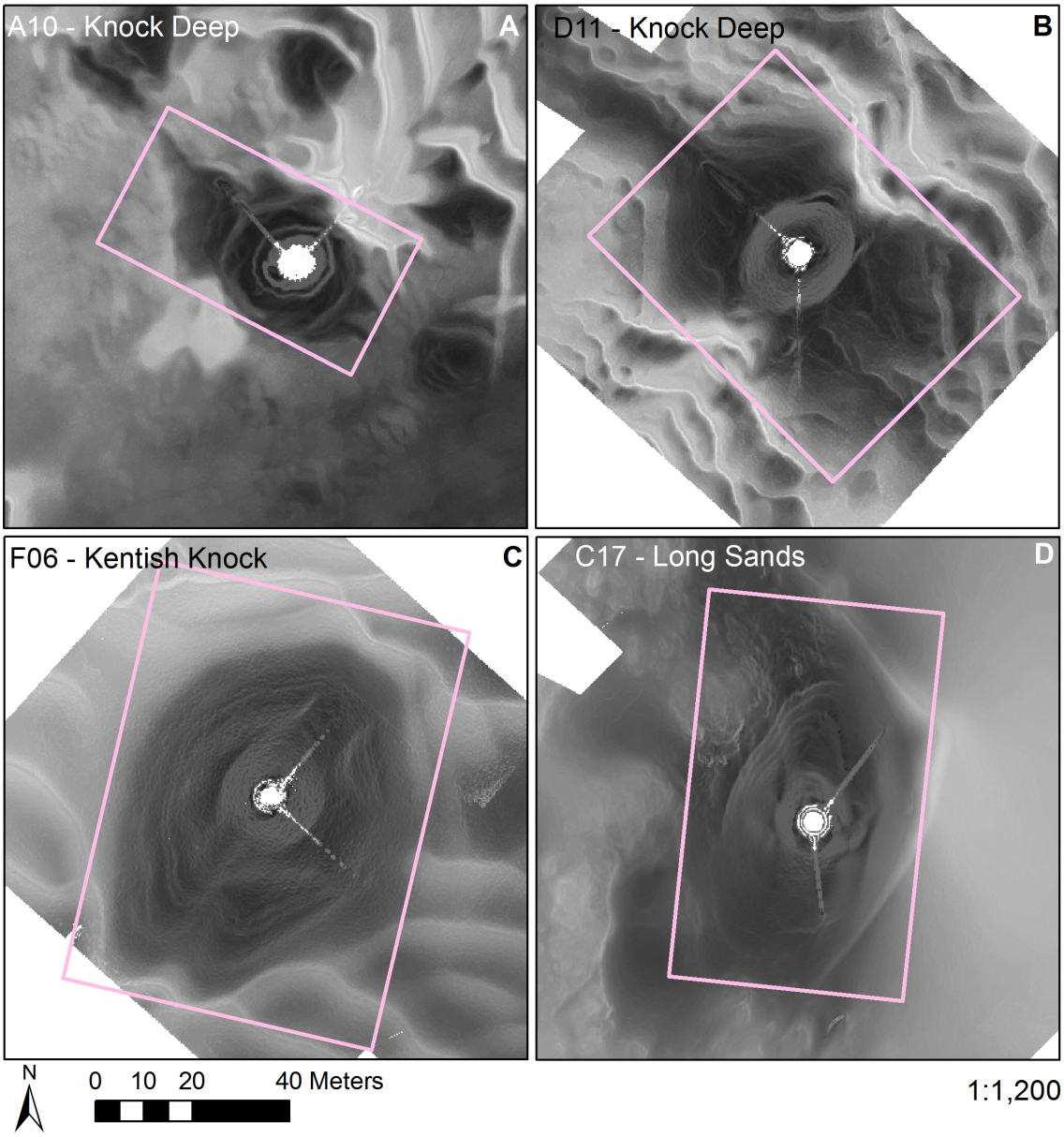

Figure 3.17: Examples of typical long and short axis orientations in Knock Deep (A:A10, B:D11) and on the sand banks (C:F06, D:C17).

at London Array wind farm can be identified. Figure 3.19 reveals that, although a wide range of shapes are observed, the majority of scour pits conform to a generally circle-type shape with $IQ \geq 0.8$ and $L/W \leq 1.4$. Examples of common scour pit shapes on the sand banks and channel are discussed below.

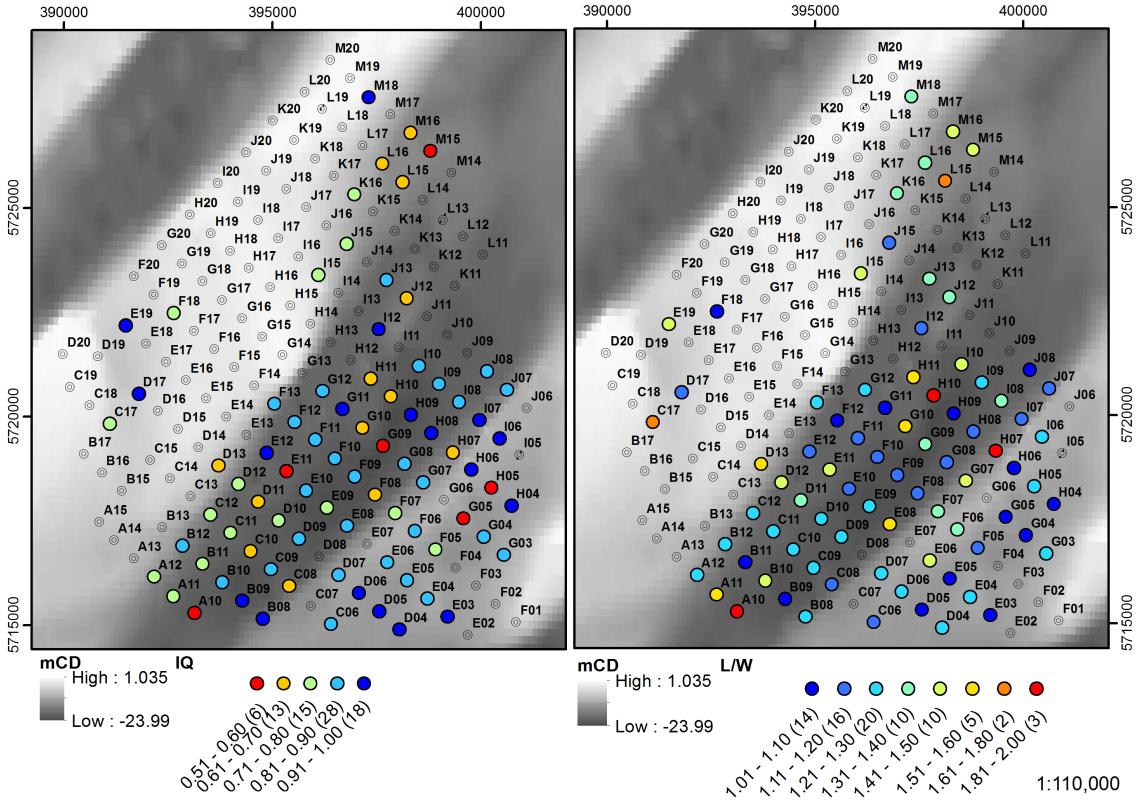

Figure 3.18: Distribution of isoperimetric quotient IQ (left) and long-short-axis ratio L/W (right) at London Array wind farm.

Due to the limited number of scour pits that are covered in their entirety by the bathymetric survey on Long Sands it is difficult to describe typical pit morphologies and the identified shapes might indeed not represent the entire breadth of morphologies present on the sand bank. As shown in Figure 3.19 the most commonly recurring shape is the modified circle. This is also confirmed by the average L/W and IQ values of 1.3 and 0.79, respectively. The other recurring shape is uni-directional with two wake limbs. Examples of the two common morphologies are shown in Figure 3.20. The uni-directional shape shows directionally preferential axial elongation with discernible wakes; however long wakes are rare. The modified circle shows a serrated edge which is observed at a large number of scour holes on Long Sands; however the origins of this phenomenon are not clear.

In Knock Deep, the shape of the scour holes is overwhelmingly near-circular with a mean of $IQ = 0.80$, i.e. merely a 20% deviation from perfect circle and a low average long to short axis ratio of $L/W = 1.30$ (see Table 3.5). Three typical scour shapes are observed in Knock Deep: scour holes with uni-directional wake features, which appear to preferentially develop in the south-western part of the Deep, circular scour pits that have little or no wake and scour patterns that bear evidence of more bidirectional flows. Figure 3.21 shows examples of the three types of scour hole encountered with shape parameter values IQ and L/W. The uni-directional pattern shows a prominent two-limbed

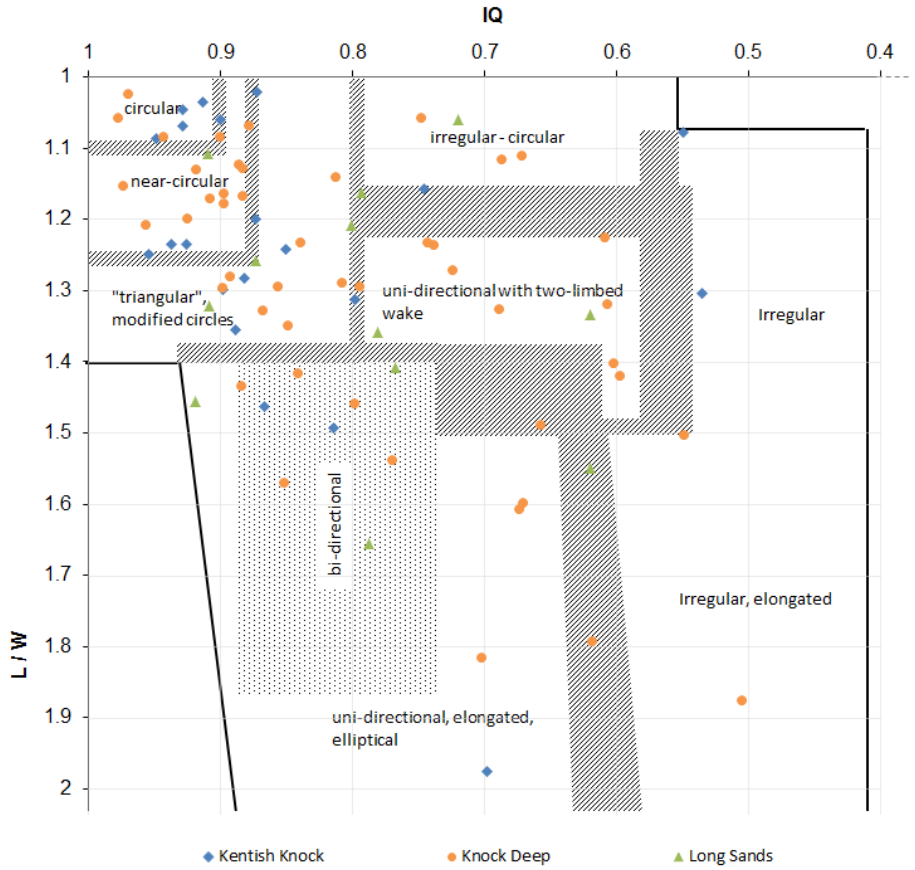

Figure 3.19: Classification of scour hole shapes at London Array.

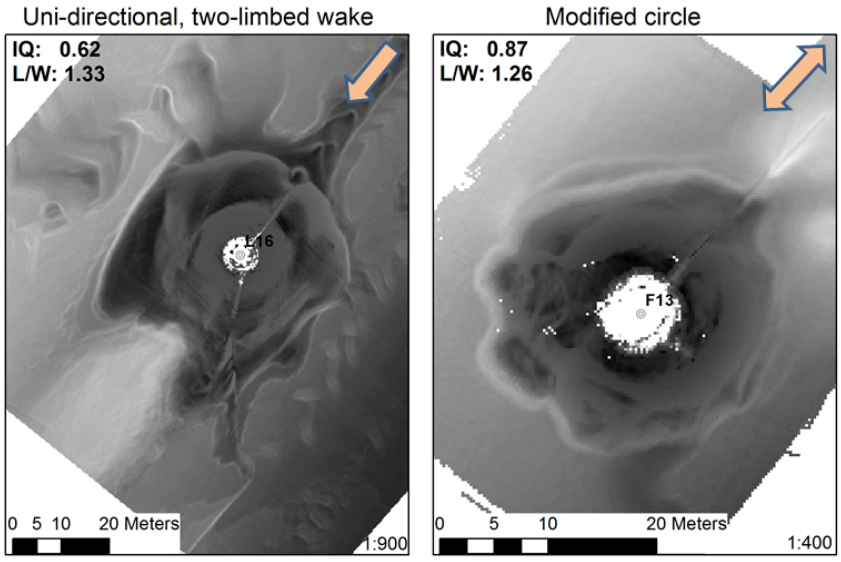

Figure 3.20: Typical scour patterns on Long Sands and arrow of dominant flow direction. Visualised as greyscale partially transparent bathymetry overlying slope plot. Foundation L16 (left) and F13 (right). For visualisation methods see Section 2.3.

wake with deposition area. Due to the wake, the IQ value is subdued at 0.75. However, as scour hole is quite wide the L/W ratio is not very high despite the presence of a wake. The downstream area around this type of scour is often characterised by the washing-out of bed features. Topographic wake impressions, where existent, are generally short and spatially limited. However, the modification of the turbulent flow-field at the structure can cause the bed forms to be washed out while no discernible seabed erosion occurs (e.g. B11 in Figure 3.21), implying a long hydrodynamic wake which while not causing appreciable erosion, does not allow seabed features to reform and is testament to the down-stream impact on the turbulent flow field. Scour holes that owe their shape to bi-directional flows show elongation along the tidal flow axis and both flood- and ebb-tidal deposition features. Despite showing a tidal pattern, one current can still be slightly dominant as exemplified in example E08 in Figure 3.21 by the weak asymmetry and the elimination of bed forms in the south-west of the pit suggest that the flood tide is still dominant in terms of the hydrodynamic impact. While the increased axial length results in a greater L/W, the IQ is only slightly reduced. The circular scour hole, shows no wakes and only very faint deposition areas either side of the pit to the north-east and south-west. It is not uncommon for circular scour holes to show depositional patterns in the absence of wake features. As such, the circular scour holes can be understood as sub-types of the bi-directional case where the extension along the flow axis has not developed, but are otherwise similar. In example G11, the scour pit is constrained by bed features. Circular holes often display bed forms in the ambient area, indicating they have not been wiped out by the modification of the flow due to the presence of the monopile. Both the IQ and the L/W are very close to unity.

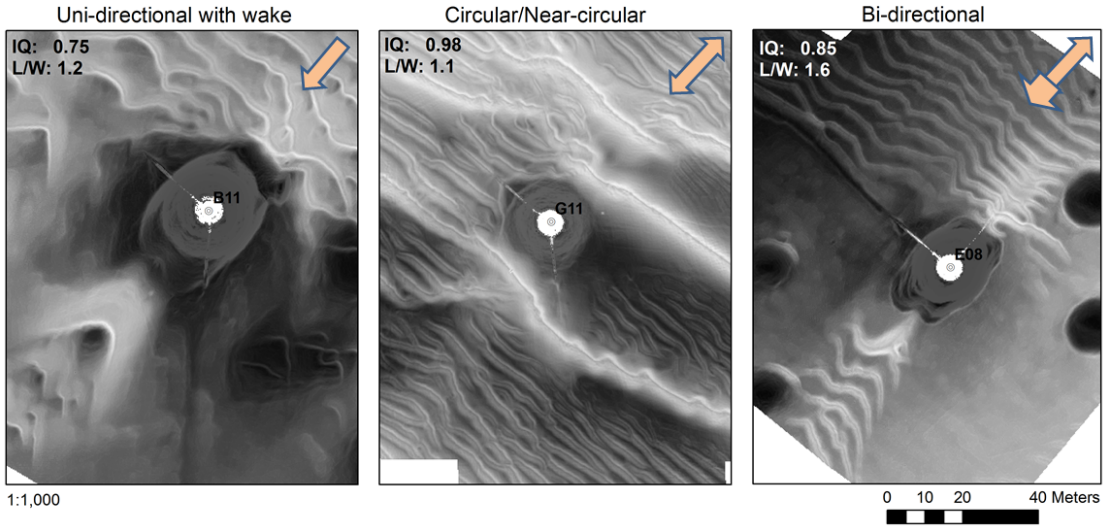

Figure 3.21: Three typical scour patterns in Knock Deep and arrow of dominant flow direction. Visualised as greyscale partially transparent bathymetry overlying slope plot. Foundation B11 (left), G11 (centre) and E08 (right). For visualisation methods see Section 2.3.

The L/W ratio is in line with the values observed at Long Sands and generally no strong asymmetry is observed. The most common found on Kentish Knock can be described as wide and near-circular. This is reflected in the median IQ value of 0.88 (see Table 3.5). Where forcings are more dominant from a particular direction, circle-type shapes morph into more elliptical patterns that generally display signs of bi-directional currents; however

one flow direction might be dominant. Lastly, there are a number of scour pits that display distinctly irregular shapes. The described scour patterns are exemplified in Figure 3.22. The elliptical or bi-directional patterns are more common near the northern flank of the Knock, while circle-type shapes appear throughout the Knock and are most common. There is a sliding scale between the near-circular and elliptical shapes as the difference is mainly just the elongation of the flow-aligned axis. Near-circular shapes have IQ and LW close to 1, while the deviation of particularly the L/W is higher for elliptical forms. The latter can display varying degrees of tidal dominance, from close to bi-directional elongation to somewhat uni-directional. The IQ is a good measure of the irregularity of the outline, as its drops to 0.54 for the misshapen scour hole. The perimeter to encompassed area ratio is much greater than for a perfect circle which causes a fall in IQ.

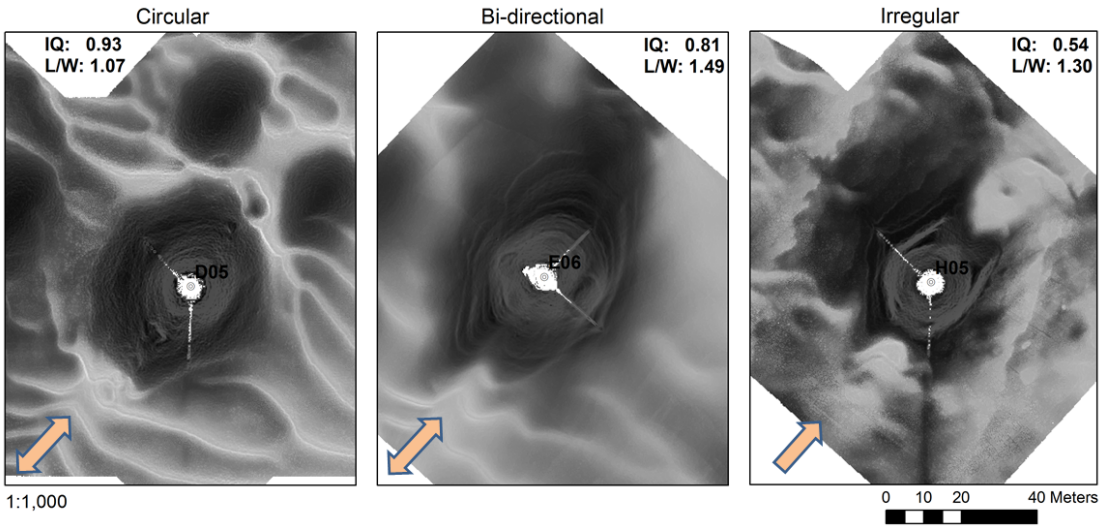

Figure 3.22: Three typical scour patterns on Kentish Knock and arrow of dominant flow direction. Visualised as greyscale partially transparent bathymetry overlying slope plot. Foundation D05 (left), E06 (centre), H05 (right). For visualisation methods see Section 2.3.

In Figure 3.23 the average scour hole slope range at London Array is shown to be between $7.5 < \beta_{av} < 30.8$. While the single representative slope angle is a function of the relative size of the steeper main scour hole and the surrounding shallower scour, the difference between the upstream and downstream slopes (as defined in Figure 2.32) has been found to be relatively limited at London Array. Upstream and downstream slope angles are similar in range to that put forward for β_{av} and the mean ratio of steep/shallow slope ratio is 1.3 with a spread from 1-2.8 (Figure 3.24). As discussed in section 1.3.1.3, slope angles in the flow axis are suggested to conform to ϕ on the upstream and $\phi/2$ on the downstream side, thus giving a range of $\beta_{u,av}$ between $26 - 45°$ and $\beta_{d,av}$ $13 - 23°$ (Hoffmans and Verheij, 1997). The distribution of the flow-aligned slopes in Figure 3.24 does not appear to follow this relationship as indicated by the similar range of slopes either side of the foundation and the mean slope ratio of 1.3. The ratio is a good indicator of directional flow dominance, since to shape varying slopes one flow direction must be stronger. Since most scour pits at London Array do not exhibit signs of strong directional dominance, as illustrated by the morphological parameters, the variance between slope angles along the flow axis is low.

The range of slope angles observed at London Array is illustrated in the histogram

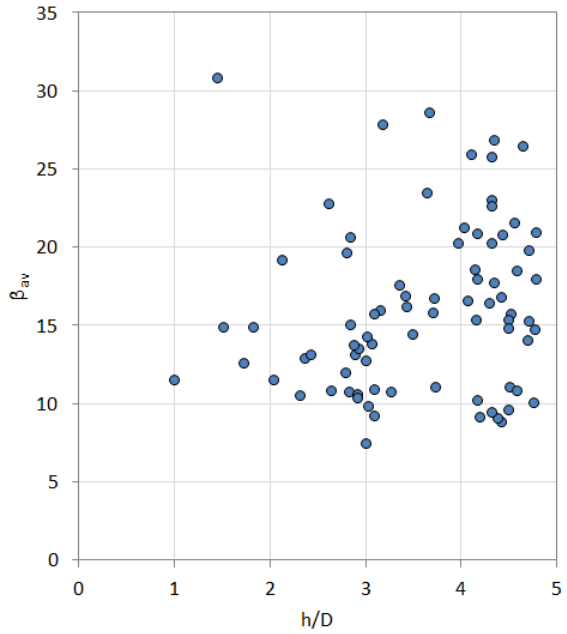

Figure 3.23: Mean slope of scour holes β_{av} as a function of relative water depth h/D at London Array.

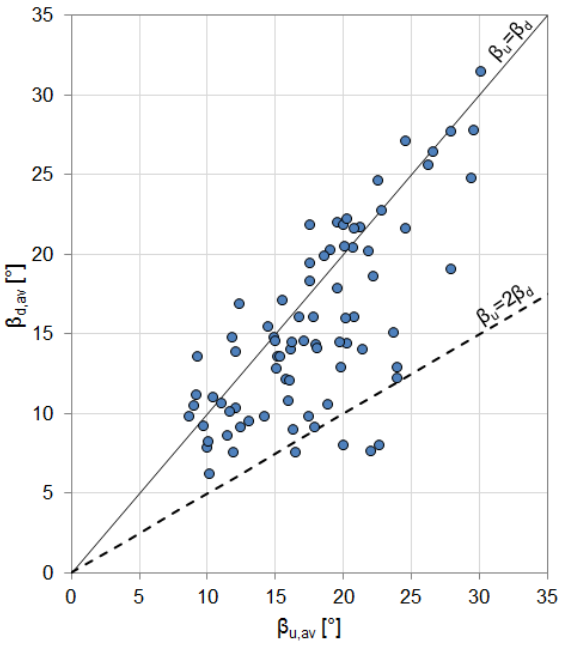

Figure 3.24: Mean upstream slope $\beta_{u,av}$ against mean downstream slope $\beta_{d,av}$ at London Array.

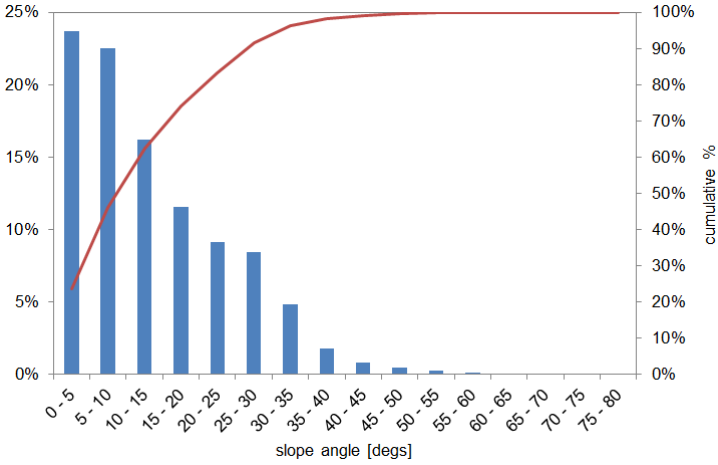

Figure 3.25: Histogram of slope angles in scour holes at London Array.

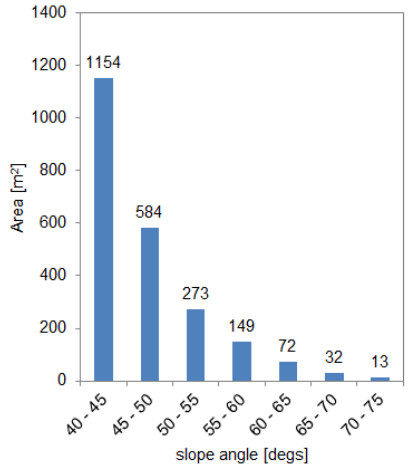

Figure 3.26: Area [m^2] exhibiting steep slopes $\beta > 40°$.

in Figure 3.25. It reveals that over 60% of the angles in the scour holes are less than 15°. However, the largest recorded slope angle is over 74.6°, albeit the occurrence of such high slopes is rare and spatially limited. That said, slope angles exceeding 60° are observed in a quarter of scour holes in the London Array data set. Nevertheless, Figure 3.26 shows that the area attributed to slope angles greater than 40° is quite limited. Figure 3.27 show high-resolution slope plots based on bathymetric sounding data and associated histograms of slope values. These plots show clearly that angles far outstripping the proposed angle of repose for sand ($\phi = 26 - 45°$, Hoffmans and Verheij (1997)) can be achieved in unconsolidated sediment. High slope angles tend to identify steep narrow bands or ridges within the scour hole (Fig 3.27B); it is also common for them to appear at the transition from main scour hole to the surrounding area (Fig 3.27A). They also appear in scour holes that show serrated edge features (Fig 3.27C). Where repeat surveys are available, it is confirmed that such high slope angles can be maintained throughout the scour development cycle and are not just ephemeral features. It is unclear how such high slope angles can be supported and maintained in what is essentially granular sediment. Based on CPT measurements, the nature of the sea bed at the example locations is interpreted to be slightly silty, clayey sand (C09), silty sand (F07) and dense sand (E19) with all locales exhibiting little geotechnical variability throughout the soil profile. As shown, the presence of fine material does not appear to be a pre-requisite for high slope angles, as they are also observed in fairly clean sand. Unfortunately, boreholes do not coincide with locations that exhibit these high slope angles, thus it is not possible to access additional information such as grain size distributions or shear tests in the vertical profile.

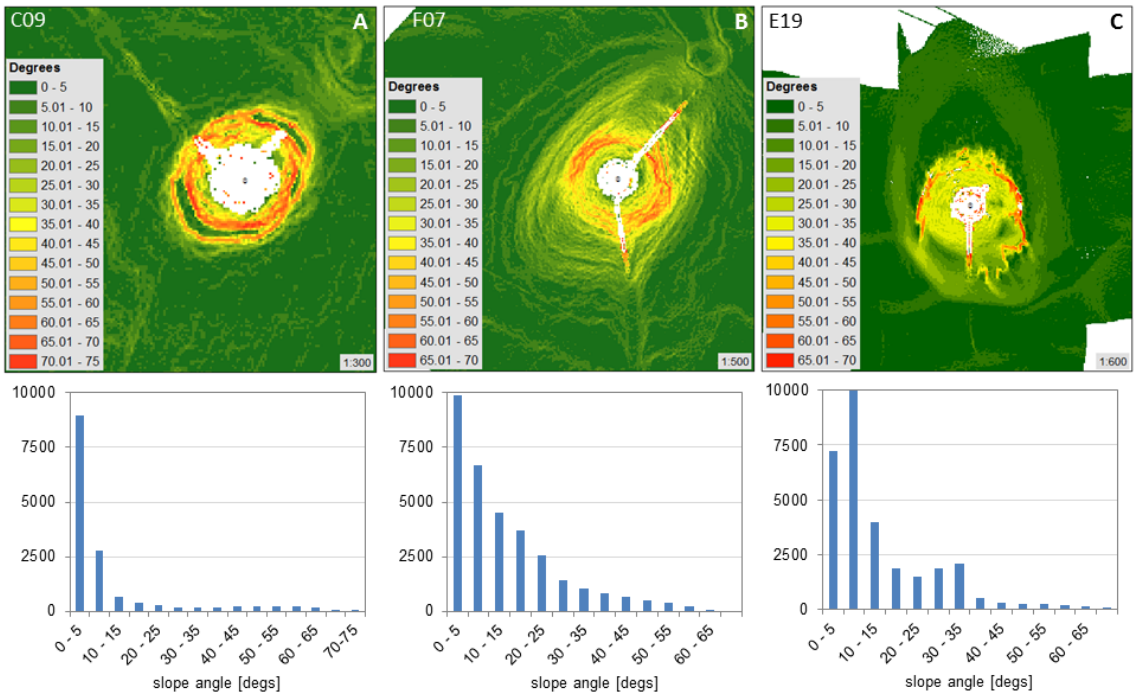

Figure 3.27: Slope plots and histograms for example scour holes with steep slopes. Foundation C09 in Knock Deep (A), F07 on Kentish Knock (B) and E19 on Long Sands (C).

It has been shown that scour dimensions show a distinct spatio-topographical organisation over the London Array wind farm, while the scour shape parameters do not reveal

such a trend. In the following sections various effects are examined in order to attempt an explanation of the observed patterns.

3.4.3 Effect of hydrodynamics

The main questions relating to hydrodynamics appears to be the development of scour in various flow types. Although, the experimental evidence is not conclusive, as outlined in Section 1.3.3, the general expectation is that scour will be greatest under uni-directional flow and some reduction in scour depth is observed under recirculating currents and oscillatory or combined current-wave action (eg. Sumer et al., 1992b; Escarameia and May, 1999; McGovern and Ilic, 2014). Since this study is dealing with field data, the hydrodynamics are not as constrained as in experiments. Notwithstanding this natural variability, it has been attempted to provide some insight into scour in different hydrodynamic forcing regimes.

Unfortunately, little detailed measured flow data were available around different locations of London Array to inform on detailed hydrodynamics to allow the dominant forcing to be identified and quantified with some confidence. However, from the examination of bed forms (Section 3.3.2), it has been shown that the topography of the area is creating some variation in flow patterns across the wind farm site. In the marine environment, pure uni-directional flow is rarely encountered due to the nature of tidal flow, nevertheless some scour holes can be identified, by means of the pattern of erosion and deposition features, that are dominated by a certain flow direction. In Knock Deep, the flows are constrained by the presence of the sand banks and thus the incoming and outgoing flows are more or less directly opposed and of relatively similar magnitude, offering prototype observations for bi-directional recirculating flows. Albeit, as the sediment transport indicators in Figure 3.9 reveal, the small asymmetry in tidal flow with the incoming tide is sufficient to effect a net transport dominance in one direction. Generally, the flow pattern in the shallows is more diverse and complex, as intricate, highly variable, local flows are set up by the interaction of the topography with the tidal current. Additionally, some wave influence on the hydrodynamics in the shallow areas is possible. Using Sumer and Fredsoe (2002)'s method for scour under combined and wave-only flows, the water depth at which waves begin influencing scour is $h/D < 2.8$, which corresponds to 13.1m (see Section 5.3.1). Within this depth range the method predicts that waves alone are incapable of causing scour, neither under average conditions or the top 10% most energetic waves from the measured record (Fig 3.2), as the resulting KC number is too insignificant. Even under combined wave and current flows, the method predicts very shallow scour of 0.4m for average conditions, indicating that wave influence is expected to be minimal. For this reason oscillatory flow is deemed insignificant in terms of the observed scour development, which is heavily dominated by currents, and will be ignored in the following analysis.

The flow regime at a scour pit is established based on the morphology of the scour. Where no directional dominance of flow can be established, the pits are classified as originating under symmetric flow. Where the scour pattern show bi-directional characteristics but a dominance in one direction, the pits are classified as directionally-dominant for the purpose of this exercise. It is recognised that the method has drawbacks. Firstly, it relies

on the scour pit and surrounding bed morphology being a reliable proxy for flow type which harbours some uncertainty. Furthermore, it assumes that the non-dominant flow can be neglected in terms of its effect on scour. However, it is quite possible that the allegedly weaker flow, the presence of which might leave any morphological evidence, can still influence the scour process, eg. by backfilling, which is the main process of scour reduction in tidal flows.

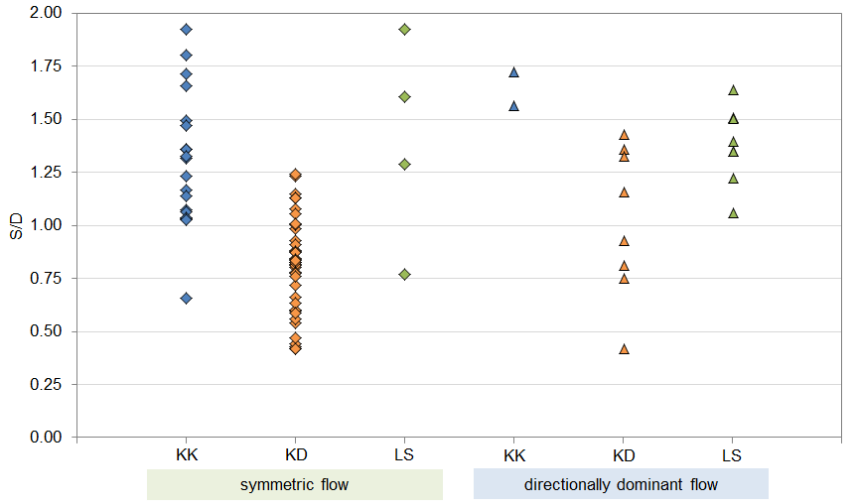

Figure 3.28: Range of S/D for symmetric and directionally-dominant flow types at London Array. KK: Kentish Knock, KD: Knock Deep, LS: Long Sands.

In Figure 3.28, scour depths in symmetric and directionally-dominated current are presented. Most scour pits show symmetric scour patterns, thus the number of data points in the directional category is small. Nevertheless, the data insinuate there is no discernible difference between these two hydrodynamic regimes, as the values and ranges are quite similar. Separating the data by topographical entity aims to reduce the effect of varying substrates, at least on the sand banks, as the soil profiles here are generally quite homogeneous.

3.4.4 Effect of sediment thickness

Judging from the largest observed scour of 9.5m, which is in an area that could potentially scour further, ie. not limited by erosion-resistant layer, the $z_{sed} = 10$m contour was chosen as an indication of the area that could be experiencing some control on scour depth from the substrate underlying the surface sediment. Figure 3.4 reveals that any such limiting effect would only be present in the central and northern part of Knock Deep. Long Sands, as a sand ridge, is characterised by a thick package of potentially mobile, granular sediment. The thickness of granular sediment is generally greater than 15m, the exception being the northern neck of Long Sands, where somewhat smaller sediment thickness is observed. Due to the depth of granular sediment and the uniformity of the sediment package (as illustrated in Sections 3.2.2 and 3.3.1), there is no reason to suggest any significant variation of scour to be introduced due to geotechnical considerations. This is possibly why, on average, the scour dimensions are greatest here and the smallest range of $1.03 < S/D < 2.02$ is observed, suggesting scour holes develop in an uninhibited manner. The smallest scour on the bank is observed at the neck and along the northern bank slopes.

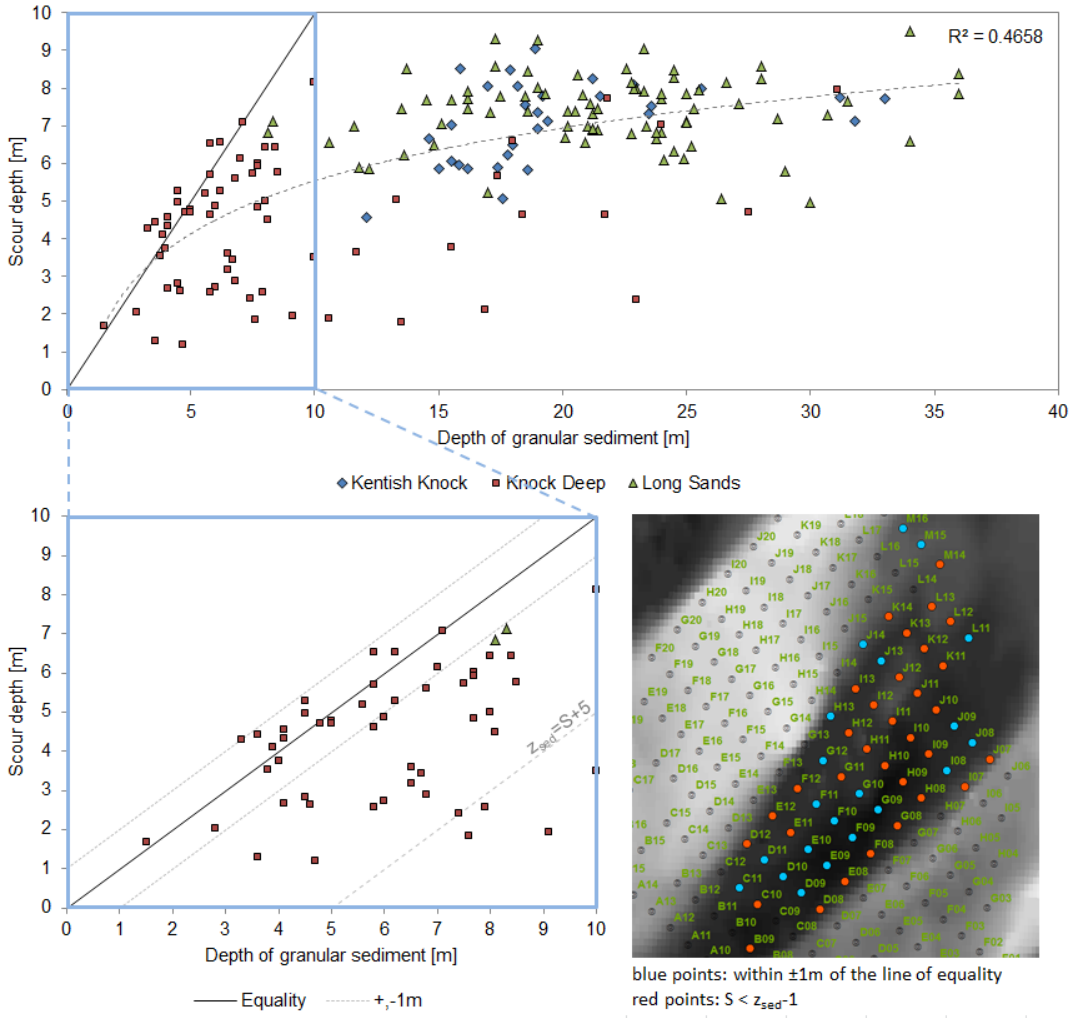

Figure 3.29: Relationship between scour depths S and thickness of granular sediment z_{sed} at London Array (top). Zoomed inset (bottom left) and location of points from zoomed inset (bottom right).

However, as shown in Figure 3.29, scour at Long Sands is not extensive enough to reach a more erosion-resistant layer at depth.

Similarly to Long Sands, at Kentish Knock, a fairly extensive layer (12-33m) of granular material is available and the distribution of surface sediment grain size coarsens from fine to medium sand in south-west to medium sand in north-east. The acoustic impedance signature and CPT measurements suggest a fairly homogeneous sedimentary consistency with simple layered structure of sediments. Observed scour values in the range of $S/D = 0.8 - 1.92$ are comparable to those at Long Sands which given similar environment and sedimentary make-up of the site is expected. Compared to Long Sands the lateral extension and volume of the scour pits are slightly smaller. The depth of granular sediment is also not a limiting factor on Kentish Knock.

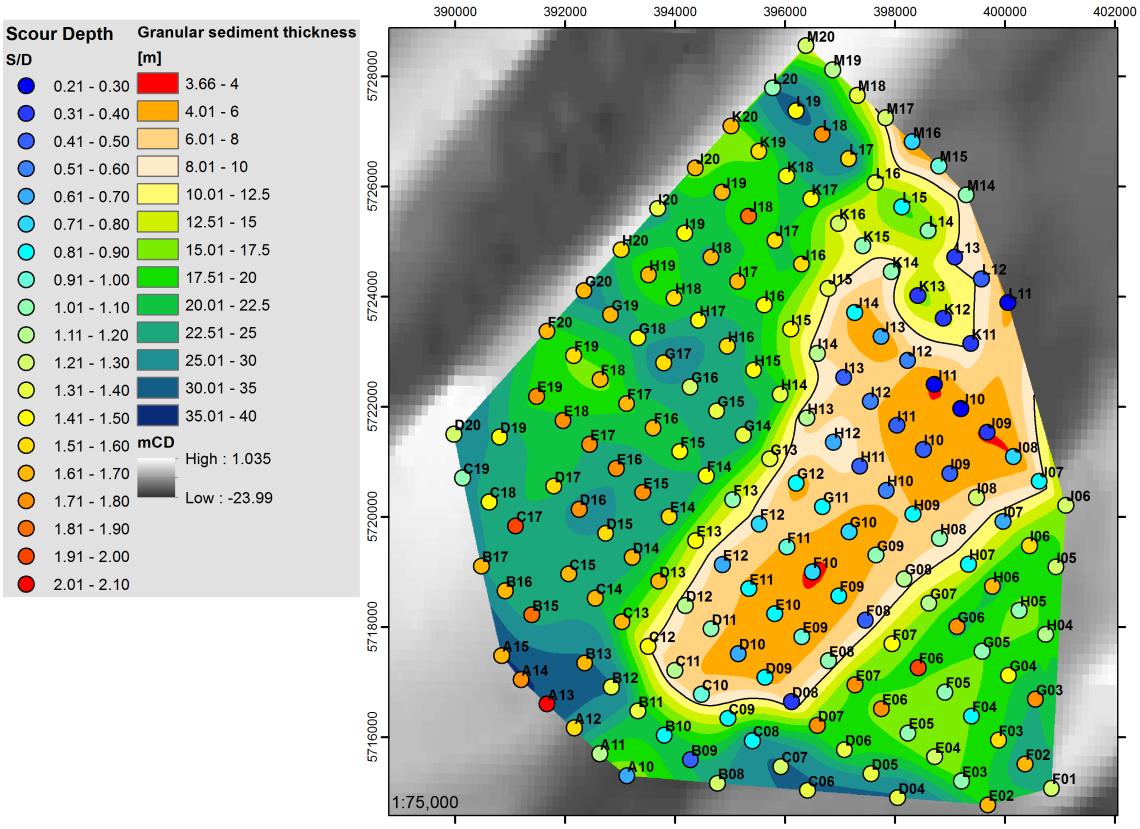

Figure 3.30: Thickness of granular sediment z_{sed} at London Array with scour depths S/D at each monopile foundation. $z_{sed} = 10$m contour in black.

The largest range of scour values is found in Knock Deep, from 1.2m in the north-east to just over 8m in the south-west. Scour depths appear to increase towards the south-west and with proximity to the banks, which bears resemblance to the pattern for increasing z_{sed}. The vertical extent of granular material varies strongly in Knock Deep. In the southern part of the channel the thickness of sand is comparable to the sand banks (> 20m) but in the central and northern section the granular package is strongly diminished and the bedrock is closer to the surface ($z_{sed} < 10$m). The sediment grab samples in Figure 3.4 indicate that surface material is fine to medium sand in the south-west and becomes medium to coarse sand in the north-eastern channel. The average is S/D =0.77, while range is between $0.21 - 1.43D$. Given that the depth of granular sediment and scour depths show similar tendencies along Knock Deep a relationship between thickness of sediment

z_{sed}(see Figure 3.30) and scour depth is examined in Figure 3.29. Although there is no unambiguous relationship between sediment thickness and scour depth, it does appear that scour is constrained by the granular package thickness where $z_{sed} < 7$m. A cluster of points from Knock Deep can be found within ± 1m of the equality line, which are scour pits that are limited by the presence of a less erosive layer beneath the surface sediment layer. Only a small number of scour depths are found to exceed z_{sed} which suggests that the depth of granular sediment can be used as an indication of the scour limit. It appears that in a small number of locations the underlying layer has experienced up to circa 0.3-0.4m (less than $0.1D$) of erosion, although most of the scatter either side of the equality line, up to approximately 1.0m, can be explained by the natural bed variability between the years of the CPT measurements, 2005 and 2007, and the post-installation surveys, as revealed on bathymetric difference plots. However, there are a large number scour holes that have not scoured even close to this limit, ie. $S < z_{sed}$. A number of factors will be examined to see if any one or a combination of them allow the inconsistent relationship between z_{sed} and S in Knock Deep to be explained. As previously mentioned, the temporal disparity between recording of CPTs and post-installation bathymetry is insufficient to account for the large discrepancies, even where the effect of migratory bed forms is included. Other considerations include hydrodynamic, geotechnical, structural and temporal details which will be investigated here.

3.4.4.1 Structural considerations

All turbine foundations in Knock Deep have a diameter of 5.7m and for this reason any structural effects can be discounted.

3.4.4.2 Substrate considerations

Where scour has not progressed through the package of granular sediment available, seismic reflection and CPT records were investigated more closely. As described in Section 3.2.2, the granular layer consists of sands and silty sands, usually becoming more dense with depth. As suggested by Fugro Engineering Services (2004) and Annandale (2006), the material strength of cohesionless sediments can be expressed using the proxy measurements for the degree of compaction in Table 2.5. Thus, the median cone resistance q_c in a band of 0.1m below scour depth, adjusted for bed level change, was extracted from the CPT measurements and plotted against S in Figure 3.31. The friction ratio and pore pressure are typically low and constant with depth in the granular layer of the homogeneous sand bank sediments, thus can be neglected in this analysis. The data does not show a limiting effect of sediment compaction as measured by q_c. Scour has stopped in sands of varying compaction, from loose ($2 - 4$ MPa) to very dense ($q_c > 20$ MPa). While the data suggest that the q_c at scour depth increases with depth, this is a function of q_c increasing down the soil profile and not reflective of scour-inhibiting conditions. Also it should be considered that the compaction grade of a cohesionless soil might be negatively affected by the process of pile-driving the foundation and the quoted values of cone resistance might not be reflective of ground conditions post-installation. Similarly, the impact of the temporary loading of the ambient sea bed by jack-up rig legs during foundation installation

is also not understood.

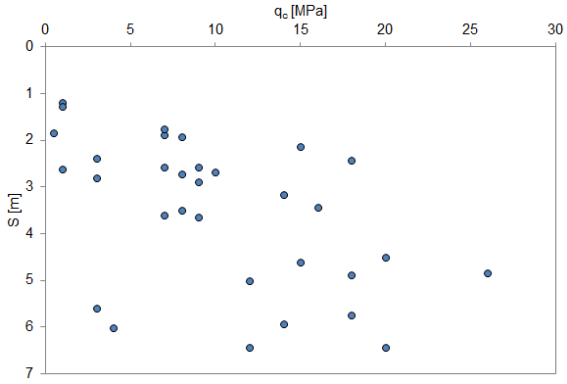

Figure 3.31: Cone resistance q_c at scour depth, for scour holes that have not reached underlying erosion-resistant layer

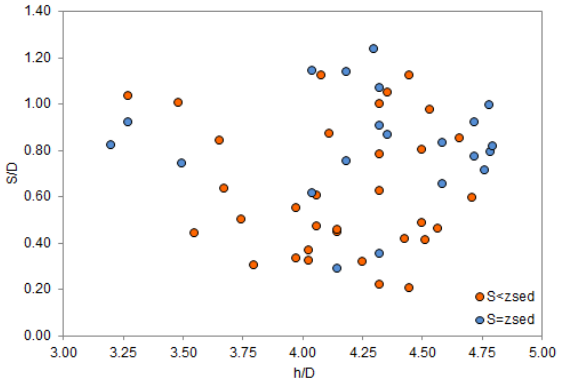

Figure 3.32: Relationship between h/D and S/D for highlighted scour holes (Fig 3.29) in Knock Deep.

3.4.4.3 Hydrodynamic considerations

Judging from the available hydrodynamic data, within London Array, the hydrodynamic regime of Knock Deep is the most uniform. The channel is dominated by tidal flow which is constrained in magnitude and direction by the presence of the sand banks, thus flow conditions are expected to be similar throughout the Deep. Even if there were local variabilities in the current, it is unlikely that they would be large enough in magnitude to explain the starkly different observations at neighbouring sites. The water depth at scour holes in the $S < z_{sed}$ population varies between $3.3 - 4.7D$, with the shallower depths in the northern part of the channel. There is no significant difference between the h/D of the two populations, as the range of water depths is very similar as shown in Figure 3.32.

Astley et al. (2014) have investigated the impact of storm events on scour at a shallow (h = 8m) ship wreck site in the Outer Thames Estuary. Over a 17 year period (1995-2012), 15 events of or exceeding a 1:1 year return period, were recorded. However, even in the restricted water depth, no evidence for scouring action by waves could be established. Hence, in the deep water of Knock Deep, it seems reasonable to assume that wave effects on scour are negligible even during extreme events. Figure 3.33 shows the wave record from the South Knock wave rider buoy in the period of time encompassing the installation and survey of the data points under investigation. The most severe storm events have been identified and numbered. The three month period before the first installation (not shown) exhibits typical benign summer conditions. During installation and surveying 6 short-duration high-magnitude events have been identified, together with a winter period of increased wave heights between November 2012 and March 2013. Based on the H_s of up to 3.52 during storm events, and Soulsby (1997)'s assertion that orbital velocities can be brought to bear on the sea bed for $h < 10H_s$, ie. $h < 35m$, then some degree of wave impact in Knock Deep is suggested. However, the surveyed scour depths (also plotted in Figure 3.33) do not appear to reflect any storm impact. This is best exemplified by the calm period prior to event 3, which displays a very similar range of scour values than the scour after event 3. Similarly, events 5 and, in particular, 6 represent longer duration events along with general increased spring wave heights and the observed S after

this period is not diminished, as would be expected after current theory, but rather scour has increased further. Further, there is no significant difference between the two scour populations ($S < z_{sed}$ and $S = z_{sed}$) at any point along the time line, thus wave action can be discounted as a factor to explain the discrepancy in the scour development.

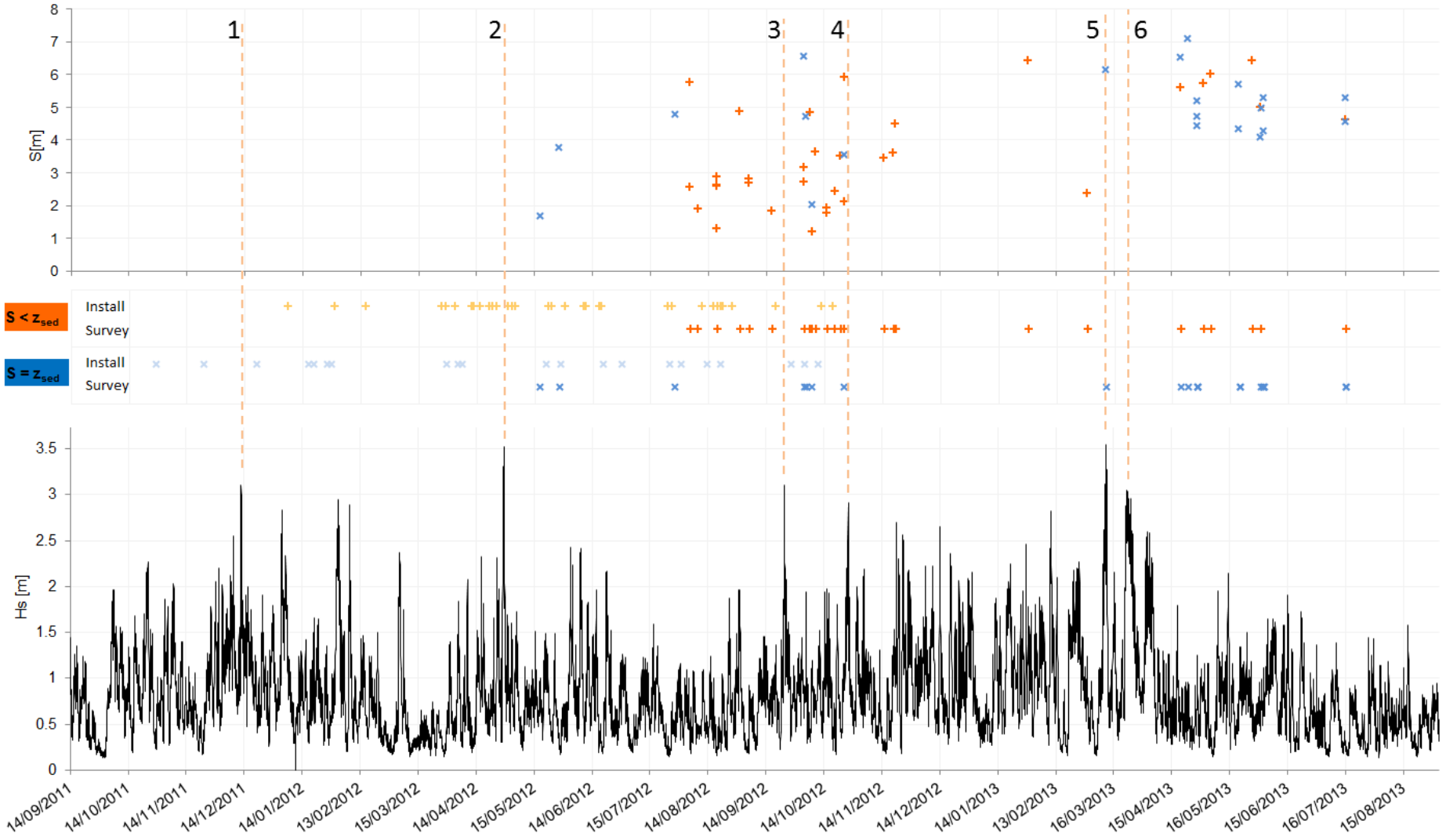

Figure 3.33: Plot showing significant wave height H_s [m] from South Knock wave rider buoy for installation and survey period of scour pits highlighted in Figure 3.29. Installation and survey dates with associated measured scour depth S [m] given for both scour pit populations $S < z_sed$ (red) and $S = z_sed$ (orange). Strom events shown as dashed lines.

3.4.4.4 Temporal considerations

Figure 3.34 shows the elapsed time T before the survey at which the scour depths in Figure 3.29 were recorded. For most of the points that show $S < z_{sed}$ the most recent survey was undertaken in 2012, ie. closer to the installation date, $T < 210$. For $S = z_{sed}$ locations, most surveys were carried out in 2013 and a longer time period passed before the survey. There is a positive trend between T and S here suggesting that there is a time-related component to the observations in Figure 3.29. The discrepancy between z_{sed} and S is plotted in Figure 3.35. It is noted that the difference decreases with T as the red points approach the equality line ±1m. Thus it seems likely that most of the difference in scour depth can be explained by survey timing. The large scatter observed in the $S < z_{sed}$ population in the $T < 210$ period seems to suggest that maybe scour progressed at a slower rate in these holes and thus there is a geotechnical constraint. However this is not corroborated in Figure 3.34, where the envelope of scour depths relative to T is similar in both populations, conveying that there is no significant difference in scour rate. This, in turn, confirms that there is no discernible geotechnical effects as suggested in the previous paragraph.

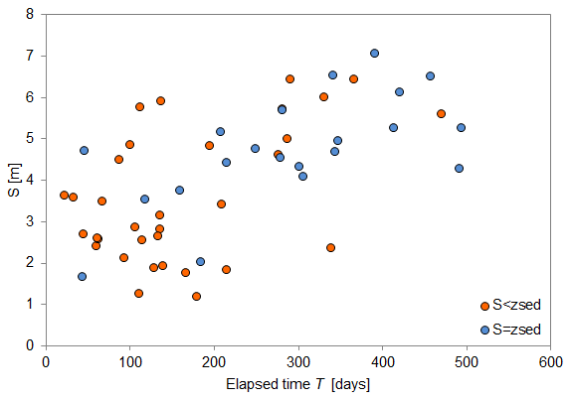

Figure 3.34: Elapsed time before survey T for scour holes in Knock Deep. Red points are scour holes where $S < z_{sed}$, blue points where $S = z_{sed}$.

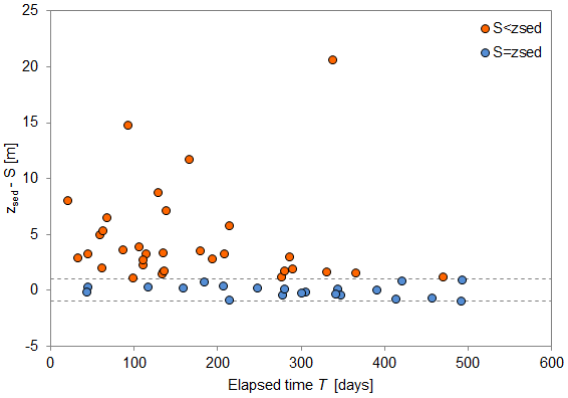

Figure 3.35: Relationship between $z_{sed} - S$ with elapsed time T. $z_{sed} - S = 0$ is the equality line, ±1m marked as dashed grey lines.

3.4.4.5 Secondary processes

The foregoing paragraphs have suggested that geotechnical effects are not responsible for the observed discrepancy between sediment thickness and scour depth, while the timing of surveys is believed to be the likely factor. However, for sake of completeness, secondary and post-scour processes will also be considered, as outlined in Section 1.4.4. One way to identify backfilling, is to observe the spud can marks created by the jack-up rig during the installation of the monopiles. Where these pockmarks have been partially or completely infilled, it is reasonable to assume that the scour hole might be experiencing a scour depth reduction by backfilling. Unfortunately, the 2012 survey is usually not extensive enough to have captured the spud can marks, thus only a smaller number of locations can be investigated. Out of the 32 locations in question, 13 clearly displayed spud can marks. In 4 locations spud can marks have been erased, while in the remaining 15 it was unclear whether the marks had been infilled or they had not been captured on the

survey. As the imprints from the jack-up rig legs have not been infilled in most locations, it can be assumed that backfilling is not a major contributor to the reduced scour depths witnessed. Furthermore, where multiple time steps are available, scour depth does not show any reduction with time. Sediment grain size information is not spatially dense enough to examine armouring in any detail. From the surface grab sample analysis (see Figure 3.4) it appears that the discrepancy between z_{sed} and S can be found in areas of both fine and coarse sand sediments. Furthermore, in theory, an extensive cover of gravels or pebbles would be required to effect armouring and the surface grabs do not suggest that sort of material to be present.

3.4.5 Effect of natural bed variability

3.4.5.1 Short-term influence

To assess whether ambient bed level changes can affect scour over the 1-2 year period between installation and hydrographic scour survey, the dimension indicators are plotted against magnitude of ambient bed mobility in Figures 3.36 to 3.38. The magnitude of bed mobility was derived from bathymetric difference plots from the amount of vertical bed level change. In Figures 3.36 to 3.38 the median value is plotted as a dashed line and, here, is a more suitable measure than the average since the effect of outliers is removed. For scour depth, the range and median S/D observed for bed mobility of up to 1m (lower two categories) are very similar, implying that moderate vertical changes do not affect prototype scour depths. In the higher mobility categories, greater than 1m, the number of data points is much lower and the low n is a caveat in the following discussion. Notwithstanding this, the median scour depth is reduced compared to the lower mobility categories. For vertical change of 1-2m, the range is also somewhat reduced. Only two data points are available show $>$ 2m mobility, so the suggested increase in median S/D is likely a result of the low n, rather than a real trend. For scour area and volume only a single data point falls into the $>$ 2m category and thus is discounted in the interpretation. Here, the largest spread of values is displayed in 0-0.5m bed mobility and the range of observed values and the median decrease with seabed dynamics, the outlier in 1-2m mobility ignored. Within the dataset available, this analysis seems to suggest that the effect of bed mobility is to dampen scour dimensions, which is contrary to current theory which suggests that scour depths are expected to increase with the presence and dimensions of bed forms (eg. Richardson et al., 2001). Vertical bed elevation changes indicate that flows are capable of moving sediment and live-bed conditions while prevail for, at least, parts of the tidal cycles. Hence, the trend towards diminished scour could be a result of backfilling by sediment, especially where bed forms are the major source of bed level change. It has also been shown in section 3.4.2 that bed forms can also constrain the lateral growth of scour pits, thus high mobility regions will display smaller areas and volumes. It is also conceivable that bed forms of significant vertical dimension in the near vicinity of the pile could alter the hydrodynamic flow, possibly providing some sheltering, disruption of the boundary layer separation or reduction of flow velocities at the structure, thus resulting in less scour.

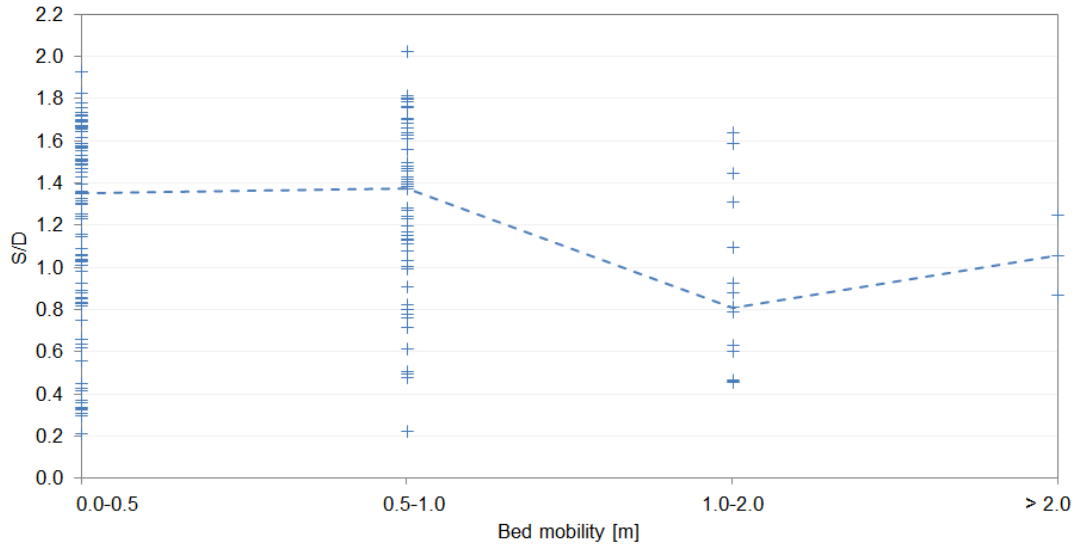

Figure 3.36: Effect of natural bed mobility on scour depth S/D. Dashed line: median S/D.

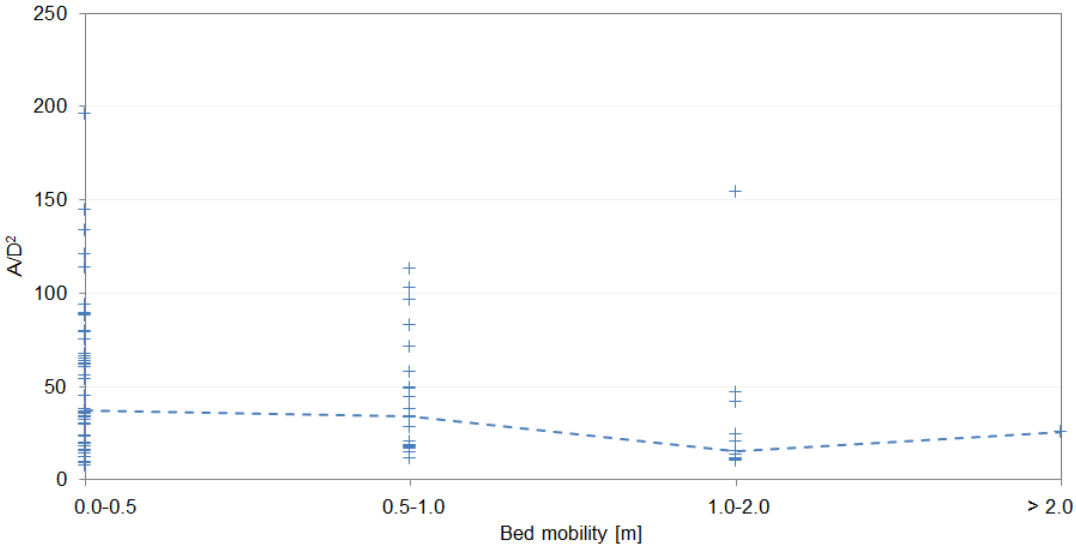

Figure 3.37: Effect of natural bed mobility on scour area A_S/D^2. Dashed line: median A_S/D^2.

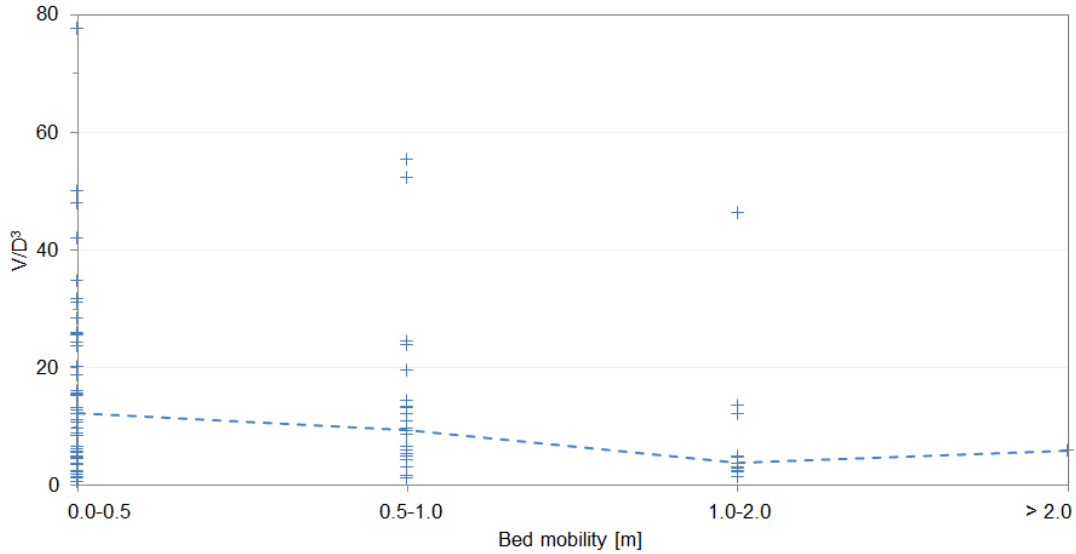

Figure 3.38: Effect of natural bed mobility on scour volume V_S/D^3. Dashed line: median V_S/D^3.

Harris et al. (2011) proposed that scour pit angles, normally following some kind of relationship with ϕ, can develop independently from sediment properties in morphologically active areas (see Section 1.3.1.3). Figure 3.39 shows the development of the average slope angle β_{av}, mean upstream slope $\beta_{u,av}$ and mean downstream slop $\beta_{d,av}$ with increasing bed mobility. The reverse trend appears to be suggested here, as slope angles tend to become steeper with higher magnitudes of bed level change. It is likely that this relationship is related to the areal extent of the scour hole in higher mobility areas. As shown in Figure 3.37 they tend to become more confined, thus the ratio of main scour hole to wider scour is reduced and steeper slope angles are witnessed.

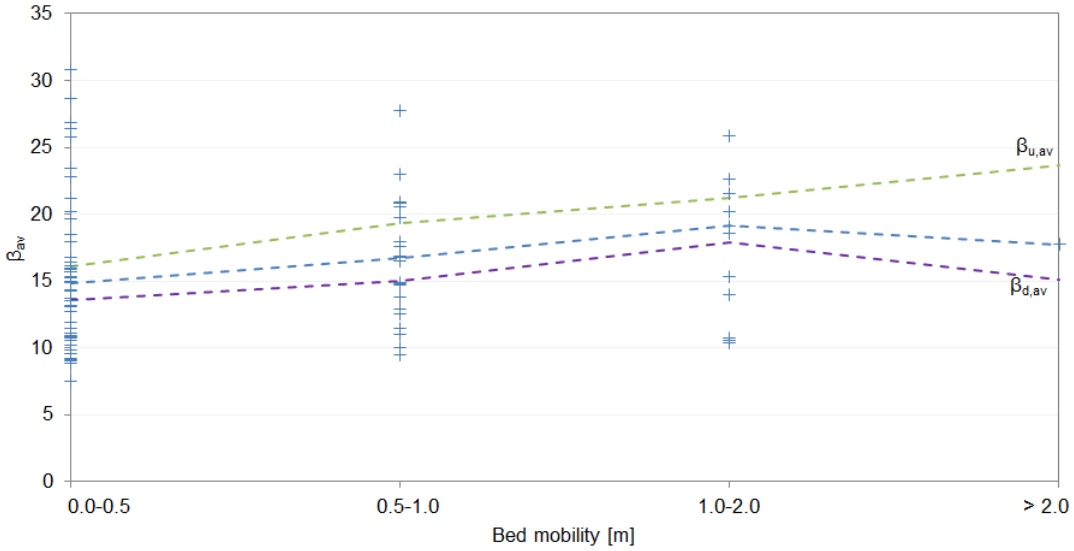

Figure 3.39: Effect of natural bed mobility on average slope angle in scour pit β_{av}. Trend of median value of β_{av} (blue dashed), $\beta_{u,av}$ (green dashed) and $\beta_{d,av}$ (purple dashed).

3.4.5.2 Long-term influence

The largest net elevation changes identified in Table 3.3 are associated with the flank and neck of Long Sand (see also Fig 3.5). Of these locations, D13 and C13 are the second and third deepest scour holes in absolute terms, shallower only than A13 another scour pit on the channel-facing slope. At these locations the bed level has dropped between some 2-4m over the 7-8 year period between 2004 and 2011. To remain in dynamic equilibrium with the hydraulic forcing, the scour hole must adapt to changes in the ambient bed level. Between 2011, the last pre-installation survey, and 2013, the last post-installation survey, the ambient area has dropped between 0-1.5m. Thus the development of this scour hole, as witnessed by the latest survey, might have only been affected to a small degree by the ongoing retreat of this area. However, if the larger-scale bank level adjustment trends continue in the future then further excavation of the foundation is likely in these areas, even if the absolute scour magnitude remains the same. In the final weeks before submission of this study, bathymetric data from 2014 became available at a selected number of foundations. While there was insufficient time to include these data in the analysis, it is used here to examine the further development of scour in the morphologically active areas. The data suggest that in both retreating and prograding areas of the bank, erosion has continued. The area of bank retreat will be discussed first. The ambient area at C13 has

retreated by circa 0.5m between 2012 and 2014. Inside the scour hole between 0.7-1.2m of erosion is witnessed at the pile in the same time period while up to 3.5m of erosion is witnessed along the cable routes (see Fig 3.40A). At D13, the ambient area has remained within ±0.2m and similarly bed levels at the pile have remained within ±0.4m; however the size of the scour hole has increased with between 0.5-1.5m of erosion along the edges of the pit (see Fig 3.40B). At F13, the ambient bed levels have increased by approximately 1.5m between 2012 and 2014 judging from changes along the cable route, yet, erosion of 2.5-2.8m is witnessed near the foundation and over 3m on the side slopes (Fig 3.41A). Due to the confined survey extent at G13, the change in ambient bed level between 2012 and 2014 is estimated from the change along the cable route which suggests circa 0.7m of aggradation in this area. Inside the pit between 0.5-1.8m of erosion at the pile is observed, while sediment has accumulated along the sides of the pit with an increase in bed levels of up to 0.75m (Fig 3.41B). The fact that erosion is continuing in areas where the scour depth is increasing by the fact that ambient bed levels are rising suggests that scour in these area has not reached its dynamic equilibrium condition.

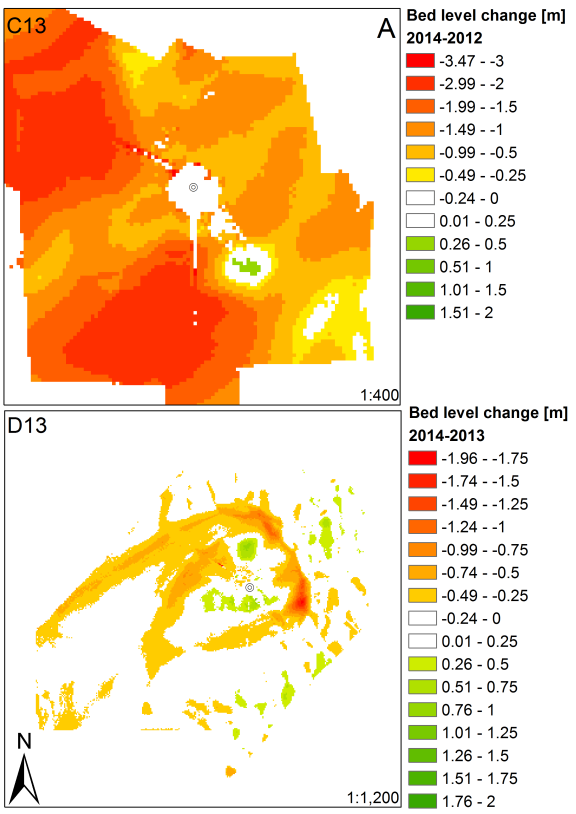

Figure 3.40: Development of scour pits C13 (A) and D13 (B) in retreating bank area.

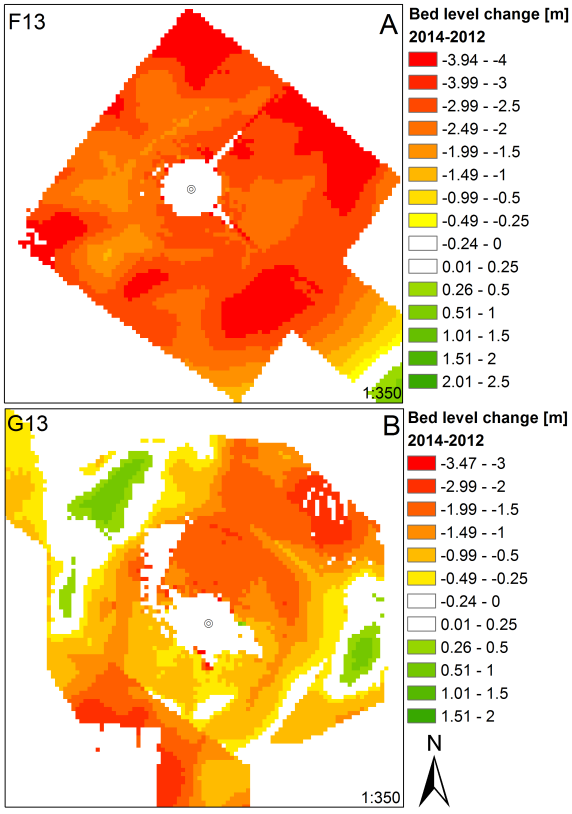

Figure 3.41: Development of scour pits F13 (A) and G13 (B) in accreting bank area.

3.4.6 Scour time evolution

The availability of repeat surveys allows an examination of the time scale of scour development at London Array. Figure 3.42 shows the time-development of relative scour depth S/S_{max} and relative scour area and volume in Figure 3.44. Under the assumption that the maximum scour dimension is adequately captured, the plots show the time required to reach the maximum condition and how rapidly scour develops. The data appear to suggest

that the timescales of scour can vary immensely. The maximum condition can be reached very quickly $\ll$ 100 days or, conversely, take over 400 days. This is also reflected in the data provided from Harris et al. (2011). With the reduced data set used to create Figure 3.44 a similar trend is observed. The maximum A_S and V_S dimension can be reached anywhere between 60 and 600 days, but typically between 200-500 days. Thus, on average it appears that the areal and volumetric "equilibrium" condition takes somewhat longer to develop. Generally, a time frame of approximately 400-500 days is suggested for most scour pits to reach their maximum vertical and lateral dimensions but the plots imply that individual scour hole growth can proceed at strongly varying rates and can continue to develop many days after installation. This assumes that the maximum condition has been captured in the surveys however, which might not be the case. Time-evolution data from the North Sea N7 pile from Rudolph et al. (2004) is plotted for comparison in Figure 3.42 which exhibits slower development of scour than most of the other data points but shows that scour in sandy sediments can continue to increase over a number of years.

To examine whether scour depth time development behaves differently in different areas of the site, the data points are separated out by topographical entity in Figure 3.43. Qualitatively, the data suggest that the maximum scour takes longest to develop on Long Sands; however the variability in scour evolution is significant, implying that individual scour holes can develop very differently. The scour development with time appears quite similar between Knock Deep and Kentish Knock; on average the latter seems to exhibit the fastest rate of scour.

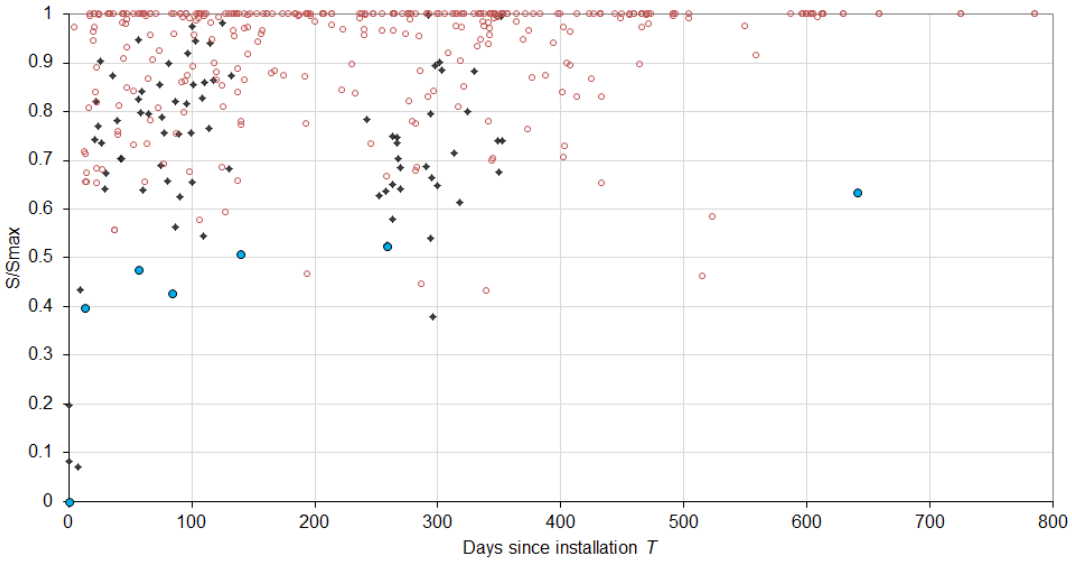

Figure 3.42: Scour depth (S/S_{max}) evolution with time. Data from Harris et al. (2011) in black. Scour data from Rudolph et al. (2004) at N7 monopile in blue.

Scour depth is understood to exhibit an asymptotic relationship against time, with rapid erosion at the beginning of the erosive process and much reduced rates of change as the scour depth approaches the equilibrium condition (eg. Sumer et al., 1992a; Whitehouse, 1998). The rate of change of scour depth ΔS, area ΔA_S and volume ΔV_S between individual surveys have been calculated and plotted in Figure 3.45. The field data from London Array confirm an asymptotic trend in all dimensional parameters. The initial scour period which is characterised by enhanced rates of erosion seems to last some 100

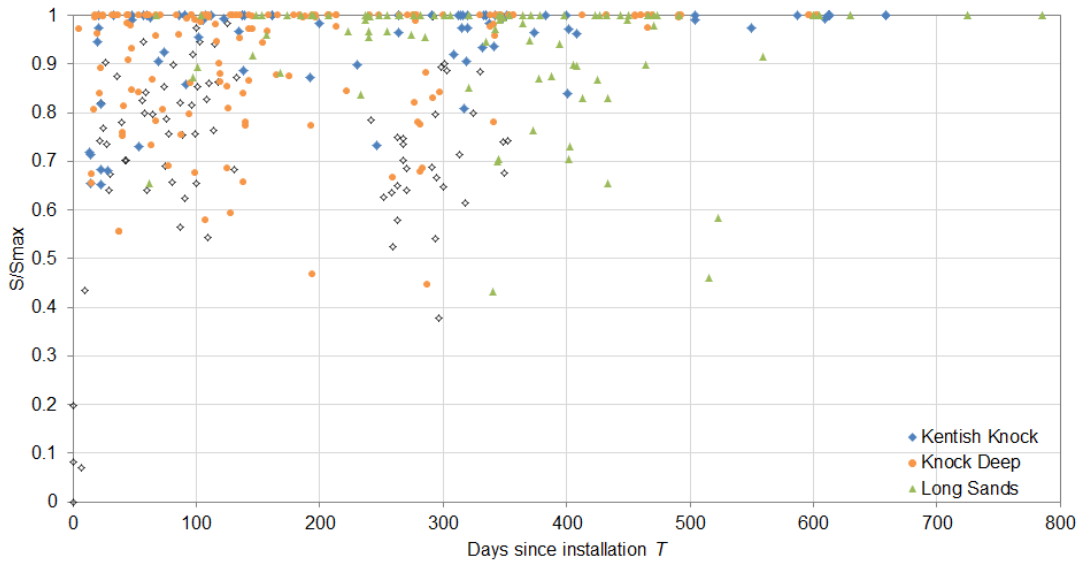

Figure 3.43: Scour depth (S/S_{max}) evolution with time by topographical entity. Data from Harris et al. (2011) in black.

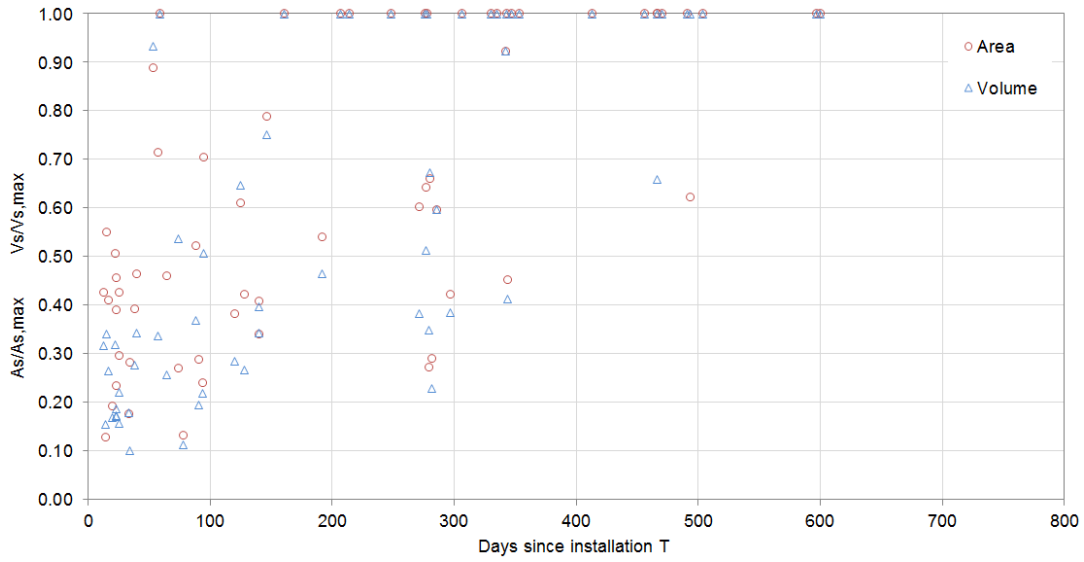

Figure 3.44: Scour area ($A_S/A_{S,max}$, red) and volume ($V_S/V_{S,max}$, blue) evolution with time.

days after monopile installation; after that, the rates show flat or linear progression. However, the most rapid change is limited to the first few days after installation. Compared to median rates of change, the initial scour occurs is typically some 10-15 times greater for vertical erosion but the maximum recorded rate, representative of the first 5 days after installation, is 0.7m/day, over 35 times the median rate. For comparison, the initial rate of scour development at N7 monopile average over the first 13 days is just under 0.2m/day. This shows that to capture the most rapid phase of scour development, scour pits should be surveyed immediately after installation and in short intervals subsequently. After approximately 100 days, the data suggest that the scour depth changes much less rapidly. Typical rates of lateral growth are between 2-5m^2/day with a median rate of 3.7m^2/day; the maximum growth rate observed is just over 35m^2/day. Initially, the scour hole expands at a rate 3-10 times the median rate. Initial rate of volume growth are typically between 10-30m^3/day although greater rates are observed. After the early stage, typical average growth rate is between 2-8m^3/day with a median of 4.3m^3/day. The areal and volumetric growth rates are an important in terms of the design of scour protection, since the amount of required protective material increases with time as scour develops.

According to the prototype data, the rate of change in scour depth S in cm/day can be approximated by equation 3.1, where T is the elapsed time in days between monopile installation and scour depth measurement. The rate of change in area [m^2/day] and volume [m^3/day] can, similarly, be calculated using equations 3.2 and 3.3, respectively.

$$\Delta S = 172.43T^{-0.906} \tag{3.1}$$

$$\Delta A_S = 88.895T^{-0.647} \tag{3.2}$$

$$\Delta V_S = 58.012T^{-0.503} \tag{3.3}$$

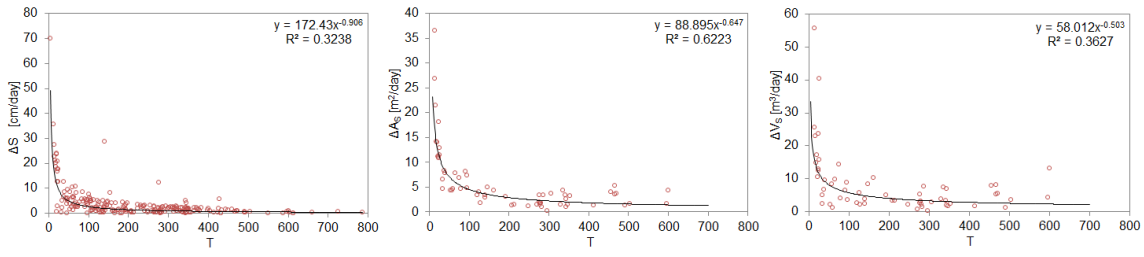

Figure 3.45: Rates of change of scour depth [cm/day], area [m^2/day] and volume [m^3/day] with time after monopile installation.

Table 3.6 shows the average rate of change of scour depth, area and volume per topographical area. Rates of change are given for the whole time series, the first 100 days of scour evolution and the period after 100 days. First of all it can be seen that evolution is more rapid in the first 100 days. The table confirms the notion that scour develops fastest on Kentish Knock, followed by Knock Deep. Long Sands shows higher rates of change for all three dimensional parameters in the $T > 100$ day period, suggesting the scour process continues here for a considerable period after installation.

Table 3.6: Average scour progression rates per topographic feature.

		< 100 days	> 100 days	overall
ΔS [cm/day]	Kentish Knock	11.6	0.9	5.5
	Knock Deep	7.2	1.6	4.1
	Long Sands	7.3	2.2	2.7
	N7 pile	6.9	0.3	3.2
ΔA_S [m^2/day]	Kentish Knock	16.0	1.7	11.4
	Knock Deep	9.0	2.4	4.8
	Long Sands	-	4.3*	3.5
ΔV_S [m^3/day]	Kentish Knock	21.0	3.5	15.8
	Knock Deep	10.8	4.9	6.4
	Long Sands	-	13.2*	10.1

* based on single data point

However, as will be outlined in the following section, caution is advised when interpreting the time-related data due to time-distortion introduced by timing of bathymetric surveys. Rates of change are calculated, for lack of alternatives, assuming the scour hole development is linear between consecutive surveys; however as will be shown below, this assumption in conjunction with large time periods between surveys can mislead the interpretations and introduce errors into the calculation of ΔS, ΔA_S and ΔV_S.

Conceptually, the aforegoing discussion raises questions about the surveying scour holes at wind farm developments. It is clear that unless scour holes in mobile sediment are surveyed immediately following installation, the initial phase of scour development that proceeds very rapidly is not recorded. In the existing data set, the smallest time period between installation and survey is 5 days. From the calculated rate of change in scour depth of 0.7m/day for this monopile it can be inferred that the scour hole changes significantly on a daily time scale. This early scour development is not captured, which from a process perspective is very interesting. On the other hand, from an engineering perspective, where the final scour depth is of most importance, the scour survey should be strategically delayed to some 400-500 after installation, so as to capture most scour holes in their near-equilibrium state. However, if the exposure of cables is of concern, surveys should be delayed further since the full lateral dimensions take longer to develop.

Foundation H05 is located on Kentish Knock and offers the opportunity to illustrate the growth of a scour hole with time on a specific case study. This particular example was chosen because it is one of the few scour pits where three time steps with known T are available and full bathymetric coverage exists. Further, the first scour survey was undertaken after $T = 14$ days, which is one of the smallest delays in the data set, thus showing the vigorous early stages of scour development. The dominant flow direction is the outgoing ebb flow in a north-easterly direction. Figure 3.46 shows the seismic profile with measurements of cone resistance q_c and friction ratio R_f. The plot reveals a package of homogeneous granular sediment of 16m thickness. The sandy sediment tends to get more dense with depth in the sand bank core as indicated by increasing q_c (see Table 2.5), although that progression is broken up by a 0.5m band of loose sediment, before becoming very densely packed $q_c > 20$MPa. The friction ratio of 1-2% suggests that only a small proportion of silts is present, although thin bands with higher percentage of fines are marked by spikes in R_f. Figure 3.47 shows the growth of a scour hole with time at this location. The sequence of images reveals that after a single spring-neap tidal cycle, a

significant scour hole of $S = 3.84$m has developed, which constitutes 66% of the maximum observed scour at this pit. The average rate of scour depth increase in this first period is just over 0.27m/day. In terms of area and volume the scour hole has only achieved 13% and 15.7% of the maximum value, respectively. This demonstrates, that scour depth progresses more rapidly, since it is a function of the vertical growth of the main conical scour hole driven by the strong excavating action of the horseshoe vortex; the full areal and volumetric extent is reached in the later stages, whose expansion is governed by weaker wake vortices and general flow acceleration around the structure (see Figure 1.3). The morphological evolution of the scour hole is illustrated in Figure 3.48. The figure shows the change in slope angles with time. As the scour hole grows in size, the maximum slope angle diminishes. The maximum angle at $T = 14$ days is 60° which drops to 58° and then to 56° in the final time step. In the first two surveys the largest angles are found at the front of the structure, whereas in the last survey the maximum slope is found in the wake. The average slope angles in the main conical scour pit, measured in profiles along the flow axis show a 25.9° slope on the upstream side and 26.2° in the downstream, implying virtually identical slope angles in the main pit. The shape of the scour hole tends to become more irregular with time as the areal extent of scour adjusts to the flow forcing. The IQ measures 0.72 at the first two time steps but drops to 0.54 at $T = 264$. The L/W ratio increases slowly from 1.14 to 1.32.

3.4.7 Scour hole age

The relationship between the elapsed time T between installation and scour survey and scour depth is examined in Figures 3.49 and 3.50. The London Array data in these plots are individual locations and represent data from the latest usable bathymetric survey (usability based on survey extent), thus can contain data from 2012 and 2013. It should be noted that this might not represent the most recent state of the scour hole, if, for example, the exact date of the last survey is not known. On the basis of above interpretation of scour time development, one would expect to find a relationship between scour depth and elapsed time for Long Sands, since the scour has been shown to proceed at the overall slowest rate of all areas (Table 3.6), whereas for Kentish Knock, any scour hole older than 100 days should display only asymptotic change. However, as illustrated in Figure 3.49 the picture appears quite differently. For Long Sands, S/D appears relatively independent from T, thus implying that most of the scour occurs in the first circa 100-200 days although the deepest scour coincides with the oldest scour pits. Conversely, data for Kentish Knock and Knock Deep display weak positive relationships with T, albeit the latter also displays large scatter. To reconcile the somewhat conflicting observations, it has to be noted that the average elapsed time between monopile installation and scour survey is longest for the scour pits in Long Sands. This introduces errors in the calculation of scour rates, ie. the $<$ 100day rate is likely to be significantly underestimated. The average time period between installation and scour survey measures 193 days for Knock Deep, 250 days for Kentish Knock and 350 days for Long Sands. So, contrary to the discussion above, Figure 3.49 demonstrates that scour on Long Sands has proceeded most rapidly, followed by Kentish Knock and Knock Deep that develop at quite similar rates on

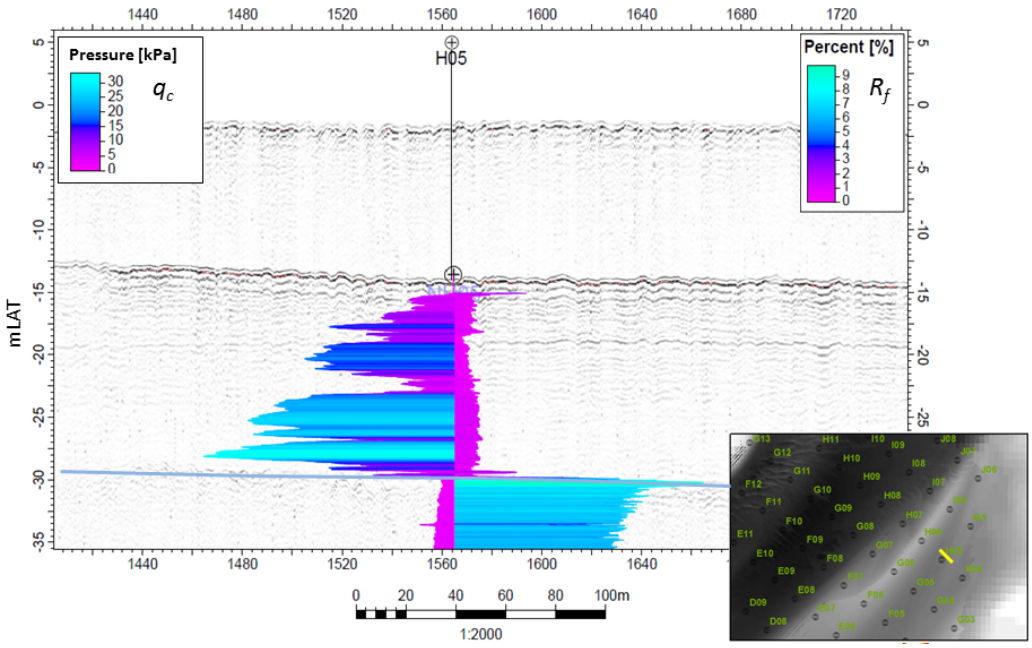

Figure 3.46: Seismic reflection and CPT records of cone resistance q_c and friction ratio R_f at foundation H05 on Kentish Knock. Top of London Clay horizon marked by blue line. Inset location map showing position of turbine and seismic profile.

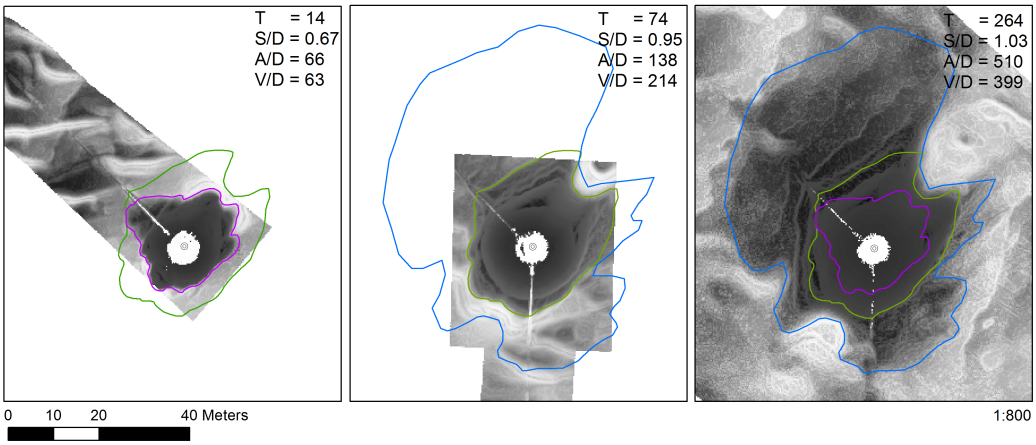

Figure 3.47: Evolution of scour pit dimensions at foundation H05 (Kentish Knock) with time. $T = 14$ (left), $T = 74$ (middle) and $T = 264$ (right). Polygons mark the scour outline of the current and consecutive time step. In the right image, all scour outlines are plotted to demonstrate progression. Scour pit visualised as partially-transparent bathymetry overlying slope map.

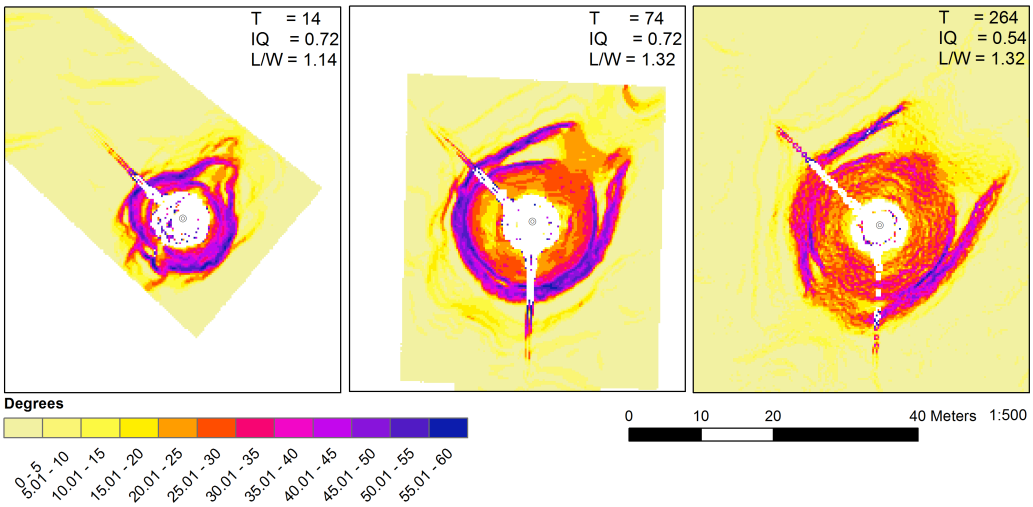

Figure 3.48: Evolution of scour pit morphology at foundation H05 (Kentish Knock) with time. $T = 14$ (left), $T = 74$ (middle) and $T = 264$ (right). Scour pit visualised as slope map.

average. For all topographies, it does appear however that the deepest scour holes are also the oldest. Based on this analysis, using all data points, an approximate estimate of S/D based on elapsed time T can be determined using the logarithmic relationship suggested in equation 3.4. Similarly, a curve-fitting exercise was undertaken to determine whether the scour time relationship by Sumer et al. (1992a), introduced in Equation 1.15, captures the time evolution of scour depth at London Array. The curve is plotted in Figure 3.49 using $S_e = 1.45$, $T_s = 160$ and $p = 1$. Notwithstanding the scatter, based on the residuals, the suggested relationship can explain 30% of the observations, which is very close to $R^2 = 0.31$ achieved with the logarithmic equation.

$$S/D = 0.3179 \ln(T) - 0.5877 \tag{3.4}$$

In Figure 3.50, existing prototype data from monopiles in sandy sediments are plotted together with data from London Array, the elapsed time T having been estimated from information provided in Whitehouse et al. (2011). As mentioned previously, the rate of scour development can be very different at individual monopiles and this notion is corroborated in the existing observations as varying S/D are observed at similar T. Considering all observations together, it appears that most of the scatter in the London Array and Gunfleet Sands data falls within an envelope (marked by blue dashed lines) suggested by the other prototype data; the lower limit is described by scour data from N7, Barrow and Egmond aan Zee wind farm and the upper limit given by Destin pier and Otzumer Balje. This suggests that the time-development here is within the expected parameters for monopiles in sandy sediments. Some scour pits in Knock Deep fall outside the envelope; however these are influenced by the underlying clay substrate (Section 3.4.4), thus are not expected to follow the time-development of sandy sediments. The upper limit is given by the logarithmic equation 3.5 and the lower boundary is described by a 2^{nd} order polynomial in equation 3.6. In theory the latter should be a logarithmic equation also; however as the rapid growth in the initial scour phase is not captured, the validity range of the lower boundary begins at $T > 15$. It is recommended that these relationships be validated with further data in the future.

$$\frac{S}{D} = 0.220 \ln(T) + 0.578 \tag{3.5}$$

$$\frac{S}{D} = -6.850 \times 10^{-8} T^2 + 4.74 \times 10^{-4} T + 0.420 \tag{3.6}$$

Due to the small number of data points on individual topographies, the scour area and volume data are discussed as a whole. The mean trend for A_S/D^2 and V_S/D^3 (Figs 3.51, 3.52) describes an increase with T, as the oldest scour holes tend to exhibit larger dimensions. This suggests that the full areal and volumetric extent can continue developing for a long time after monopile installation. However the variability in the scour hole growth increases with time illustrated by the large range of dimensionless area and volume values witnessed at $T > 500$.

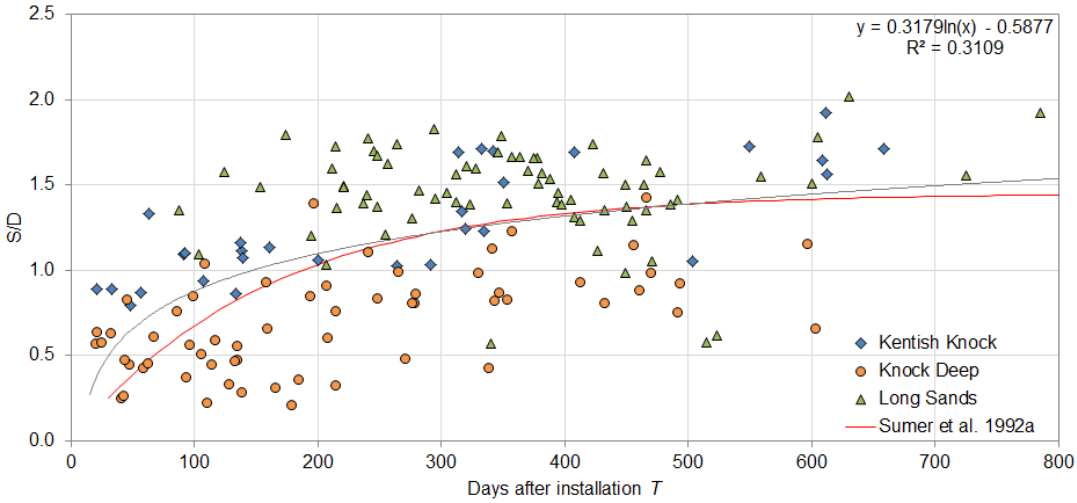

Figure 3.49: Relationship between scour hole age and scour depth S/D at London Array.

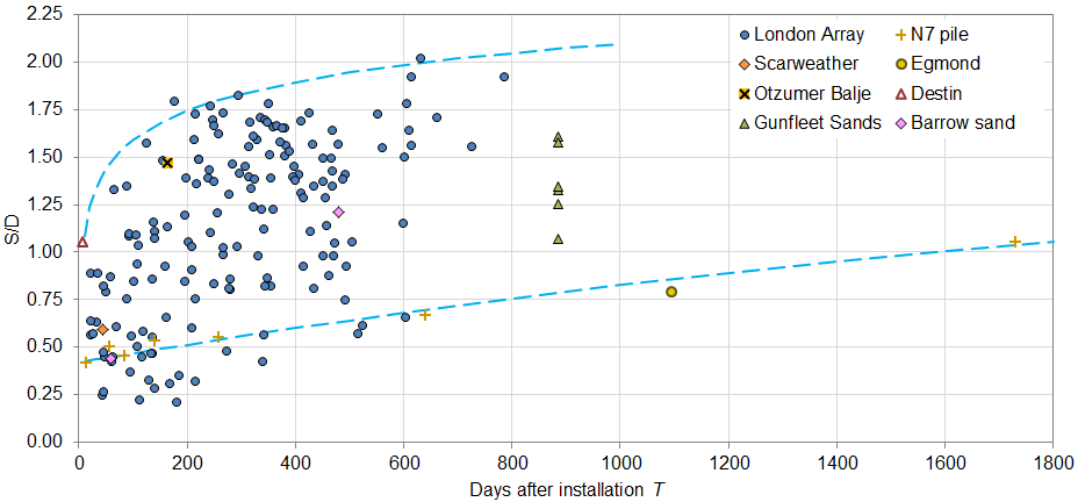

Figure 3.50: Relationship between scour hole age and scour depth S/D in sandy sediments. Envelope of scour development in sandy sediments given as blue dashed lines.

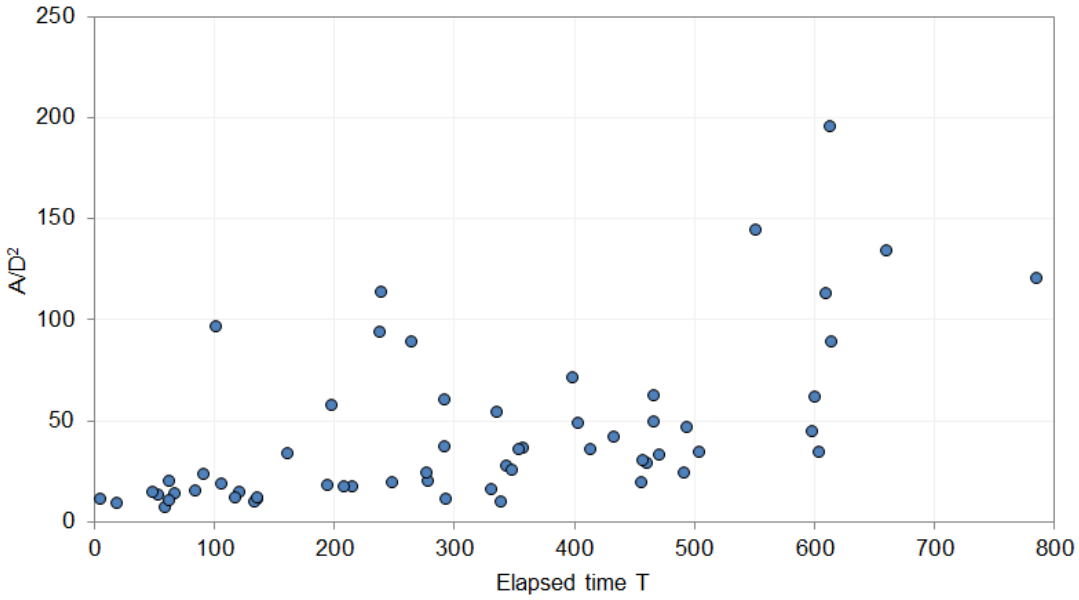

Figure 3.51: Relationship between scour hole age and scour area A_S/D^2 at London Array.

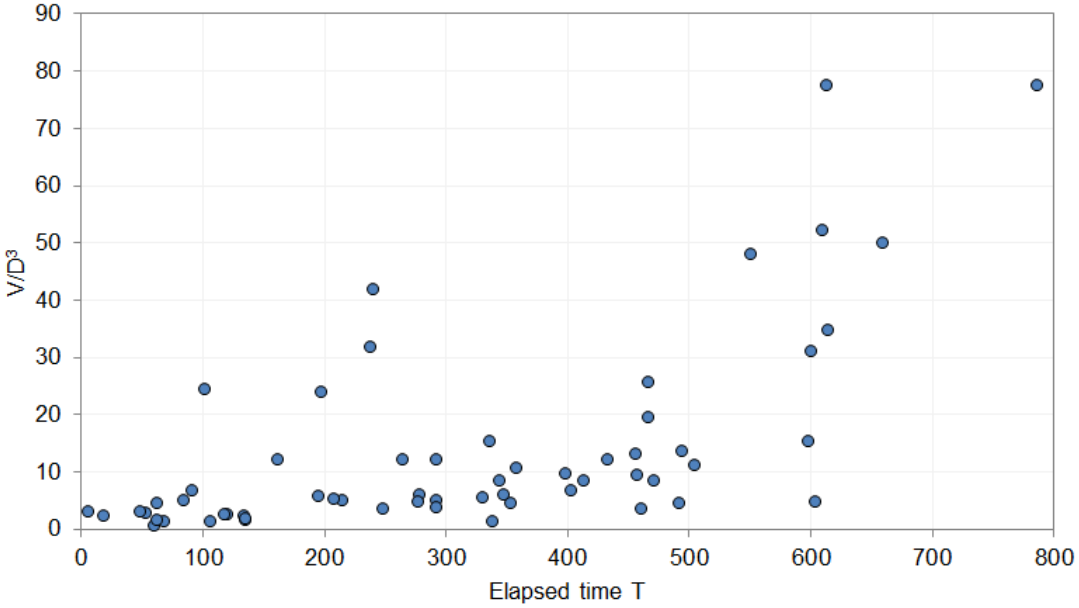

Figure 3.52: Relationship between scour hole age and scour volume V_S/D^3 at London Array.

3.5 Summary

The above discussion has conveyed the variability of scour from 175 offshore monopiles at a single wind farm location in what is relatively uniform substrate. The analysis of prototype data has shown a considerable variation in scour depth, area and volume, at London Array offshore wind farm. Scour depths vary between $0.21-2.02D$ ($1.20-9.50$m), with $7.9 < A_S/D^2 < 196.1$ ($256-5013$m^2) and $0.6 < V_S/D^3 < 77.7$ ($119-8590$m^3). The spatial distribution of scour dimensions follows the topographic setting to a certain degree with larger scour found on the sand banks and lesser erosion in the channel of Knock Deep. Scour hole shape has proven to be, on average, less variable than the dimensional parameters as most scour holes exhibit circle-type outlines ($IQ > 0.8$ and $L/W < 1.3$), albeit the range of circularity and axial elongation is considerable. Also, the morphological descriptors do not appear to follow any organisation by topography and the pattern is more chaotic. The lateral extension ranges strongly from confined scour holes to very laterally extensive scour holes and follows the distribution of scour area with more confined holes in the channel and more extensive pits on the sand banks. The lateral extent of scour controls the exposure of high-voltage cables and volume of scour protection required. The mean W/D and L/D have been determined as $6.7D$ (36.4m) and $8.6D$ (46.8m), respectively.

The analysis of slope angles in scour holes revealed that there is a lack of knowledge about possible slope angles in marine substrates. Slope angles are reported as a single average slope value β_{av} per scour hole ($7.5-30.8°$), which has been found to be a function of the relative dominance of the main scour pit to the wider scour area. Upstream and downstream slope angles display similar ranges as β_{av} and on average the upstream slope was found to be a factor of 1.3 steeper than the downstream slope. A histogram of all slope values observed at the foundations showed that the majority of recorded slopes are below 15°, but in terms of maximum slope angles, the main scour pit and edge features in the wake can display small areas with angles of over 70°, which is significantly greater than the expected ϕ of sandy sediments. Slope angles in cohesionless substrate greater than 50° are common and observed in most scour holes. The effect of hydrodynamic variation was investigated to establish whether there is a significant difference between scour holes that develop under the influence of one dominating flow direction as opposed to the more balanced symmetric flow condition; the range of scour values in both flow regimes were found to be very similar. The scour in thick deposits of unconsolidated sediments appear to develop unaffected by variations in ground conditions (eg. compaction degree) throughout the vertical profile. However, where London Clay bedrock is close to the sea bed surface in Knock Deep, the thickness of granular sediment was found to be an effective limiter of vertical erosion. Interestingly, in the same area, a large number of relatively shallow scour pits appear to have been limited within the granular sediment package. A variety of factors were considered to explain this observation and it was found that the most plausible explanation is the timing of scour surveys which appears to have skewed the analysis.

The effect of natural bed mobility at London Array appears to be a decrease in scour, albeit the number of data points in the higher-mobility categories is low, thus the significance of the trend is ambiguous. The scour development with time follows the general

pattern expected from experimental evidence in loose sediment; very rapid rates of erosion are witnessed in the first few days of erosion and scour commences immediately upon installation. Subsequently, the scour progression slows and, from approximately $T > 100$, the rate of change approaches zero asymptotically. Exponential relationships have been established to predict the rates of change ΔS, ΔA_S and ΔV_S on the basis of the number of days since installation T. Similarly, a logarithmic equation is provided to estimate the dimensionless scour depth S/D from elapsed time T. The observed temporal development of scour raises the question of survey time planning; unless hydrographic surveying is conducted immediately after monopile installation the exponential change in scour depth is not captured. From a process perspective, not much is known about the early phase of scour at prototypes and there is a case for a dedicated study to investigate this in a suitable offshore location. Conversely, from an engineering perspective where merely the "final" scour depth is required, a single survey after approximately 400-500 days seems appropriate to effectively capture most of the change in cohesionless sediments; longer delays are recommended if the full lateral extent is required. As a general rule, the more erodible a substrate, the more important the notion of survey timing.

Chapter 4

Thanet offshore wind farm

The Thanet offshore wind energy project is a Round 2 wind farm located approximately 14km off the coast of Margate, eastern Kent (see Fig 1.2). The development covers an area of 35km^2 and consists of 100 Vestas V90 turbines with a rating of 3.0MW, providing a total capacity of 300MW and capable of covering the energy needs of 200,000 homes[1]. The wind turbines are mounted on monopile foundations with diameters of 4.1-4.9m, installed over a period of 10 months between March 2009 and January 2010; turbine rows are spaced at 670m distance and the inter-turbine interval is 480m. This development is the most southerly within the Outer Thames Estuary and is located on a flat plateau in relatively deep water of 17-30m. Thus, the topographical variation is considerably less than at London Array. However, the heterogeneity of the sea bed is much greater, with a typically thin veneer of mobile sediment above different bed rock types. The general hydrodynamics are similar, in terms of magnitude, to London Array.

4.1 Hydrodynamic regime

In addition to the regional hydrodynamic regime outlined in Section 2.1.1 some more detail from measured data (Ramboll, 2009) and numerical modelling studies (HR Wallingford, 1992, 2002a,b; ABPmer, 2008) will be introduced. It will be shown that the gross hydrodynamics are similar to those at London Array; however, due to the low topographic variability, the resulting flows are less variable in magnitude and direction throughout the site.

Tides The tidal range at Gunfleet Sands lies within the range suggested in section 2.1.1 and is given as 2.4m and 4.1m in neap- and spring-tidal conditions, respectively, based on measured data. Admiralty tidal diamond data (see Figure 2.2) suggest that the flood current direction is southerly (189°N) and due north (004°N) on the ebb, which is in strong contrast to the E-W flows closer to the Kent headland. The flood tide dominates with spring and neap tidal streams of 1.0ms^{-1} and 0.6ms^{-1} respectively; on the ebb tide, slightly lower velocities of 0.8ms^{-1} and 0.5ms^{-1} are reached. Modelling by ABPmer

[1] Vattenfall, unknown, Thanet offshore wind farm in Kent, http://www.vattenfall.co.uk/en/Thanet-offshore-wind-farm.htm. Accessed: 08/05/2014

(2008) shows current speeds of 0.8-1.1ms^{-1} for springs and 0.6ms^{-1} for neaps with the larger magnitudes observed over the southern part of the site. Tidal residuals on the spring tide are directed in a south-south-easterly direction as shown in Royal Haskoning (2005) with a residual velocity of circa 0.1ms^{-1}; on the ebb tide, weaker northerly residuals are observed with approximately 0.03-0.05ms^{-1}. During extreme conditions of a 1:50 year return period the surge conditions cause an increase in depth-averaged tidal current of up to 0.6ms^{-1} (HR Wallingford, 1992), which agrees well with the depth-average current speed $\overline{U_c}$ = 1.62ms^{-1} for a 1:50 year return period event suggested by Ramboll (2009). Under the given average current conditions, scour is expected to occur in a live-bed regime, at least in respect to sand-sized sediments, as corroborated by the presence and migration of bed forms (section 4.3.2).

Waves The site is exposed to waves from northern and eastern sectors originating in the North Sea, southerly and south-westerly waves from the English Channel and locally generated waves from the north-west (see Figure 2.4). Waves approach predominantly from the south-west but the largest waves are generated from a northerly and north-easterly direction where the fetch is greatest. A short-term deployment of a wave buoy at the Drill Stone reef (see Figure 4.5) between February 2004 and December 2004 revealed the largest recorded waves to have originated from both south-westerly and north-easterly directions with $H_s = 3.25m$. Due to proximity and low sea bed relief, the average wave conditions are expected to be similar to those measured at Southern Kentish Knock, presented in Figure 3.2.Numerically modelled wave conditions suggest the winter mean significant wave height in a range of $H_{s,wi}$=1.2-1.4m and $H_{s,su}$=0.7-0.8m in summer (ABPmer, 2008). The summer values agree well with the summer average derived from South Knock Wave Rider in Section 3.1, but the winter range is greater than simulated. It is possible that due to the location of the buoy on southern Kentish Knock (Fig 3.5), that winter waves from the north-east are limited in height over the sand bank, thus actual winter wave conditions at Thanet are larger than suggested from that location. For extremes, significant wave heights with return periods of 1, 10 and 100 years are given as 3.9m, 4.9m and 5.7m respectively (HR Wallingford, 2002b). For 1:50 year wave conditions H_s = 5.1m and T_p = 10.4s is proposed (Ramboll, 2009). Given the mean water depths at the site (h > 17m), the effect of waves on sediment transport and erosion around turbine foundations should be negligible in anything other than extreme events, as for average conditions $L_0/2 \approx 10$m, based on T_z = 3.6s (see Section 3.1).

4.2 Geology

The underlying geology of the area is characterised by three north-north-westerly dipping formations, ranging stratigraphically from the Upper Cretaceous to the Late Palaeocene/ Early Eocene (see Fig. 2.5). The southern part of the Thanet site is located on the edge of a chalk plateau that stretches offshore from the Kent coast as illustrated in Figure 2.6, while the central and northern site is underlain by the Thanet Sand and Lambeth Group formations. A variable, but generally thin, cover of Quaternary sediments is observed throughout the site. The stratigraphy and the geotechnical properties of the bedrock and

Quaternary sediments will be discussed below.

4.2.1 Bedrock

As outlined in Section 2.1.2 the solid geology at this wind farm site is characterised by three cycles of deposition in the Cretaceous and Thanetian.

4.2.1.1 Upper Chalk

In the south-west, the bedrock consists of Cretaceous Upper Chalk that is outcropping or within 1-2m of the sea bed surface. The chalk at Thanet can be described as low-density, weak to very weak, very fine-grained limestone originating from deposition of planktonic algae (coccoliths) during warm, tropical marine conditions that prevailed in the Late Cretaceous period. The chalk is formed to over 98% of calcium carbonate ($CaCO_3$) and incorporates frequent flints which are registered as pronounced spikes in cone resistance q_c in the CPT record. Lab analysis of samples from borehole cores show dry densities of between $\rho_{dry} = 1.45 - 1.6 g/cm^3$, bulk densities between 1.9-2.0g/cm^3 and water contents between 25-32%. The Upper Chalk can be described as non-plastic and in unconfined axial shear tests has been shown to fail in a brittle fashion (Gardline Lankelma, 2008). The undrained shear strength c_u, derived from CPT measurements, lies in a range of $100 < c_u < 700$kPa, with 400-700kPa (described as "hard", Table 2.6) associated with unweathered lithology and the reduced material strength range of 100-400kPa (stiff to very stiff) commonly observed in the top 3-10m of Chalk that has undergone subaerial weathering during episodes of emergence in the Late Cretaceous/Early Tertiary. CPT records reveal that in terms of engineering properties, the Upper Chalk behaves similarly to stiff to very stiff hard clays. Structurally and compositionally, the Upper Chalk is quite homogeneous over the study area and are found to be either structureless or densely fractured, in the vertical depth of interest. The thickness of chalks in this area is approximately 200m in this area (Bomel, 2006).

Figure 4.1 shows the stratigraphy at Thanet wind farm. The top of the Upper Chalk horizon, dipping away to the north, is readily identifiable as a strong reflector and can be traced throughout the site. The lack of acoustic signal from within the chalk bedrock is very typical and conveys the notion of solid structure and homogeneous material with little lithological or sedimentological variation in lateral and vertical directions. Above the Upper Chalk, lies unconformably the Thanet Sand Formation, which displays layered reflectors that follow the dip direction. Above that is a layer of 1-3m of loose Quaternary sand and further to the north-west, the Upnor Formation which is the lowest litho-stratigraphic unit of the Lambeth Group.

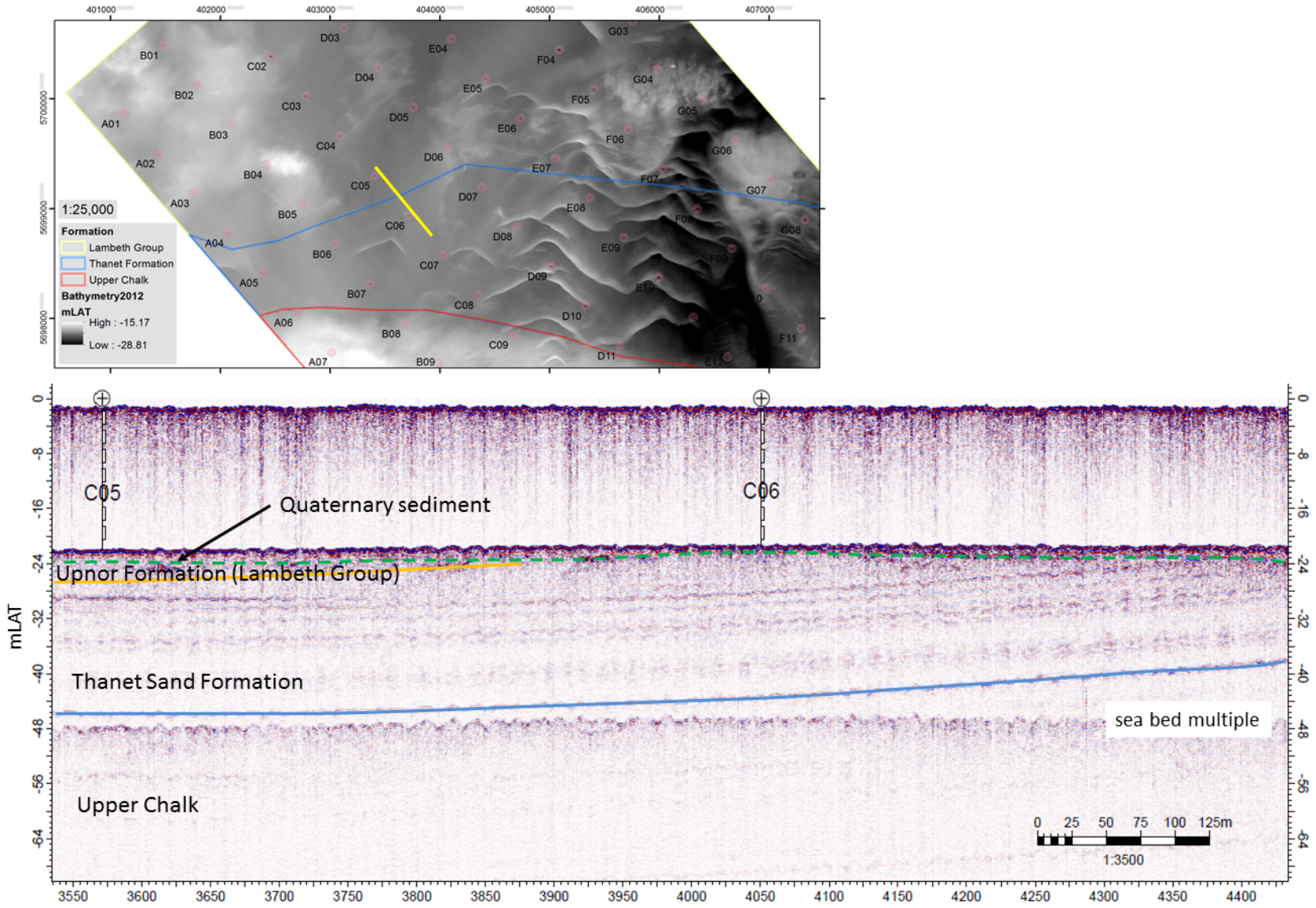

Figure 4.1: Seismic reflection data the stratigraphy at Thanet wind farm. Top of Upper Chalk (blue), Top of Thanet Sand Formation (orange), Top of Lambeth Group (green dashed). Loose sediment cover of between 1-3m. Upper Chalk seismic signal typically feature-less implying homogeneous structure.

4.2.1.2 Thanet Sand Formation

Where the chalk dips away in the mid- and eastern sections of the site, the bedrock is made up of the Palaeocene Thanet Sand Formation (also referred to as, simply, the Thanet Formation), dominated by glauconitic sands, silts and clays. After a depositional hiatus of 10-15Ma, caused by tectonic uplift, a small-basin shallow-sea depositional environment was created that resulted in a shift from carbonate sedimentation to the deposition of inner-shelf and coastal siliciclastic sediments of the Thanet Sand formation (Entwisle et al., 2013). The bedrock consists of sediments that are generally well sorted owing to re-working prior to deposition. At this location, the Thanet formation measures approximately 30m thick. The unconformable basal boundary is marked by the flint conglomerate of the Bullhead bed which is, however, not universally present around the site. Boreholes and CPT records at turbine locations show that fine material ($d_{50} < 0.063$mm) can be found ubiquitously within the Thanet Formation, often also close to the surface. Laboratory examination of borehole samples exhibit typical values for dry density of $\rho_{dry} = 1.5 - 1.7$g/cm^3 and water contents between 25-35%. The bedrock can be described as dense to very dense which is reflected by relative density values, that although variable, tends toward $D_r \longrightarrow 100\%$ (see Table 2.5). At Thanet the CPT records in this formation show a large proportion of clay, sandy clay and clayey sand lithologies as revealed by elevated friction ratios on CPTs. The cohesive layers found within this stratigraphic entity are firm to very stiff clays and sandy clays with undrained shear strength values between $c_u = 100 - 300$kPa, occasionally up to 500kPa ("very stiff" to "hard"). The seismic data reveal some internal organisation within the Thanet formation. Figure 4.2 shows a typical acoustic reflection pattern with cone resistance q_c and friction ratio R_f from CPT investigations. The stratigraphy shows a 2-3m cover of loose silty sand over a 12m package of clay with a layer of gravelly clay. Sandy gravel marks the basal boundary of the Thanet Formation. The sub-parallel, northerly dipping inclined reflectors can be cross-referenced with the CPT information and reflect changes in sediment density and lithology within the Thanet Sand Formation. The strong reflector between -37− -40mLAT is Upper Chalk interface.

4.2.1.3 Lambeth Group

The Lambeth Group (formerly known as Woolwich and Reading beds, Entwisle et al., 2013), deposited between 55-56Ma ago, unconformably overlies the Thanet Formation in the north and west of the wind farm site. The Upnor Formation is the lowest litho-stratigraphic unit of the Lambeth Group. Sediments of the Lambeth Group are structurally and compositionally highly inconsistent and is made up of shallow marine and estuarine clays and laminated silts and sands. For this reason, the highly heterogeneous bed rock is characterised by strongly variable rock strengths. Much of the knowledge about the Lambeth Group is derived from terrestrial investigations and outcrops and is discussed comprehensively in Entwisle et al. (2013) however less is known about this formation offshore. The mentioned source is drawn upon here and is augmented with additional insights gleaned from CPTs, boreholes and seismic reflection data. The heterogeneity of the Lambeth Group is explained by the variety of depositional conditions experienced

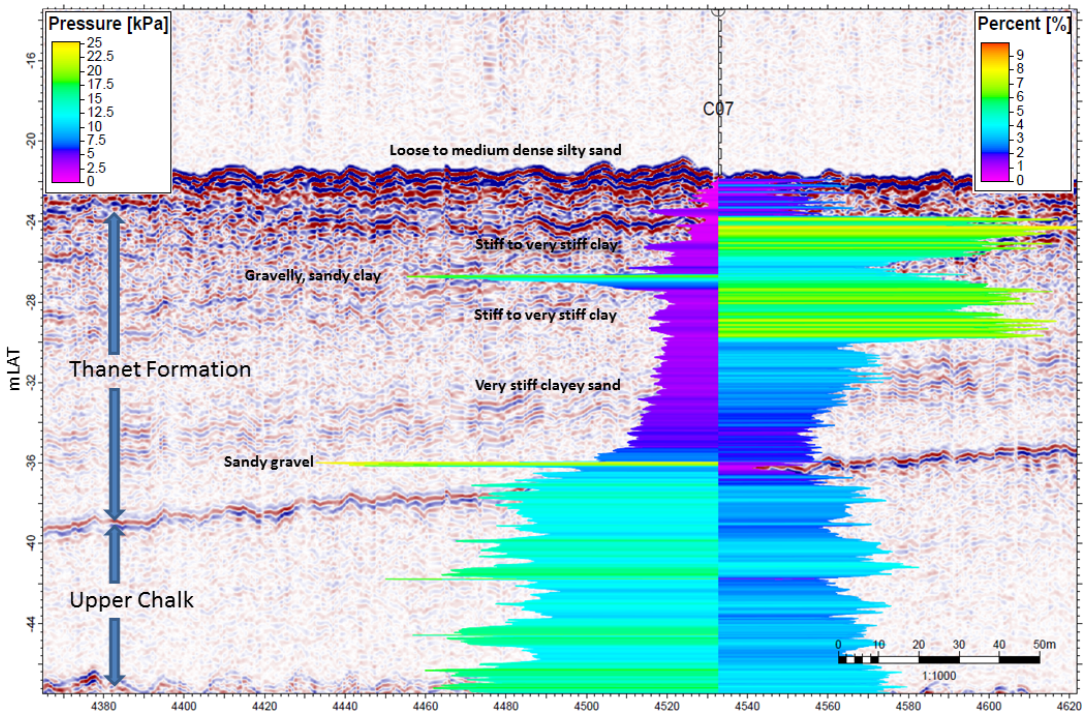

Figure 4.2: Representative seismic reflection of the Thanet Sand Formation with CPT records of cone resistance q_c [kPa] and friction ratio R_f [%] exhibiting a variety of clay-rich lithologies. Top of Chalk at depth.

during sedimentation. At the beginning of the Palaeogene the region was on the margin of a sedimentary basin resulting in intermittent deposition periods during cycles of transgression and regression caused by global sea level changes. The depositional environment at this marginal sea location fluctuated between shallow marine to lagoonal and estuarine. During periods of regression, fluvial erosive and terrestrial weathering and pedogenic processes took hold (Entwisle et al., 2013). Thus, it is not uncommon to find concreted hard layers such as sandstones (Sturt et al., 2009) silcretes, calcretes or ferricretes in this formation as a result of weathering under subtropical conditions. In fact, concreted layers have been picked up on a number of the CPTs within this formation; usually, the CPT cannot penetrate these hard surfaces and tip resistance spikes of $q_c \gg 80$MPa are typical (as shown in Figure 4.3). Lithostratigraphically, the base of the Lambeth Group consists of the Upnor Formation which is 4m thick in this area (pers. comm Mike Clare (email)). The Upnor/Thanet boundary is characterised by a change in grain size and colour and can display one of two forms; a gradational boundary mixed by bioturbation which is difficult to identify, or a more unambiguous sharp flint gravel boundary. In the former case the greenish grey sands of the Upnor formation are somewhat coarser, less dense and more clayey than the grey fine sand deposits of the underlying Thanet formation (Entwisle et al., 2013). At Thanet, some uncertainty remains over the bottom boundary of the Lambeth group as it has proven difficult to identify from geotechnical and geophysical data even where boreholes are present. Similarly, the interface between recent unconsolidated sediments and the top of the Lambeth Group can also equally difficult to establish. Due to the typically low material strength and low consolidation, the CPT measurements are similar to those of the overlying unconsolidated sediment and the boundary can often not be placed with confidence on CPTs. The very high lateral heterogeneity of the Lambeth

Group also complicates the interpretation as even small positional discrepancies between individual sub-bottom data records (seismic, borehole, CPT) can be sufficient to confuse cross-referencing between the sources. Borehole samples from the Upnor Formation reveal similar dry densities as observed in the Thanet Formation but somewhat lower moisture contents between 10-30% reflecting the lower porosity and poor sorting of the sediment. From a large database of terrestrial samples, Entwisle et al. (2013) shows median water contents of 19% and dry density of 1700kg/m^3. The CPT recordings reveal that the cohesive material found within the Lambeth Group typically exhibits unconfined shear strength values between $c_u = 100 - 400$kPa ("stiff" to "hard", Table 2.6). The strong spatial heterogeneity of sediments is demonstrated in the seismic data. Figure 4.3 shows a characteristically chaotic acoustic reflection with multiple internal sub-parallel reflectors. The northerly dip of the stratigraphy is appreciable but the inconsistency of the lithological facies is evident in the irregularity in length, orientation and acoustic impedance of the reflectors and presence of discontinuities, incisions and fills (Sturt et al., 2009) bears witness to the complex deposition and genetic history of the sediment in this stratum. In this particular example a surface layer of loose sand (0.8m) lies above a narrow band of clay (0.3m). The underlying layer of sand becomes progressively more dense with depth until a hard concreted layer is hit, where the CPT cannot progress.

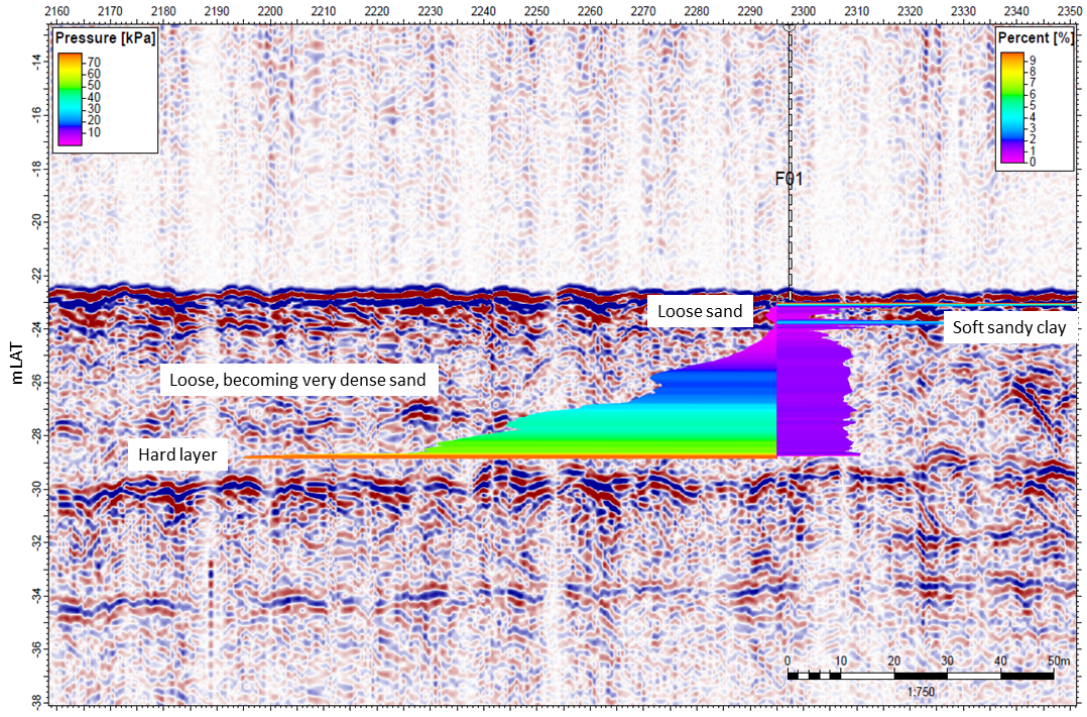

Figure 4.3: Seismic reflection in the Lambeth Group and CPT records of cone resistance q_c [kPa] and friction ratio R_f [%]. Concreted layer at depth stopped CPT penetration as marked by spike in q_c.

4.2.2 Quaternary sediments

The Quaternary sediment layer consists of recent post-transgressional and re-worked pre-Holocene sediments predominantly fine to medium silty, sometimes gravelly sands. As mentioned above the boundary between Quaternary sediment and underlying Lambeth Group and Thanet Sand Formation can not always be distinguished with confidence,

since the sedimentary bed rock and can be weak or weathered and thus does not exhibit a distinct boundary in terms of geotechnical properties. The thickness of granular sediment z_{sed} is used as a parameter for unconsolidated, potentially mobile sediment and identified from the CPT measurements by means of the relative density of the deposit. Hence, it should be noted that the chosen parameter does not necessarily discriminate by age or origin of sediment and, as such, can include any Quaternary sediments as well as Tertiary sediments as long as these are granular and unconsolidated. The justification for this is that, for scour purposes, the consolidation state and mobility characteristics of a deposit are more important than the precise determination of stratigraphic origin. In the CPT records, the encountered spikes in q_c relate to the concreted horizons in the Lambeth Group which are found between 1.5-6m depth below the sea bed.

4.2.2.1 Pre-transgressional sediments

Sediments deposited before the Holocene transgression are typically confined to the palaeochannels. A prominent branching depression, discernible in the bathymetry in Figure 4.4, runs approximately north-south along the eastern edge of the sand wave field marking the location of the defunct channel. Boreholes and grab samples in this area reveal that the channel infill is comprised of 1-2.5m of fine sediments such as silty sands, clayey silts and sandy clays. Cuspate seismic reflections suggest that local patches of gravels can be found at the channel bed. None of the turbine foundations are situated directly in the channel although D14 and E14 are on the margins of the southern channel.

4.2.2.2 Post-transgressional sediments and thickness of sediments

Only a small amount of grab sample information is available. Additional median grain size values were extracted from particle size distributions of near-surface borehole samples. Furthermore, Crown Estate data were added, that while not providing grain size values, inform on the percentage of gravel in surface sediments. The data, plotted together, are shown in Figure 4.4. The distribution of gravel shows that surface sediments are distinctly different between the Chalk plateau and the lower rest of the site. The latter is mostly devoid of gravels, bar local patches (e.g. at A03, B02 or E06), with very fine to medium sands ($0.63 < d_{50}[\text{mm}] < 0.25$), locally coarse, being the dominant size fraction. On the chalk plateau gravel percentages between 60% and as high as 95% are found. The predominance of coarse material here is due to a shallow veneer of heterogeneous sediments generally 0.2-0.5m thick, locally up to 1m thick, which are typically composed of mixed gravel lag deposits with clasts of chert, flint or chalk.

The thickness of granular sediment z_{sed}, as derived from CPT measurements, ranges from a thin veneer of 0.2m to circa 6m as shown in Figure 4.4. Over much of the southern part of the site, the cover of loose material is less than 0.5m, locally up to 1.5m. Thicknesses of 0.5-2m are common in the northern area with locally greater z_{sed} in the central and north-eastern areas. The maximum loose cover in a turbine location, as extracted from the interpretation of CPT records, was found to be 6.5m at E02. The analysis of CPT records has revealed that 26% of turbines are effectively situated in bedrock, 45% percent

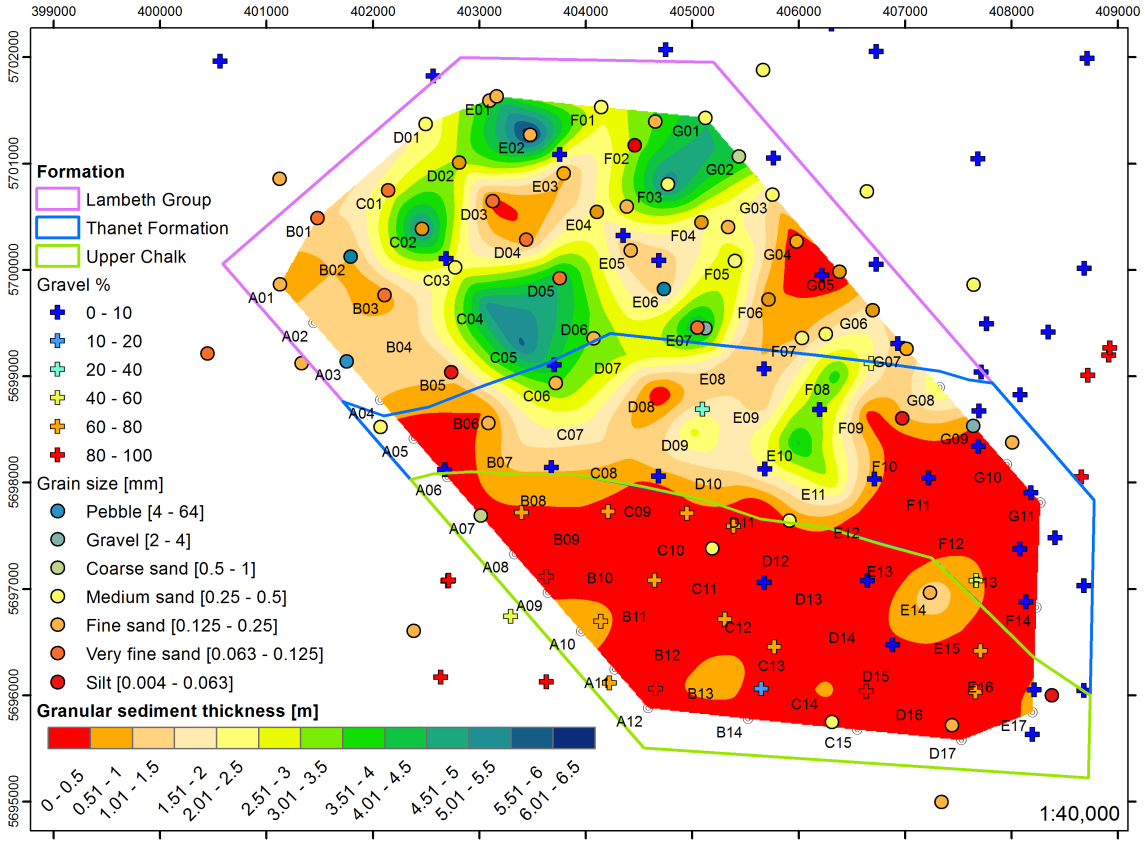

Figure 4.4: Nature and thickness of granular sediments at Thanet wind farm. Grain size d_{50} and sediment composition (gravel %) data from surface grab samples.

are on a veneer of 1m or less, leaving a mere 29% with a larger sediment cover. It should be noted that the CPT survey was undertaken in 2007 and, where mobile, the thickness of veneer at a specific turbine location might have changed prior to installation of the turbines in the period between March 2009 and January 2010. This has been found to only affect a three locations (D09, E10, E11) in the central sand wave field.

4.3 Seabed Morphology

As mentioned before, the topography of the site is relatively benign compared to the sand bank and channel environment of London Array. Figure 4.5 shows the relief of the sea bed at the wind farm. The majority of the area is flat and bed morphology is a function of the presence of sand waves. However, sea bed levels are typically higher along the western side of the development. In the south-west of the area the Upper Chalk outcrop manifests itself as an erosional platform elevated by some 4-6m from the surrounding seabed. The slope at the transition varies between 1:50 and 1:150. To the south-east of the development, the sea bed drops rapidly to greater depths into the Lobourg Channel. The prominent Drill Stone reef is found to the east of the site.

4.3.1 Natural variability of seabed levels

This analysis was carried out on the basis of difference plots between consecutive bathymetric surveys. Bathymetric surveys were taken in 2005, 2007 and 2012. The spatial

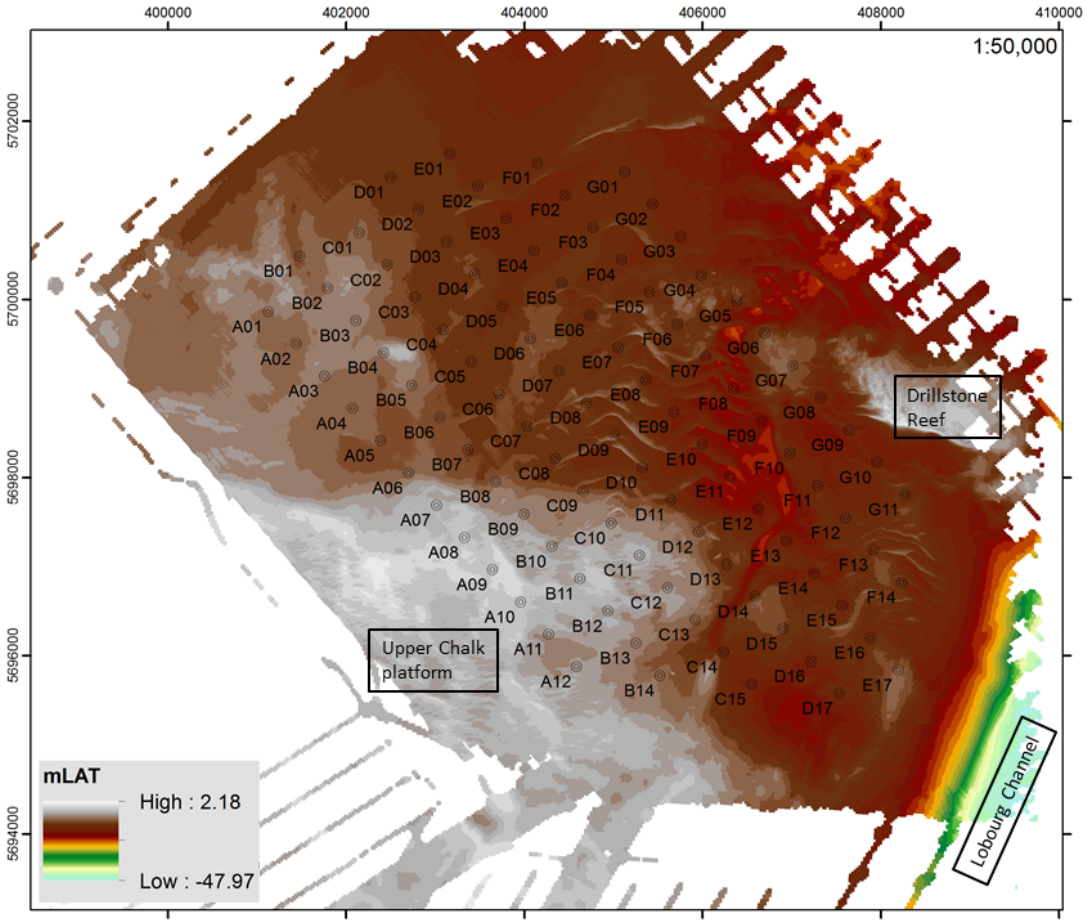

Figure 4.5: Sea bed topography at Thanet offshore wind farm. Mosaicked from bathymetric surveys dating from 2005, 2007 and 2012.

resolution of the 2005 dataset is quite coarse at 25m; both the following surveys were recorded at 1m resolution. A total of 3 difference plots were generated (2012-2007, 2012-2005 and 2007-2005) to inform on magnitude and trends of seabed level changes across the site. To allow for a meaningful interpretation of calculations using the 2005 dataset, the other surveys were coarsened to 25m resolution using nearest neighbour resampling prior to conducting the subtraction. The most accurate picture can be drawn from a comparison of the 2012 and 2007 surveys (Fig 4.6). All noteworthy bed level changes observed in that 5 year span can clearly be attributed to migration of bed features. The direction of movement can be inferred from the bed level change and is directed in a southerly to south-westerly direction. This coincides with the direction of the southerly flood tide, implying this is the main transport agent. Over the rest of the site, virtually no change in seabed levels is observed (seabed variation of ±0.5m is plotted transparently). The 2012-2005 and 2007-2005 plots are, expectedly, very similar (Figs 4.7 and 4.8, respectively). Even at the coarser resolution, the main pattern is the migration of the large-scale bedforms and otherwise negligible ambient bed level change, although more noise is visible. Much of this noise is due to resolution effects and is not considered to represent actual physical changes in bed elevation.

4.3.2 Bedforms and sediment mobility

As described in Section 4.2.2, the availability of readily moveable sandy sediments is limited over large parts of the site and consequently the seabed, in large parts, does not exhibit any significant bed features. Nevertheless, a wide range of bed forms are found at the site, from localised small-scale megaripples to large sand waves. Using the technique outlined in Section 2.2.4.2, the dimensions of the bed forms present in the vicinity of turbine foundations are determined and the calculated parameters were cross-checked against visual assessment of seabed topographical profiles to ensure accuracy. The bed form dimensions and orientation of the crest normal are summarised in Figure 4.9. Firstly, the plot reveals that most foundations are located in featureless surroundings. Otherwise, three common types of bed forms are identified; a closer look at these is offered in Figure 4.10 and the nature of the bed morphologies will be discussed below. The plot includes tidal residual sediment transport vectors for a grain of $d_{50} = 0.16$mm diameter derived from hydrodynamic modelling results from Carrizales (2010). Although the bed form configuration suggests southerly migration, the numerical model implies a sediment transport divide, with the northern half showing west to west-south-westerly pointing tidal residuals while in the southern half of the site net transport is due south to south-west. This could be related to the influence of the flow around the Kentish headland, which forces a re-direction of the flow, to the west of Thanet as mentioned in section 4.1.

4.3.2.1 Sand wave field and localised megaripples

This area encompasses the sand wave field in the north-east, the main central sand wave field and south-eastern sand wave field. All are characterised by distinct, well-developed crescentic sand waves with similar plan form. The largest bed forms within the site are

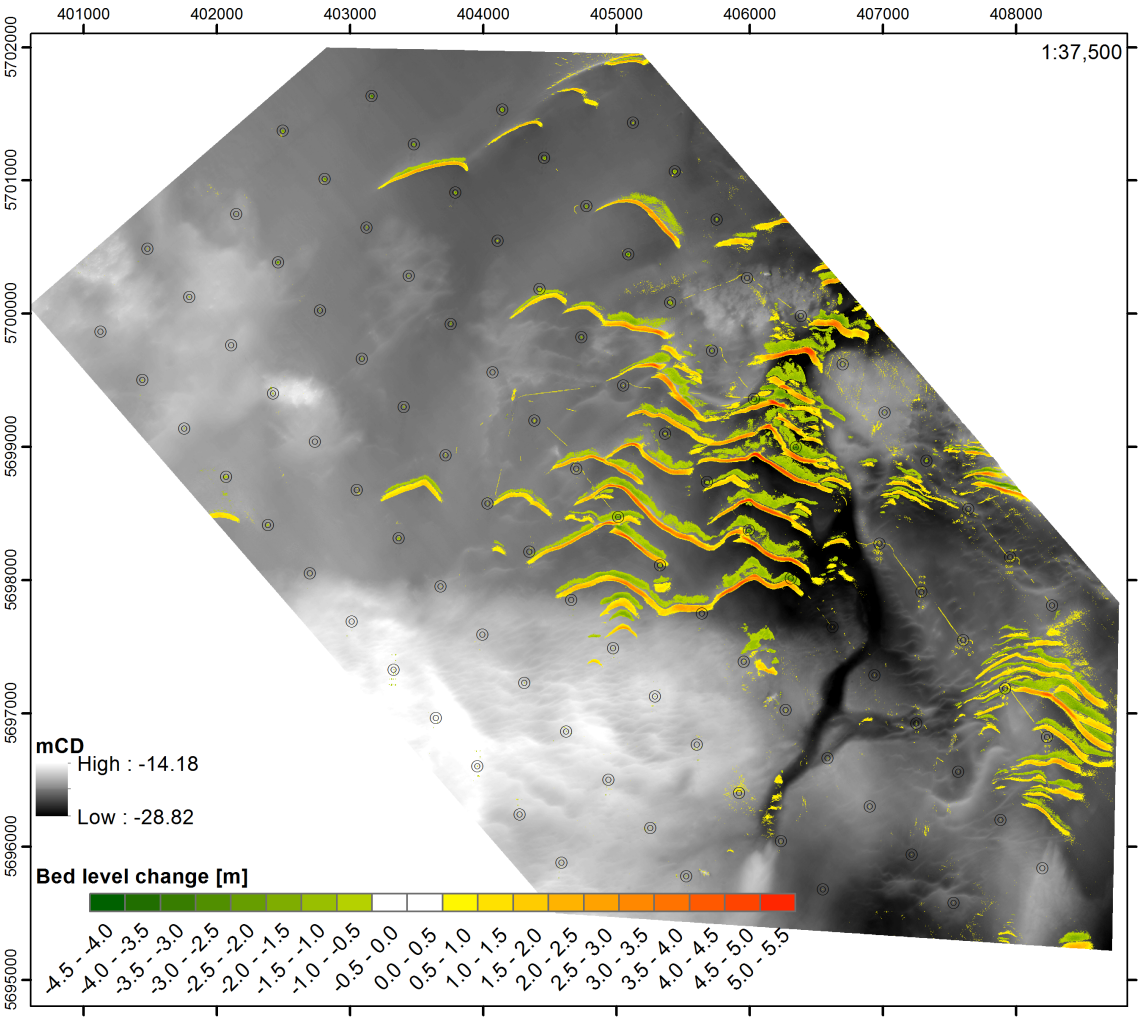

Figure 4.6: Natural bed level change between 2007 and 2012.

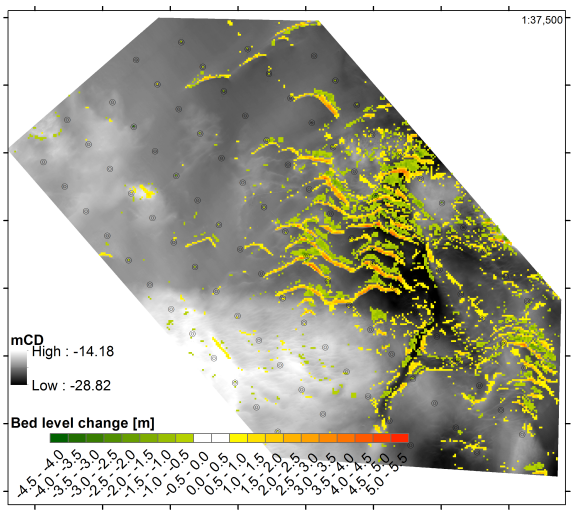

Figure 4.7: Natural bed level change between 2005 and 2012.

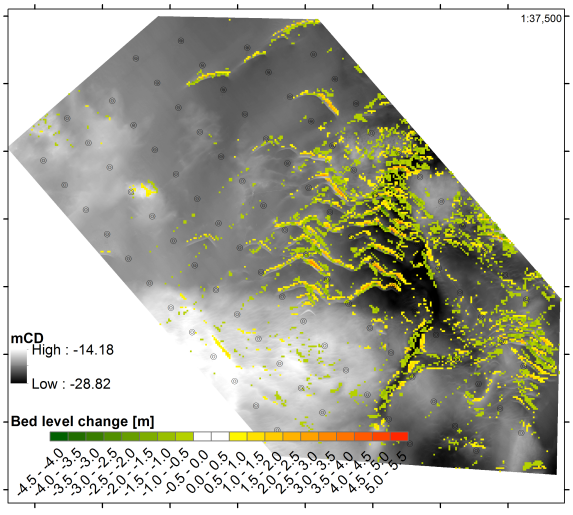

Figure 4.8: Natural bed level change between 2005 and 2007.

found in the main sand wave field with feature dimensions of $H = 3 - 6$m and $\lambda = 200 - 300$m. On the stoss side of these dunes well-developed megaripples are observed (Fig 4.10, A). In the north-east the sand waves are more isolated and exhibit heights of $2.5 - 3.5$m. Somewhat smaller sand waves are encountered in the south-east with dimensions of $H = 1.5 - 2.5$m, $\lambda = 50 - 100$m. The central and northern sand wave fields appear to be part of or an extension of a system of large-scale bed forms in deeper waters to the east of the site. These features, up to 7m in height, are likely to be the source of sediment to the area, entering the site in the east, constrained and funnelled into the area by the Drill Stone reef. Once within the site, their trajectory changes anti-clockwise to a more southerly direction as indicated by the bed form asymmetry and the positional change between consecutive bathymetric surveys. Latter analysis suggests that the rate of southerly movement of the bed forms in this area is 4-6m/yr; a faster rate of 8-10m/yr is observed in the south-eastern field (see Section 4.3.1), which demonstrates the very high mobility of sediment in this area and strong relief created by the large features. A number of foundation locations (D09, E09, E10) could be affected by the presence or movement of these features and will be investigated in more detail in section 4.4.4.1. For the megaripples found across the site as either localised bed features (Fig 4.10, C) or parasitic on sand waves (Fig 4.10, A), typical wavelengths of $5 - 15$m and crest heights of $0.1 - 0.5$m are observed. Bed features of similar heights $H = 0.3 - 0.5$m but narrower spacing of $\lambda = 5 - 10$m are found in the southern part of the palaeochannel. The bed forms in the fossil channel have experienced movement of about 1m/year in the period between 2007 and 2012. For the bed forms on the lower plateau the transport direction is south to south-westerly. The sediment budget will be controlled mainly by migration of these bed forms in sandy sediment. HR Wallingford (2002a) calculated a south to south-westerly directed net tidal sediment flux rate in the area in the range of 1000 to 10,000kg/m/tide for a grain of 0.1mm diameter in spring tidal current.

4.3.2.2 Chalk platform

On the Chalk platform bed forms are present in the gravel lag deposits. The features display wave heights of $H = 0.4$m consistent with megaripples; however the distance between crests is typically much larger with $\lambda = 50 - 70$m (Fig 4.10, B). Comparisons of consecutive bathymetric surveys in Figure 4.6 seem to suggest that these features have not migrated, at least not between 2007 and 2012, and are possibly moribund or only move in extreme events, when hydraulic forcing is sufficient to move the coarse sediment. Unlike the S-SW direction of transport on the lower plateau, the crest orientation on the chalk plateau suggests a migration in southerly direction.

4.4 Scour at Thanet offshore wind farm

At Thanet wind farm a single scour survey is available from 2012 that was taken approximately 2.2-3 years after the installation of the turbine foundations at a resolution of 1m. Due to the availability of a single survey only, the time development is not captured here; from the findings in section 3.4.6 it is likely that scour depths are fully developed, at least

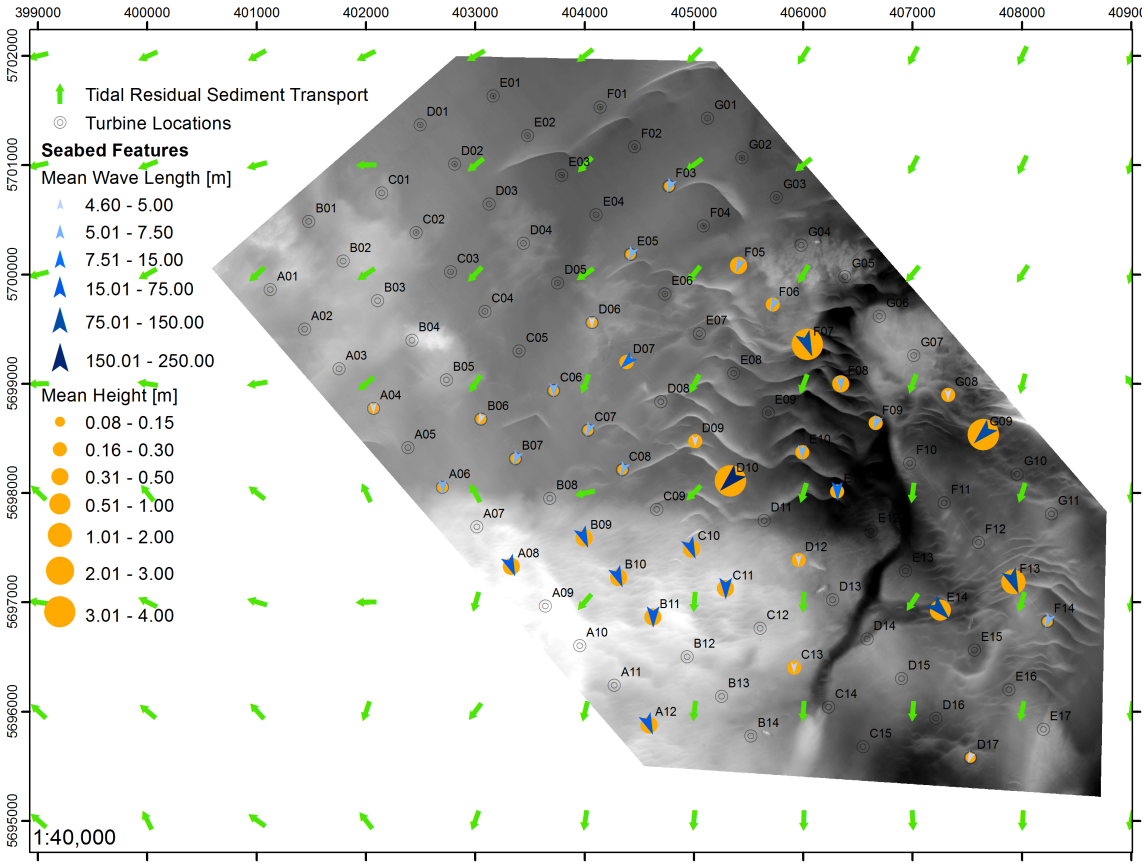

Figure 4.9: Mean bed form wave height and wave length derived from the quantitative bed form analysis. Predicted tidal residual sediment transport from numerical modelling by Carrizales (2010).

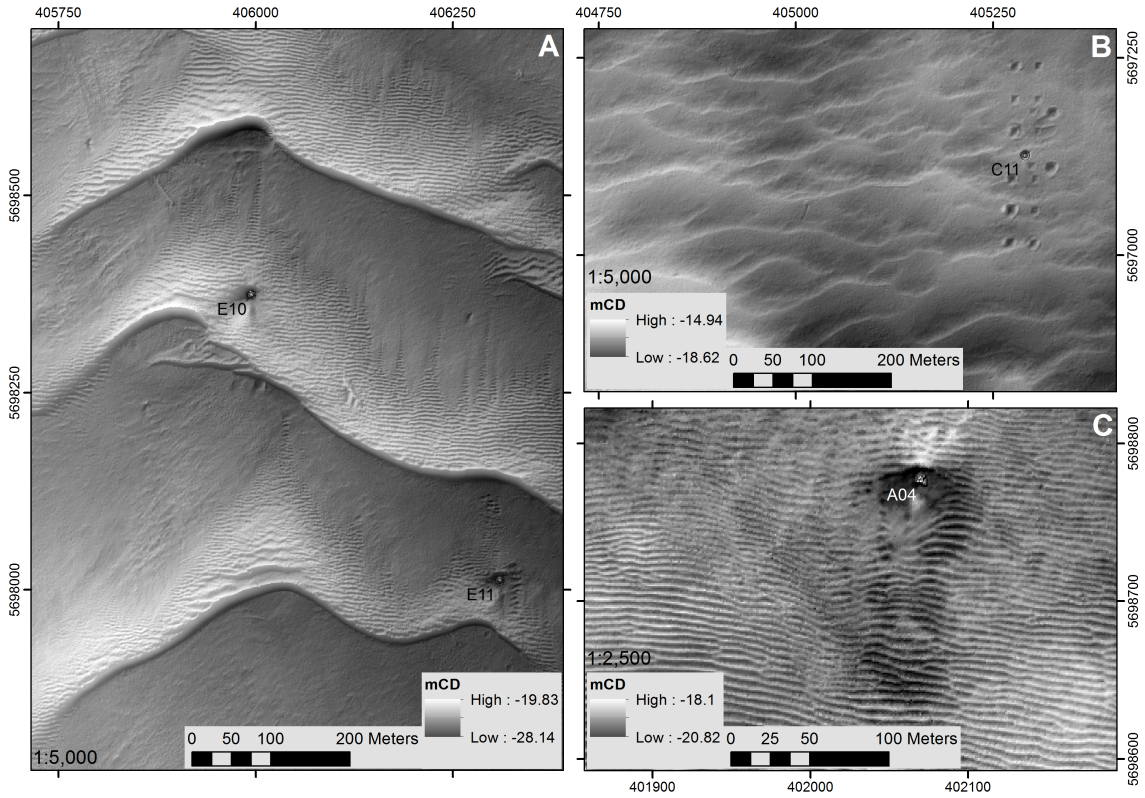

Figure 4.10: Typical bed features at Thanet: sand waves (H=4-6m, λ=200-300m) with parasitic megaripples (H=0.3m, λ=5m) at foundation E10 (A), moribund bed forms in gravel lag above Upper Chalk at foundation C11 (B) and local megaripple field (H=0.2m, λ=5m) at foundation A04 (C).

in sandy sediments. For complex substrates the time developments is yet unclear but is assumed to develop less rapidly thus might still be progressing. The coverage of the survey is complete, thus allowing all foundations to be considered, giving $N = 100$, for all aspects of the scour analysis.

4.4.1 Scour dimensions

The distribution of scour depths, areas and volumes across the wind farm site is shown in Figure 4.11 while the scour statistics are shown in Table 4.1. Scour here is much less pronounced than at London Array. Very shallow scour depths of less than $S/D < 0.4$ (approximately $S = 1.8$m) are prevalent in the southern area and along the western edge of the site, while somewhat deeper scour can be found in the rest of the site, although the distribution of scour depths does not appear to follow a clear pattern. The largest observed scour depth is $0.93D$ (4.54m) at E10 in the central sand wave field, while four locations display no scour (F10, F11, G04, G10). The mean scour depth over the site is $0.36D$ or 1.68m. All observed scour is less than $S = 1.3D$ ($S = 5.1 - 6.4$m), the expected value after Det Norske Veritas (2013), and also significantly less pronounced than at London Array.

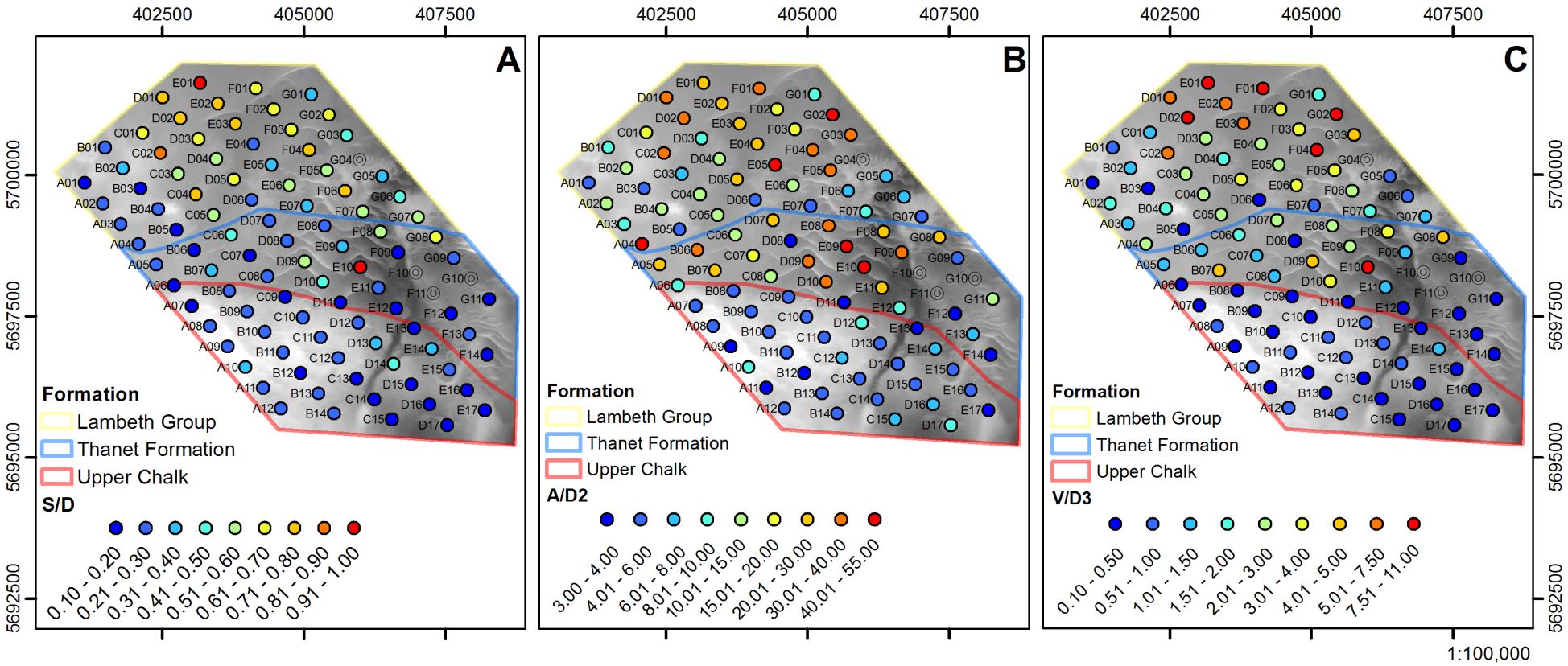

Figure 4.11: Scour depth S/D (A), area A_S/D^2 (B) and volume V_S/D^3 (C) at Thanet offshore wind farm.

Table 4.1: Statistics of dimensional scour parameters by geological formation at Thanet wind farm.

		S/D	A_S/D^2	V_S/D^3	S [m]	A_S [m^2]	V_S [m^3]
All	Min	0.10	2.9	0.1	0.43	54	8
	Max	0.93	52.6	10.1	4.54	1262	1048
	Mean	0.36	15.2	2.0	1.68	324	201
	σ	0.21	12.8	2.3	1.02	282	240
Upper Chalk	Min	0.12	2.9	0.1	0.56	54	8
	Max	0.42	9.7	1.4	1.89	214	144
	Mean	0.23	5.8	0.5	1.01	114	39
	σ	0.08	1.7	0.3	0.36	37	27
Lambeth Group	Min	0.10	0.0	0.0	0.43	95	14
	Max	0.93	46.8	10.1	4.38	947	1048
	Mean	0.50	18.3	3.1	2.34	499	323
	σ	0.21	12.7	2.6	1.02	262	272
Thanet Formation	Min	0.12	0.0	0.1	0.52	60	9
	Max	0.93	52.6	7.7	4.54	1262	904
	Mean	0.31	19.4	2.0	1.47	481	213
	σ	0.19	15.4	1.9	0.94	331	215

A similar pattern can be seen on the scour area and volume plots (Fig 4.11, B and C), at least for the southern area, where small scour area and volumes are found, typically $A_S/D^2 < 10$ ($A_S < 200\text{m}^2$) and $V_S/D^3 < 1.5$ ($V_S < 135\text{m}^3$). The north-western area shows the most extensive scour and areal and volumetric dimensions over $30D^2$ and $3D^3$, respectively, are common. For the rest of the site no particular organisation or clustering can be discerned and, overall, the range of scour areas and volumes is considerable. The most confined scour hole covers an area of just $2.9D^2$ (54m^2), while the most extensive covers $52.6D^2$ (1262m^2); scour volumes range between $0.1-10.1D^3$ ($8-1048\text{m}^3$). Although the spread is large, the distribution of A_S and V_S is heavily skewed towards low values with mean values are $15.2D^2$ (324m^2) and $2.0D^3$ (201m^3) only. The predominance of low scour values is illustrated in Figures 4.12 to 4.14, where the scour dimesions are plotted against relative water depth h/D. These plots show that scour in Upper Chalk shows the most confined values, whereas much larger variability is observed in the other two formations. Scour appears to be independent from water depth.

Although a weak organisational pattern of scour dimensional parameters for individual geological formations can be interpreted, it is not as clear as the topographical organisation in London Array. Nevertheless, the statistics (Table 4.1) for the individual formations suggest there is a statistically significant difference in scour dimensions between the three geologies. The statistics reveals that, on average, the shallowest and smallest scour pits are associated with turbines located in the Upper Chalk. Good clustering of all dimensional parameters is revealed by the consistently small standard deviations in this geology. The average scour hole depth in the Thanet formation is only just under 0.4m deeper than in the Chalk however the spread of values given by σ is much greater indicating that the scour in this geology is more variable. On average, scour depth and volume is greatest and most variable in the Lambeth Group, whereas the scour extent is the greatest in the Thanet Formation. A number of reasons for the described distribution of scour dimensions will be discussed below; based on the discussion of the lithological properties and sediment distribution the spatial pattern of scour could be controlled by variable characteristics of the bedrock, the varying distribution and thickness of unconsolidated sediment, or both.

Figure 4.15 shows the distribution of scour depths with area (left) and volume (right).

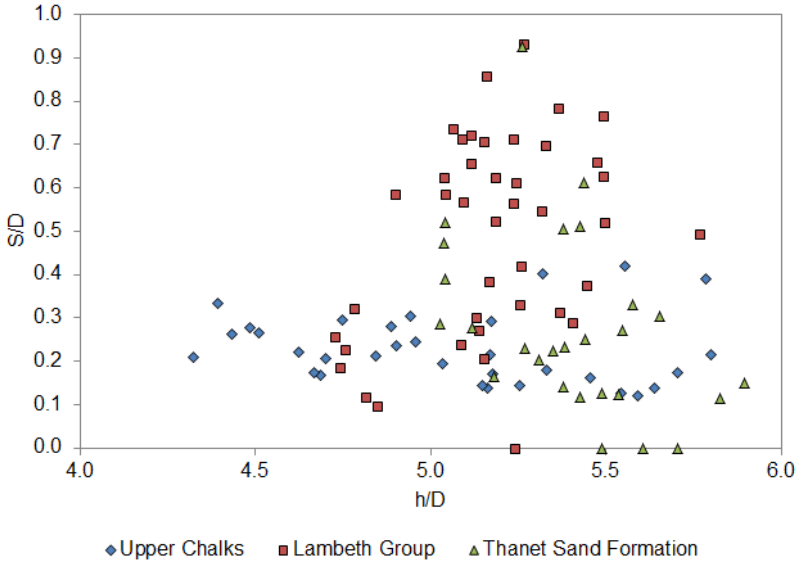

Figure 4.12: Observed scour depth S/D as a function of mean relative water depth h/D at Thanet wind farm.

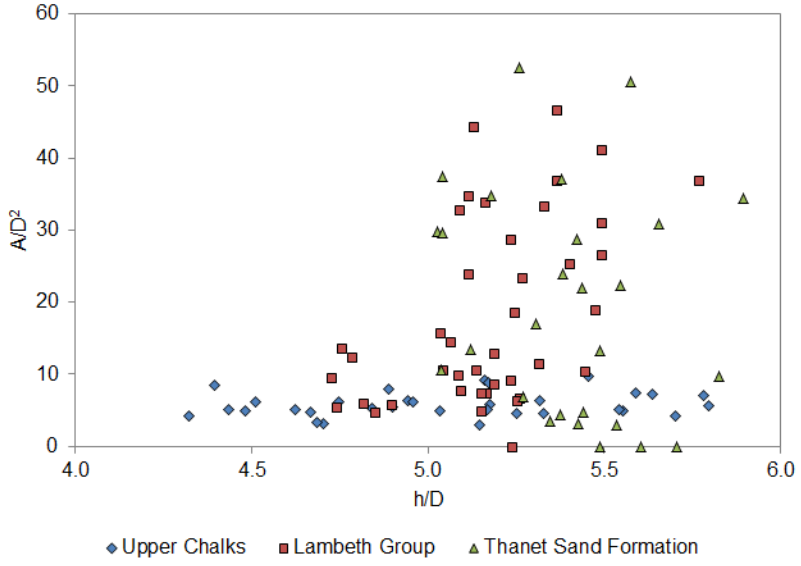

Figure 4.13: Observed scour depth A/D^2 as a function of mean relative water depth h/D at Thanet wind farm

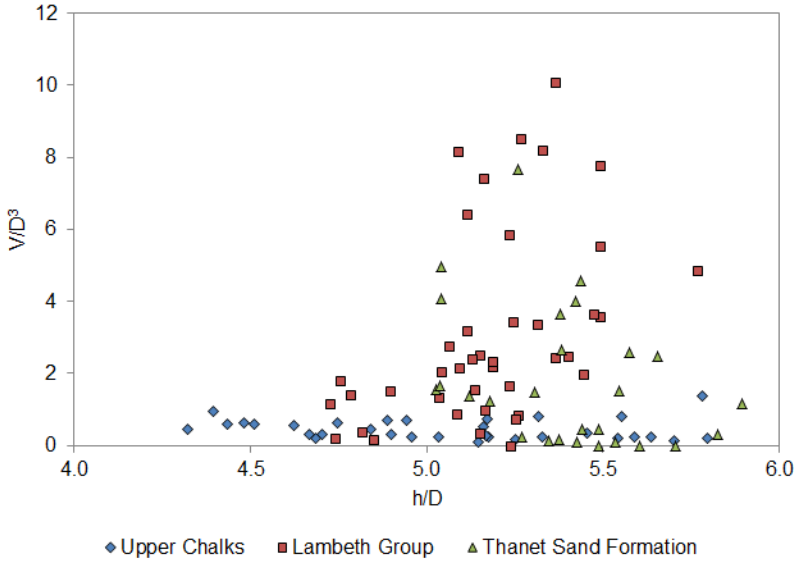

Figure 4.14: Observed scour depth V/D^3 as a function of mean relative water depth h/D at Thanet wind farm

Unlike at London Array, only a weak relationship between S/D and A_S/D^2 is observed, implying that even quite shallow holes can have extensive lateral scour. The distribution of points suggests that scour holes in the Thanet Formation are typically shallow but laterally extensive, whereas scour in the Lambeth Group is similarly wide but deeper. The relationship with volume is generally much stronger, indicating that most of the scoured material originates from the main scour hole which is a function of scour depth. Scour hole volumes in the Upper Chalk show a particularly strong correlation with S/D indicating that most of the eroded sediment volume is from the main scour pit.

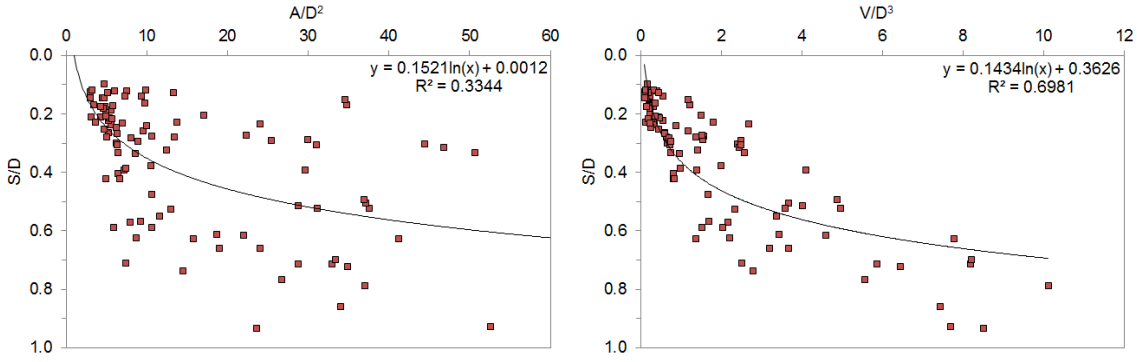

Figure 4.15: Scour depth S/D as a function of scour area A_S/D^2 (left) and volume V_S/D^3 (right) at Thanet wind farm.

4.4.2 Scour morphology

The extent and orientation of the long and short axes are plotted in Figure 4.16. This plot also reveals the orientations, relative to °N, of the long and short axis. The scour holes in the southern and north-western section of the site appear to be considerably more confined than in the rest of the site. The largest scour extents are found in the central and northern areas of the development. The scour hole widths W across the site vary between $2-8D$ (approximately 10-40m), with an average lateral extent of $3.9D$, approximately 17.7m (see Table 4.2 for statistics of morphological parameters). Scour hole extension along the flow axis L is relatively similar between $2-13D$ ($\approx 10-58$m) and a mean of $5.1D$ (≈ 23.4m). The similar values of L and W already indicate that flow-parallel and flow-transverse scour pit dimensions are very alike. On average, scour holes exhibited more confined lateral extent than previously reported for sandy beds by Whitehouse et al. (2011). The distribution is similar to that of scour area, with the scour in Upper Chalk exhibiting the most confined scour pits.

The orientation of the long axis α_L is also shown in Figure 4.16 and displays high variability, from approximately flow-aligned (ie. north−south to north-east−south-west) to flow-transverse. The latter are mostly found in the central area of the site, eg. in the sand wave field. Wakes are present here; however these are stubby and seem to be confined in length by the presence of the large sand wave crests, resulting in the observed orientation of the long axes (similarly to Figure 3.17). As will be shown below, the axis dimensions described by L/W are typically very similar, thus, even a small asymmetry can affect α_L. The long axis is hence not diagnostic for the dominant flow direction.

The L/W ratio, shown in Figure 4.17, reflects the previous observation that the length

Table 4.2: Statistics of morphological scour parameters by geological formation at Thanet wind farm.

		W [m]	W/D	L [m]	L/D	L/W	IQ	α_L	β_{av}
All	Min	9.1	2.12	10.2	2.36	1.03	0.43	-87.88	2.72
	Max	37.7	7.70	57.8	12.85	2.95	0.97	89.60	28.89
	Mean	17.7	3.86	23.4	5.11	1.32	0.81	9.09	11.89
	σ	7.3	1.52	10.9	2.31	0.29	0.12	50.47	5.21
Upper Chalk	Min	9.1	2.12	10.2	2.36	1.03	0.62	-87.88	5.71
	Max	14.3	3.22	29.8	6.33	2.95	0.96	89.60	19.79
	Mean	11.7	2.66	15.1	3.42	1.30	0.84	36.91	11.67
	σ	1.2	0.26	3.9	0.81	0.37	0.08	44.85	3.39
Lambeth Group	Min	11.4	2.53	14.5	3.23	1.03	0.43	-83.17	3.98
	Max	34.9	7.42	57.8	12.85	2.19	0.97	87.51	28.89
	Mean	20.3	4.39	26.3	5.70	1.28	0.82	-2.77	14.01
	σ	6.5	1.40	10.3	2.28	0.21	0.13	42.53	6.03
Thanet Formation	Min	9.6	2.13	12.6	2.80	1.06	0.48	-82.96	2.72
	Max	37.7	7.70	56.3	11.50	2.41	0.95	87.88	17.68
	Mean	21.5	4.59	29.7	6.36	1.40	0.74	-8.26	54.09
	σ	8.2	1.72	11.5	2.42	0.26	0.12	54.09	3.81

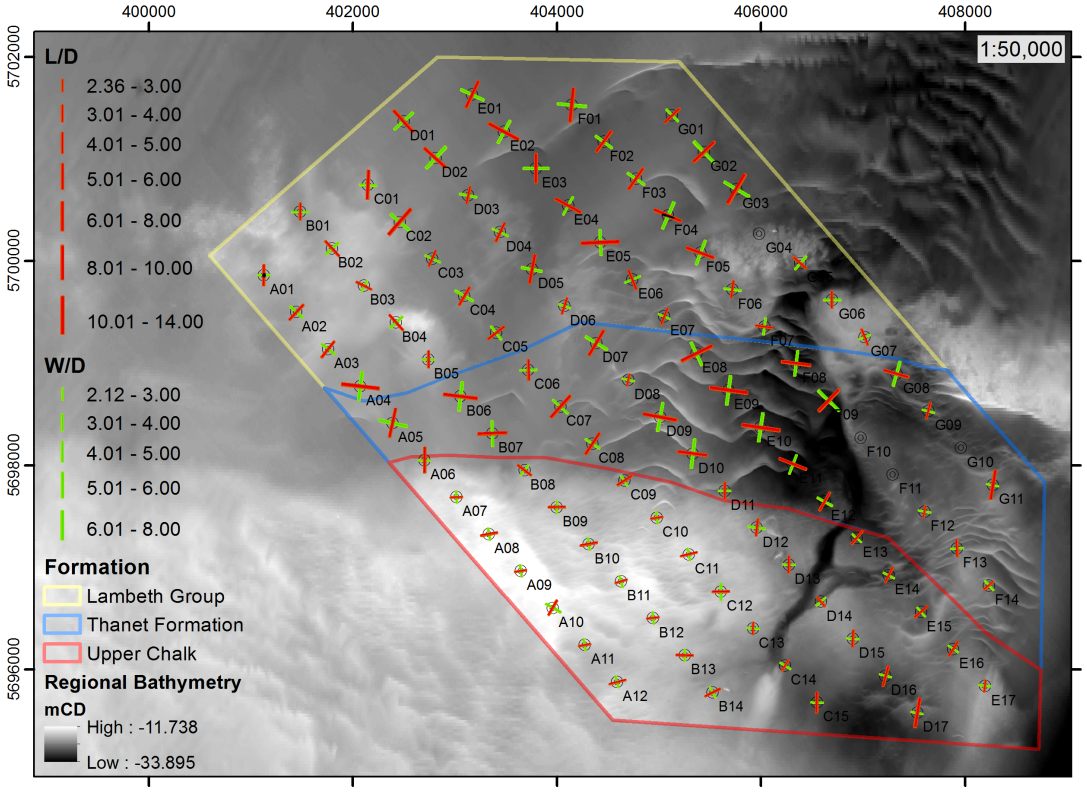

Figure 4.16: Scour hole length L/D and width W/D and orientation of long and short axes at Thanet offshore wind farm.

and width of the scour pits at Thanet are overwhelmingly similar. The average value for the ratio is 1.32, although it ranges from very close to unity to nearly 3; 70% of scour holes are below $L/W < 1.4$ and only in five cases is the long axis over twice as long as the short axis. Interestingly, the smallest values, on average, for the ratio is found in the Lambeth Group, which displays the largest scour depths. However, the spatial pattern described by the morphological parameters is less pronounced compared to the dimensional factors and variability is high. The areas identified as having the smallest scour generally show quite circular scour. The distribution of the isoperimetric quotient indicates that the majority of scour pits less than 20% from a perfect circle ($IQ = 0.81$, Table 4.2) and the greatest mean deviation is observed in the Thanet Formation, which is due to the presence of large sand waves. The availability of sediment is a prerequisite of wake development, which also explains why the largest scour holes by area are found in this region. However, it will be outlined in section 4.4.4.1 that due to the transient nature of the sediment supply, the observed scour dimensions should be considered temporary. The most circular scour pits are observed in the Lambeth Group and Upper Chalk which agrees well with previous observations about the likeness in magnitude of the long and short axis in this area.

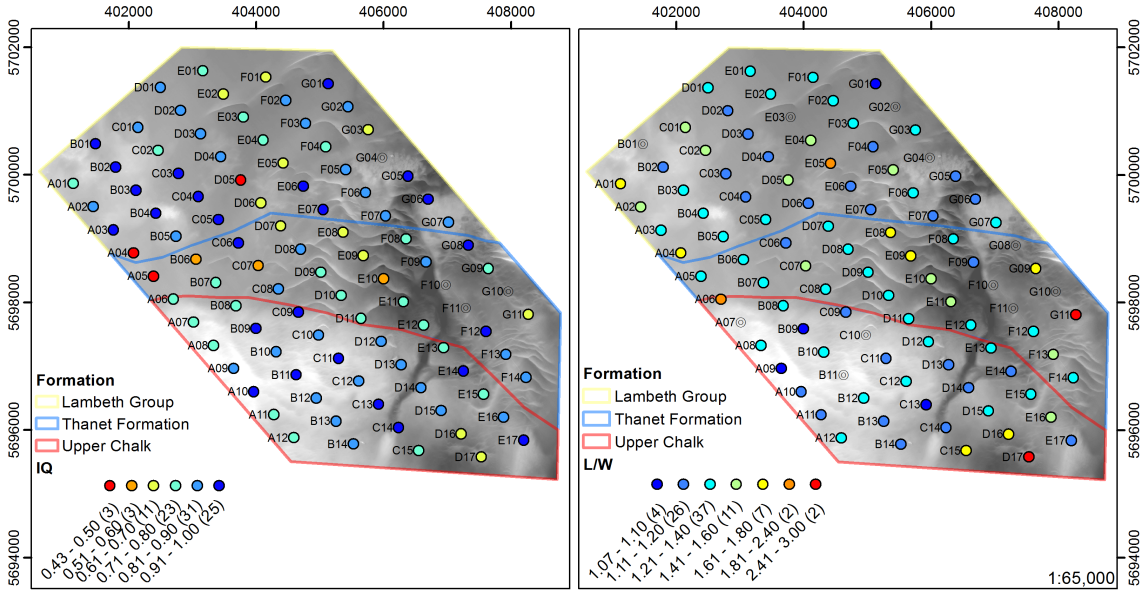

Figure 4.17: Distribution of isoperimetric quotient IQ (left) and long-short-axis ratio L/W (right) at Thanet offshore wind farm.

Figure 4.18 illustrates that circle-type morphologies, i.e. circular, near-circular and modified circle ($IQ > 0.8$; $L/W < 1.4$), are most common over the site (see Fig 4.19, A and B), although uni-directional (see Fig 4.19, D) and irregular (see Fig 4.19, E and F) shapes dominate in the area of the Thanet Sand Formation where loose sediment is available and hence more extensive wakes and lateral scour. Nearly all scour pits in the Upper Chalk fall into these three circle shape categories, which is testament to their confined nature and the absence of lateral scour. Although the Lambeth Group displays mostly circle morphologies, the range of observed shapes is great. Holes with explicitly bi-directional shapes as in London Array are not common; typically more uni-directional somewhat elongated shapes are found (similar to Fig 4.19, D). While increasing irregularity of scour pit outlines is not that uncommon, significant preferential axial extension ($L/W > 2$) appears rare.

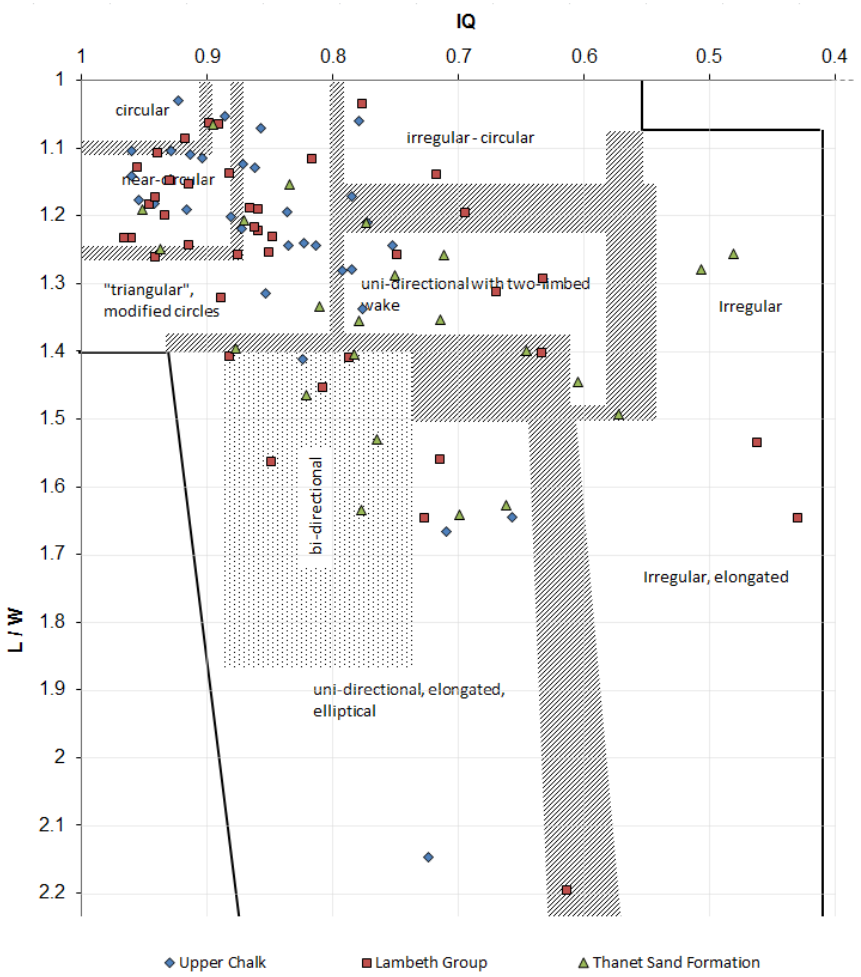

Figure 4.18: Classification of scour hole shapes at Thanet offshore wind farm.

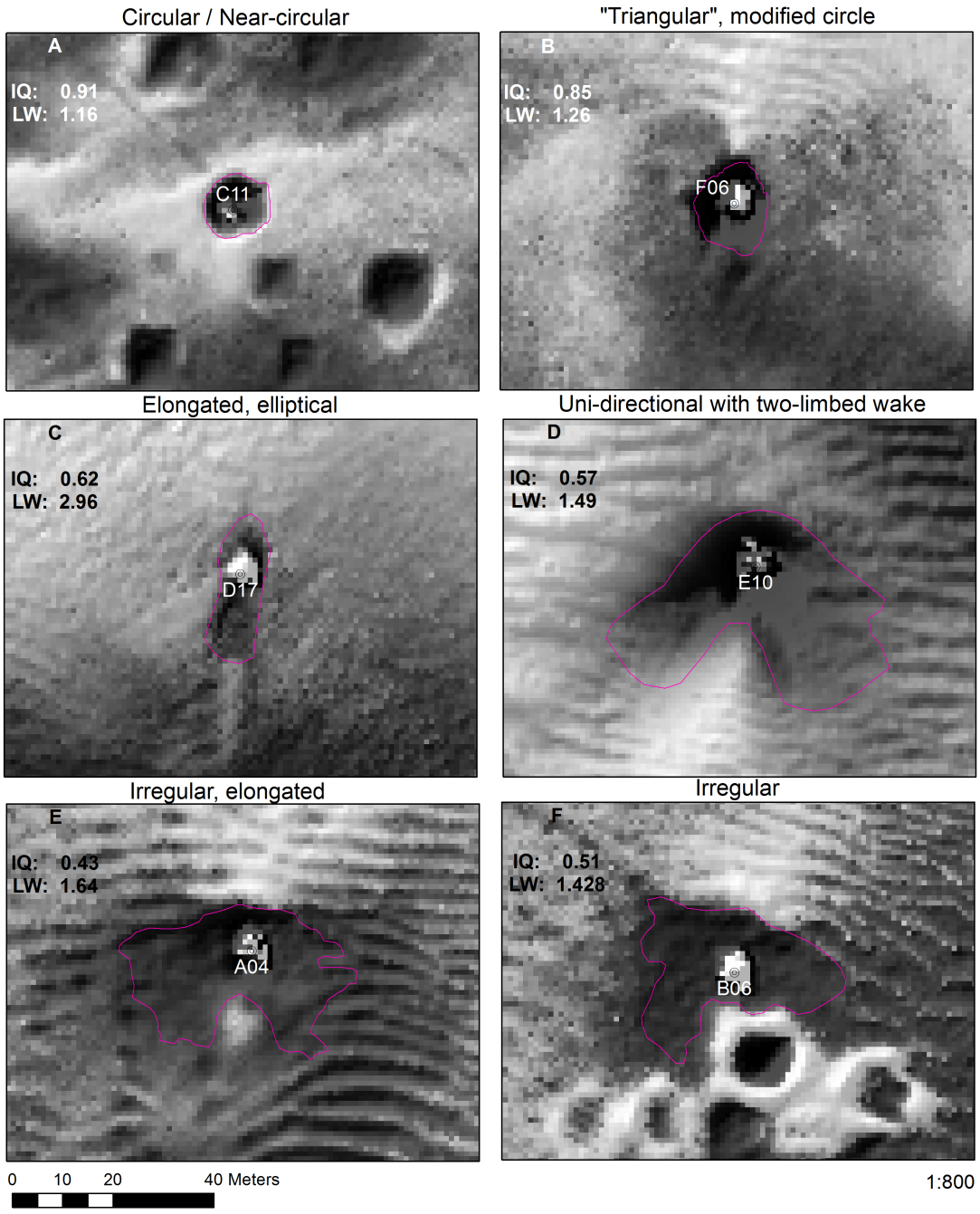

Figure 4.19: Typical scour patterns observed at Thanet wind farm and arrow of dominant flow direction. Circular shapes (A), modified circles (B), elliptical (C) and uni-directional (D). Visualised as partially transparent bathymetry overlying hillshade plot.

In Figure 4.20, the range of mean slope angles is between $2.7 - 28.9°$ (Table 4.2). While the single representative slope angle is a function of the relative size of the steeper main scour hole and the surrounding shallower scour, at Thanet, confined scour holes also exhibit low slope angles. The flow-axial slope ratio $\beta_{u,av}/\beta_{d,av}$ is generally less than 1.5, with an average of 1.3 and a maximum ratio of 2.5 (Fig 4.21). On average, this is less than the factor of 2 suggested by Hoffmans and Verheij (1997), which is likely to be due to the overwhelming absence of wakes. Interestingly, the slope ratio range and average value is very similar to that observed at London Array, although the ground conditions are very different. Figure 4.22 shows the histogram of slope values observed at Thanet wind farm. The maximum slope angle is 48°, while 60% of slope angles are less than 10°. Since cohesive materials are, in theory, not limited in the maximum attainable slope angle by physical constraints of granular friction, the comparatively low maximum slope angle is thought to be an artefact of insufficient spatial resolution of the bathymetric survey as discussed in Sections 2.2.1 and 5.1.2.5.

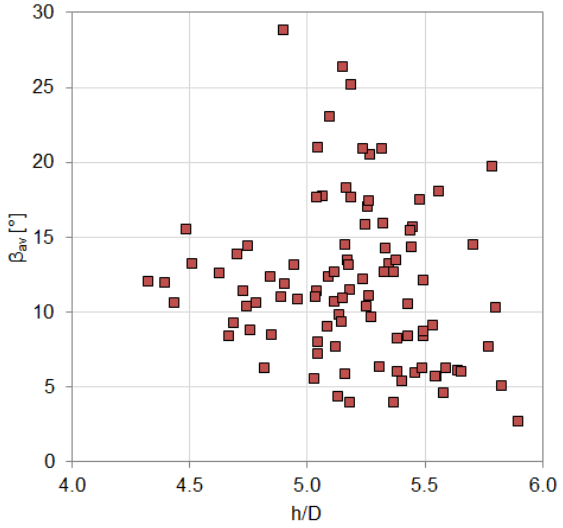

Figure 4.20: Mean slope of scour holes β_{av} as a function of relative water depth h/D at Thanet wind farm.

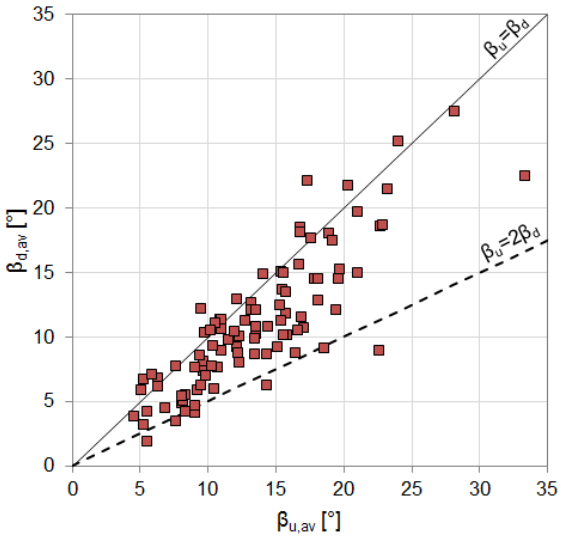

Figure 4.21: Mean upstream slope $\beta_{u,av}$ against mean downstream slope $\beta_{d,av}$ at Thanet wind farm.

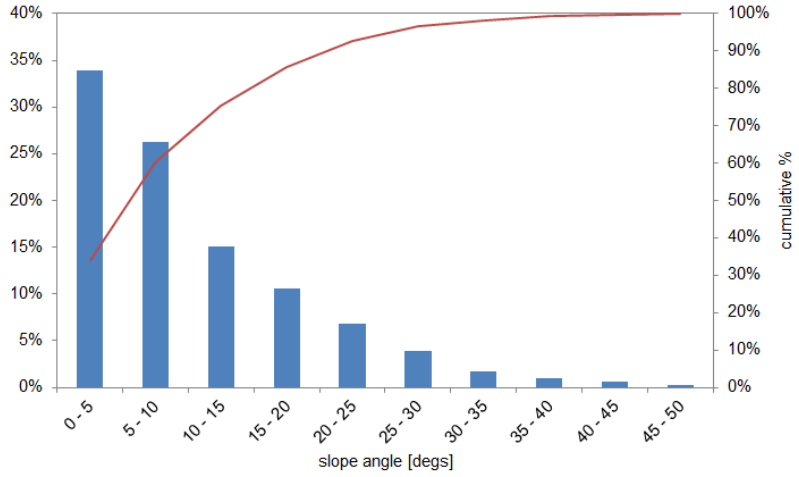

Figure 4.22: Histogram of slope angles in scour holes at Thanet wind farm.

4.4.3 Effect of hydrodynamics

Repeating this analysis, previously undertaken at London Array (Section 3.4.3), is not straightforward at Thanet. Previously, the distinction between symmetric flow and directionally dominated flow was evaluated based on the scour pit and ambient bed morphological evidence. This was aided by the relative abundance of mobile sediment and the homogeneity of the sediment properties. Due to the limited sediment availability and large swathes of featureless sea bed, the categorisation of the dominant flow mode is less certain. The outcome of the analysis is presented in Figure 4.23.

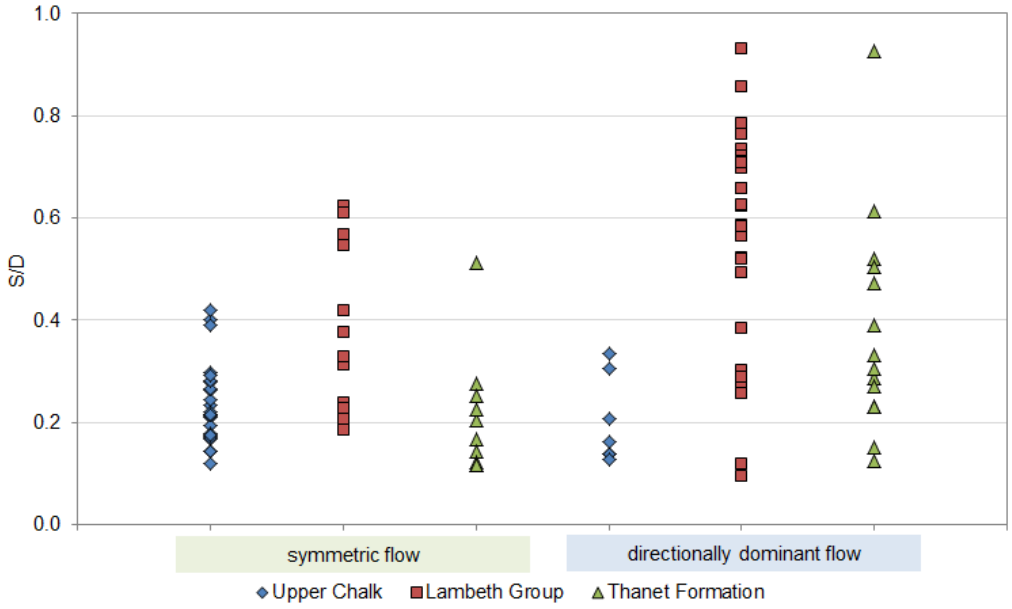

Figure 4.23: Range of S/D for symmetric and directionally-dominant flow types at Thanet wind farm.

The data suggest that larger scour is possible under directionally-dominant flow in areas underlain by Lambeth Group and Thanet Sand Formation, whereas Upper Chalk shows more confined range of S/D in this flow type. Generally the variability is greater under directionally dominant flows. The scour in symmetric displays a similar range in all three areas.

4.4.4 Effect of sediment thickness and geotechnics

At Thanet wind farm, the substrate in which monopiles have been installed is very diverse. It ranges from different types of bed rock to cohesive substrates to mixed granular sediments. At London Array, generally a large vertical package of mobile granular sediment is available other than in some areas of Knock Deep. This is typically not the case at Thanet where, overwhelmingly, the surface sediment layer is thin as illustrated in the isopach plot in Figure 4.4. Large areas in the southern part of the site display a veneer of less than 0.5m thickness, while in the north z_{sed} varies from about 1m to, very locally, over 5m. In the central area, spot depths of granular sediments are a function of the sand wave crest locations and should be considered relatively ephemeral covers given the migration rates put forward in section 4.3.2.1. First, scour will be investigated in terms of the available depth of sediment, followed by an investigation into the erodibility of underlying cohesive

substrates and bed rock.

4.4.4.1 Granular sediment availability

Figure 4.24 displays the relationship between the thickness of granular sediments z_{sed} and the observed scour depth S. At first glance, there appears to be little correlation between these two parameters as scour depth seems to develop fairly independently from sediment availability; however, three different response patterns between scour and vertical sediment availability can be identified based on underlying geology: a bed rock pattern (Upper Chalk), an independent pattern (Lambeth Group), and a mixed response that shows characteristics of both previous patterns (Thanet Formation) as well as a weak relationship between scour and z_{sed}. The orange highlighted points in Figure 4.24 identify data points that are subject to more detailed scrutiny in this section.

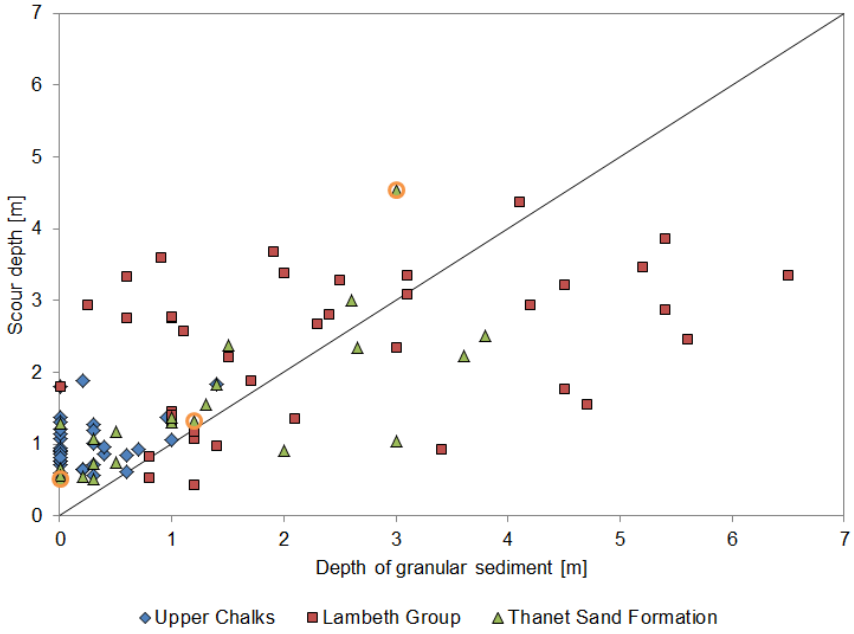

Figure 4.24: Scour depth vs thickness of granular sediment at Thanet wind farm. Highlighted data points will be discussed in more detail in this section (Fig 4.25).

Bed rock scour response pattern As shown in Table 4.1, the scour depth observed in Upper Chalk is quite uniform in dimension and shape. Furthermore, the erosion response of the monopiles in Upper Chalk appears to be significantly different to that around most of the rest of the site which is illustrated in Figure 4.15 which conveys constrained clustering of the scour dimensions when plotted against one another. Typically, little to no lateral extension is developed in Upper Chalk, thus a strong positive relationship is observed between S and V. Scour depths are small, in the range of $S/D = 0.12 - 0.42$ ($0.56 - 1.9$m). 60% of scour depths are less than 1m and 90% less than 1.5m. The two largest scour values are in foundations on the edges of the palaeochannel (D14, E14). In the Upper Chalk formation, where only thin sediment veneers of typically coarse particles are present, scour depth exceeds z_{sed}, implying that the weathered chalk is indeed erodible (Figure 4.24). Albeit, the erosion depth into bed rock ($S - z_{sed}$) is overwhelmingly limited to less than 1.5m ($< 0.35D$) suggesting that this is potentially the maximum possible

scour in this material, at least in the observed time frame. As previously mentioned in Section 4.2.1.1, the upper horizon (some 3-10m) of the chalk is weathered to a certain degree and the Upper Chalk is considered quite weak in terms of strength. Nevertheless, the material still offers significant resistance to erosion as suggested by the limited depths. It is possible that erosion resistance is enhanced by armouring action of gravel lag deposits, thus offering some shelter to the bed rock and reducing the potential for abrasion (see Section 1.4.4). Due to only a single post-installation survey being available, it is not clear whether the observed scour depths are final or whether scour is still developing here. If these scour holes develop at a slower rate, comparable to, say, cohesive materials, then further deepening of the scour depressions can potentially be expected. The presence of spud can marks raises the question how much of the observed near-turbine seabed deformation is hydraulically forced erosion and how much (if any) was contributed by drawdown due to skin friction during piling or compaction. The response of the chalk to piling is not known and to the authors knowledge no studies are available that investigate the deformation and change in engineering properties of a sediment during the piling operation. In Section 4.2.1.1 the Upper Chalk is, however, described as responding in a non-plastic manner to a vertical force, thus it can be assumed that no plastic sea bed surface deformation is likely. Nevertheless, if the bed rock fails brittly during piling, then fractures and weaknesses introduced at the surface can facilitate erosion (see Section 1.4.3).

Independent scour response pattern The surface sediment layer overlying Lambeth Group is highly inconsistent in thickness between 0-6.5m, generally fine- to coarse sand (Fig 4.4). As illustrated in Figure 4.24, the scour in this formation shows very similar scour depths, irrespective of the depth of the availability of granular sediment. This suggests that the Lambeth Group bed rock lithologies do not offer much resistance to scour and allow erosion to a similar depth as the granular sediment. Up to 2.7m ($0.57D$) of erosion into the underlying substrate is witnessed. In Section 4.2.1, the chaotic facies, high heterogeneity and relatively weak rock strengths of the Lambeth Group facies were conveyed and this is reflected in the observed substrate-independent scour development. Nevertheless, a wide range of scour is observed. Scour depths vary from no scour (at G04) to 4.4m ($S/D = 0.93$). At G04, a pedogenic layer is identified at the surface which inhibits scour from forming. Similarly, scour is limited by concreted layers at eg. A03, B01 and B02. However, it was noted that hard layers do not universally inhibit scour as a number of examples in the north-eastern area of the site exist where scour has progressed past these concretions (eg. at D04, E06, F04, F06). This is at odds with the observation made in Section 4.2.1.3 that in the undisturbed sea bed, these bands have represented barriers to deep CPT investigations. Again, this raises the question of the modification of sea bed geotechnical properties after the installation of the monopile.

Mixed scour response pattern The data from the Thanet Sand Formation display a mixed response based on the thickness of available sediment in Figure 4.24. Where sediment is available, from approximately $z_{sed} > 1.5$m, there is a weak trend towards higher scour with increasing granular layer depth, indicating that sediment availability does have some bearing on erosion depths. Hence, spatially within the Thanet Formation

the large scour values are found at foundations located in the loose sediment of sand waves or where locally thicker depth of sediment is found (see Figure 4.11). On the other hand, where scour has exceeded the thin granular layer ($z_{sed} < 1.5$m), the erosion depth in bed rock has, as in the Upper Chalk, been limited to less than 1.5m, suggesting the erosion response of the underlying materials is similar in these two areas, although again it is unsure whether these are final scour depths. Considering the CPT readings this observation is plausible, as the Thanet Formation facies is often very clay rich as described in Section 4.2.1.2 and Upper Chalk behave in manner similar to hard clays as mentioned in Section 4.2.1.1. The mixed response to scour in bed rock and scour in granular sediment can explain the large range of scour depths $0.12-0.93D$ observed, but the scour depths are skewed towards low values as 70% of scour holes are less than 1.5m deep ($\approx 0.33D$). The largest scour value is observed at E10 which is located on the lee side of a sand wave which will be shown to be a function of the thickness of sediment. Sediment availability can also be linked to the wide range of scour areas observed here as unconsolidated sediment, such as in sand waves, can accommodate a larger degree of lateral extension leading to large areas and volumes.

The importance of sediment availability over less-erodible substrates is demonstrated in a case study of three foundations in the sand wave field; these were previously highlighted in Figure 4.24. Figure 4.25 shows the post-installation bathymetry at D08, E10 and E11, which show different levels of sediment cover. From geotechnical field measurements, the substrate at these locations is interpreted as firm to very stiff sandy clays and clays, which is interpreted to be Thanet Formation bed rock. D08 illustrates the case of scour in bed rock. A small, very confined scour pit is observed with a depth of $S = 0.51$m, area of $A_S = 72\text{m}^2$ and volume of $V_S = 11\text{m}^3$. These are similar dimensions to the depressions of the spud can marks caused by the jack-up rig which are between 0.2-0.6m deep. Thus, it is not clear whether the depression in this substrate is caused by hydraulic erosion or whether the drawdown occurred due to downward vertical pressure during the piling and no scour has taken place. The fact that the spud can marks are still visible 2.7 years after the installation was carried out speaks for the sediment starved nature of the area and is indicative of the idea that sediment only moves in the form of migrating sand waves. At E10, the scour survey was undertaken after the crest of a 4m high sand wave had passed through and the foundation was located in the lee of that feature. The bathymetric cross-section $B - B'$ shows that from the flat surrounding sea bed, there is a thickness of approximately 3m of sediment. The scour depth was measured to be 4.53m which suggests that a depression of circa 1.5m is found in the underlying clay. Consequently, this is essentially the real scour depth at this site. The large scour depth is merely temporary and will keep diminishes with the continuing migration of the sand wave. The large scoured area of 1262m^2 and volume of 904m^3 are also transient values demonstrating the large difference in the scope for lateral scour in granular sediment as opposed to cohesive and consolidated substrates. Some evidence towards the impact of monopile installation is given here. Judging from the available bathymetric surveys, the foundation at E10 was installed through the sand wave, which implies the underlying will not have been exposed to flows since; this in turn implies that the depression witnessed in the clay should be of mechanical origin. The scour at E11 is similar to E10 but has

progressed further in the transition toward the low-sediment condition. The scour depth of 1.33m just exceeds the sediment thickness of 1.5m which is reducing as the sand wave moves on. Similarly to the situation at E10 evidence implies that the depression in clay is caused by the piling operation. Based on the observations made at D08, the depression will remain benign after exposure to flows.

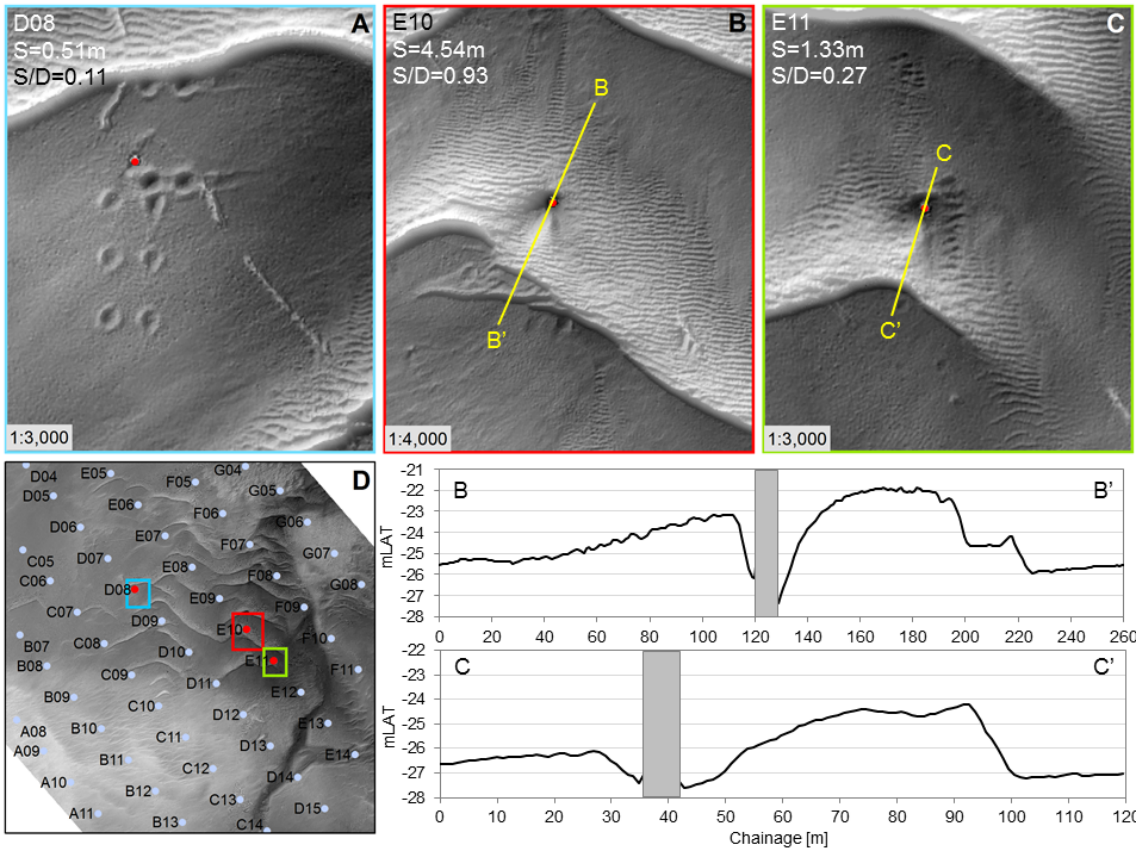

Figure 4.25: Illustration of importance of sediment availability in sand wave field. Post-installation bathymetries at foundation D08 (A), E10 (B) and E11 (C) with location map (D) and bathymetric profiles for (B) and (C).

4.4.4.2 Geotechnical considerations for scour

Scour control in unconsolidated sediments The material strength of cohesionless material can be quantified by the relative density D_r (Fugro Engineering Services, 2004; Annandale, 2006), which effectively measures the density and compaction of granular materials, or cone resistance q_c as suggested in Table 2.5. Thus it is investigated whether these factors act as a scour depth control. Figure 4.26 shows the median D_r and q_c in a band of 0.1m below the recorded scour depth. No particular pattern is discernible, as the scour depth S/D appears independent from either parameter. This implies that neither q_c nor D_r is a discriminating factor for scour depth. In fact, from inspection of CPT records it is found that highly compacted, partially lithified material is routinely scoured at Thanet. Similarly, it was found that the cone resistance of a granular material is also not a limiting factor in scour development, confirming the outcome of the analysis in Figure 3.31 of London Array.

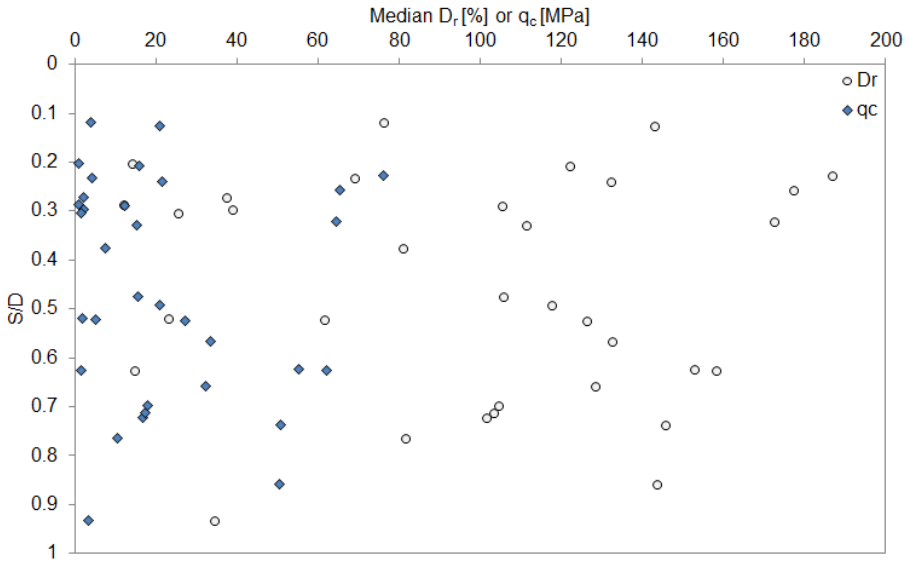

Figure 4.26: Scour in cohesionless sediments. Median relative density D_r [%] and cone resistance q_c [MPa] in a 0.1m band below scour depth.

Scour control in cohesive and consolidated substrates The analysis in section 4.4.4.1 has shown that supposedly erosion-resistant materials do not completely inhibit scour and can experience a certain degree of erosion. For this reason, the scour into bed rock and cohesive substrates will be investigated in more detail. Where erosion occurs in such material, although scour is generally moderate, it is the variability and establishing a causality with geotechnical parameters that is of interest. As established above, scour in Upper Chalk and in cohesive strata of the Thanet Sands Formation seem confined to $S < 1.5$m, while in the Lambeth Group up to 2.7m of erosion into the underlying material has been witnessed. The CPT records were investigated to determine whether there is a quantifiable geotechnical control or threshold for scour in consolidated substrates that can offer an explanation for the range of values observed.

Work by Rambabu (2003); Annandale (2006) and Whitehouse et al. (2011) has suggested that the undrained shear strength c_u influences scour depths in consolidated substrates. This parameter can be derived from CPT measurements as shown in Table 2.4. To evaluate whether there is a control on scour depth by c_u, the median value of c_u in a 0.1m band below the scour depth is plotted in Figure 4.27, indicating what strength of material is potentially capable of limiting scour at a certain depth in the sea bed. The data distribution implies a relationship between c_u and S/D as indicated by the blue line, which defines the largest recorded $c_{u,med}$ that limited scour at the respective depth. This relationship, given in Equation 4.1, can be used to determine an estimate of required material strength to control scour depth at a certain position in the vertical profile. As expected, when attempting to relate scour to a geotechnical parameter, the scatter is considerable (Briaud et al., 2001; Whitehouse et al., 2011). The significance of the suggested relationship could be improved by adding more data points in future studies, thus increasing the confidence in the suggested threshold values and extending the prediction range beyond $S/D > 1$. To corroborate the above relationship with existing data, the maximum shear strength value in ±0.2m of the scour depth was plotted, assuming that the largest c_u and not the median will be the actual limiting value. A very similar pattern to Figure 4.27

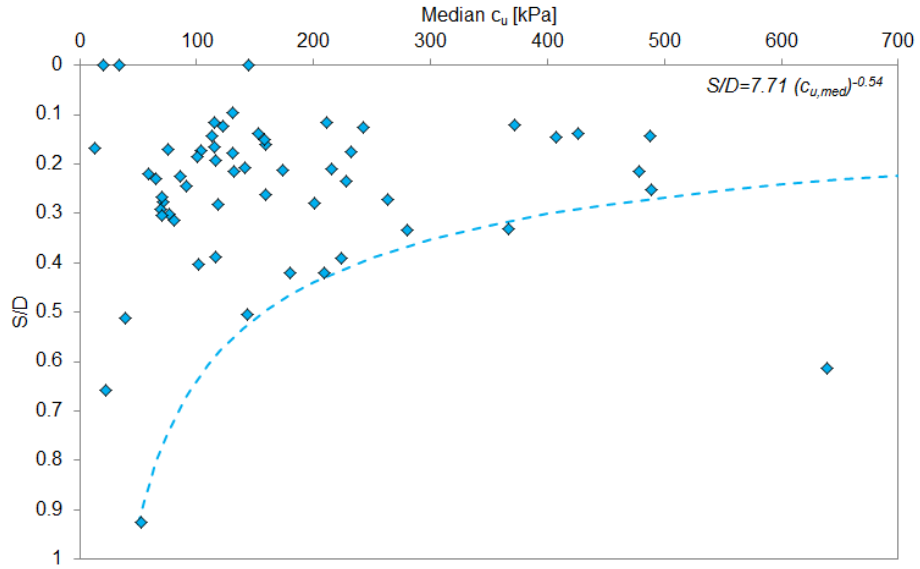

Figure 4.27: Scour in consolidated material. Median c_u [kPa] in a 0.1m band below scour depth.

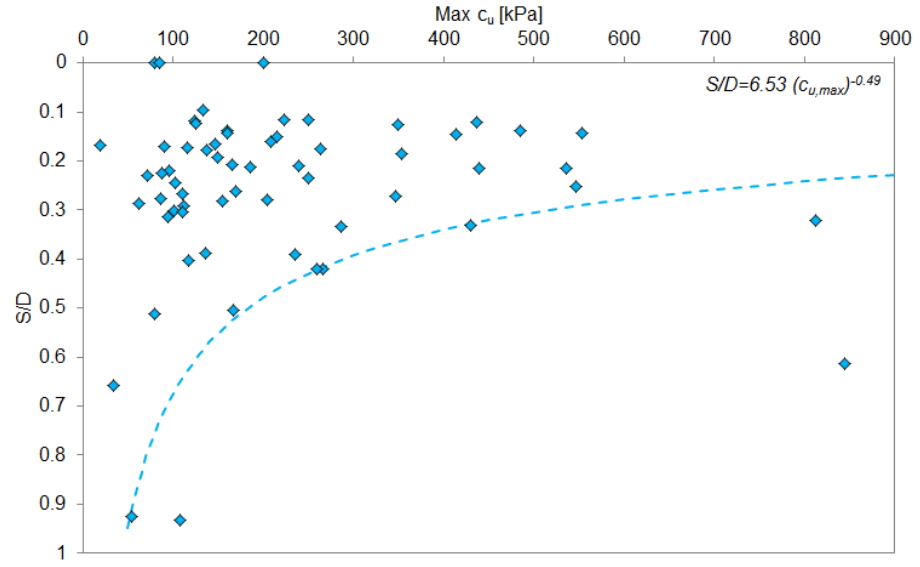

Figure 4.28: Scour in consolidated material. Maximum c_u [kPa] in ±0.2m of scour depth.

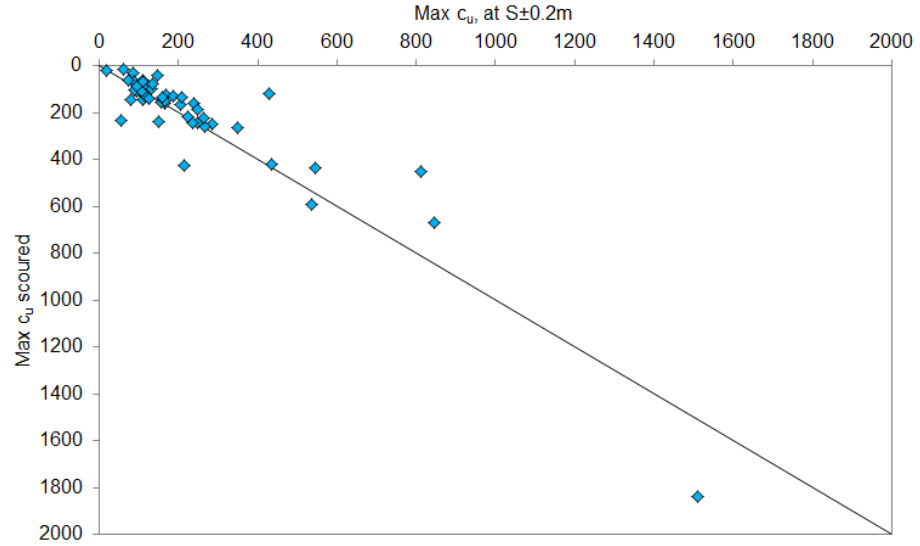

Figure 4.29: Scour in consolidated material. Maximum c_u [kPa] in ±0.2m of scour depth and maximum c_u [kPa] that has experienced erosion.

is revealed in Figure 4.28, resulting in the estimation S/D from the maximum c_u after equation 4.2. The analysis is based on a relatively small N of 60 and more data should be added in future to improve the relationships.

Whitehouse et al. (2011) suggested that clay with an undrained shear strength of order 100kPa is likely to be resistant to scour in the marine environment. Although Figures 4.28 and 4.27 suggests that very soft material with shear strengths as low as 13kPa can inhibit scour, typically stiff to very stiff material (after Table 2.6) with c_u in the range of $70 - 240$kPa can act as scour inhibitor. Considering the complexities of feedback between geotechnical properties and erosion it is unlikely that a single threshold value is appropriate, not last because it ignores the suggested relationship between threshold c_u and diminishing turbulent flow energy with scour depth, as the required material strength to control erosion appears to diminish with scoured depth. Nevertheless, the value of 100kPa lies within the range suggested here. According to the data, the maximum expected scour depth in a cohesive substrate can be estimated from the median $c_{u,med}$ or maximum $c_{u,max}$ material strength from equations 4.1 and 4.2, respectively.

$$S_{max}/D = 7.71 c_{u,med}^{-0.54} \tag{4.1}$$

$$S_{max}/D = 6.53 c_{u,max}^{-0.49} \tag{4.2}$$

Figure 4.29 plots the maximum c_u at a ± 0.2m band against the maximum shear strength that was eroded above the scour depth. Most points cluster very close to the equality line, implying that only a small difference in material strengths is required to facilitate scour control.

4.4.5 Effect of natural bed variability

As shown in Figure 4.6, the sea bed levels have been stable over large areas of the site and natural bed variability is limited to areas of migrating bed forms. For this reason, the overwhelming majority of data points in this analysis fall into the lowest mobility category, where vertical elevation changes are within ± 0.5m, limiting the informational value and confidence in the interpretation of the analysis. The observed scour depths are plotted in Figure 4.30. Notwithstanding the lack of data points in higher-mobility categories, the overall trend suggests that the median S/D increases with bed mobility. For scour area, Figure 4.31 displays a similar trend, while also displaying larger spread of values with higher mobility. The maximum A_S/D^2 also increases, but is reduced again for bed mobility greater than 2m. Volumes also tend to be greater where the bed is mobile. This is counter to observations made at London Array in Section 3.4.5 and it is believed that the scarcity of mobile sediment can be used to explain the trend; this will be illustrated in more detail in Section 5.1.5, when data from all three wind farms is contrasted.

To test whether the scour pit slope angles are affected by morphological dynamics of the bed as suggested in Section 1.3.1.3, the average slope angle β_{av} is plotted in Figure 4.33 along with the trends for median values for β_{av}, $\beta_{u,av}$ and $\beta_{d,av}$. The number of data points

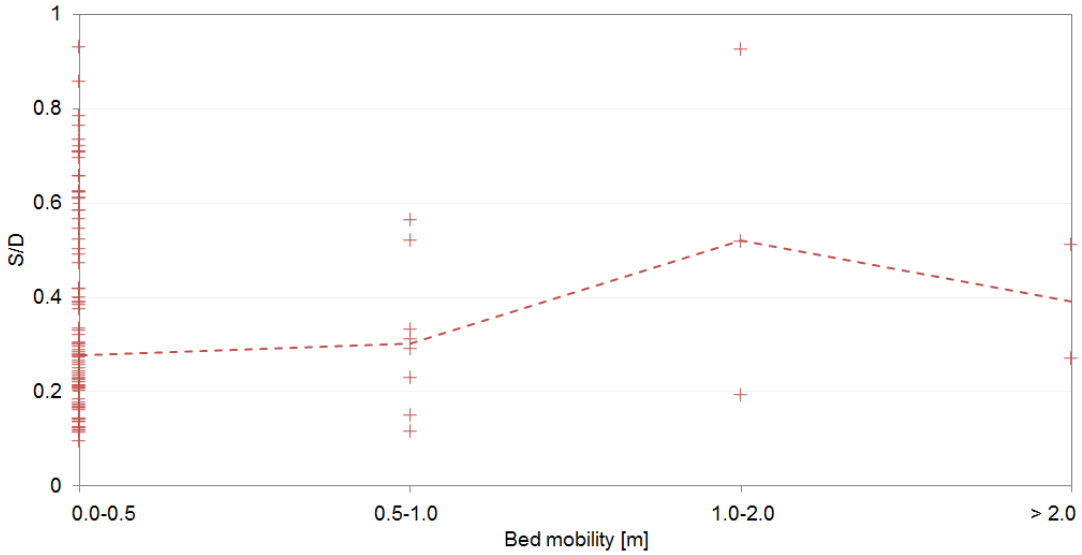

Figure 4.30: Effect of natural bed mobility on scour depth S/D. Dashed line: median S/D.

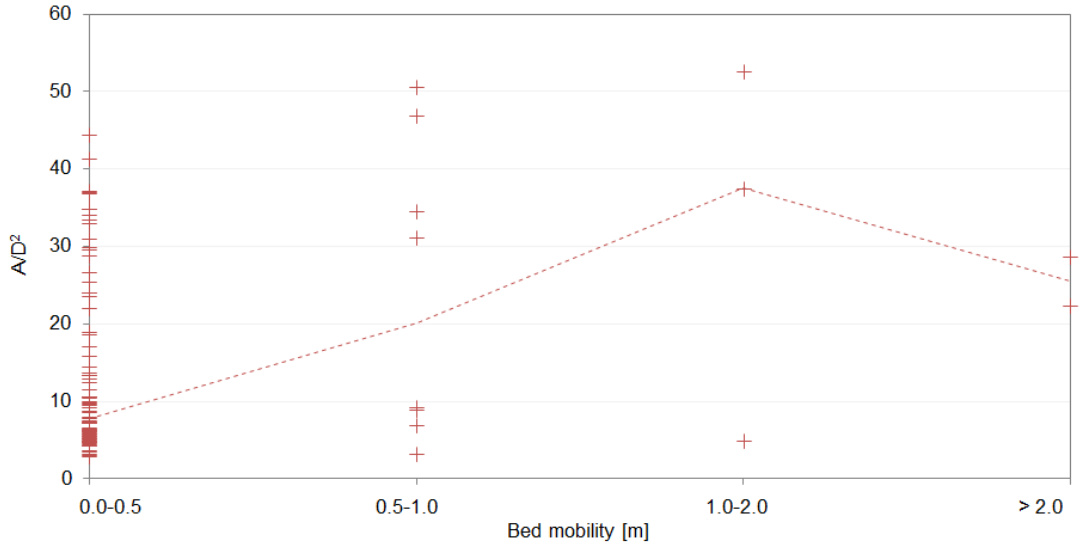

Figure 4.31: Effect of natural bed mobility on scour area A_S/D^2. Dashed line: median A_S/D^2.

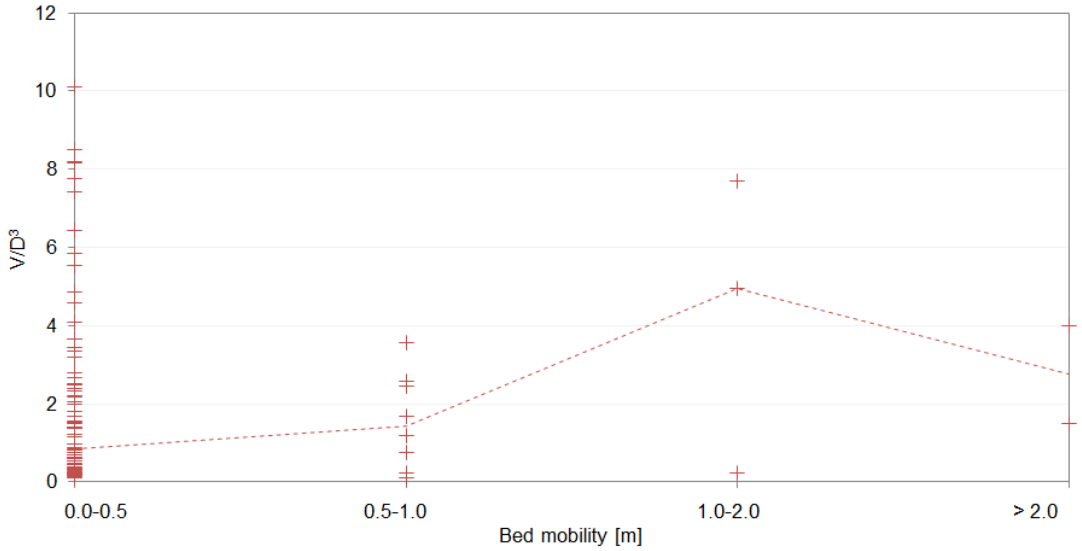

Figure 4.32: Effect of natural bed mobility on scour volume V_S/D^3. Dashed line: median V_S/D^3.

for bed mobility greater than 0.5m is only 13, but the range of slope values diminishes with higher bed mobility and the largest observed angles are reduced. That said, the median value in each bed mobility category for the three slope parameters shows no particular trend, suggesting that on average there is no influence of morphological activity.

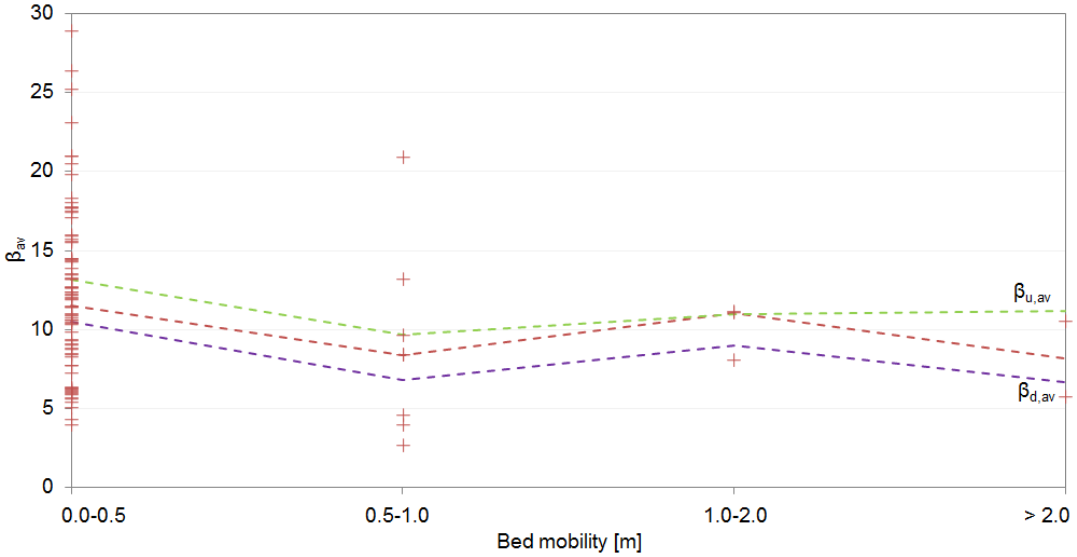

Figure 4.33: Effect of natural bed mobility on average slope angle in scour pit β_{av}. Trend of median value of β_{av} (red dashed), $\beta_{u,av}$ (green dashed) and $\beta_{d,av}$ (purple dashed).

4.4.6 Scour hole age

Although, details of the scour hole time development cannot be examined, as multiple post-installation time steps are not available, the scour can be evaluated against the time between installation and scour survey. This can serve to determine an average rate of scour hole development, notwithstanding the skewing effect of survey delay. Especially in cohesive substrates and bed rock it is interesting to see how scour has progressed and what similarities exist between time-development in these substrates. Figure 4.34 shows the non-dimensionalised scour depth S/D in various substrates (following the categorisation in the conceptual model in Figure 1.11) in respect to elapsed time between the monopile installation date and the hydrographic survey.

Generally no relationship is observed between the age of the scour hole and scour depth. Only in stiff clay, does the data suggest that older scour holes show deeper scour holes. Since erosion in this substrate is expected to develop at a very slow rate (eg. Briaud et al., 1999, 2001) the survey delay appears to play less of a role.

Based on the elapsed time between installation and the single scour survey, the rates of scour in various consolidated and cohesive substrates have been calculated and presented in Table 4.3. The values suggest that on average, scour in chalk progresses at a similar rate as in clay, while scour in stiff clay is somewhat slower. Based on the average scour rates in sandy sediments at London Array between $27 - 55$mm/day (see Table 3.6), the scour in the listed substrates develops slower by a factor of between $20 - 70$. The same analysis with scour pits in sandy sediments in Thanet suggests the difference between scour progression in granular and cohesive sediments is only a factor of $2 - 3$. Two factors

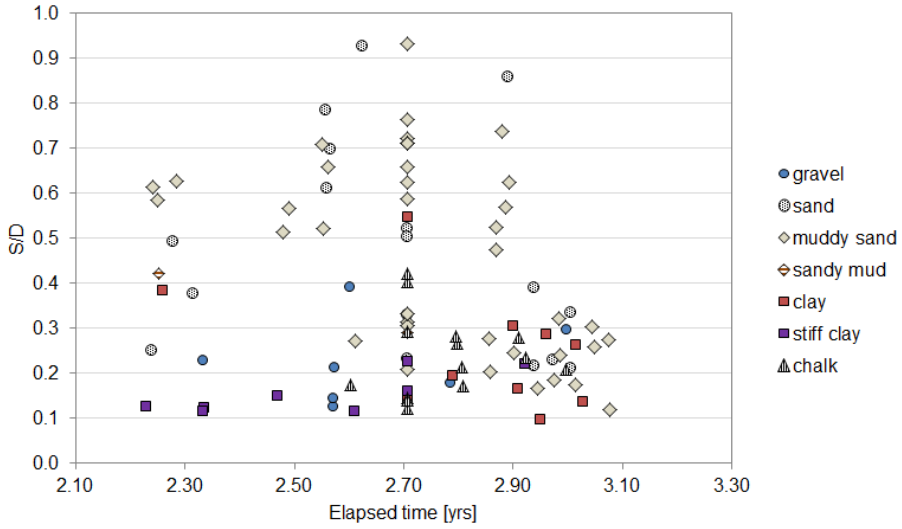

Figure 4.34: Scour depths S/D in various substrate types against elapsed time at Thanet wind farm.

Table 4.3: Rates of scour development in consolidated and cohesive substrates at Thanet wind farm.

Substrate	Min [mm/day]	Max [mm/day]	Mean [mm/day]
chalk	0.6	1.9	1.1
clay	0.4	2.6	1.1
stiff clay	0.6	1.0	0.8

can potentially explain this large discrepancy. Firstly, due to the long delay before the hydrographic survey, the scour rates in unconsolidated granular sediment at Thanet are likely to be underestimated; for sandy sediment average rates of $0.5 - 4.8$mm/day with a mean of 2.22mm/day are calculated which is significantly less than at London Array. Secondly, the granular sediments at Thanet are generally more heterogeneous (less well sorted, interbedding with fine material) than the relatively uniform sand banks deposits at London Array thus some of the slower rates could be explained by this. At Gunfleet Sands, where an estimated 2.5 years passed before the scour survey was undertaken, the rates of scour in sandy sediments based on this single post-installation survey are between $5.6 - 8.5$mm/day with a mean of 7.2mm/day, suggesting a factor of $2 - 11$ decrease in cohesive sediments. All calculated time factors are are significantly less than the factor of up to 1000 suggested by Briaud et al. (2001).

4.5 Summary

In terms of geological and geotechnical considerations, the conditions at Thanet wind farm are most diverse. The variability of the substrate makes the scour analysis complex but interesting, since geotechnical factors can be explored. The analysis of prototype scour at 100 foundations has showed a large variability in scour dimensions. While the scour depths are overwhelmingly limited to $S < 1.5$m ($S < 0.35D$), some foundations exhibit no scour at all while at the other extreme 4.5m ($0.93D$) of erosion are witnessed. The range of scour areas ($2.9 < A_S/D^2 < 52.6$) and volumes ($0.1 < V_S/D^3 < 10.1$) is similarly great but the distribution is heavily skewed towards lower values with means of $A_S = 15.2D^2$ and $V_S = 2.0D^3$. The statistical distribution of scour dimensions can be partially explained

by the presence and thickness of a surface layer of mobile granular sediment. Where erosion proceeds into underlying bed rock, the scour development in vertical dimensions is typically limited to less than 1.5m ($0.35D$), other than in Lambeth Group bed rock where larger scour, up to 2.7m ($0.57D$), is possible ; the larger scour values are observed in areas of greater sediment availability as, for example, in the sand wave fields. For this reason, the most confined and shallowest scour pit can be found in the Upper Chalk, and the other two formation show larger variance. For scour in unconsolidated sediment the compaction of the deposit, as expressed by q_c and D_r was investigated in a bid to identify the mechanism of scour depth control; however these parameters could not explain the distribution of S and appear to be irrelevant in terms of limiting scour depths. Similarly, it was attempted to causally link the undrained shear strength c_u of consolidated sediments to the observed scour depths. This resulted in two relationships, based on $c_{u,med}$ and $c_{u,max}$, being put forward to determine the required material strength capable of limiting scour at a given depth. The comparison of limiting $c_{u,max}$ and $c_{u,max}$ of eroded material further up in the profile suggests that only small increases in material strength are needed to effect scour control. However, it is recommended that these relationships are improved and validated with additional data in the future.

Another outcome of the geotechnical scour analysis calls for an investigation into the impact of the piling operation on the engineering properties of different types of consolidated and unconsolidated sediments, to investigate whether these are altered during the installation of monopiles; this would have implications on the use of pre-installation geotechnical information for scour analysis. Discrepancies in the geotechnical analysis suggest that the material strengths recorded during pre-installation ground investigations may not be representative of the sea bed properties after the monopile is driven into the ground.

The mean extension of the scour pits in horizontal directions was found to be $W = 3.9D$ and $L = 5.1D$. However, spatially constrained scour pits can show lateral extension as low as $2D$. Consequently, the scour pit shapes show limited L/W ratios, typically less than 1.4 and circle-type shapes are dominant with the majority in the range of $0.8 < IQ < 1.0$. Major deviation from this pattern is observed where loose sediment is available for lee-wake scour development and more irregular scour shapes. The observed slope angles in the scour holes have shown that shallow scour holes tend to produce low average slope angles, especially when scour occurs in bed rock. The difference in slope angles in either flow direction is generally quite less than 1.3, indicating limited wake scour and the dominance of the horseshoe vortex in the scour process. The maximum observed slope angle is 48°; however it is believed that the analysis of slope angles at Thanet is unreliable due to survey resolution effects which skew the results towards small values. The effect of natural bed variability was found to be opposite to London Array, in that increased bed level changes result in larger scour dimensions. This can be explained by the availability of sediment. Low mobility areas are sediment-starved areas, where scour is limited due to geotechnical conditions, whereas high-mobility areas are associated with the migration of bed features, and the increased package of mobile sediment allows greater scour. In terms of time evolution, it was found that scour at Thanet appeared independent of T for all substrates but stiff clays, bearing in mind that only a single time step at $2.2 < T < 3.1$ years

is available. The rates of change ΔS in consolidated material, based on this single post-install survey, is 1.1mm/day for chalks and clays and 0.8mm/day for stiff clays. Compared to scour rates in non-cohesive sediments at Thanet, this was found to be only by a factor of 2-3 times slower, although it is likely that the scour rate in sandy sediments is strongly underestimated due to the survey timing. Compared to ΔS in loose sediment at London Array, the erosion progresses by a factor of 20-70 times slower, which is likely to be a more realistic value.

4.6 Gunfleet Sands offshore wind farm

To complete the discussion of the wind farm sites as individual wind farm data sets, the scour recorded at a small number of foundations at Gunfleet Sands wind farm is discussed here. Gunfleet Sands is a Round I wind farm located 7km off the Essex coast and encompasses two phases with a total of 48 turbines with 3.6MW rating. The combined capacity of 172MW is sufficient to power 125,000 households[1] . The installation of the 4.7m diameter foundation was conducted between October 2008 and March 2009. Subsequently, a small amount of scour data along a turbine row (A6-F6) has become available in the public domain from the Crown Estate. A post-installation survey was undertaken in early 2011, along a single row of six turbines along a mild topographic slope (circa 1:200) as shown in Figure 4.35. Although only a small amount of scour information is available from this site, some interesting scour patterns can be extracted and the additional data points will bolster the analysis of the compound data set.

4.6.1 Hydrodynamic regime

Field measurements were undertaken at two locations on the site by Thales (2002) for a period of 2 months (January-March 2002) and by RPS Hydrosearch (2004) over a period of 13 months (January 2002 to February 2003). The information captured in these field campaigns is analysed in order to gain an understanding of the average hydrodynamic conditions experienced. The mean spring and neap tidal range are measured as 3.9m and 2.5m, respectively. Current speeds are weaker than at London Array and Thanet with an average flow speed of 0.21ms^{-1} and peak flow speed on springs tides of 0.5-0.6ms^{-1}. However, flows have been demonstrated to vary strongly based on external forcing, thus magnitudinal fluctuations are high on the scale of days and weeks; the maximum observed current speed, during the 13 month period, was $U_c = 0.94$ms^{-1} (RPS Hydrosearch, 2004). It is likely that this creates a mixed regime where clear-water and live-bed conditions are possible depending on state of tide and wind effects. Currents tend to be stronger in the northern part of the site. The flood tide travels towards WSW (250°N) and the ebb, directionally slightly more variable, returns in a NE-NNE direction, between 45-60°N. However, the local flow direction varies strongly in specific locations on the bank. Measurements by RPS Hydrosearch (2004) show that the flow dominance can vary between ebb and flow depending on the wind direction; westerly winds enhance the ebb tide while east and south-easterly winds increase the flow speed during the incoming tide. The average wave climate is benign with over 60% of measured H_s below 0.25m. The largest wave captured on record by RPS Hydrosearch (2004) measures $H_s = 2.1$m. Due to the proximity of the coast in the north and the limited fetch to the south, locally generated short-period waves from the east and south-easterly sectors dominate (60% of occurrences), followed by southerly and south-westerly directions (28%) (see also Figure 2.4). Thales (2002) measured wave periods and the records reveal mean values of $T_p = 4.1$s and $T_z = 3.7$s. Due to the exposure and the topographic configuration of the site, the largest waves are encountered at the south-eastern corner of the site, however, Thales (2002)

[1]Dong Energy, unknown, About Gunfleet Sands, http://www.gunfleetsands.co.uk/en/about-gunfleet-sands/about-gunfleet-sands, Accessed 04/09/2014.

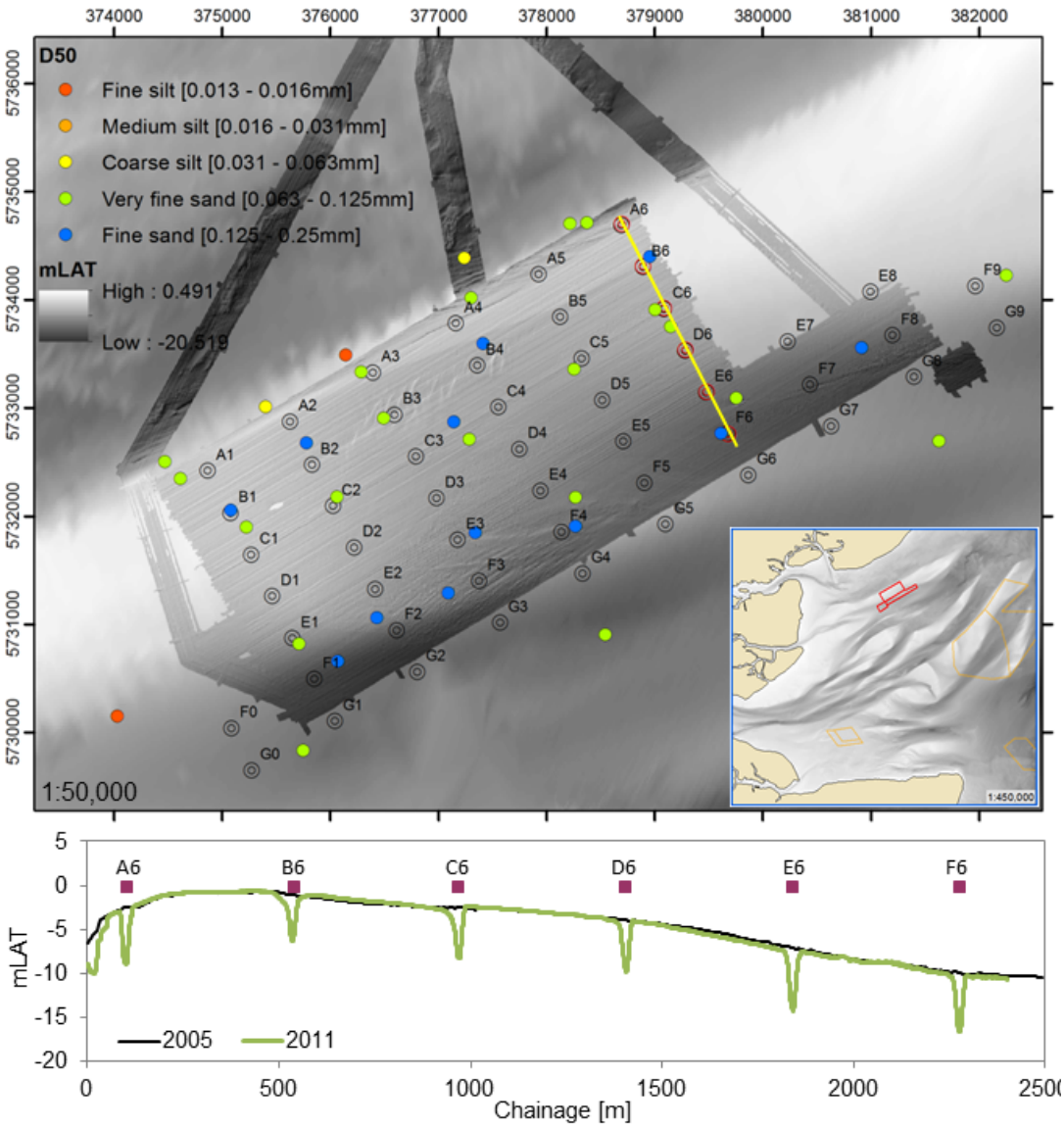

Figure 4.35: Location and topography at Gunfleet Sands wind farm. Coverage of foundation scour survey indicated in red. Surface sediment median grain size d_{50} from grab samples. Bathymetric cross-section along the surveyed foundations shows decreasing bed levels towards the south; bed levels in 2005 in black, those in 2011 in green. Inset map shows location of wind farm (red) within the Outer Thames.

have reported the influence of waves on current-induced flows and bed shear stresses to be minimal. Based on numerical modelling, ABPmer (2004) have suggested extreme wave heights, generated from local winds, of $H_s = 2.66$m and $T_z = 5.15$s, $H_s = 2.84$m and $T_z = 5.33$s and $H_s = 2.90$m and $T_z = 5.40$s, for return periods of 1:10, 1:50 and 1:100, respectively. As mentioned in section 3.4.4.3, Astley et al. (2014) have demonstrated that within the relevant time period no storm events greater than 1:1 have been experienced in the Outer Thames.

4.6.2 Geology

The stratigraphy at Gunfleet Sands is similar to that at London Array. The area is underlain by Tertiary London Clay which forms the bed rock in most of the Outer Thames Estuary (see Figure 2.6). The engineering properties of London Clay have been previously discussed in Section 3.2.1. The sand bank of Gunfleet Sands is postulated to have formed during the Holocene transgression with large amounts of sandy sediments being sourced from the surrounding coastline as a result of sea level rise (British Geological Survey, 2002). Over the site 13-28m of Quaternary sediments are witnessed; along the relevant section (A6-F6) the thickness of Holocene sediments, as determined from CPT and boreholes are between 9-14m, with the thickest cover in the north-west and diminishing to the south-east. The nature of the post-transgressional sediments describes two distinct units; the top unit comprises of loose mobile sediments, typically 1-2m thick which are underlain by dense partially lithified sands (GE Gunfleet, 2002) and silty sands with clay layers which make up the compact core of the sand bank. From seismic reflection data, the core deposits are described as cross-bedded and planar-bedded reflectors (British Geological Survey, 2002). Surface grab samples reveal the top unit to consist of very fine to fine sands ($0.063 - 0.25$mm) on the sand bank (Fig 4.35) and along the turbines of interest. It has been suggested that sediments become coarser and muddier on the flanks of the bank (British Geological Survey, 2002) however this is not reflected in the grab sample data. These two Holocene units are of most relevance for the scour analysis and between locations A6-F6, the CPT and borehole information suggest lateral homogeneity of sediments. Cone resistance ranging from $1 < q_c < 18$ (loose to dense, Table 2.5) and relative density of $30 < D_r < 100$ (loose to very dense). Where clay layers are present, the lab analysis of borehole samples suggests shear strengths c_u in the range of $50 - 300$kPa, with $50 - 150$kPa more common. Below the granular sediments, a wide band of Pleistocene clays and silts (5-8m thick, along A6-F6) marks the transition to London Clay bed rock.

4.6.3 Seabed morphology

Gunfleet Sands is located on one of the most northerly sand banks in the Thames Estuary (Figure 2.1), with King's Channel to the south. Bed levels across the site vary from 0−-10mLAT with deeper water depths increasing from north-west to south-east as illustrated in the bathymetric profile in Figure 4.35 which also shows that the north-west facing slope is significantly steeper than the offshore slope. The topography of the area is best described as gently undulating with a generally smooth surface as large parts of the site

are devoid of bed features. However, according to British Geological Survey (2002) and GE Gunfleet (2002) the area is understood to display highly dynamic bed form evolution, where transient sedimentary features form, then disappear and reform again according to changes in the hydrodynamics as periods of bad weather are conducive to the destruction of bed features; however insufficient bathymetric surveys were available to corroborate this. Where present, megaripple dimensions were assessed and typical dimensions were found to be $H = 0.3 - 0.6$m and $\lambda = 10 - 40$m; the orientation of the crest normal indicates a net west-south-westerly transport direction, pointing towards a net dominance of the flood tide. Towards the north-eastern part of the site, bed forms reveal more ambivalent transport directions. Around the foundations of interest bed forms are only observed around location F6, the most southerly site, with megaripples of $H = 0.15$m and $\lambda = 5 - 10$m. Historical analysis of Admiralty Charts from 1968 and 1988 in GE Gunfleet (2002), suggest that the main shape of Gunfleet Sands has remained stable over the years; however the shifting of the mobile sand layer can cause crest level fluctuations around the bank and it was found that bed levels have dropped by an average of 1m across the sand bank in the investigated time period. Along A6-F6, the natural change of bank crest levels between 2005 and 2011 displays some sub-metre scale variability as minor aggradation of 0.1-0.35m is observed in an area from A6 to just north of D6, while between D6 and F6, bed levels have diminished by 0.1-0.6m (see cross-section in Fig 4.35).

4.6.4 Scour at Gunfleet Sands

The scour at each of the six foundations has been visualised in Figure 4.36. The range of scour depths varies from $S = 1.07 - 1.61D$ $(5.02 - 7.54\text{m})$, where B6 exhibits the shallowest scour depth and E6 the deepest. The average scour depth is $1.36D$ which is slightly over the suggested equilibrium value of Det Norske Veritas (2013), as 4 out of 6 sites exceed this value. The timing of the scour survey is not expected to have any bearing on the observed differences as all scour pits were surveyed after more than 2 years post installation. Based on an estimate of elapsed time T of approximately 2.4 years, the average scour rate is calculated as between $5.6 - 8.5$mm/day, however, it is likely that these are underestimations due to the long survey delay. Visually, the extensive areal nature of the scour at Gunfleet Sands is clear. As opposed to London Array and Thanet, all the scour holes exhibit some type of lee-wake scour. The orientation of the long axis α_L as controlled by the direction of erosive wake reflects the change of hydrodynamics across the bank. In section 4.6.1 the directional dominance of flow was found to be variable and depend on external forcings. However, the shape and orientation of the scour pits are distinct indicators of the dominant flow and a transition in dominance is witnessed along F6 to A6. At foundations F6 and E6, a pronounced uni-directional wake is witnessed, indicating the flow dominance of the incoming flood tide. At D6, a large flood wake is complemented by a smaller ebb-tidal wake and α_L has shifted from SW at F6 to due west. Further to the north, at C6, the scour pattern reveals both flood and ebb-tidal wakes, with the first being slightly stronger; the orientation of the wakes suggest that flow are no longer directionally opposed as the flood wake points towards north-west and ebb wake towards north-east with an inter-wake angle of approximately 100°. At B6, the ebb wake

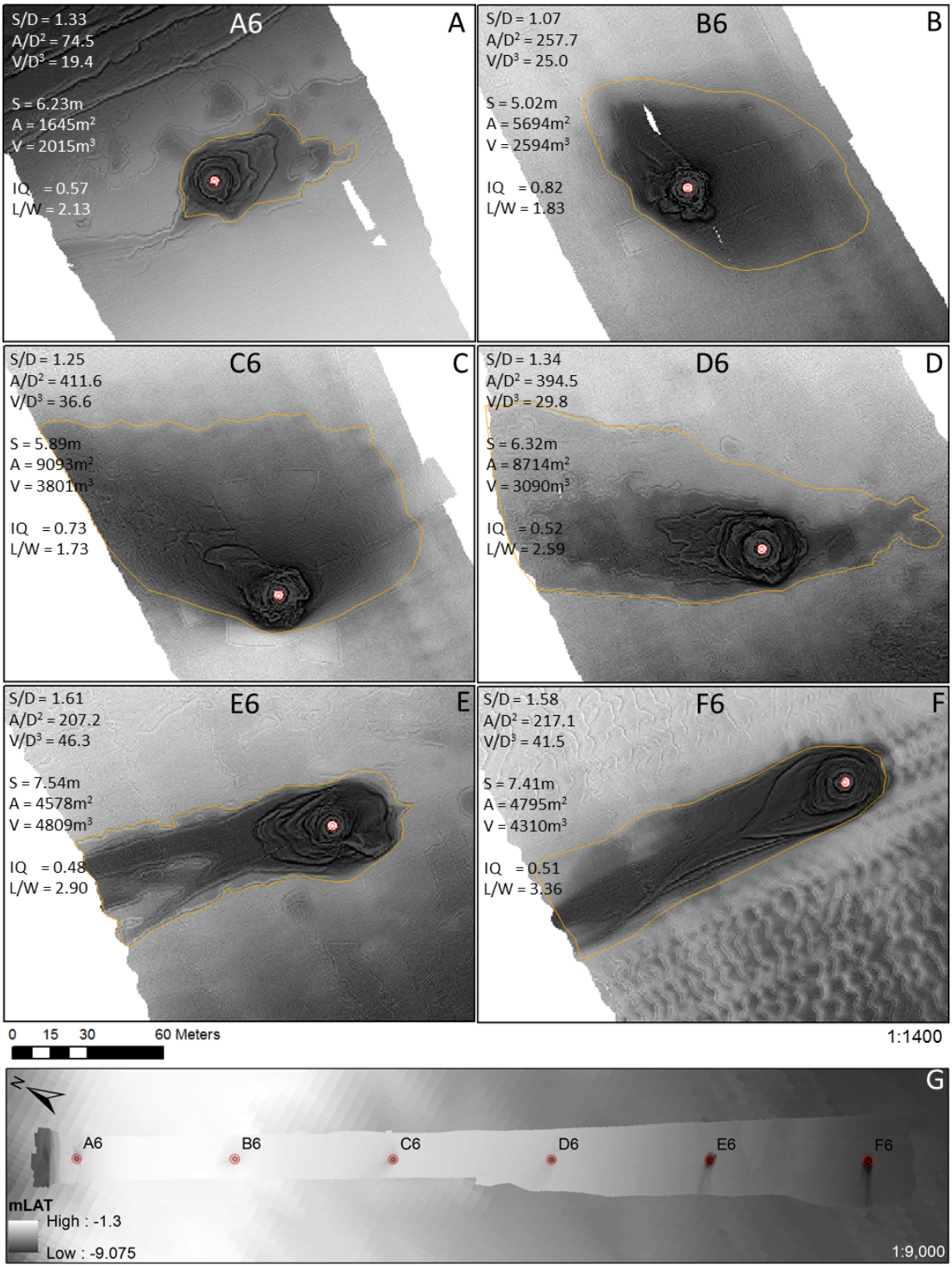

Figure 4.36: Scour at Gunfleet Sands foundations A6-F6 (panels A-F) visualised as partially transparent bathymetry overlying profile curvature plot with scour outline in orange. Nature and direction of wake indicates change in dominant hydrodynamic forcing. Rotated location map (G) indicating foundation locations.

appears to dominate with most of the wake erosion exhibited to the east of the foundation. The considerable width of the scour hole is attributed to the action of the flood tide. The most northerly scour pit A6, shows a clear dominance of the outgoing tide, with a north-east orientated wake, which is less pronounced due to the absence of loose sediment and the exposed compacted bank core which in less favourable to wake development. The pattern of scour depths over this hydrodynamic change, assuming geotechnical factors are negligible, appears to suggest that scour diminishes with increased symmetry of the flow (smallest scour depths at B6 and C6) which confirms the experimental conclusions of McGovern and Ilic (2014) and Escarameia and May (1999) (Section 1.3.3).

Most of the scour holes are not captured in their entirety due to the limited spatial extent of the surveys, however, the very extensive nature of the scour is demonstrated with A/D^2 between 74.5 (A6) and 411.6 (C6), where the latter is a minimum value. Scour pit length L shows a range of $15.5 - 39.9D$ ($73 - 187$m); however as lee-wakes are not entirely covered in the bathymetric survey, scour lengths actually exceed the top values. Nevertheless, these large dimensions illustrate the remarkable capabilities of the scour process where flow and ground conditions are favourable (ie. easily erodible fine to medium sands); even in the relatively moderate current observed at the site, a 4.7m diameter turbine can cause scour of well over 180m in length. Scour pit widths W vary from $7.3D$ (34.3m) to $18.6D$ (87.3m). Due to the large horizontal expanse, the isoperimetric quotient is lower (mean $IQ = 0.6$) than at the other wind farms and the L/W (mean $L/W = 2.4$) ratio is greater. The L/W ratio is closest to unity where the flows are most symmetric in terms of magnitude, but not in direction (B6, C6). The average slope and the upstream and downstream slope are shown in Figures 4.37 and 4.38. The data suggest that the lowest average slope is found at scour pits where the dominance of a certain flow direction is less pronounced (eg. C6), ie. double wake patterns produce lower average slope angles due to the increased area of the wake scour relative to the main scour pit, especially when flow directions are not 180° opposed. The most laterally confined scour hole A6, exhibits the greatest average slope. Comparing the upstream and downstream slope angle, the ratio approximated by $\beta_{u,av} = 2\beta_{d,av}$ (Hoffmans and Verheij, 1997) fits well at 4 out of 6 scour pits; the other two (C6, F6) show ratios of 4.8 and 6.1, implying that the difference in flow-axial average slope angle can be significant, in both symmetric and directionally-dominated flow. The maximum observed angle is 52° in the main scour pit at A6.

Recalling the geotechnical conditions at the site (Section 4.6.2), the analysis of scour depths suggests that scour can progress in compacted, partially lithified granular sediments in a relatively uninhibited manner, as the core of the sand bank has experienced significant erosion. This is in agreement with the investigation into scour controls in unconsolidated sediments in Sections 3.4.4 and 4.4.4, where the degree of compaction (q_c and D_r used as proxy after Table 2.5) was not found to have any bearing on the observed scour depth. This statement assumes, that the pre-installation CPT readings are representative of post-installation ground conditions.

Gunfleet Sands exhibits the most pronounced lee-wake scour of all three wind farms. This begs the question why wake scour is not similarly frequent and prominent at London

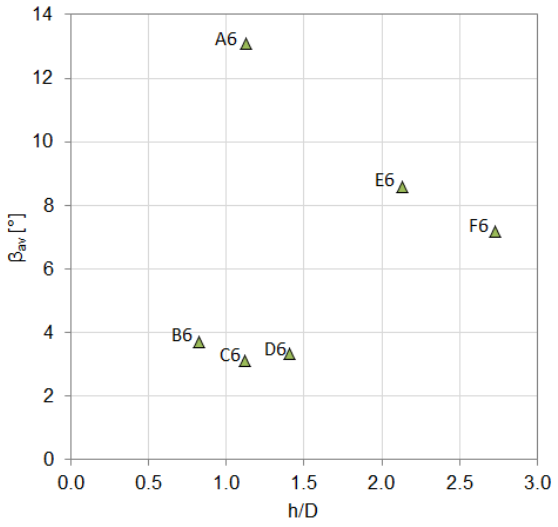

Figure 4.37: Mean slope of scour holes β_{av} as a function of relative water depth h/D at Gunfleet Sands wind farm.

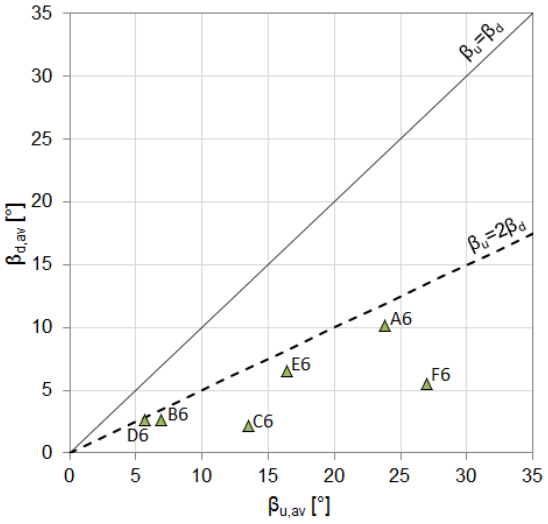

Figure 4.38: Mean upstream slope $\beta_{u,av}$ against mean downstream slope $\beta_{d,av}$ at Gunfleet Sands wind farm.

Array, at least on the sand banks. Both locations are similar in terms of surface sediment grain size (fine and medium sands) and tend to show increased compaction with depth, albeit the depth to core is greater at London Array than at Gunfleet. Still, it is unlikely that geotechnical factors are playing a role in determining the prominence of the wake here. It is believed that the greater flow asymmetry at Gunfleet, in magnitude and direction, together with generally lower current speeds favours the lee-wake scour development here. The slower flows mean that the ambient sediment movement is limited and clear-water conditions can prevail over, at least parts, of the tidal cycle. This reduces the capacity for the wake scour to be destroyed or infilled during the reverse flow and this is further aided by lesser magnitudes of returning flows (eg. A6, D6-F6), or, where flows are more equal in magnitude, the angle described between incoming and outgoing tide (eg. B6, C6).

4.6.5 Summary

The observed scour depths at Gunfleet Sands wind farm varies between $1.07 - 1.61D$ ($5.02-7.54$m). It was shown that the scour here is horizontally extensive ($74.5 < A_S/D^2 < 411.6$) and the scour patterns reflect changes in hydrodynamic conditions (uni-directional to bi-directional) and flow dominance along the turbine row where scour data are available. Out of all wind farm sites under investigation Gunfleet Sands shows the most pronounced lee-wake scour and the highest degree of scour hole elongation with mean $L/W = 2.42$ and $L = 28.7D$ (134.8m). The length of erosion along the dominant flow axis can be over 180m long.

Chapter 5

Wind farms in the Outer Thames Estuary

This chapter aims to build on the interpretation of scour data from individual wind farms by collating the information into a single compound data set. This will facilitate the identification of universal relationships emerging from the data distributions over all wind farm sites, which have a similar hydrodynamic regime but diverse bathymetric and geotechnical settings. Geographical and scientific context will be given by including existing prototype scour data (COWRIE, 2010; Whitehouse et al., 2011) in the analysis where appropriate. Further to the trends analysis, the compound data set will be manipulated to readdress some of the research questions outlined in Chapter 1.

5.1 Scour in the Outer Thames Estuary

Now that the nature of scour at all three sites has been discussed, all the data are summarised and re-interpreted in order to derive general statements about scour around marine offshore monopiles.

5.1.1 Scour dimensions

The range and statistics of all scour parameters observed within the OTE is summarised, in absolute terms, in Table 5.1 and in non-dimensionalised values in Table 5.2. The sample size for scour depth statistics is 281, of which 175 data points from London Array, 100 from Thanet and 6 from Gunfleet Sands, while for the extended analysis of all 7 scour parameters 186 data points are available (due to survey restrictions not all parameters could be calculated at London Array, see Section 3.4). The reduced data set is composed of 100 foundations at Thanet, 80 from London Array and 6 from Gunfleet Sands. Despite the entire horizontal extent of scour not always being captured at Gunfleet Sands, the data is nevertheless included as these scour pits are still the most areally extensive scour holes in the OTE data set and it was deemed appropriate to capture this. A large range of values can be observed for all dimensional parameters (S, A_S and V_S). Scour depths vary between $0.43 - 9.50$m ($0.10 - 2.02D$), with the mean of 4.65m ($0.93D$) falling centrally

between these values. Large value spreads are also observed for A_S and V_S; however the mean area and volume of 966m^2 ($37.7D^2$) and 1224m^3 ($8.9D^3$) indicate skewing of the distribution towards lower values. Relatively large standard deviations are calculated for all three parameters quantifying the variability of the parameters within the OTE.

Table 5.1: Statistics of absolute scour dimensional parameters for study dataset from three wind farms. For S, sample size $N = 281$, for other parameters $N = 182$.

	S [m]	A_S [m^2]	V_S [m^3]
Min	0.43	54	8
Max	9.50	9093	8590
Mean	4.65	966	1224
σ	2.72	1304	1704

Table 5.2: Statistics of non-dimensionalised scour parameters for study dataset from three wind farms. For S/D, sample size $N = 281$, for other parameters $N = 182$.

	S/D	A_S/D^2	V_S/D^3
Min	0.10	2.9	0.1
Max	2.02	411.6	77.7
Mean	0.93	37.7	8.9
σ	0.55	55.9	13.6

Figure 5.1 displays the relationship between scour depth S/D and scoured area A/D^2. There is a positive relationship between these two parameters as expressed by the exponential equation 5.1. The proposed relationship can explain 67% of the variance in the observations, allowing an estimate of area to be made based on S/D. Similarly, the scour volume V_S/D^3 can be approximated from the dimensionless scour depth (Figure 5.2) by equation 5.2 with $R^2 = 0.84$. Both equations are suitable to estimate the scour area and volume of scour holes that do not show extensive wakes. Figures 5.1 and 5.2 reveal that scour pits that display large lee-wake features, eg. as found at most scour pits at Gunfleet Sands, are not captured by the proposed relationship for scour area. The scatter increases for deeper scour holes where approximately $S/D > 1.4$ and the equations will be less accurate in this range. The scour volumes at Gunfleet are in the range of those at London Array for similar S/D, although much larger areas are exhibited, which suggests that the dimensions of the main conical scour hole are less at Gunfleet and the proportion of the scoured volume in the wake is greater as is exemplified in Figure 5.3. The two scour pits are plotted at the same scale revealing that the main scour hole at D13 (Fig 5.3B) is considerably wider than at E6 (Fig 5.3A), which makes up for less scour volume in the smaller wake. A possible explanation relates to the potential restriction of main pit lateral scour in the partially lithified core. Further, the sphere of influence of the structure-related increase in bed shear stresses (see Section 1.2.2) is controlled by the structure diameter and current speeds. Since the latter are lower at Gunfleet, this could contribute to the more confined main scour pit. This image also illustrates the engineering implications of lateral scour extent. First, it highlights the need for inter-array cables not to be laid in the direction of the lee-wake if possible. More significantly, where cables are laid at right-angles to the predominant flow, it is the lateral dimension of the main scour pit that gives an indication of free-spanning cable lengths.

$$\frac{A_S}{D^2} = 5.396e^{1.859S/D} \tag{5.1}$$

$$\frac{V_S}{D^3} = 0.320e^{3.149S/D} \tag{5.2}$$

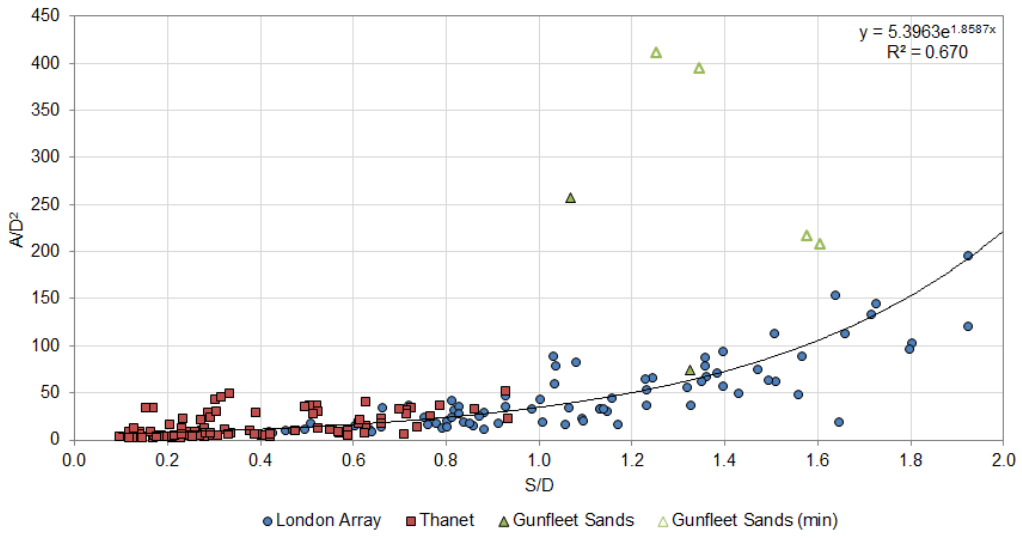

Figure 5.1: Relationship between S/D and A_S/D^2 at all wind farms.

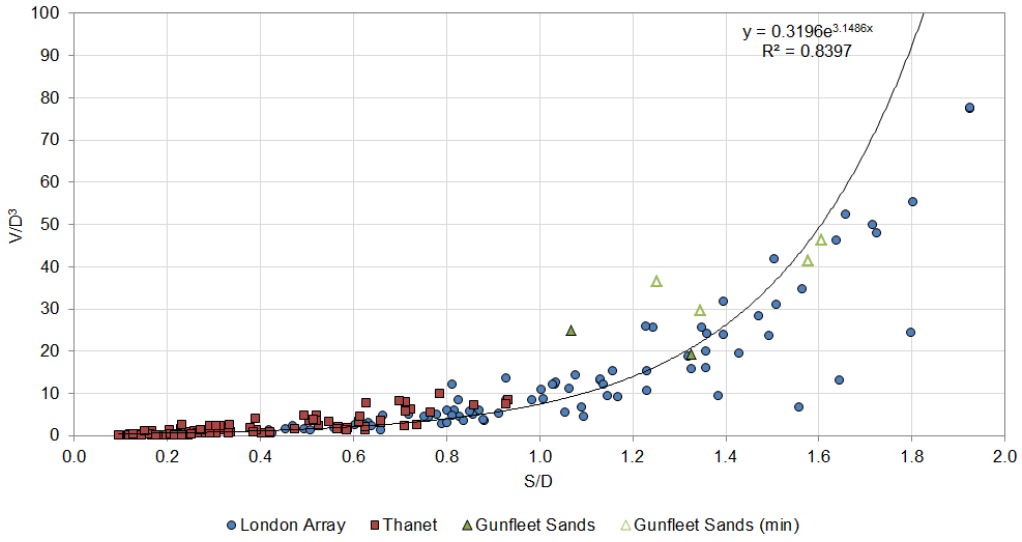

Figure 5.2: Relationship between S/D and V_S/D^3 at all wind farms.

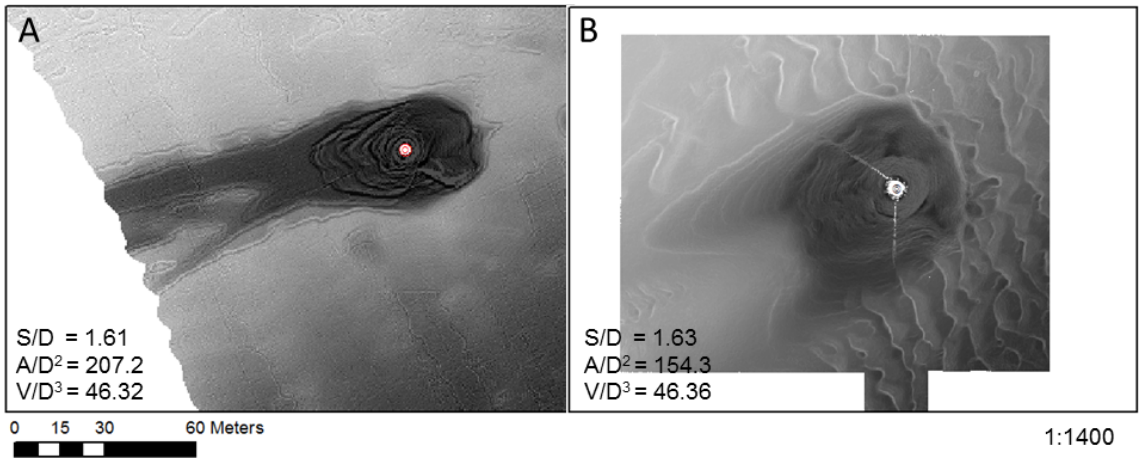

Figure 5.3: Comparison of scour pits with similar S/D and V/D^3 but varying A/D^2. Scour pit at foundation E6 at Gunfleet Sands (A) and D13 at London Array (B).

5.1.1.1 Effect of structure diameter

The observed scour depths are plotted against foundation diameter in Figure 5.4. The data distribution conveys a large range of values for various pile diameters. The range of scour values for individual monopile diameters is considerable and no clear scaling of scour depth with D is discernible, as eg. the range of S is essentially the same for diameters of 4.7m and 5.7m. In scour studies, it is customary to report scour depths as dimensionless magnitudes S/D, normalised over the foundation diameter, owing to the assumption that the scour depth scales with the diameter by means of a positive feedback between D and the hydrodynamic force, as explained in Section 1.2. The foundation diameter has been suggested as the main controlling parameter for scour hole depth in the overwhelming majority of experimental studies and empirical scour equations (see Section 1.3.1); however, the field data suggest that D is not a strong determinant for scour depth at prototypes; in fact scour depth S appears largely independent from D, although it appears that the upper limit of observed is well captured by $2D$. This implies that although, there is a sound theoretical underpinning for the relationship between S and D in controlled conditions, it does not necessarily manifest itself strongly in the prototype scour situation. It is likely that the positive feedback is "overprinted" by geotechnical factors which have a much greater influence on scour than the fluid-structure interaction. This calls into question the basis for non-dimensionalisation of scour over D.

For comparison, the equation 1.3 for S_e and equation 1.4 for the largest expected scour depth S_{max} are also plotted in Figure 5.4, revealing that the data do not scale according to this relationship. The average dimensionless scour depth S/D of all scour observations in this study is determined as 0.93 (4.65m) (Table 5.2 and 5.1) with a standard deviation $\sigma_{S/D} = 0.55$, which suggests more confined relationship than the experimentally derived values of $1.3D$ and $\sigma_{S/D} = 0.7$. However, despite the relationship not being able to accurately predict scour at any one location, the theoretical limit of $S_{max} = 1.3D + 0.7D = 2.0D$ is only just exceeded by a single data point ($S = 2.02D$) and would appear appropriate as a conservative estimate of the largest expected scour depth. The maximum expected scour using the mean and standard deviation from the prototype data set is calculated as $0.93+2\sigma = 2.03$. The deepest scour is within the limit of $S_{max}/D = 2.4$ as suggested by Melville and Sutherland (1988).

One implication of the findings is that predictive methods (Section 1.3) based on diameter D cannot be expected to perform satisfactorily. Furthermore, it infers that the theoretical underpinnings of the positive $S - D$ trend (based on controlled flows in loose sandy sediments) is not sufficient to explain prototype scour where complex geotechnical factors need to be accounted for. The scour area and volume show similar independence from D as the spread of A_S and V_S is very similar for $D = 4.7$m and $D = 5.7$m. The Thanet data reveals a trend towards the largest observed scour to diminish with decreasing D. However, it should be noted that the foundation diameter is designed in respect to the environmental conditions, ie. smaller diameter foundations are used where the ground conditions have good bearing capacity. These substrates are also less erodible which is more likely to explain the observed pattern.

Figures 5.4 to 5.6 also demonstrate that the smallest scour is generally found at Thanet

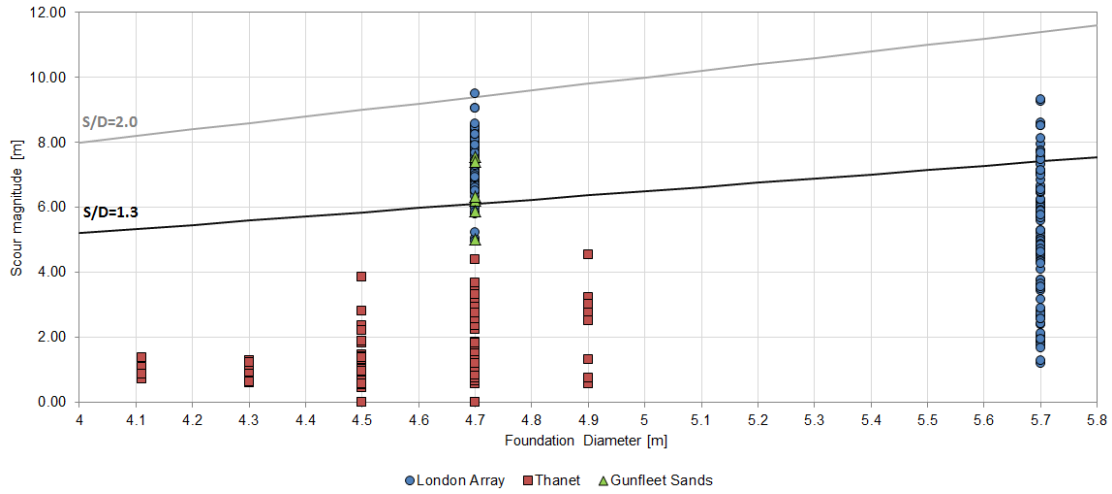

Figure 5.4: Observed scour depth S as a function of foundation diameter.

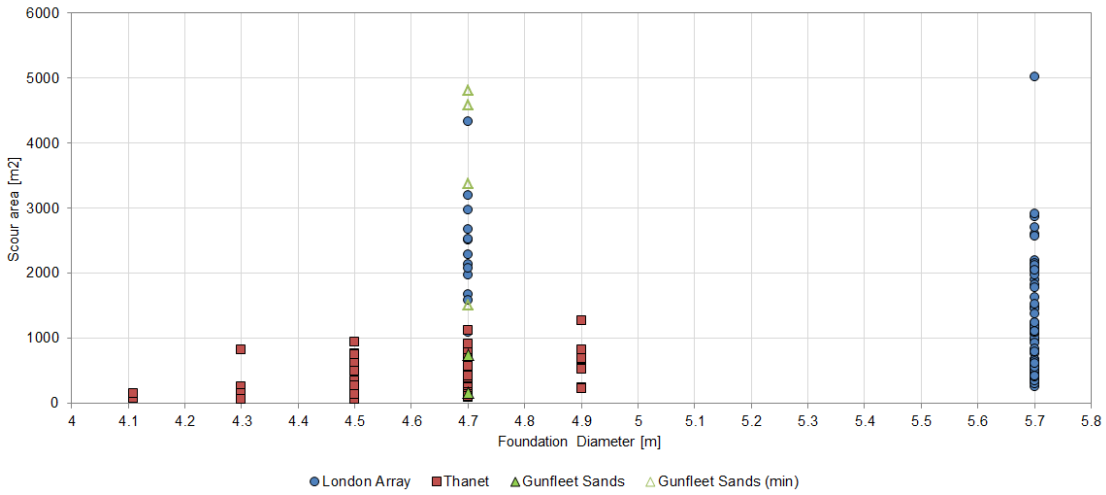

Figure 5.5: Observed scour area A_S as a function of foundation diameter.

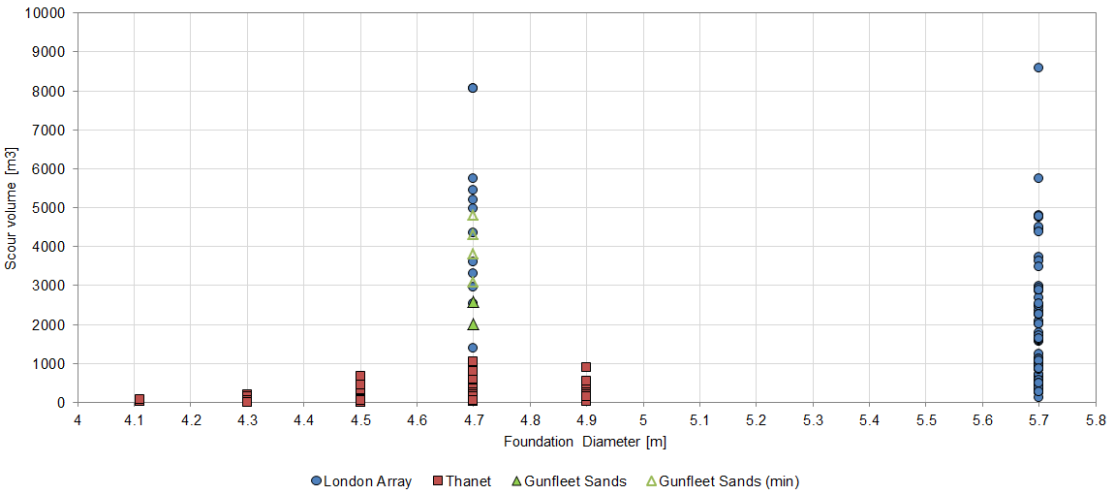

Figure 5.6: Observed scour volume V_S as a function of foundation diameter.

wind farm and the largest at London Array. The scour holes with the most extensive lateral growth are located at Gunfleet Sands and London Array with large scatter observed in both locations. The Gunfleet Sands (min) points should be understood as minimum values since the post-installation survey did not cover the full extent of the very extensive wake scour so the exact value cannot be determined. The smallest volumes and deviation of values is again observed at Thanet while London Array shows the largest volume of eroded material V_S.

5.1.1.2 Effect of water depth

Experimental work suggests that scour around a monopile in shallow water $h/D < 2-5$ is expected to diminish with reducing water depth (eg. May and Willoughby, 1990; Whitehouse, 1998). For this reason many empirical formulae, particularly for fluvial scour, include water depth as a parameter in the equations (eg. Laursen, 1963; Hancu, 1971; Breusers et al., 1977; May and Willoughby, 1990; Richardson et al., 2001). Figure 5.7 shows the distribution of non-dimensionalised scour depth S/D with relative water depth h/D in the prototype data. A 4^{th} order polynomial equation can be employed to explain a significant proportion of the variance in observations ($R^2 = 0.79$). The average properties of the data distribution as described by the trend line suggests some control on scour by water depth. The scour behaviour appears to be governed by a maximum at $h/D = 1.66$, circa $h = 8-9$m, as either side of this value the average S/D is diminished. While this explains the average trend in the data, the inflection point does not adequately explain the distribution of the upper extrema observed; this will be investigated closer in Section 5.2.1 where existing prototype observations are included in the analysis. Although there appears to be a correlation between h/D and S/D variables, it must be considered that other factors might be responsible. In shallow water ($h/D < 1.66$), the envelope of scour depths is well constrained with $\sigma_{S/D} = 0.18$. These points are located on topographical highs of sand banks, where typically, the substrate is fairly uniform, non-cohesive sand or silty sand and due to this similarity of substrates it is unlikely that the reduction is caused by geotechnical factors. Thus, a water depth control in shallow water as suggested by, for example Breusers et al. (1977) or Richardson et al. (2001) seems plausible. The scour in the shallowest water will also be most affected by wave action, which is generally, albeit not unanimously, considered to produce a reduction of scour hole depth (Section 1.3.3.3); thus the reduction effect could potentially also be a function of wave action. But, as will be shown in Section 5.3.1, using a semi-empirical formula, the effect of waves alone is insufficient to cause scour under average conditions. In combined flow, very small scour is predicted ($S < 0.07D$, $S < 0.3$m), which suggests that waves can likely be discounted in terms of their relative impact on scour as the tidal current will heavily dominate all aspects of scour development. In deeper waters, the range of S/D values for equal water depths is considerably greater, although a mean trend of reduced scour cannot be denied. However, when the Thanet data are considered in isolation as in section 4.4.1 then no relationship is found. Although, these data appear to follow a general trend, it is also clear that there are stark differences in substrate between the scour data points in deep water (especially between London Array and Thanet) and it is possible that geotechnical factors

are influencing the distribution of data points. Existing prediction methods developed for fluvial scour expect scour to be greatest in deep water; however this is contrary to what is observed in the data. Experiments by Hjorth (1975) have shown a reduction in bed shear stresses with water depth for equal flows and structure diameters (Fig 1.5), which is a possible explanation for the scour depth reduction in deeper waters.

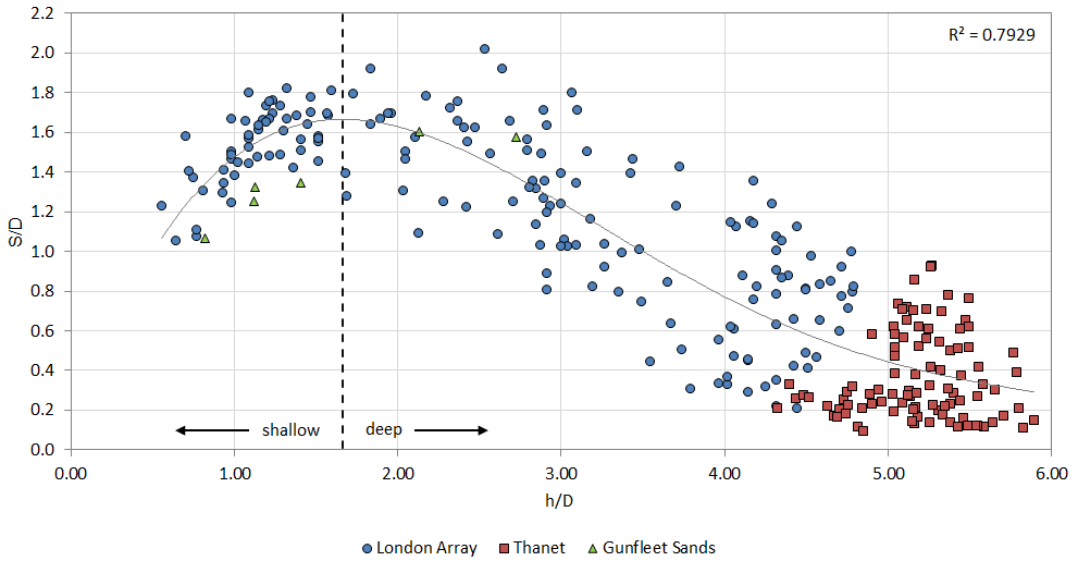

Figure 5.7: Observed scour depth S/D as a function of mean relative water depth h/D.

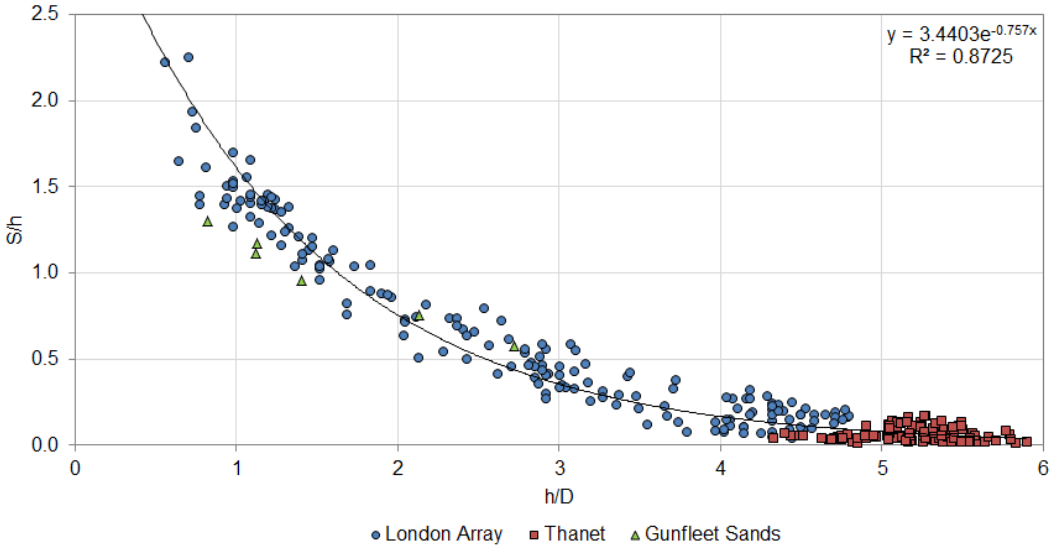

Figure 5.8: Relationship between water depth h/D and normalised scour depth S/h.

To investigate further the effect of water depth, scour depths S can also be normalised over h as shown in Figure 5.8 (Harris, 2014, pers. comm.), based on an assumption of implied relationship between these two factors. A strong exponential relationship ($R^2 = 0.873$), given in equation 5.3, is suggested between S/h and h/D. The validity range of the equation will be discussed in more detail below.

$$\frac{S}{h} = 3.440e^{-0.757h/D} \tag{5.3}$$

While a strong correlation between S/h and h/D is exhibited, it does not necessarily imply a causation. It is potentially problematic having h on both axes, as it is in both the

dependent and the explanatory variable. Nevertheless, this strong correlation cannot be simply dismissed as a mathematical effect, as will be illustrated in tests with a randomly generated data set of S/h and h/D. Of each individual variable, a thousand values were randomly computed, restricted within observed ranges ($0.5 < S < 9.0$, $1 < h < 30$ and $1 < D < 6$), and then the correlation between the two ratios was investigated. This was repeated 100 times with new random data for every iteration. The average R^2 over the tests was 0.38 and Figure 5.9 indicates the range of R^2 achieved from random data sets.

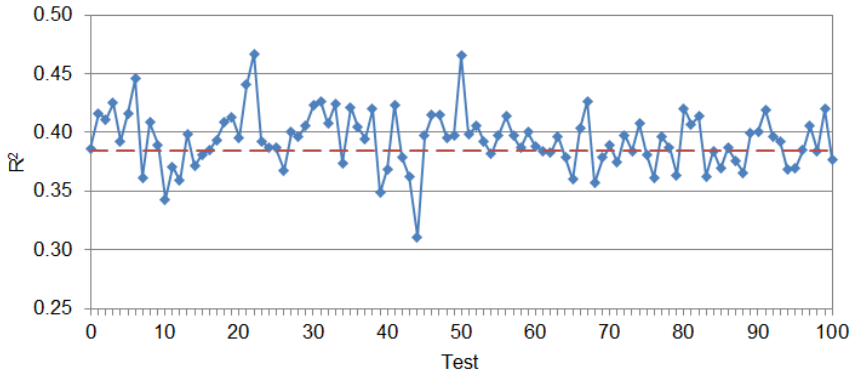

Figure 5.9: Correlation coefficient R^2 for each of the 100 iterations of the relationship between randomly generated ratios of h/D and S/h.

The fact that the correlation of the prototype data are much greater than what is achieved with random data, corroborates the notion that there is a real underlying trend and not just a fabricated relationship. Furthermore, the proposed relationship should be considered, not on its own, but in conjunction with Figure 5.7 which shows quite convincingly that there exists a strong relationship between water depth and scour depth, indicating that this is worth exploring in more detail. It is an interesting notion to suggest that a relatively good estimate of scour depth can be achieved, using equation 5.3, based on knowledge of mean water depth and structure diameter only, although the latter variable is not strictly necessary but is included as traditionally the relative water depth h/D is used in scour studies. If an, at least partial, causation is assumed, which appears legitimate following the preceding discussion, then water depth can be said to be the overriding scour depth control, where the deviation from the trend relates to, what appear to be, less influential factors. By inference, this suggests that h/D somehow represents the scour-relevant properties of the flow, and is an effective proxy for the erosive action of the horseshoe vortex, which is responsible for erosion at the pile and controls the scour depth (Section 1.2.1). The exact physics and mechanism of this control are not well understood at the time of writing, however, the performance of the model will be investigated further to gain more insight into the significance and validity of equation 5.3.

To test the relationship, the analysis is broadened to include existing prototype observations. Figure 5.10 shows normalised scour depths S/h from COWRIE (2010) and Whitehouse et al. (2011) with those from the Outer Thames in the background. To derive the S/h values, plots in the aforementioned publications were digitised and the individual parameters h and S were reverse calculated using information on turbine diameters from the public domain. Equation 5.3 is plotted in red. Visually, the majority of observations seem to fit well the suggested relationship; however it is clear that scour depths from

cohesive sediments (eg. Kentish Flats, North Hoyle and parts of Barrow and Robin Rigg) increase the scatter considerably, which is illustrated more clearly when the data are plotted in logarithmic scale (Fig 5.11). The scatter in Thanet is also quite large however due to the water depths it happens to be located, it still fits around the proposed model, as is the case for Princess Amalia data.

To determine an objective measure of how well the model fits with existing observations, scour predictions are conducted using equation 5.3 and compared to the field values, thus indicating how accurately scour can be predicted based on h and D alone. Based on all prototype data (not including the OTE data used to derive the equation), the accuracy of the model is quantified as $RMSE = 0.30$ and a model efficiency of $E = 0.28$. But the agreement between predicted and observed scour is naturally diminished by substrate outliers. Hence, the forecast is repeated removing scour associated with cohesive and consolidated sediments (Kentish Flats, North Hoyle and parts of Barrow and Robin Rigg); this shows a much improved model performance with an $RMSE = 0.18$ and $E = 0.80$, highlighting the capability of equation 5.3 to give accurate estimates of scour in sandy sediments based on h. While this gives further weight to the notion that water depth, as a proxy for flow conditions, is the overriding influence in such sediments, it also implies that geotechnical effects in granular sediments play a subordinate role, or at least that the sea bed properties between the plotted sites are similar. Taking this issue further and considering the variability of the substrate in Figure 5.11, three validity ranges can be defined based on which the model performance can be critically evaluated.

In the range from $0.5 < h/D < 3$, the bulk of the data, which are derived from sand bank locations, fit the model very well (substrate-influenced sites are omitted). This represents scour in relatively homogeneous unconsolidated granular materials. The scatter in these data can be likely explained by differences in sea bed properties between the sites and some survey time considerations (section 5.2.1). The good agreement in this area suggests that, in general, in granular media, geotechnical differences do not create large differences in scour depths and the model can be used with some confidence here.

In depths between $3D$ and approximately $5-6D$, but including Kentish Flats and low-scour sites at Robin Rigg the stronger deviation from the trend illustrates the effects of sea bed configuration. The data here are at sites that are either influenced by underlying erosion-limiting layers (e.g Kentish Flats, Knock Deep at London Array, Thanet, Princess Amalia) or are located in less-erodible complex substrates and bed rock (e.g. North Hoyle, Barrow, Upper Chalk at Thanet). This variability increases the scatter and decreases the confidence in the model, as the overriding factor is no longer adequately described by water depth, but erodibility considerations of the sea bed become much pertinent. The fact that these sites deviate strongly from more conventional granular scour, which has typically been the focus of research, demonstrates the need for further research into scour in complex substrates (see section 5.1.4), greater field data density and developing scour relationships for cohesive and consolidated materials. The circumstantial lack of scour data in unlimited granular sediments in this water depth range increases the uncertainty of the model for sandy sediments in this range; Figure 5.12 shows those sites from London Array and Thanet that have been identified as scour in granular sediments. At Thanet

those sites tend to display greater scour than suggested by equation 5.3, suggesting that in these depths the curve should potentially be corrected upwards. At London Array there is significant scatter below the line. However, drawing on the analysis carried out in section 3.4.4.4 it was found that all, bar 3 data points that fall below the line, have been surveyed with a time delay between 21-166 days, thus are not fully developed and are likely to show larger scour depths if surveyed again. All identified scour depths have been surveyed less than 1 year after installation thus it is likely that scour is progressing at all points.

Due to the nature of the exponential relationship approaching zero, the model predicts very low S in water depths deeper than $5 - 6D$, thus there is an upper limit of water depths that this model can be applied to. For a diameter of 5m, this corresponds to a water depth of 25-30m, which roughly coincides with the limit of water depths at Round 2 wind farms. Plans for future wind farms include construction in deeper waters, thus the relationship should be reappraised when scour data from deep sites becomes available.

Further to equation 5.3, from the aggregated data, a relationship for the maximum possible scour depth can be derived, described by the orange dashed line in Figures 5.10 and 5.11 and given by the following equation.

$$\frac{S_{max}}{h} = 0.15 + 3.10e^{-0.66h/D} \tag{5.4}$$

For the future, it is recommended that the applicability of equations 5.3 for S/h and 5.4 for S_{max}/h is tested against more monopile scour data to validate and increase the confidence in these models. For the time being, to validate further the relationship between h/D and S/h, physical test data from various studies are plotted in the same way in Figure 5.13. The data presented, originate from a variety of experimental conditions, including uni-directional and reversing flows, uniform, mixed and layered granular beds (no cohesive scour) and circular and square piers.

Firstly, it can be seen that despite the variety of experimental conditions, the data follow a similar distribution with a high correlation, which increases confidence in the relationship between S/h and h/D. However, the best fit is described by the power relationship given in equation 5.5, as opposed to the exponential law for prototype observations. Figure 5.14 plots both prototype and experimental data with the respective best fit lines (black line: experimental best fit, power law, eq. 5.5; red line: prototype best fit, exponential law, eq. 5.3). This graph illustrates the deficiency of equation 5.3 for greater h/D ratios.

$$\frac{S}{h} = 1.064(h/D)^{-0.788} \tag{5.5}$$

To test the performance of the power law, the predictive performance of equation 5.5 was evaluated against all existing prototype scour data. This resulted in agreement described by an $RMSE = 0.26$ and $E = 0.69$, which can be considered quite good forecasting ability. To have a direct comparison with the exponential law developed from OTE data, the power law is validated against all prototype scour, bar the OTE data, resulting in

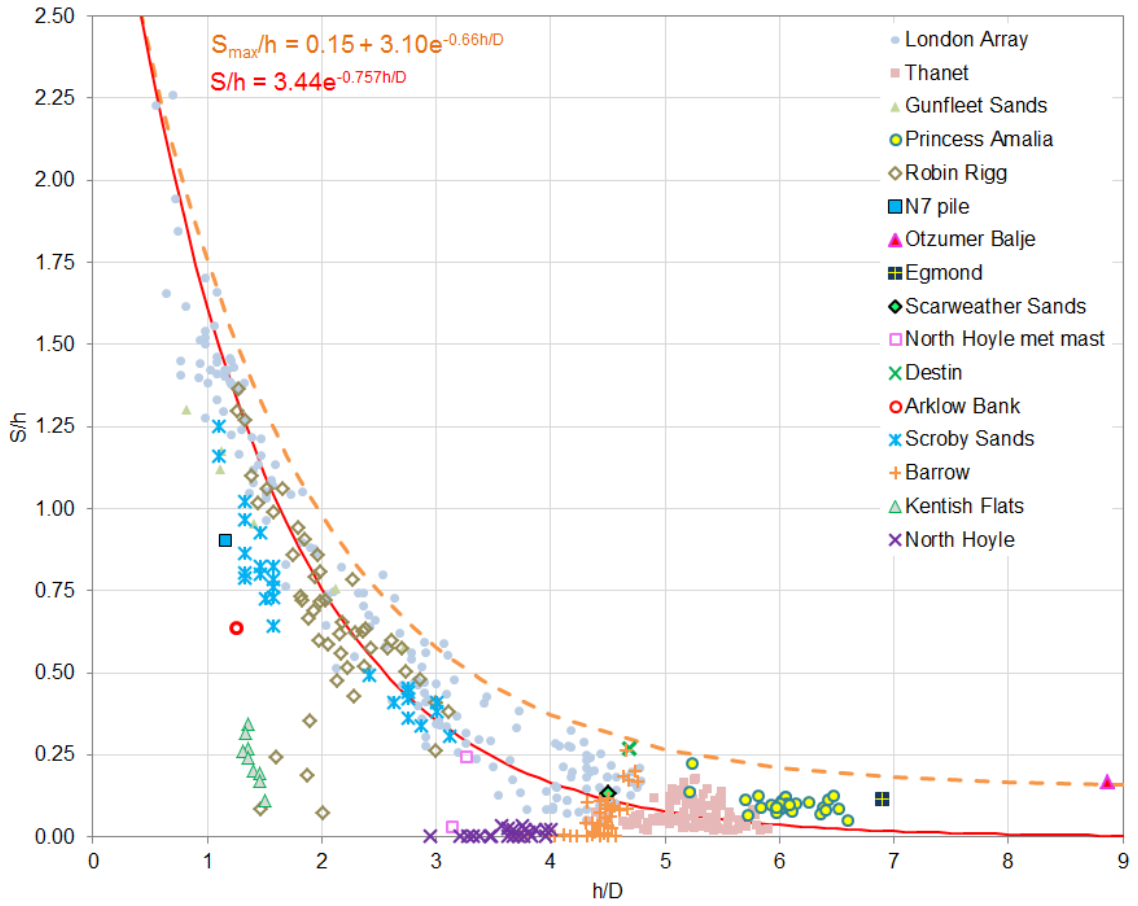

Figure 5.10: Normalised scour depth S/h as a function of relative water depth h/D for all existing marine monopile prototype observations. Includes data from COWRIE (2010) and Whitehouse et al. (2011). Orange dashed line describes maximum S_{max}/h. Red line is equation 5.3.

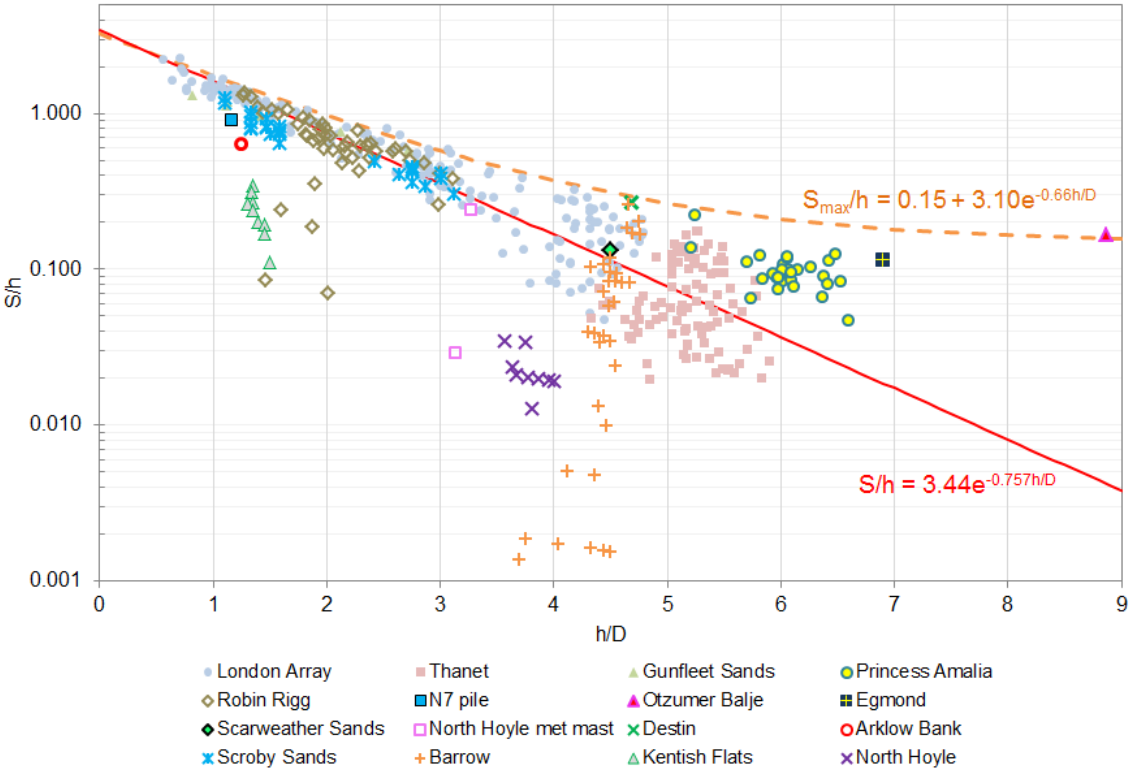

Figure 5.11: Logarithmic normalised scour depth S/h as a function of relative water depth h/D for all existing marine monopile prototype observations. Includes data from COWRIE (2010) and Whitehouse et al. (2011). Orange dashed line describes maximum S_{max}/h. Red line is equation 5.3.

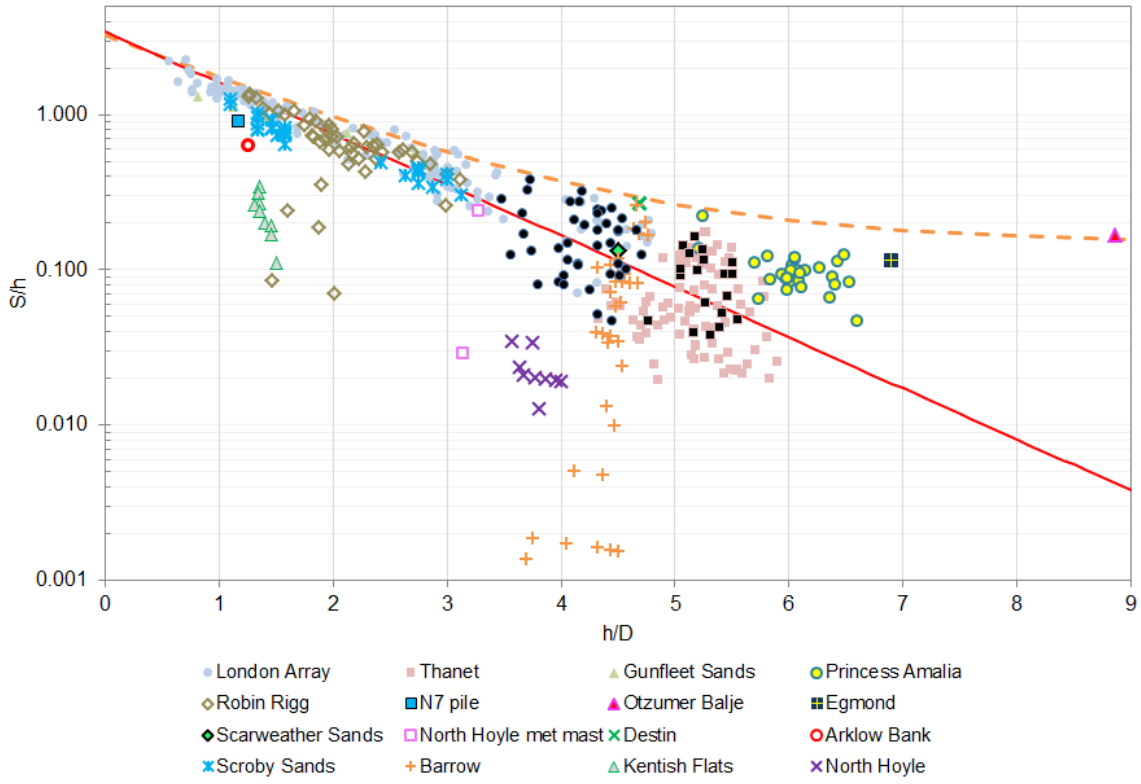

Figure 5.12: Logarithmic normalised scour depth S/h as a function of relative water depth h/D for all existing marine monopile prototype observations. Data points from London Array and Thanet that are considered to have developed within granular sediments marked in black.

Table 5.3: Comparison of model performance for prediction of prototype data sets.

	Power law, equation 5.5, developed from experimental data		Exponential law, equation 5.3, developed from OTE data	
	$RMSE$	E	$RMSE$	E
All prototype data	0.26	0.69	–	–
All prototype data, excluding OTE data	0.27	0.39	0.30	0.28
Prototypes in granular sediments only	0.17	0.76	0.16	0.80

$RMSE = 0.27$ and $E = 0.39$, which is an improvement over equation 5.3 ($RMSE = 0.30$, $E = 0.28$). When tested against prototypes in sandy sediments only, the power law gives $RMSE = 0.17$ and $E = 0.76$, which is slightly less good fit than from the exponential relationship. The comparison of the performance indicators for the two models is summarised in Table 5.3. The developed equations are deemed to be improvements over currently existing prediction methods, based on the statistical performance measures. As will be shown in Section 5.3, the capabilities of existing formulae lie much below the proposed relationships.

Similarly, relationship with water depth is investigated for scour area and volume. Scour area and volume are plotted against the relative water depth in Figures 5.15 and 5.16, respectively. Here, large scatter is found with decreasing water depth suggesting scour areas can vary greatly in shallow water. The data indicate that scour holes, while being shallower, also tend to become more confined in deeper water. This could be explained by experimental observations on the extent of bed shear stress amplification M outlined in section 1.2.2. In deeper flow depths the magnitude and lateral sphere of influence of

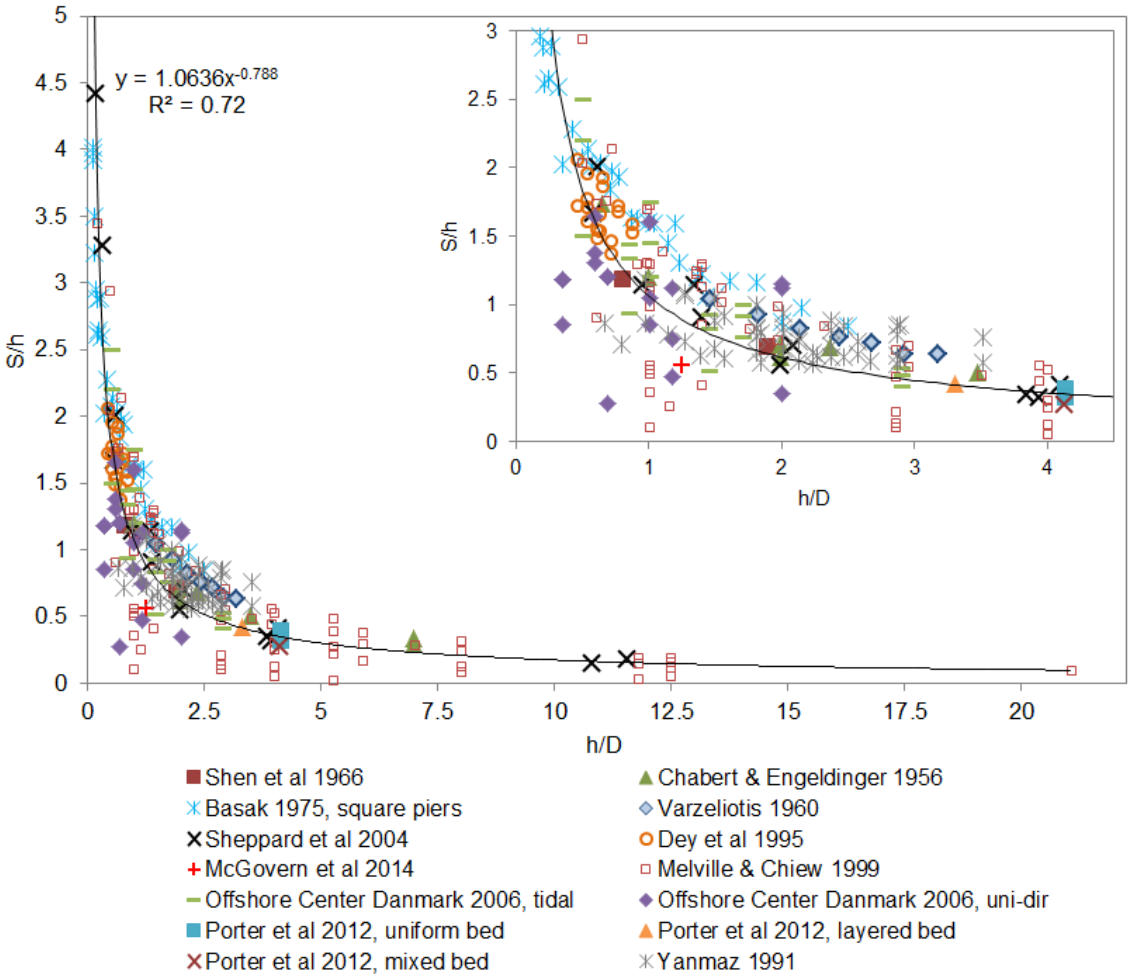

Figure 5.13: Normalised scour depth S/h as a function of relative water depth h/D taken from various experimental studies. Black line is equation 5.5. Inset zoom plot for clarity.

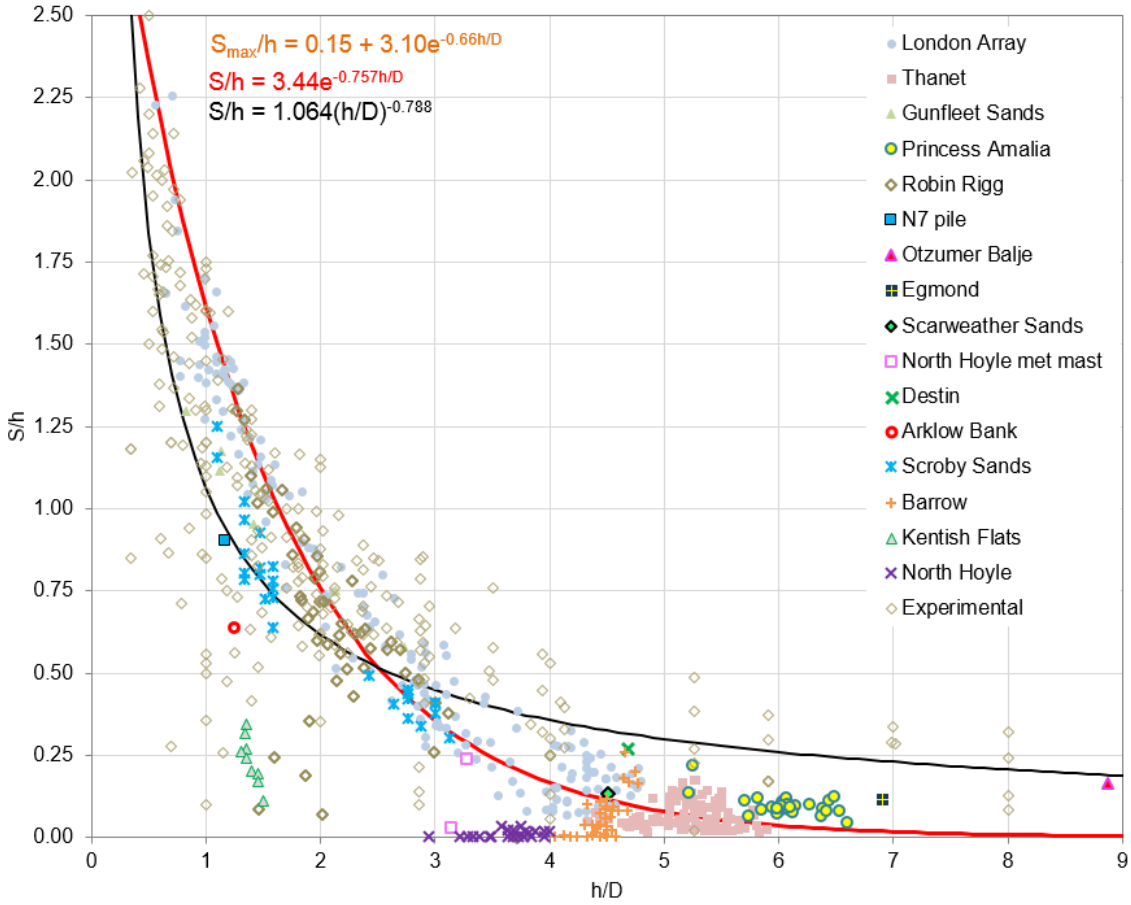

Figure 5.14: Normalised scour depth S/h as a function of relative water depth h/D for both prototype data (Fig 5.10) and experimental data (Fig 5.13). Red line is best fit for prototypes equation 5.3, black line is best fit for experimental data equation 5.5.

M is reduced. However, it should also be noted that substrate effects come into play here as will be discussed in Section 5.1.4.2. Figures 5.17 and Figure 5.18 show the area and volume normalised over water depth plotted against relative water depth. The relationship between these parameters is not as strong as for S/h and less of the variance can be explained by water depth alone ($R^2 = 0.614$ for area and $R^2 = 0.545$ for volume) indicating that the relationship here is not as straightforward as seen for scour depth.

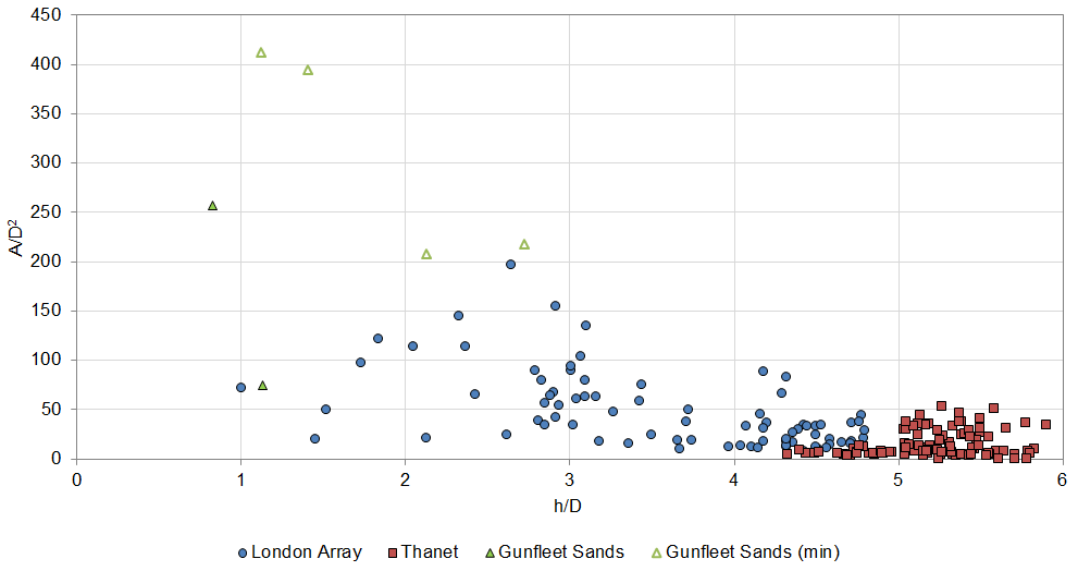

Figure 5.15: Observed scour area A_S/D^2 as a function of mean relative water depth h/D.

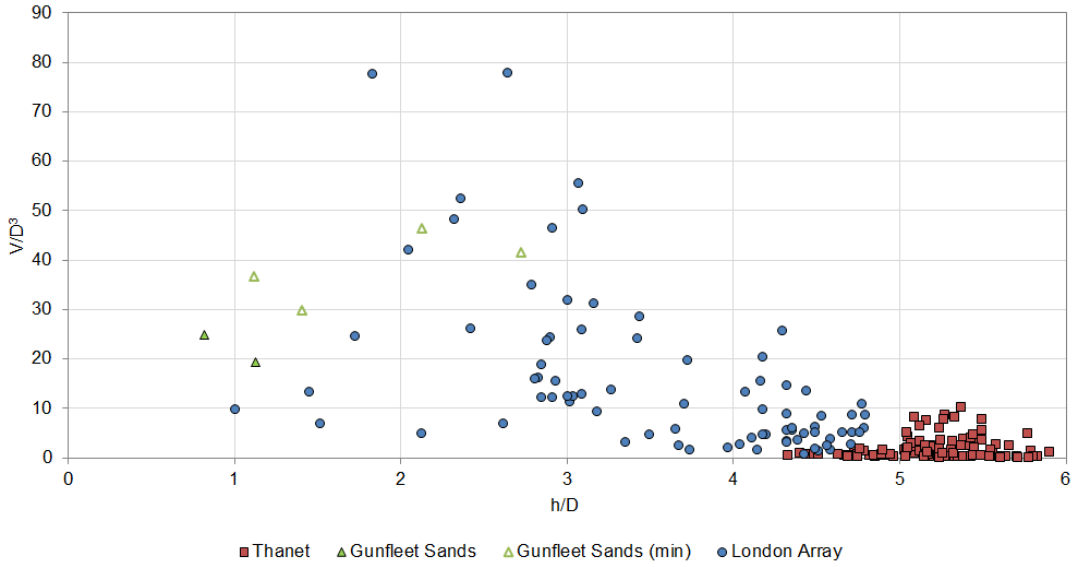

Figure 5.16: Observed scour volume V_S/D^3 as a function of mean relative water depth h/D.

5.1.2 Scour morphology

The systematic quantification of scour hole shape is worth examining as an engineering parameter of interest (eg. to quantify potential lengths of excavated and unsupported cable runs, or to calculate volume of required scour protection), but also to elucidate scour hole evolution and genetic processes. For example, scour hole patterns, such as wake orientation or axial elongation, can indicate dominant flow conditions and nature of forcing (i.e. uni-directional, symmetric or oscillatory). The morphological indicators, introduced

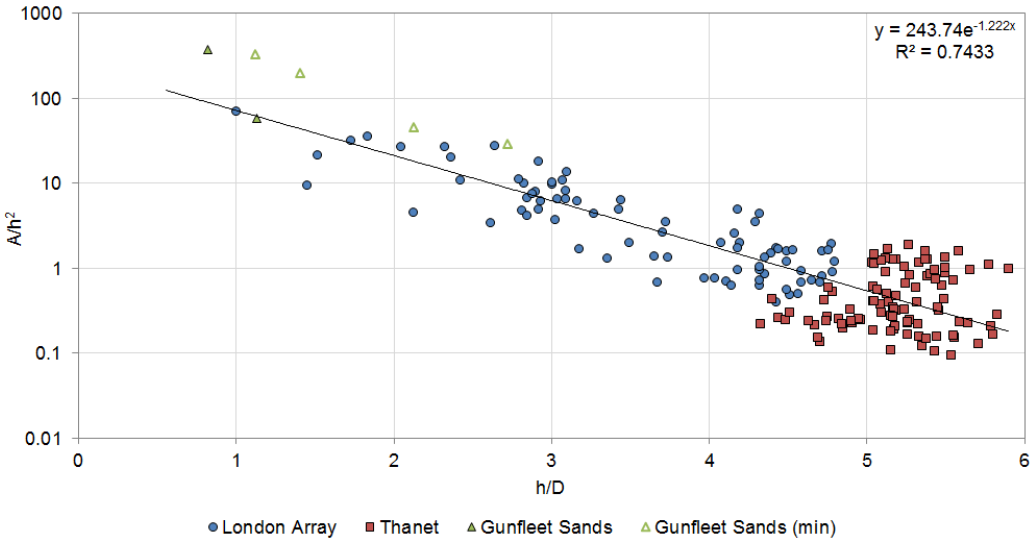

Figure 5.17: Relationship between water depth h/D and normalised scour area A/h^2.

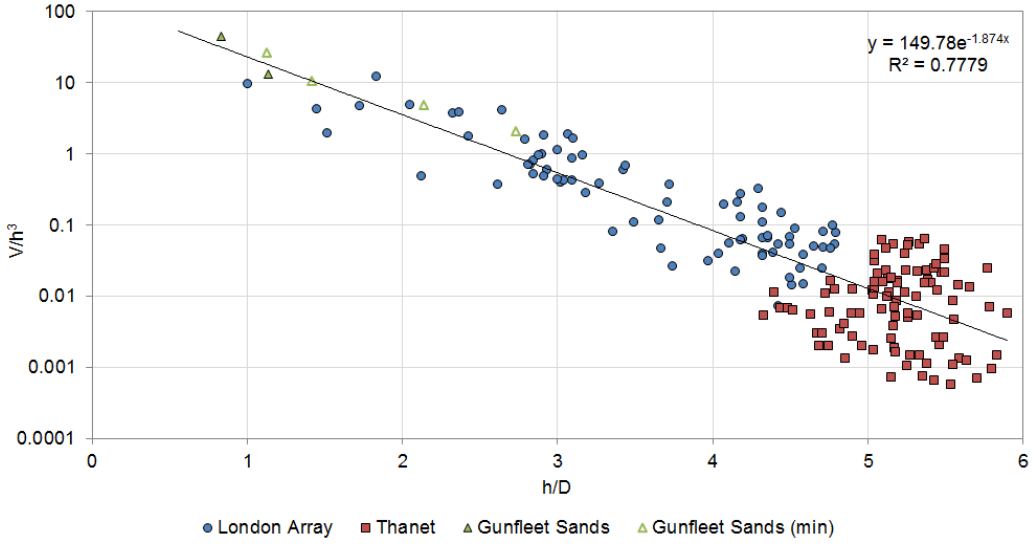

Figure 5.18: Relationship between water depth h/D and normalised scour volume V/h^3.

in Section 2.4.2, are subsequently plotted against water depth to exhibit the range and magnitudes of observed values in the OTE. The statistics for the shape parameters are given in absolute and dimensionless form in Table 5.4.

Table 5.4: Statistics of scour shape parameters for study dataset from three wind farms. Sample size $N = 186$.

	W [m]	L [m]	W/D	L/D	L/W	IQ	β_{av}	$\beta_{u,av}$	$\beta_{d,av}$
Min	9.1	10.2	2.1	2.4	1.02	0.43	2.7	4.5	1.9
Max	87.3	187.4	18.6	39.9	3.36	0.98	30.8	33.3	31.5
Mean	27.3	37.4	5.4	7.4	1.34	0.80	13.5	15.4	12.7
σ	15.0	26.2	2.9	5.3	0.34	0.13	5.7	5.8	6.0

5.1.2.1 Axial elongation

Scour hole width Current appreciation of scour hole lateral extent is low, both from experiments and from prototypes. A range of scour hole widths ($3.05 \leq W/D \leq 7.54$) based on assumptions about S and ϕ have been calculated in Table 1.3. From field data, Whitehouse et al. (2011) describe the lateral extent to be typically 4-5D for a monopile in a sandy bed while there appears not to be any distinction between width and length. In this study a much larger range of scour hole widths is observed; for foundations in sandy sediments values between 18-78m or $W/D \approx 3 - 19$ are found, while the entire range of observed values lies between 9-87m (see Figure 5.19). The data distribution suggests a negative relationship between W/D and h/D. Using the observed S/D and an assumed $\phi = 30°$, the lateral extent W/D was estimated using equation 1.13 and compared to observed values in Figure 5.21. The root mean square error of the prediction is 1.58 and model efficiency $E = 0.32$. The plot shows that using this equation with real scour depths, the scour hole width is typically overestimated implying that, on average, scour holes are more confined than would be expected based on geotechnical assumptions for sand. The best agreement between observed and predicted W/D, based on $RMSE$ and E, is achieved with $\phi = 50°$, giving $RMSE = 1.40$ and $E = 0.51$. The reasons for this could be that sea bed substrates deviate from sand and support greater internal friction angles, or that sandy sediments can show greater ϕ than presumed (as suggested by Link et al. (2013)), or that ϕ is not a controlling factor of lateral extent. It is also clear that for scour pits with complex wider scour patterns, as exemplified at Gunfleet Sands, the relationship with ϕ is not suitable. To test whether the width of the scour pit is a function of scour depth, the two parameters are plotted in Figure 5.23. A relatively strong link between S/D and W/D is witnessed ($R^2 = 0.678$). Based on the field data the dimensionless scour hole width W/D can be approximated from the non-dimensionalised scour depth S/D using the exponential relationship in Equation 5.6. As the scour width is linked to the erosion at the foundation, the proposed equation is a better predictor of the observed scour widths ($RMSE = 1.07$, $E = 0.74$) than ϕ.

$$\frac{W}{D} = 2.60e^{0.85S/D} \tag{5.6}$$

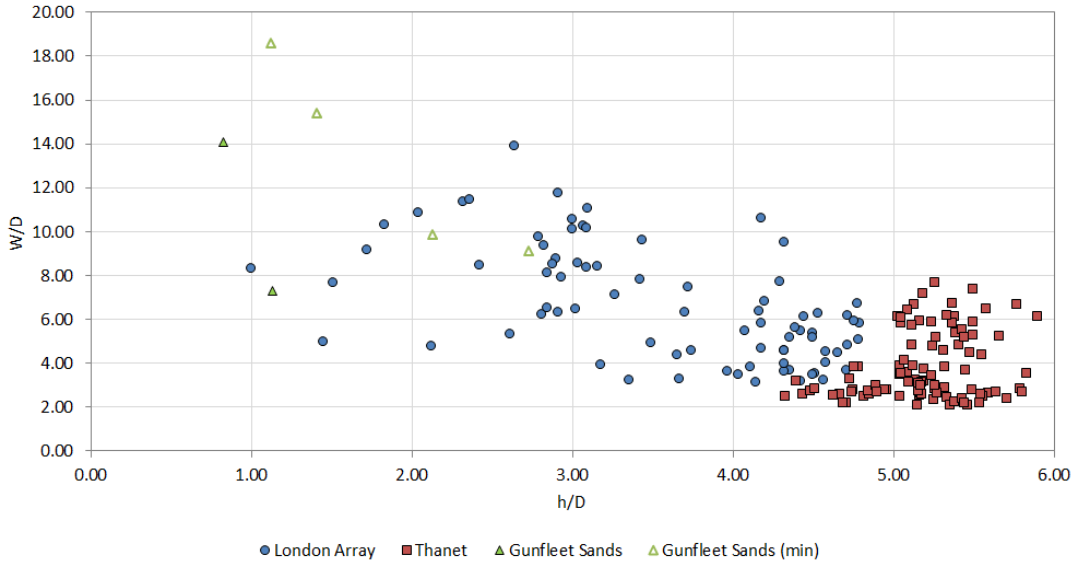

Figure 5.19: Observed scour hole width W/D as a function of mean relative water depth h/D.

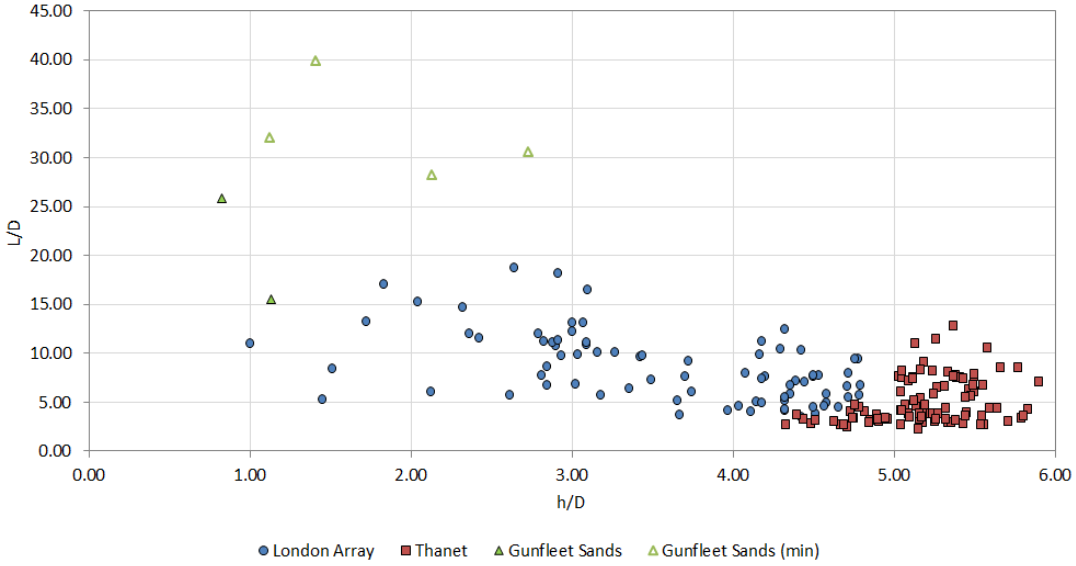

Figure 5.20: Observed scour hole length L/D as a function of mean relative water depth h/D.

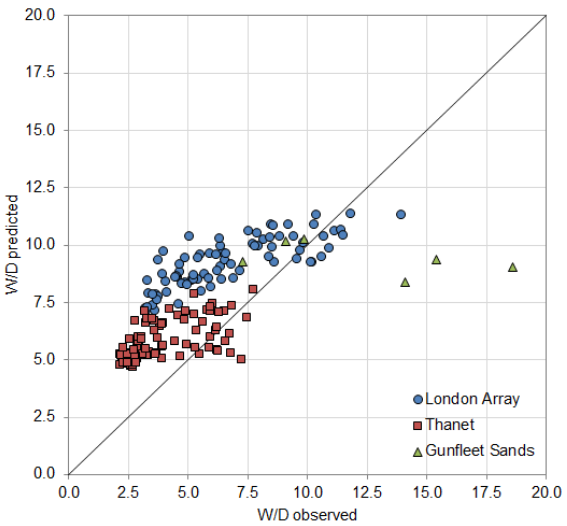

Figure 5.21: Observed W/D against predicted W/D using $\phi = 30°$.

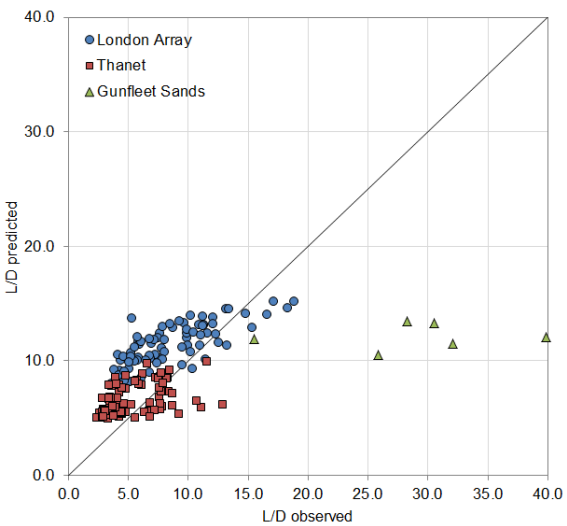

Figure 5.22: Observed L/D against predicted L/D using $\phi = 30°$.

Scour hole length Only a single observation of scour length from prototypes was found in the literature. Whitehouse et al. (2011) document scour wakes of up to $100D$ at monopiles with scour protection at Scroby Sands wind farm. The range of scour pit lengths in this study is shown in Figure 5.20 and ranges from approximately $2 - 19D$ or $9 - 87$m. Using the relationship for upstream and downstream angles given in Equation 1.14 and substituting the assumed $S = 1.3D$ with observed scour depths and $\phi = 30°$, the predicted scour pit length is compared to observed L in Figure 5.22. The $RMSE = 3.1$ and $E = -2.58$ shows that the prediction is unsatisfactory as the model fit is low. Large wakes, such as observed at Gunfleet Sands, do not follow a relationship with ϕ. Similar explanations as mentioned for W apply, indicating ϕ is a weak control. The relationship between L and S/D, plotted in Figure 5.24, is less pronounced than for W/D owing to the fact that the presence of wake length of a lee wake is not primarily controlled by the development of the main conical scour hole. Since most scour pits in this study have no or only limited wake, the relationship between S/D and L/D is still significant and the non-dimensionalised scoured length can be approximated by equation 5.7. This equation is an improvement over the ϕ-based appraoch; however due to the relative independence of lee-wake scour from the scour depth at the foundation, as illustrated in the Gunfleet Sands data, the model fit is still unsatisfactory with $RMSE = 2.88$ and $E = -2.29$.

$$\frac{L}{D} = 3.34e^{0.88S/D} \tag{5.7}$$

Hoffmans and Verheij (1997); Whitehouse (1998) and Harris et al. (2010a) have suggested that the internal friction angle ϕ controls the width, length and slope angles of scour holes; however in this analysis it was established that, for scour holes without significant wake development, scour depth S/D is a better predictor of pit axial dimensions.

5.1.2.2 Long-short axis ratio

The long to short axis ratio L/W indicates whether a scour hole is elongated along a certain axis. An interesting distribution is visible in Figure 5.25. The overwhelming majority of scour holes in the London Array and Thanet developments show $L/W \leq 1.5$ indicating that there is overwhelmingly less than 50% difference in the axes dimensions. In contrast, much greater uni-directional axial elongation (up to $L/W = 3.4$) can be observed at Gunfleet Sands as a result of the extensive wake scour.

5.1.2.3 Circularity

The plot in Figure 5.26 shows the distribution of IQ values, calculated using Equation 2.3. All three wind farms show a considerable and similar range of values. The isoperimetric quotient ranges from 0.43 to 0.98, implying shapes can be highly variable from near-perfect circle to very irregular. This spread of morphologies is found to be fairly similar within the data of every wind farm site. The average $IQ = 0.8$ (Table 5.4) indicates that the majority of scour holes in the OTE deviate by less than 20% from a circle.

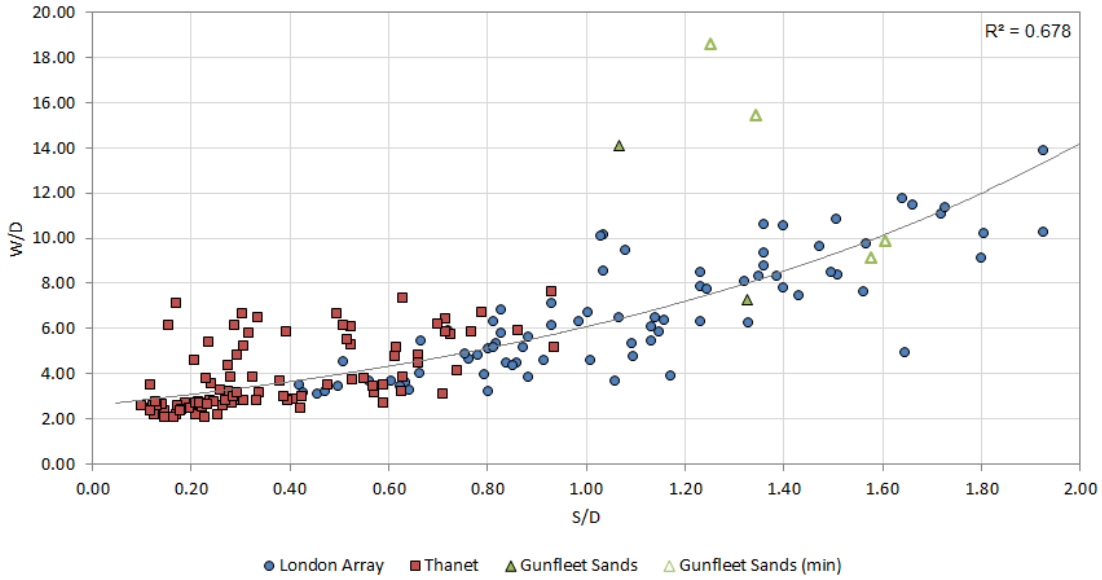

Figure 5.23: Scour hole width W/D against scour depth S/D.

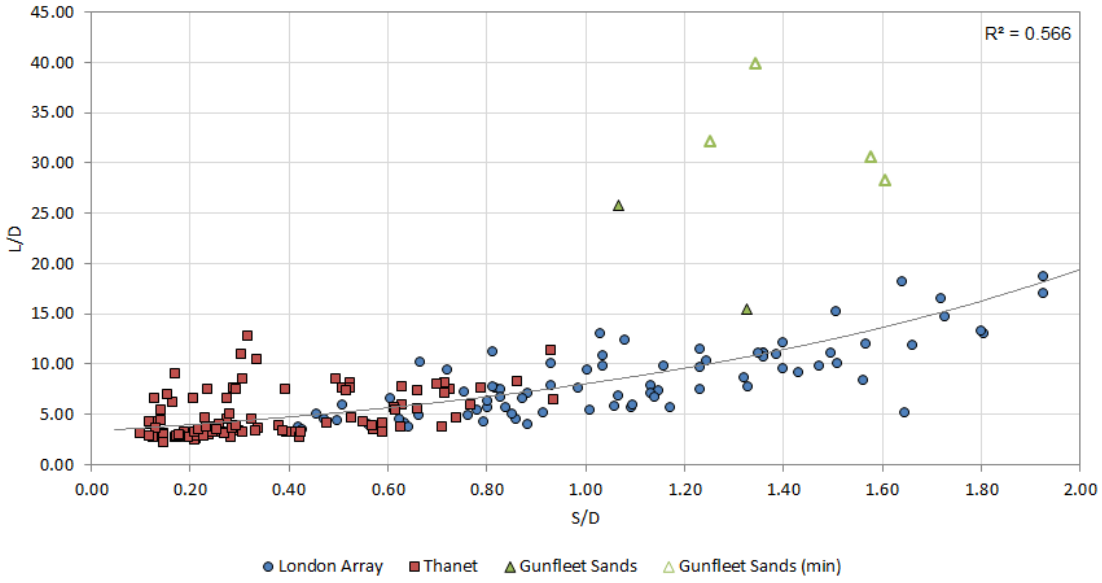

Figure 5.24: Scour hole length L/D against scour depth S/D.

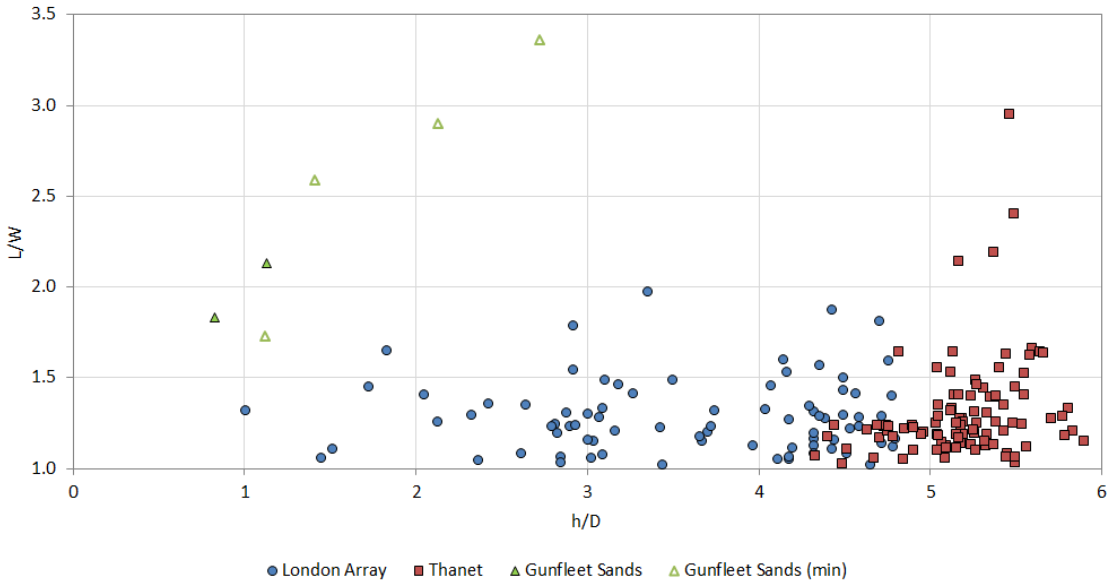

Figure 5.25: Scour hole long-short-axis ratio L/W as a function of relative water depth h/D.

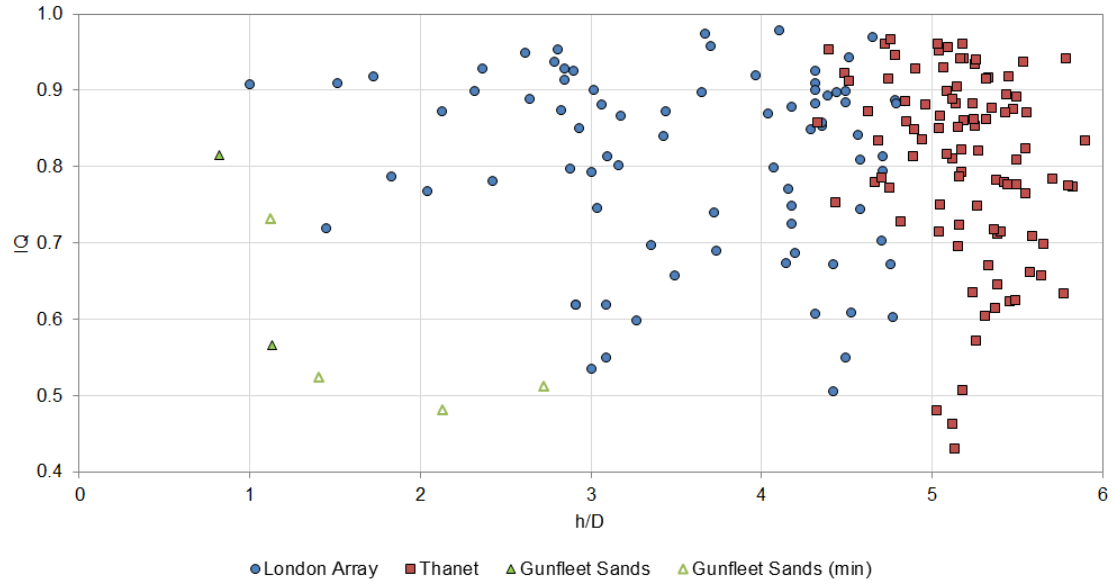

Figure 5.26: Scour hole isoperimetric quotient IQ as a function of relative water depth h/D.

5.1.2.4 Shape classification

The range of morphologies across the OTE is displayed in Figure 5.27. The data distribution in the shape classification system plot reflects the description of morphological parameters in Sections 5.1.2.2 and 5.1.2.3 with, on average, limited axial elongation high circularity. Thus, the majority of scour pits for London Array and Thanet fall into one of the three circle-related categories where $IQ > 0.8$ and $L/W < 1.4$, although significant scatter and plan form shape variability is observed at both sites. Scour pits at Gunfleet Sands are decidedly more stretched along the L axis and are characterised by bi-directional and uni-directional elongated and irregular elongated shapes.

5.1.2.5 Slope

Histograms of the slope value distributions for each scour hole were calculated as well as associated statistics. Figure 5.28 shows the mean slope angle β_{av} of the scour holes. The data show that the average slope can vary significantly between approximately $3 - 30°$. There is no direct relationship with scour depth. Shallow scour displays relatively moderate slope angles as illustrated by Thanet data points with $S/D < 0.4$). Similarly, deep scour holes tend to have reduced average angles due to the two components that make up a typical scour hole. The main scour pit, idealised as an upturned conical frustum, at the structure is generally steep and assumed to be controlled by the internal friction angle of the sediment ϕ (eg. Hoffmans and Verheij, 1997; Whitehouse, 1998). In reality slope angles in this area vary approximately between $10° < \beta < 75°$. However, section 5.1.2.1 has shown that ϕ is actually not a good predictor for the scour hole slopes, as lateral extents appear to be independent of ϕ. The wider scour hole is characterised by low slope values, of typically less than 10° other than at edge features where much steeper angles (up to 65°) can be witnessed. The mean slope angle, as illustrated in Figure 5.28, is a function of the relative dominance of these two components. Hence, scour holes at Gunfleet Sands can display such low average slopes, while confined scour holes that have no wider scour tend to show steeper average slopes. To better capture some of this detail, the upstream slope $\beta_{u,av}$ and downstream slope $\beta_{d,av}$ (as defined in Figure 2.32) are plotted in Figure 5.29. Most points cluster close to the equality line, which agrees with the observation that scour holes are generally circular and have little preferential extension, as such up- and down-stream slope angles are similar as a consequence of relatively symmetric tidal flows. Hoffmans and Verheij (1997) suggested the downstream angle is typically half the upstream angle, which in turn is equal to ϕ, while Harris et al. (2010a) quotes $\phi/2$ $\pm 2°$. This relationship can be considered a rough approximation where one flow direction is dominant, but $\beta_{d,av}$ can be as much as a factor of six smaller than the upstream slope. Typically, the more pronounced the wake, the greater the ratio of $\beta_{u,av}/\beta_{d,av}$. However, as will be shown below, shallow slopes are not limited to scour holes with extensive wake features.

A histogram of scour hole slopes observed over the three wind farm data sets is presented in Figure 5.30. The plot also shows the cumulative percentage lines for the individual wind farms, indicating that Gunfleet Sands has a greater proportion of shallow angles

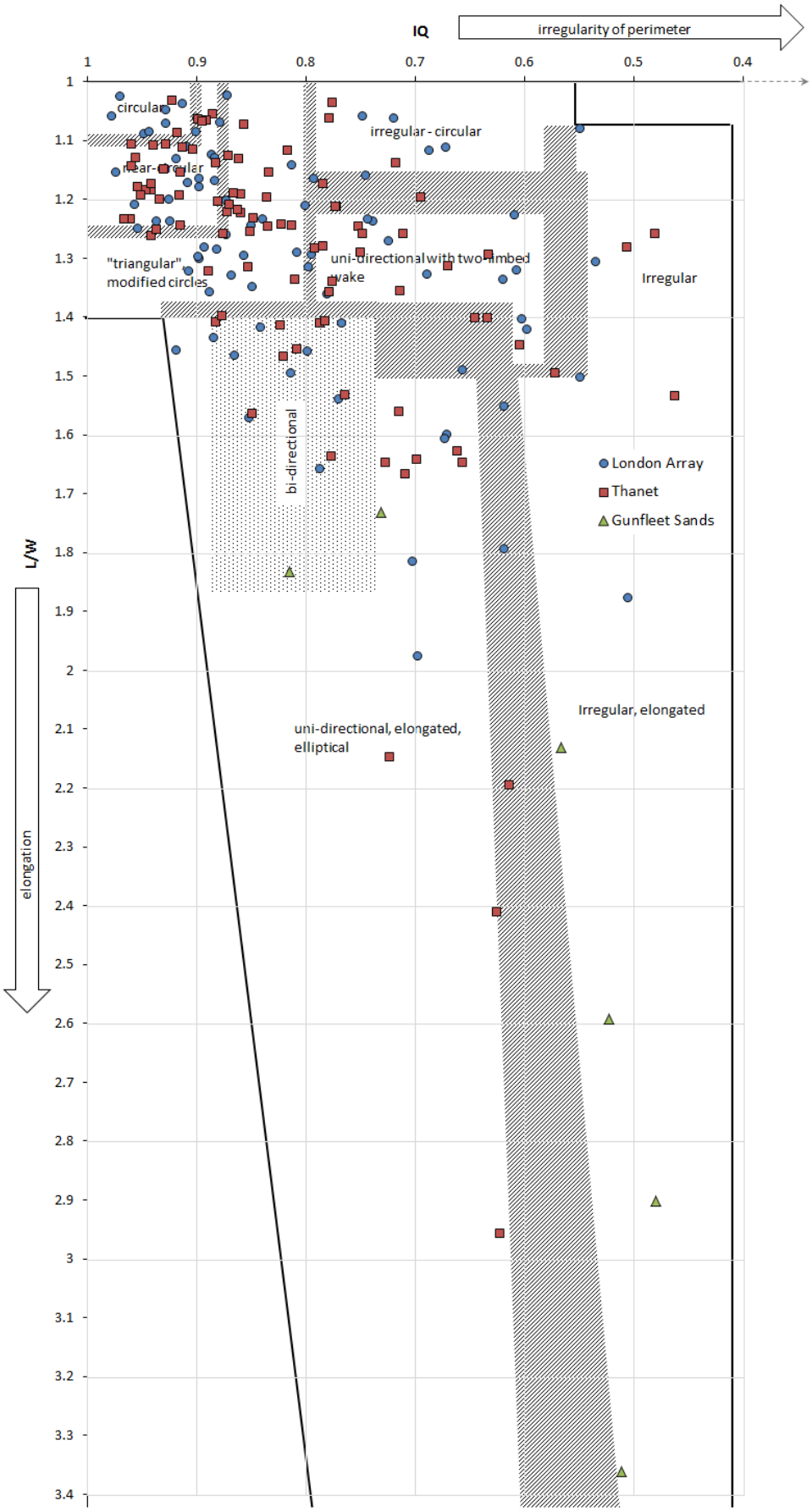

Figure 5.27: Scour hole shape classification chart, based on IQ and LW. Populated with data from Thanet, London Array and Gunfleet Sands wind farms.

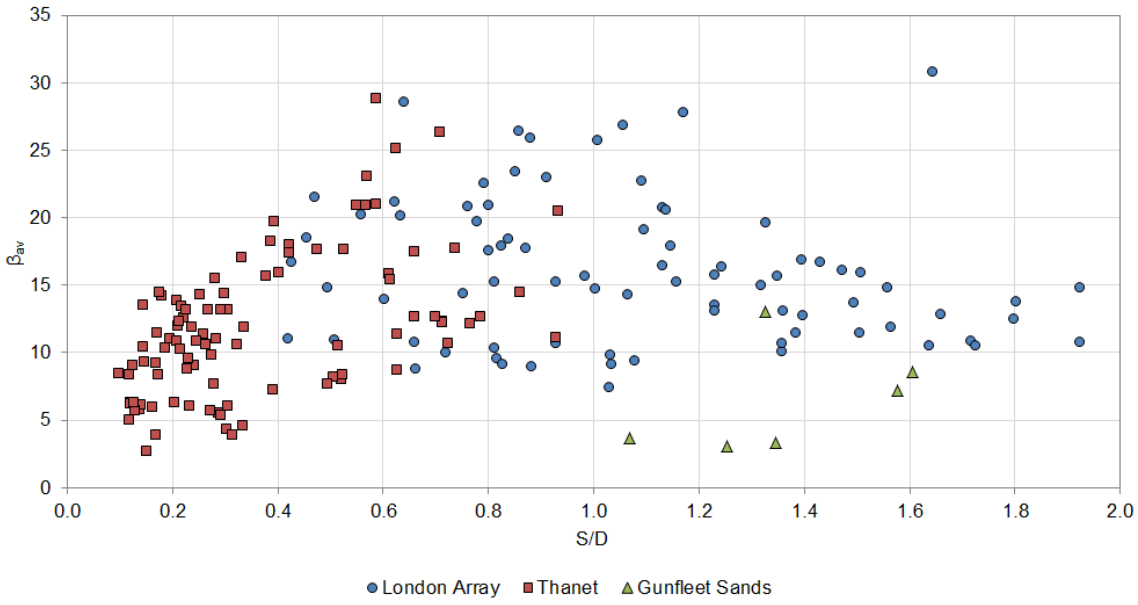

Figure 5.28: Mean slope of scour holes β_{av} as a function of scour depth S/D.

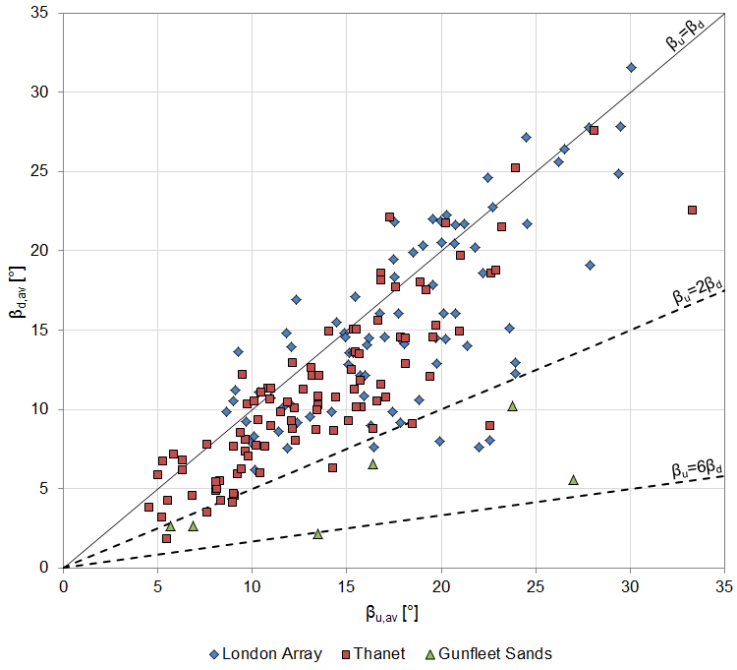

Figure 5.29: Mean upstream slope $\beta_{u,av}$ against mean downstream slope $\beta_{d,av}$.

due to the extensive wake, whereas London Array has a larger amount of steeper angles. Generally, over half of the observed angles are below 10° while 5% of angles are in the range of $30° < \phi < 40°$ for sands and sandy sediments after Peck et al. (1974) and Carter and Bentley (1991) and 12% of slope angles are encompassed in the $26° < \phi < 45°$ range put forward by Hoffmans and Verheij (1997). This shows that the intra-pit variability of slope inclines is so large that a single ϕ is not going to be representative of the actual slopes. The histogram also reveals that slope angles of up to 74.6° can occur in natural sandy sea bed sediments, as seen at London Array. This exceeds even the suggestion of Link et al. (2013), that slope angles of $\phi + 15\%$ are possible in sandy substrates. Interestingly, quite such high slope angles are not observed at Thanet or Gunfleet Sands wind farms. At the latter, in similar sandy substrates, the steepest slope is just over 50°. While this confirms the notion that the angle of repose can be exceeded in scour pits, the question as to why the extremes are not witnessed here leads to the issue of survey resolution. It is likely that the degree of detail captured by the bathymetric data influences the range of slope angles observed in individual data sets as less detailed surveys are liable to average out thin bands of high slope angles. This could explain why the steepest angles are only observed in the high-resolution (0.25m bin size) London Array data.

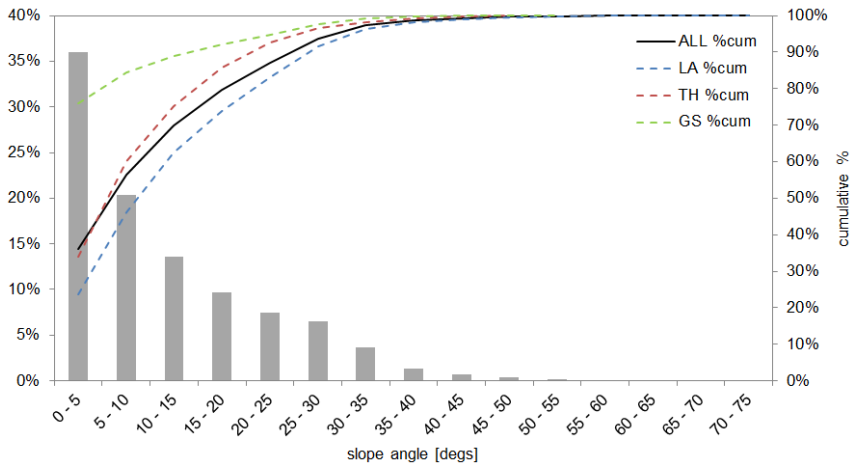

Figure 5.30: Histogram of scour hole slope angles for all three wind farms. Cumulative percentage curves for London Array (blue dashed), Thanet (red dashed) and Gunfleet Sands (green dashed).

For comparison, den Boon et al. (2004) report scour hole slope angles between $18 - 34°$ for a monopile in uni-directional current and wave flow. While it is not explained how these angles were determined, it is assumed that these are based on profile measurements along the flow-aligned symmetry-axis of the cylinder, thus are likely to be higher than angles calculated using the method outlined in section 2.4.2. Here, the data show flow-axial slope angles in the range of approximately $4 - 33°$ and Figure 5.31 reveals that shallow slope angles are not limited to areally extensive scour holes. In fact, very confined scour holes can display very low slope angles. The data from Thanet wind farm reveals a remarkable range of slope angles. For London Array and Gunfleet Sands a tendency for $\beta_{u,av}$ and $\beta_{d,av}$ to diminish with increasing area is discernible.

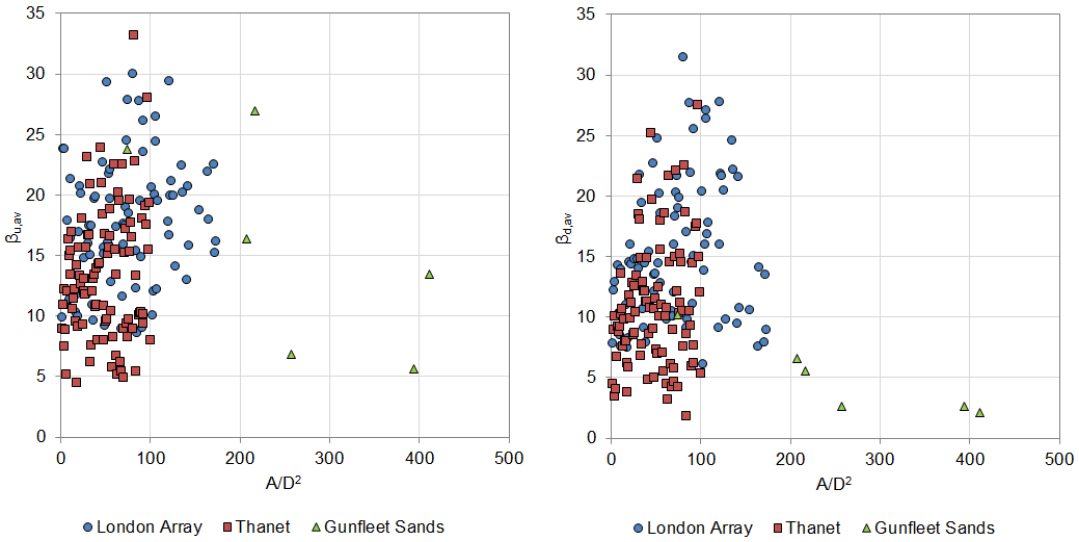

Figure 5.31: Relationship between $\beta_{u,av}$ (left) and $\beta_{d,av}$ (right) with scour area A/D.

5.1.3 Effect of hydrodynamics

Using the same methodology as in Section 3.4.3, the scour pits were categorised as either directionally influenced or symmetric on the basis of pit morphology and presence, location and magnitude of depositional features. In addition to the caveats mentioned in Section 3.4.3, this analysis is further complicated by large variabilities in the sea bed substrates which are going to influence the outcome.

Figure 5.32 shows the differences in scour depths observed under symmetric and directionally dominant flow. London Array shows the maximum scour and the largest range in symmetric flow, whereas at Thanet the maximum scour depth and greater range is observed in directional flow. Since the geotechnical conditions between London Array and Gunfleet Sands are relatively similar, these data sets offer some scope for comparison. At London Array, scour occurs in live-bed conditions as indicated by migrating bed forms under ambient conditions. At Gunfleet Sands, scour is thought to develop in a mix of clear and live-bed conditions depending on the state of tide and external forcings (see Section 4.6.1). Due to the small sample size it is difficult to draw conclusions about the effect of the scour regime on scour depths, as Gunfleet Sands scour is slightly less, but comparable to the scour observed at London Array. Also, for vertical scour, it is questionable how much impact the regime will have compared to potential water depth control (section 5.1.1.2) or substrate effects (section 5.1.4.2), which appear to have a greater bearing on erosion. However, the regime distinction is believed to be important factor in lateral scour development as suggested in Section 4.6.4 and discussed further in section 5.1.5. It is clear that large geotechnical variability exists between London Array/Gunfleet Sands and Thanet, thus it is likely that substrate controls have superseded any hydrodynamic effects.

In terms of scour hole shape, the two populations show different characteristics. The scour holes attributed to symmetric tidal flow exhibit higher average IQ of 0.83 and $L/W = 1.26$. In directionally-dominated flow, the scour holes deviate stronger from the circular pattern as the mean IQ drops to 0.75 and lateral extension becomes more prevalent

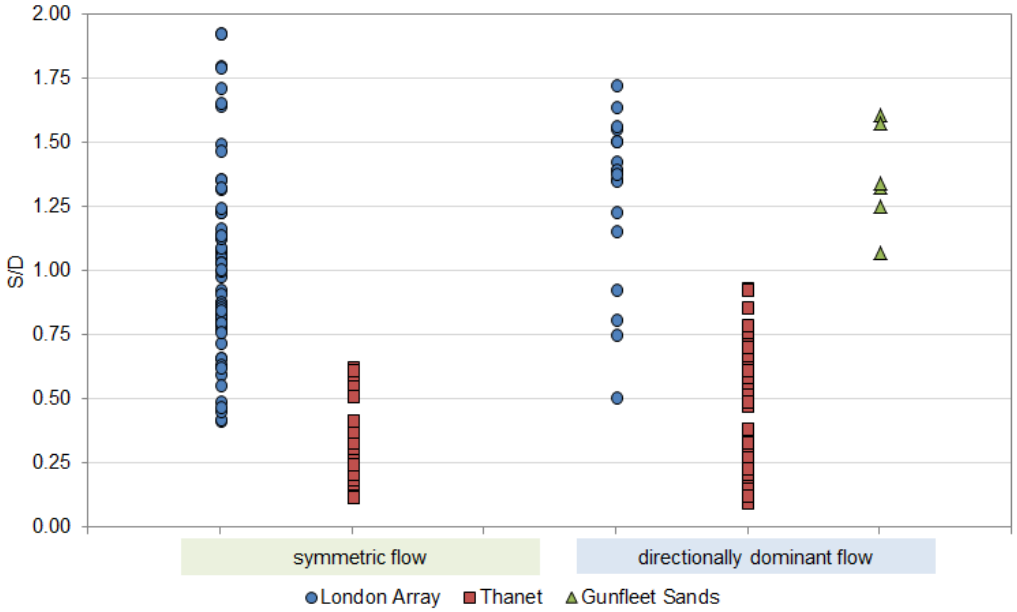

Figure 5.32: Range of S/D in symmetric and directionally dominant flow regime at London Array (blue), Thanet (red) and Gunfleet Sands (green).

as indicated by an average long-short axis ratio of 1.46.

5.1.4 Effect of sediment thickness and geotechnics

5.1.4.1 Granular sediment availability

Following on from the detailed discussion of the effect of sediment thickness at London Array (section 3.4.4) and Thanet (section 4.4.4), all of the data from the Outer Thames are plotted in Figure 5.33. At London Array it was shown that scour is limited at the London Clay, allowing for some vertical adjustments due to bed level changes between CPT measurements (z_{sed} taken from these) and scour surveys, and notwithstanding small amounts of erosion in this layer. However, at Thanet it was shown that bed rock does not necessarily always function as a scour control as it was demonstrated that scour can continue in granular (poorly-) lithified sediments; clays and chalks do experience erosion, but the magnitude of scour is benign from an engineering perspective. At Gunfleet Sands the scour does not reach the underlying layer, at least not at time of surveying, although one data point is within 0.6m of a more erosion-resistant band. The scour holes at Gunfleet are estimated at just under 2.5 years old (see Figure 5.1.6), it is likely that the final depth has been reached, although scour can develop for many years after installation in sandy sediments. Putting aside the aspect of scour limiting by erosion resistant layers, the variability of scour depths that lie within the granular package is worth investigating, especially where this package is relatively homogeneous in the vertical dimension (ie. at London Array and Gunfleet Sands). At Thanet, where the granular layer is not in form of mobile bed forms, the sediment can show strongly varying characteristics in profile and lateral, which is the likely cause of the variability as illustrated in section 4.4.4. Focussing on London Array and Gunfleet Sands, the range of scour depths in thickness of granular sediment $z_{sed} > 10$m is remarkable, especially in the first location. In sections 3.4.4.2

and 4.4.4.1 a geotechnical causation was investigated, examining a relationship between engineering parameters of granular sediments (cone resistance q_c and relative density D_r) and scour depths. However, no correlation could be established, suggesting that those parameters, indicative of the compaction grade, and hence strength of the sediment (see section 2.2.3), do not exert control on scour depth (assuming pre- and post-installation engineering properties of the sediment are comparable). As shown in section 3.4.4 and the timing of scour surveys is believed to explain most of this discrepancy at London Array, such that the low-scour outliers are young scour holes that are still developing. This has been confirmed in section 5.1.1.2 and has been shown to explain the high variability in observed scour in water depths between $3-6D$ in Figure 5.12. This survey timing issue makes it difficult to consider geotechnical factors within the granular sediment package that might affect scour. Nevertheless, the range of scour observed at Gunfleet suggests that some subtle effects might be present, as these were, to the authors best knowledge, surveyed on the same day. These remain once the effect of water depth has been taken into account. This question should be revisited in future, where the temporal aspect can be excluded to explain the varibility in scour depths.

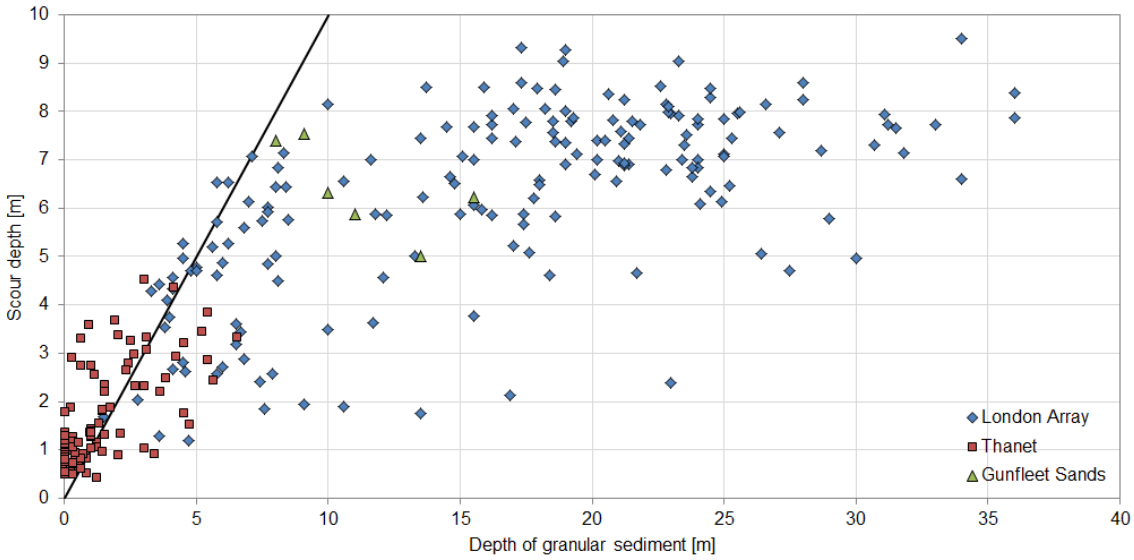

Figure 5.33: Relationship between thickness of granular sediment z_{sed} and scour depths S at wind farms in the Outer Thames Estuary. Equality line $S = z_{sed}$ in black.

5.1.4.2 Geotechnical considerations for scour in cohesive and consolidated substrates

As explained in section 5.1.1.2, geotechnical influences are expected to be responsible for deviations from the $S/h - h/D$ relationship in equation 5.3. These deviations have shown to be greatest in complex sea bed configurations. For this reason, the scour in different substrate types is examined here. Figures 5.34 to 5.36 show the observed scour depth, area and volume in terms of substrate using the substrate classification after Whitehouse (2006) (see Figure 1.11). The sediments at London Array and Gunfleet Sands are sand and silty sand (muddy sand in the conceptual model), while the diversity of substrates at Thanet allows scour in gravelly, cohesive and consolidated substrates to be evaluated. An additional category of chalk was added.

Table 5.5: Statistics for A/D^2 (top) and A_S [m^2] (bottom) for substrates encountered in the Outer Thames Estuary. Substrate classification after Whitehouse (2006).

A_S/D^2	sandy sediments		cohesive/consolidated sediments				
	muddy sand	sand	sandy mud	stiff clay	clay	chalk	gravel
Min	4.74	4.20	6.62	0.00	3.41	3.08	2.92
Max	411.62	257.75	25.40	34.49	29.88	8.89	7.11
Mean	40.86	49.55	16.01	7.46	8.68	5.88	5.47
σ	81.93	46.91	9.39	9.54	7.45	1.52	1.34
Mean	46.59			7.65			
σ	61.28			7.28			

A_S [m^2]	sandy sediments		cohesive/consolidated sediments				
	muddy sand	sand	sandy mud	stiff clay	clay	chalk	gravel
Min	80.0	71.0	134.0	0.0	63.0	57.0	54.0
Max	9092.7	5693.7	561.0	828.0	605.0	180.0	157.0
Mean	928.9	1336.4	347.5	167.0	176.0	117.4	113.4
σ	1810.4	1119.4	213.5	228.5	152.5	33.1	32.0
Mean	1197.6			160.4			
σ	1407.1			165.4			

The scour dimensions are largest in sand and muddy sand and these categories also display the greatest range of values. Scour depth and volume is largest in sand, while the largest area was observed in muddy sand, which is attributed to the extensive scour in silty sands at Gunfleet. However, sand encompasses grain sizes from 0.063mm to 2mm, which have quite different mobility characteristics based on Figure 1.12, thus it is possible that some of the variation is explained by the coarse categorisation. Also scour in mixed sandy sediments is more complex than in uniform sediments. In general, increasing the heterogeneity of sediments and adding fine materials increases the erosion resistance as discussed in sections 1.4.1 and 1.4.2. This subtle variability is not captured in this analysis, but potentially a reason for the large range of values observed. It should also be noted that some residual temporal effects can still be contained in the data, ie. not all scour holes have reached "final" condition (as suggested eg. in section 3.4.4.4). Scour dimensions in the other substrates are more limited and a similar range of values is observed between clay, gravel and chalk, while stiff clay exhibits the least erosion. The number of observations in sandy mud is small. The statistics of scour depth in various substrates was given in Table 5.8, while the statistics for scour area volume are summarised in Tables 5.5 and 5.6. The statistics show that, on average, scour depths in sandy sediments are greater by a factor of 5, than scour depths in cohesive and consolidated sediments. Even more significant are the differences in scour area and volume between sandy and cohesive/consolidated sediments as areas are 7.5 times and volumes are 28.7 larger. The scour dimensions in granular sediments show much greater variability as indicated by the larger standard deviations for the dimensional parameters.

Based on the prototype data and the statistical distribution of dimensional factors, some modifications to the original conceptual model are proposed as shown in Figure 5.37. The range of scour depths observed in muddy sand and sand are considerably larger than suggested in Whitehouse's model and the range in clay and gravels was more confined. This does not mean, however, that larger scour values are not theoretically possible in these substrates. Only a small number of observations is available in sandy mud, thus the confidence in the modified range is low. The scour depth values in Upper Chalk at Thanet

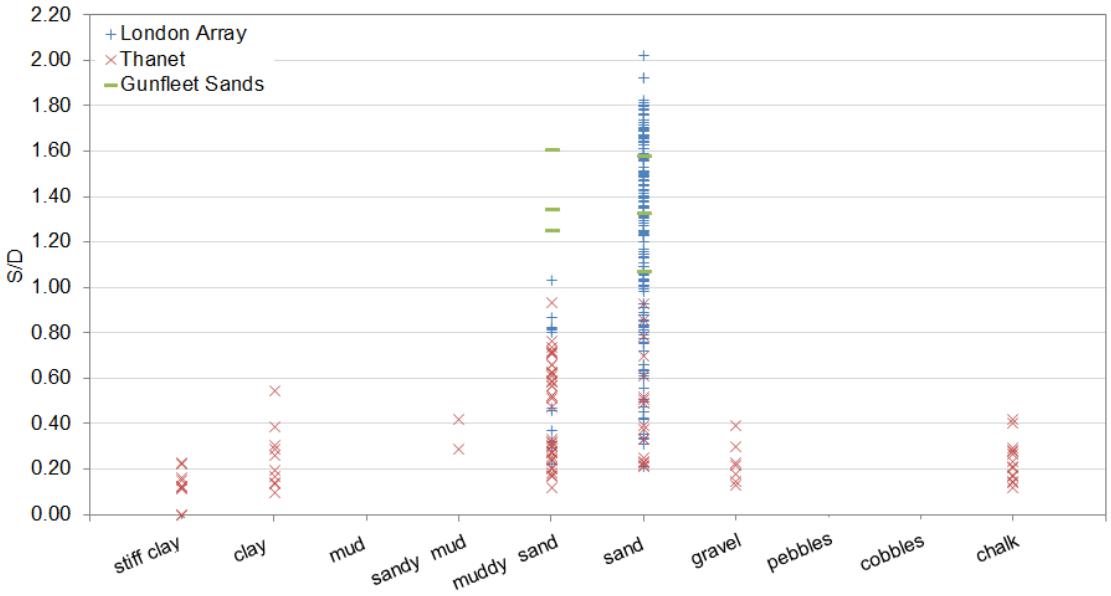

Figure 5.34: Scour depth S/D by substrate type.

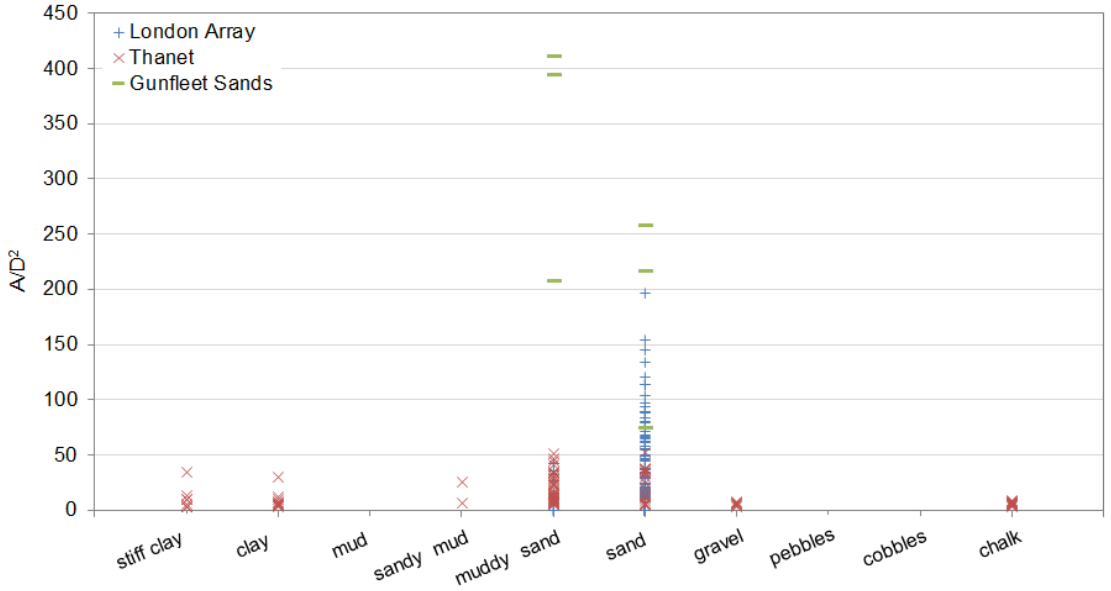

Figure 5.35: Scour area A_S/D^2 by substrate type.

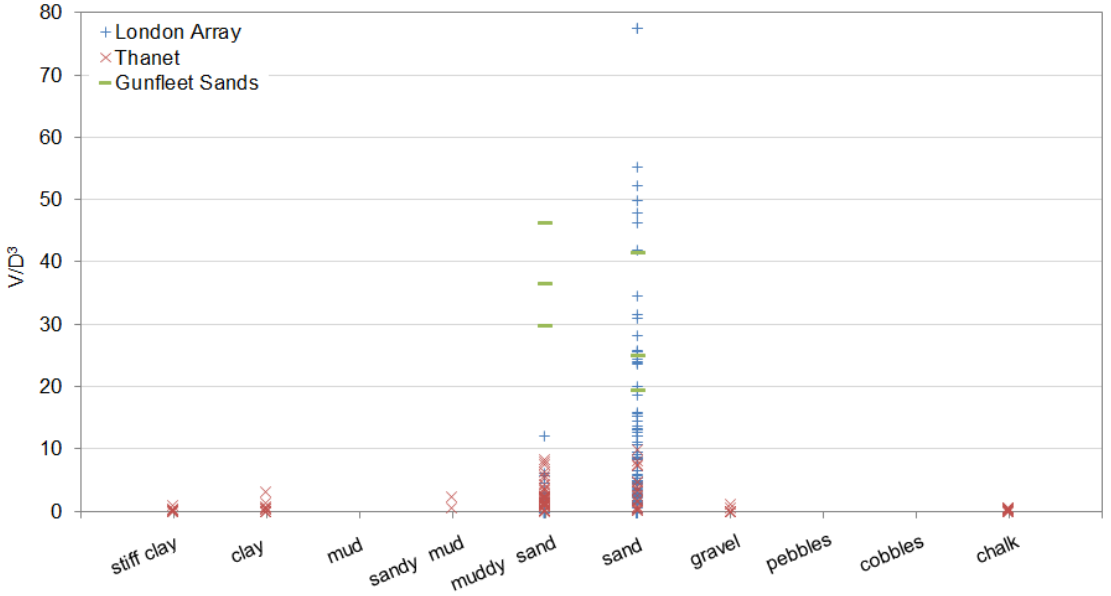

Figure 5.36: Scour volume V_S/D^3 by substrate type.

Table 5.6: Statistics for V/D^3 (top) and V_S [m^3] (bottom) for substrates encountered in the Outer Thames Estuary. Substrate classification after Whitehouse (2006).

V_S/D^3	sandy sediments		cohesive/consolidated sediments				
	muddy sand	sand	sandy mud	stiff clay	clay	chalk	gravel
Min	0.22	0.26	0.83	0.00	0.16	0.13	0.10
Max	46.32	77.7	2.48	1.18	3.35	0.81	1.39
Mean	5.34	14.4	1.66	0.28	0.85	0.45	0.42
σ	8.94	16.1	0.82	0.33	0.93	0.24	0.43
Mean	11.32			0.58			
σ	14.72			0.66			

V_S [m^3]	sandy sediments		cohesive/consolidated sediments				
	muddy sand	sand	sandy mud	stiff clay	clay	chalk	gravel
Min	19.8	20.7	76.0	0.0	14.3	14.0	8.1
Max	4809.3	8590.0	257.6	138.6	347.9	73.7	144.1
Mean	611.2	2036.8	166.8	29.4	80.8	39.4	40.7
σ	962.1	1926.6	90.8	38.2	97.3	20.7	44.0
Mean	1551.3			54.5			
σ	1794.2			68.9			

are similar to those observed in clay.

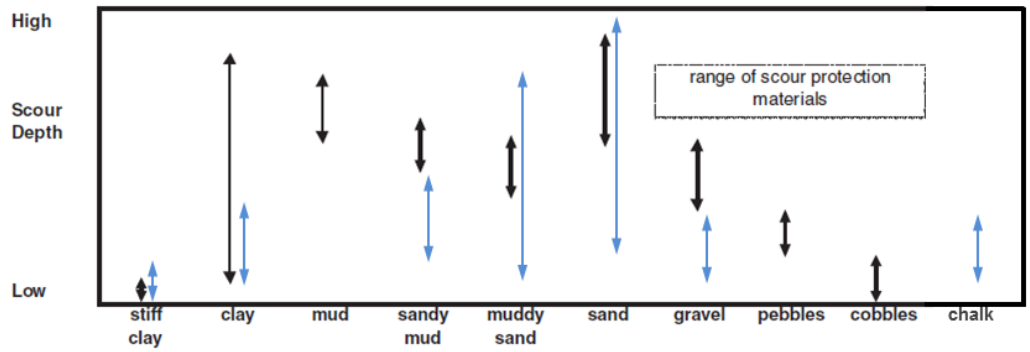

Figure 5.37: Conceptual model for scour in various substrates by Whitehouse (2006). Proposed modifications, based on prototype data, in blue.

The morphological scour parameters are plotted against substrate type to investigate whether the nature of the sea bed has an influence on the scour shapes witnessed. The range of IQ values is greatest in muddy sand and sand as shown in Figure 5.38. Other substrates show more confined ranges. Although cohesive and consolidated substrates exhibit more confined scour holes (as shown in Fig 5.35), the average IQ is slightly lower than that in sandy sediments (Table 5.7). A very similar distribution to IQ is observed for the long-short ratio L/W with the largest range of values found in sandy sediments. Further, the most elongated scour pits are also located in sandy sediments; the other substrate types reveals more equitable axis dimensions (see Figure 5.39) with a lower mean L/W (Table 5.7). An interesting pattern is observed for the average slope angle (Figure 5.40). Again, the largest range of values is observed in muddy sand and sand. However, the confined scour holes in cohesive and consolidated substrates that are able to support very high slope angles actually exhibit quite low average angles. Scour in clay exhibits similar angles as scour in chalk, whereas stiff clay shows the shallowest angles. The statistics show that, on average, slope angles in cohesive and consolidated sediment are lower than in sandy sediments, which appears somewhat counter-intuitive, since slope angles in these substrates are in theory capable of sustaining steeper angles due to cohesive

Table 5.7: Statistics for IQ (top), L/W (middle) and β_{av} (bottom) for substrates encountered in the Outer Thames Estuary. Substrate classification after Whitehouse (2006).

IQ	sandy sediments		cohesive/consolidated sediments				
	muddy sand	sand	sandy mud	stiff clay	clay	chalk	gravel
Min	0.00	0.00	0.72	0.00	0.48	0.66	0.77
Max	0.96	0.97	0.94	0.94	0.96	0.96	0.94
Mean	0.69	0.43	0.83	0.83	0.81	0.84	0.85
σ	0.28	0.41	0.11	0.11	0.13	0.08	0.06
Mean	0.79		0.75				
σ	0.13		0.25				

L/W [m^3]	sandy sediments		cohesive/consolidated sediments				
	muddy sand	sand	sandy mud	stiff clay	clay	chalk	gravel
Min	0.00	0.00	1.11	0.00	1.10	1.03	1.11
Max	2.90	3.36	1.56	2.95	2.15	1.66	1.46
Mean	1.25	0.70	1.33	1.16	1.31	1.23	1.27
σ	0.57	0.69	0.23	0.90	0.29	0.19	0.12
Mean	1.35		1.24				
σ	0.33		0.53				

β_{av} [m^3]	sandy sediments		cohesive/consolidated sediments				
	muddy sand	sand	sandy mud	stiff clay	clay	chalk	gravel
Min	0.00	0.00	5.41	0.00	5.60	6.15	5.71
Max	28.89	30.84	17.45	13.24	20.97	18.08	19.79
Mean	11.00	8.02	11.43	5.77	11.70	12.43	11.94
σ	7.23	8.48	6.02	4.59	4.73	3.23	4.25
Mean	14.16		10.20				
σ	5.90		5.16				

forces.

5.1.4.3 Effect of grain size

In data compiled by Melville and Sutherland (1988) scour was diminished for large relative grain sizes of $D/d_{50} < 50$. Later, Melville and Chiew (1999) concluded that this effect disappeared from $D/d_{50} > 25 - 100$, thus making it effectively irrelevant for prototype scour situations, where much higher ratios of D/d_{50} are common. In Figure 5.41 S/D is plotted against D/d_{50}, showing a range of $362 < D/d_{50} < 58,750$ in the OTE data set. The median grain size information was taken from surface grab samples and therefore might not necessarily be representative of the particle size distribution of the entire sediment profile. However, where granular sediment is available, the surface sediment size is usually a relatively good approximation of the characteristics in the vertical profile, as typically, the grain size is similar (trend towards slight downward fining) but the density of packing increases. At Thanet, from the sparse data available, there appears to be more heterogeneity in the sediment profile; however due to the limited and spatially discontinuous data on sub-surface grain sizes, detailed statements about the effect of sediment changes cannot be made. However, it is clear that, for example, where gravels have been found at the surface, these are not representative of the d_{50} below this lag deposit, which is typically chalk bed rock. This is a factor that should be considered in future data collection as providing a more continuous record of grain size changes with vertical depth would improve the assessment of this factor in granular sediments. CPTs allow grain size changes to be inferred from soil behaviour classifications (see Section 2.2.3); however

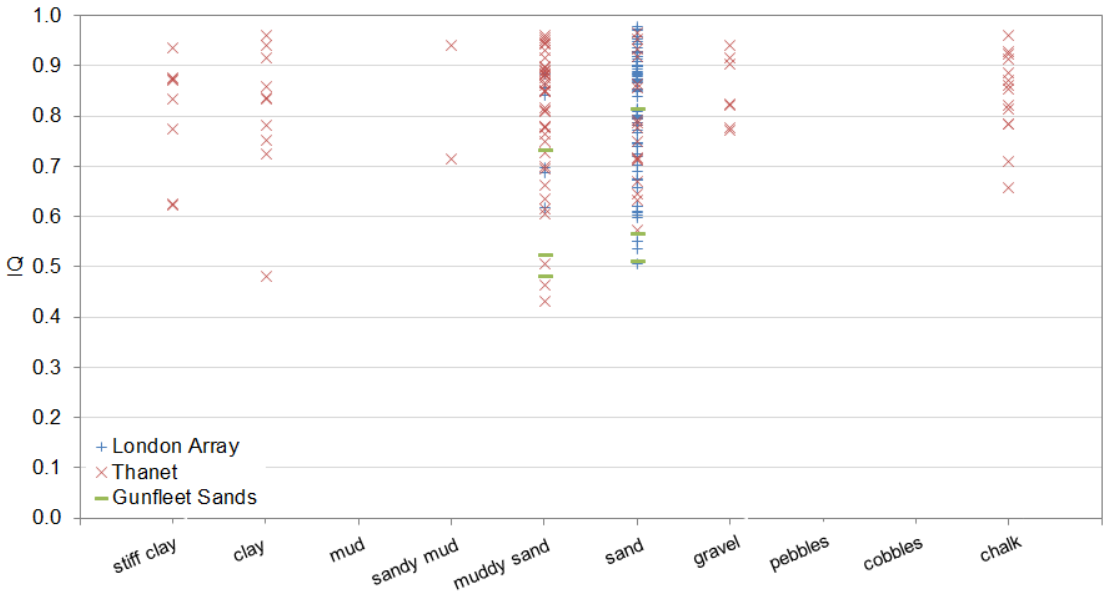

Figure 5.38: Isoperimetric quotient IQ by substrate type.

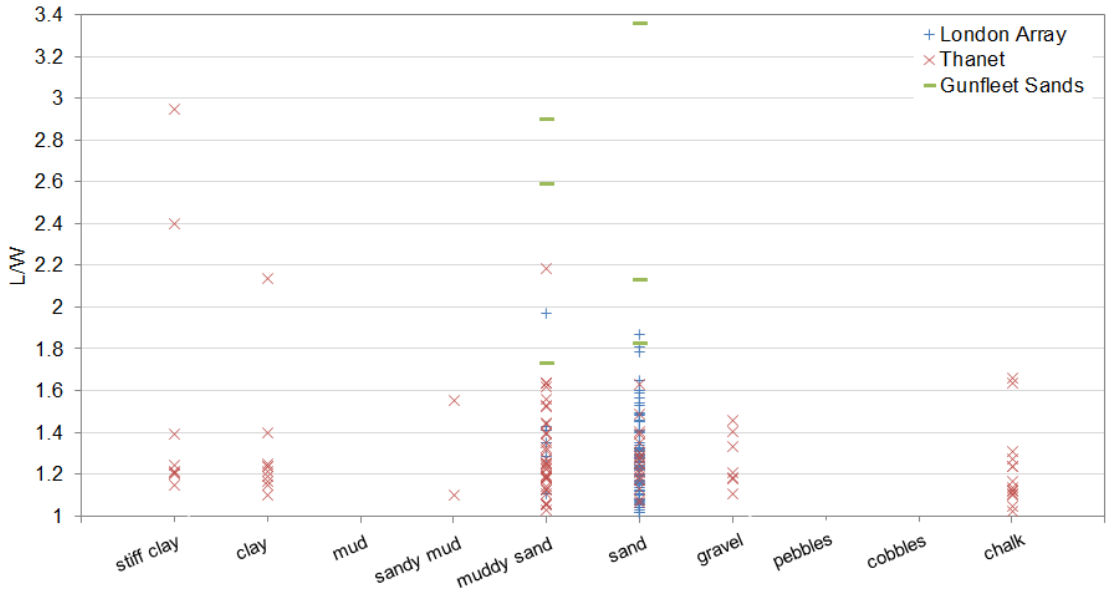

Figure 5.39: Long-short-axis ratio L/W by substrate type.

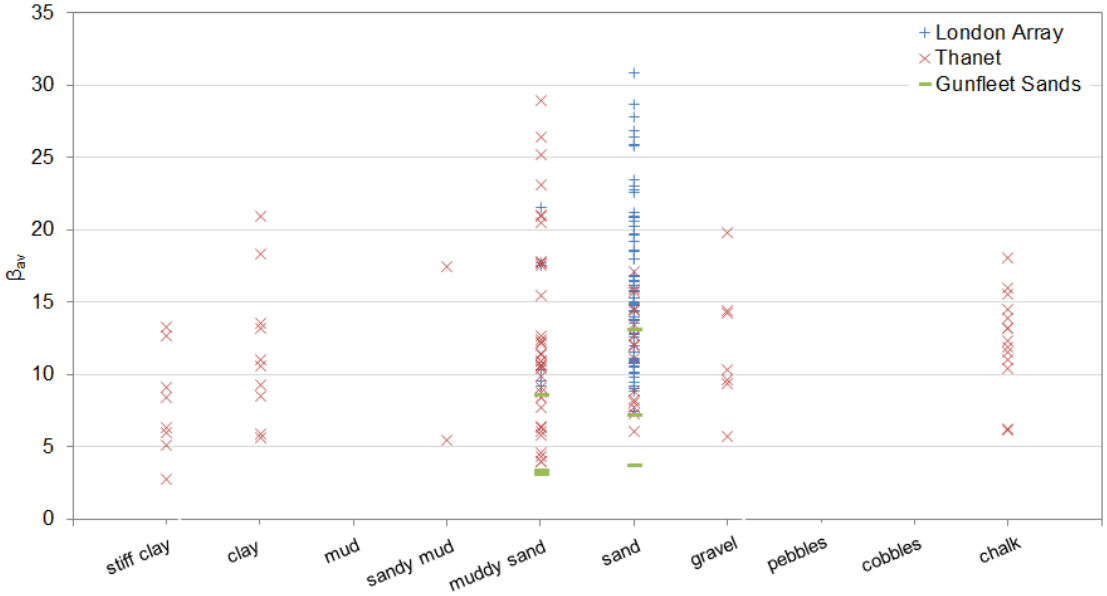

Figure 5.40: Average slope angle β_{av} by substrate type.

distinguishing between, for example, different sands with confidence is not possible.

Experimental data from Sheppard et al. (2004) covering $142 < D/d_{50} < 4,155$ are also plotted in Figure 5.41. All experiments were carried out with different water depths and flow velocities, that were just under critical, ie. clear-water conditions. Sheppard et al. conclude from the experiments that scour is reduced for $D/d_{50} > 50$, although the dependence of S/D on D/d_{50} is diminished compared to the range of $D/d_{50} < 50$, where scour reduces as the grain size approaches the characteristic length scale of the structure. However, this pattern is not observed in the prototype data. There is no dependence with D/d_{50}, other than what is the result of simply d_{50} and the erodibility of unconsolidated sediments. The observed distribution shows the largest scour in fine to medium sands and lesser scour either side of this range (as shown in Figure 5.42). It appears that the largest scour values for each D/d_{50} are controlled by grain size (as suggested by yellow line in Figure 5.42), whereas a range of scour depths can be observed over all D/d_{50}, thus no significant general trend can be established. Again, it should be noted that the largest number of data points are in this range and thus the interpretation of this figure could be misleading. Referring to Figure 1.12, shows that typically medium and coarse sands have the lowest erosion threshold. The smaller range of scour depths in coarse sand is either a function of the smaller amount of data points in this type of sediment or that the coarse sediments do not erode as easily here, eg. due to heterogeneity effects that are not captured by a single d_{50} value. However, it should also be noted that the effect of grain size on scour is ambiguous. In the review of pre-1977 experimental studies, Breusers et al. (1977) has shown that grain size was found to have typically negligible to little effect on scour, at least for uni-modal sediment (Ettema (1976)), which suggests the smaller n might be responsible for the observed pattern. Furthermore, since the d_{50} value is not necessarily representative of the entirety of the eroded sediment, more caution is advised when interpreting the graph. For example, the large grain sizes mostly represent gravel lag deposits on top of Upper Chalk bedrock where scour would be limited anyway, so this does not necessarily reflect what scour depths can be achieved in gravels. Conversely, the large scour values in fine to medium sandy sediments are from sand banks where the surface grain size is a reasonable approximation. The yellow line traces the proposed limit, based on the OTE data, for scour in various grain sizes.

Examining the data given in Sheppard et al. (2004) it is suggested that what is observed in the experiments is potentially not a dependence of S/D on D/d_{50} at all. Based on the findings in section 5.1.1.2, in particular Figure 5.13, the results appear to be nearly fully explained by the different water depths used in the tests as shown in Figure 5.43. When the effect of water depth on scour is accounted for, 98.4% of the variability in Sheppard et al.'s results can be explained by h/D, leaving only the remaining deviation to be explained by grain size effects.

5.1.5 Effect of natural bed mobility

Figures 5.44 to 5.46 show four ranges of bed mobility and scour dimensions observed within each category range, aggregating the data from the three wind farms. The bin sizes were chosen so as not to reduce too much the number of records n in each category.

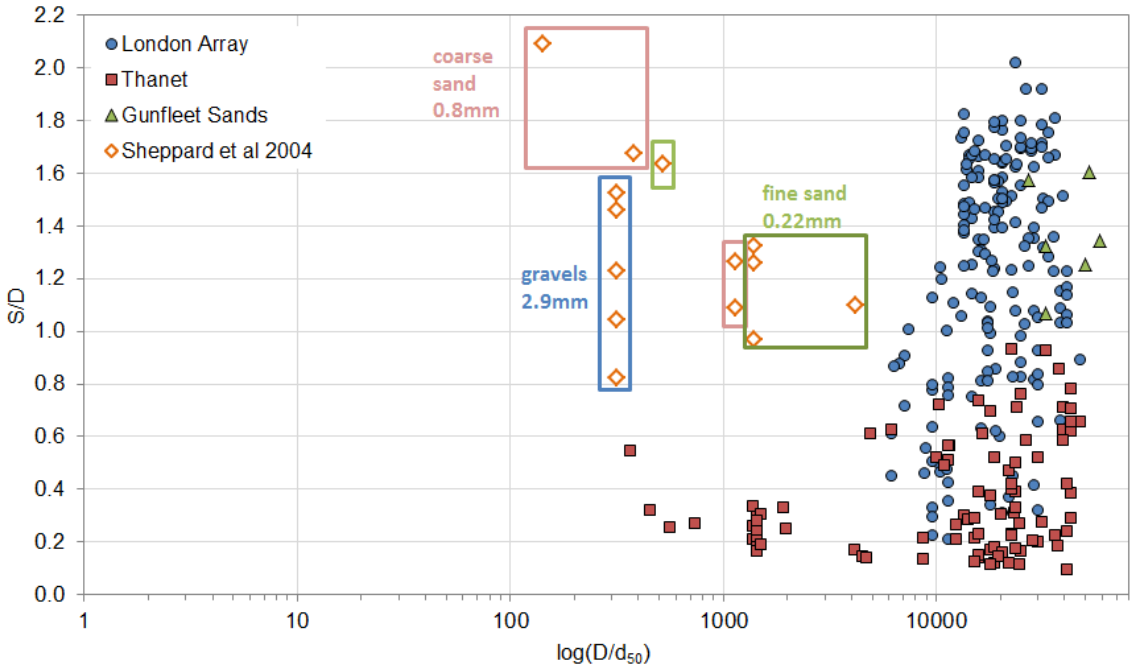

Figure 5.41: Scour depth S/D against relative grain size D/d_{50}. Data by Sheppard et al. (2004) included, with coloured boxes indicating size of sediment used in the experiments.

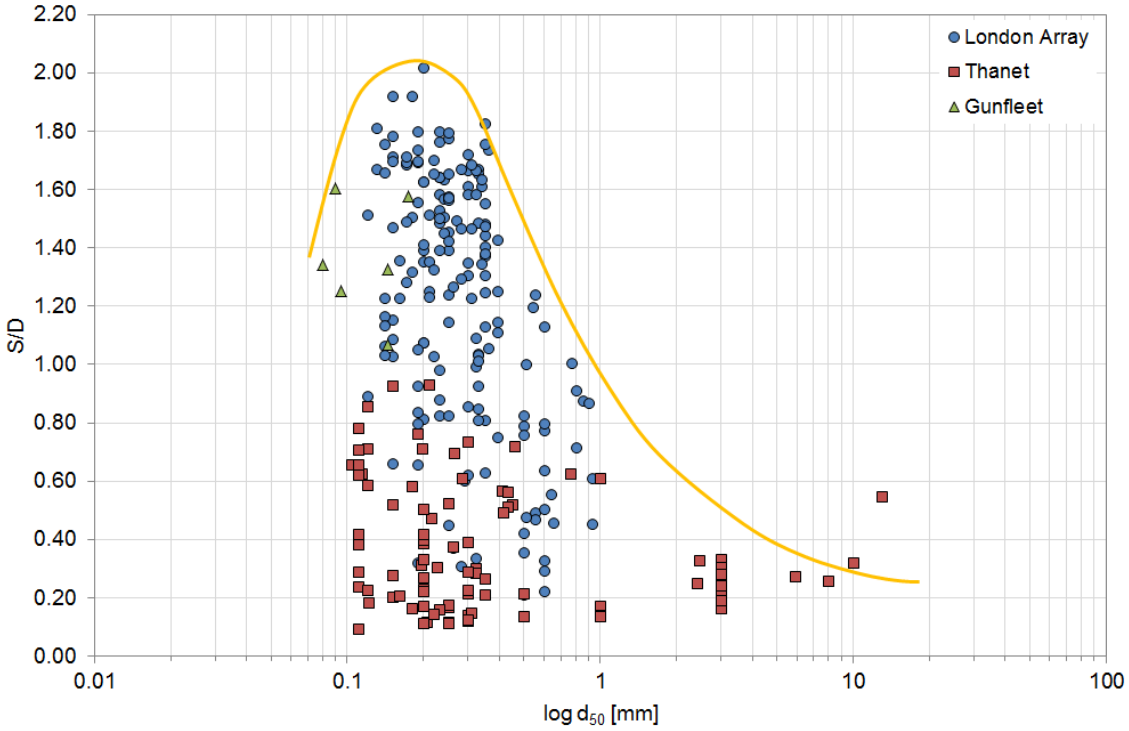

Figure 5.42: Scour depth S/D against grain size d_{50}. Yellow line gives approximate upper limit of S/D for various d_{50}.

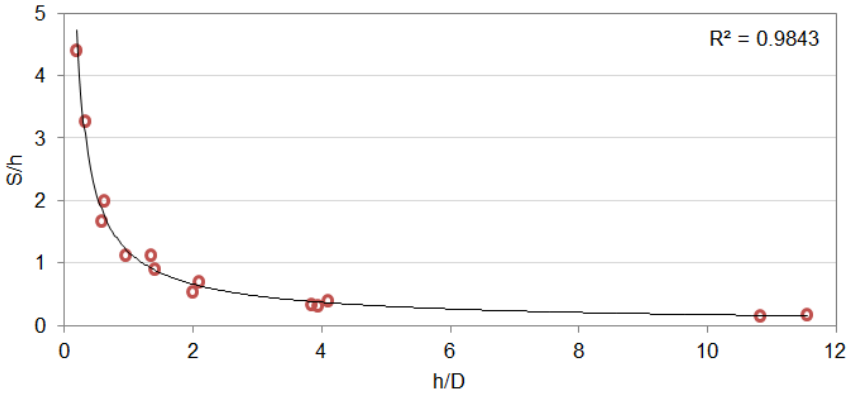

Figure 5.43: Experimental results from Sheppard et al. (2004) replotted as relative water depth h/D against normalised scour depth S/h.

Nevertheless, most data points are in the low-mobility categories of less than 1m of vertical change between pre and post-installation bathymetric survey. The median values for each data set and mobility bin are plotted to reveal any potential trends. As a large amount of scatter is visible, the median was chosen over the mean since it is less susceptible to effect of outliers. In Section 3.4.5 the effect of vertical bed elevation changes at London Array has been discussed and it was found that the median scour dimensions diminished with increased bed mobility. At Thanet, the same analysis (Section 4.4.5) appeared to suggest that scour increases with larger magnitude bed fluctuations. The data from Gunfleet Sands do not add much information since little bed level fluctuation has been experienced there. Considering the environmental conditions at the individual sites, both of the opposing trends described appear plausible as the discrepancy is believed to be the result of different levels of availability of mobile granular material. From the observation of migrating bed forms at both sites, it can be concluded that live-bed conditions prevail under ambient flow conditions.

At Thanet the layer of mobile granular sediment is generally thin (Fig 4.4) over much of the site. In these areas the scour dimensions are moderated by underlying substrates (Fig 4.24) and these areas naturally show little to no bed elevation changes due to the absence of mobile sediment, thus the median in the 0-0.5m bed variation category is skewed towards low values. The larger scour dimensions are found in areas of greater thickness of the granular sediment layer. Since the availability of sediment at the site is related to the presence and migration of large sand waves, ie. areas of large bed mobility, the increase in S/D, A_S/D^2 and V_S/D^3 with bed mobility is actually a function of z_{sed}. At London Array, over the majority of the site a thick layer of unconsolidated material is available (Fig 3.4), thus sediment availability is typically not a limiting factor, bar at a small number of sites in Knock Deep (Fig3.29). The diminishing scour depths with increased bed mobility can be explained by backfilling effects, which are favoured by flows that are symmetric in magnitude and direction (Fig 5.32 shows that most scour pits at London Array were deemed to have been created by symmetric flows). The scour area and volume is thought to be restricted by the presence of bed forms in high-mobility areas. This leads to the conclusion that there are two separate issues when considering the effect of bed mobility on scour. Firstly, there is a distinction between live-bed and clear-water scour which depends on the current speeds and symmetry, in magnitude and

direction, of flows. This controls the capability for backfilling and is illustrated by the differences in wake development between Gunfleet Sands and London Array. Secondly, the general availability of sediment and the nature of how this sediment becomes available is of importance. Current knowledge expects scour to increase where moving bed forms are present, at least in uni-directional flow (Richardson et al., 2001). The results of this analysis suggest that this must be further qualified with a statement on the nature of sediment availability. Narrowly-spaced megaripples have been shown to restrict lateral scour development and potentially influence the near-structure flow field (Section 3.4.5) at London Array, whereas large sand waves with long wave lengths at Thanet have increased both vertical and lateral scour dimensions; thus it is postulated, that apart from providing erodible sediment, the relative size of the bed form in relation to the structure and scour pit has a bearing on the impact of bed mobility. This notion should be investigated further in future when suitable data becomes available.

5.1.6 Scour hole age

The findings on the time evolution of scour at London have been discussed in section 3.4.6 where multiple post-installation surveys were available. The Thanet and Gunfleet Sands data set only offers single time step snapshots of scour, which is why only the scour hole age is discussed here. To increase the evidence base, data from other prototypes are included in the analysis, where the elapsed time between surveys was known or could be estimated with some confidence. All the data are plotted in Figure 5.47. In the previous analysis of scour in sandy sediments in section 3.4.7, based on data from the Outer Thames and other prototype data, an envelope that describes scour development with time in sandy sediments was developed, shown in Figure 5.47 as blue dashed lines. Scour depths from Gunfleet Sands lie comfortably within this range, offering some corroboration. When data from other substrates are plotted, it can be seen that these plot below the lower limit for sandy sediments, indicating that scour progresses slower and that the scour depths are less. For Princess Amalia, where a variable layer of granular sediment (0-3m) is underlain by less erodible substrate (see Table 1.2), the data distribution suggests some locations are developing as in sandy sediments (presumably until clay reached) and others are influenced by the underlying clay and would thus be an ideal site to test the accuracy of the lower limit. Unfortunately, the data were not accessible in this study and no later survey data are available to investigate how these two scour populations have developed subsequently. The larger scours at Thanet seem to confirm the validity of the curve, as the data points that exceed the limit are associated with thicker layers of granular sediment. The scour data from Kentish Flats follow a similar pattern described for the depth-limited locations in Knock Deep (section 3.4.4), where the overlying granular layer is eroded but scour finds a barrier at the underlying London Clay, thus keeping them below the limit. The erosion in tillite at Barrow shows progress that suggests similar development to the scour at Thanet which is influenced by cohesive and consolidated substrates. It would be interesting to compare the scour development in tills to that in Upper Chalk and stiff clays at Thanet if another survey became available at Barrow. Future data should be used to corroborate the validity of the given curves (equations 3.5 and 3.6) for scour in sandy

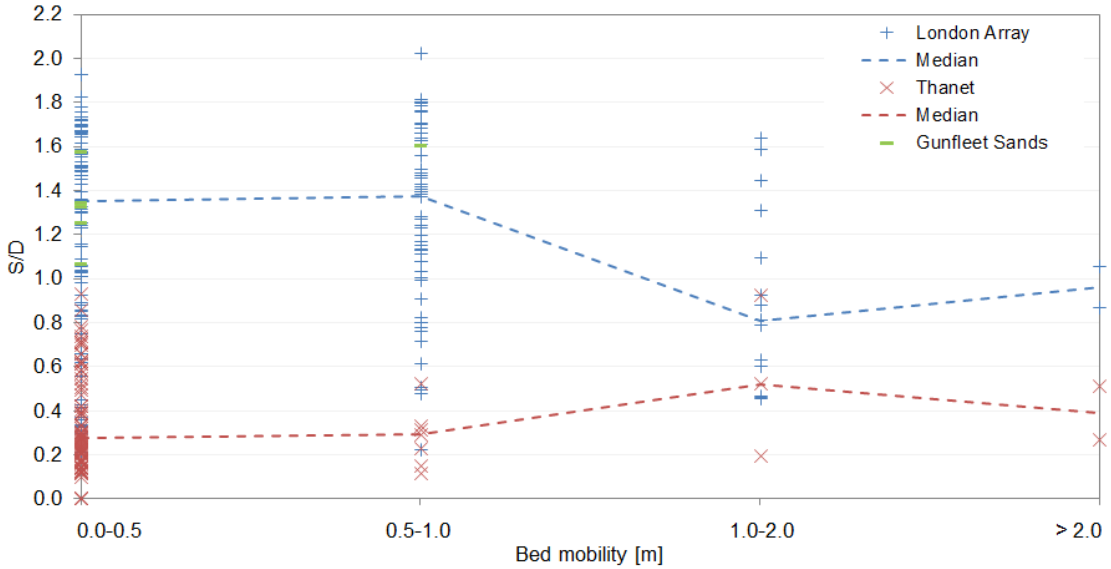

Figure 5.44: Scour depth S/D by bed mobility.

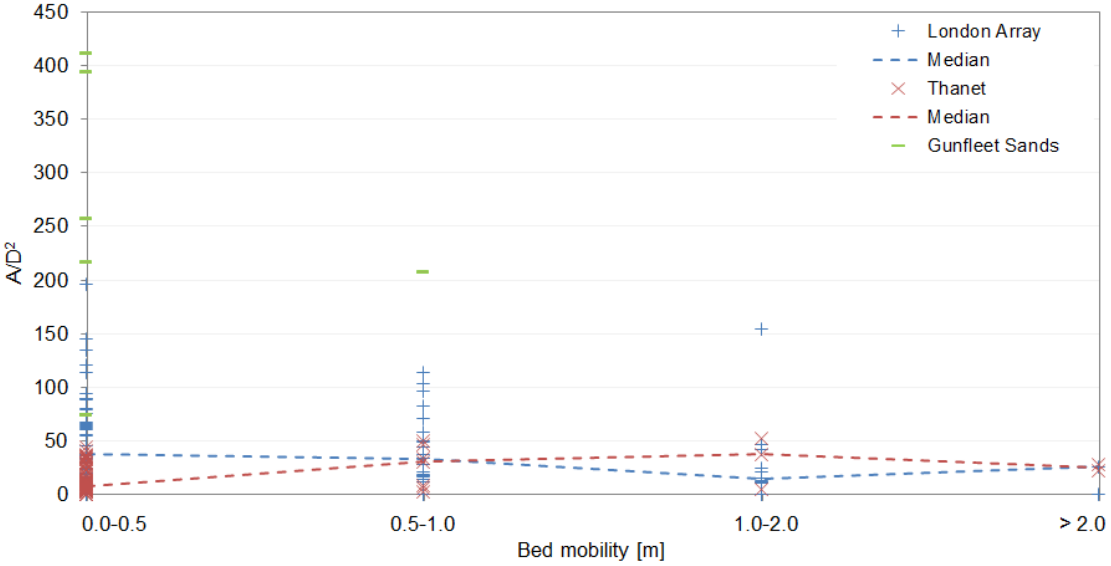

Figure 5.45: Scour area A/D^2 by bed mobility.

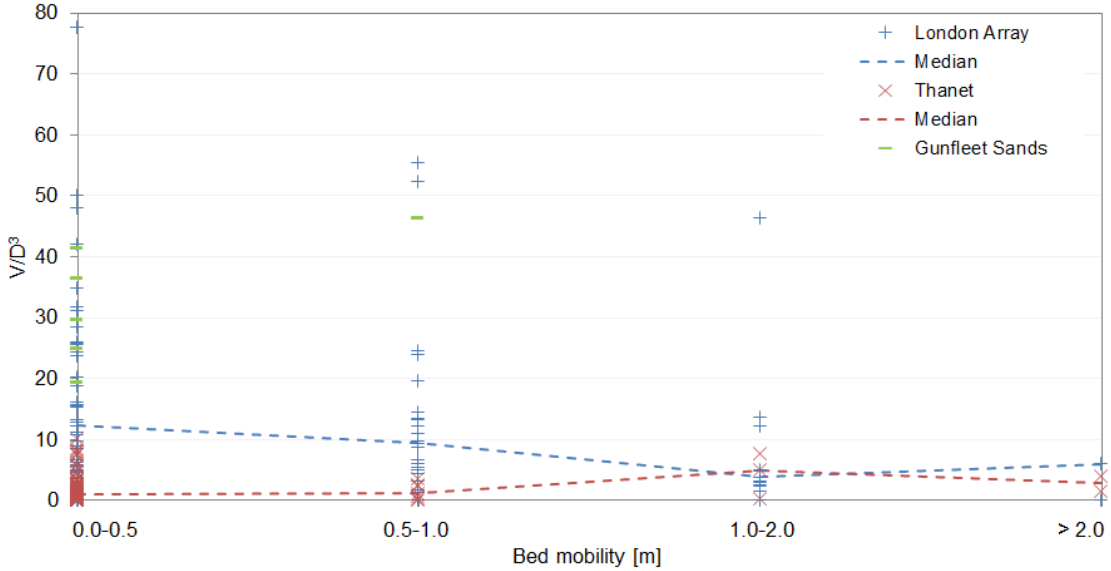

Figure 5.46: Scour volume V/D^3 by bed mobility.

sediment and develop similar boundaries for scour in consolidated/cohesive substrates and for locations in mixed stratigraphies of granular mobile sediment above inerodible or less erodible materials. Also, the long-term development of scour in sandy sediments ($T > 1000$) should be investigated further as hitherto only a single data point is available and the confidence in the lower limit is, necessarily, reduced in this range of T. This could answer questions about whether scour keeps growing in mobile sediments and whether the envelope reduces in width with greater T and what is the maximum S/D at prototypes.

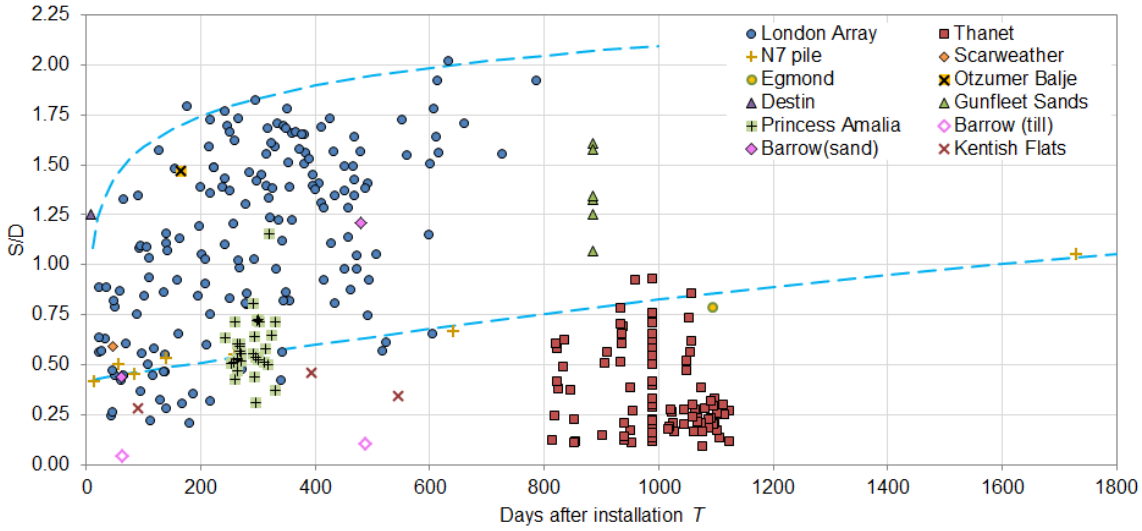

Figure 5.47: Relationship bewteen scour hole age and scour depth S/D for all prototype data where T is known or can be reasonably estimated. Envelope for scour development in sandy sediments (after equations 3.5 and 3.6 given as blue dashed lines.

5.2 Regional context

The existing field observations compiled in COWRIE (2010) and Whitehouse et al. (2011) and their hydrodynamic and geotechnical environments, were described in Section 1.3.1. To put the prototype scour from this study into the larger regional context, the data points are plotted together with existing data from other UK wind farms and monopile structures in Figure 5.48. The distribution of the scour depth data reveals the complexity of the scour phenomenon at prototypes, with a large variability being observed. In the following sections it will be attempted to pick apart some of the trends within the data on the basis of the substrate considerations, which after section 5.1.4 are believed to be the overriding determinant of scour depth.

5.2.1 Scour in sandy sediments

In terms of water depths and scour depths, the sand banks at London Array and Gunfleet Sands are comparable to Robin Rigg and Scroby Sands. In fact, the geotechnical and hydrodynamic conditions at these 4 sites are remarkably similar, despite their geographic spread. As described in Table 1.2, Robin Rigg wind farm is located on a sand bank in the Solway Firth where the sediment consists of fine to medium sands, interbedded with silts and clays. The thickness of sediment above the glacial till deposits, which underlie

the area, is between 17-29m (COWRIE, 2010), thus no limiting effect of the bed rock is expected or reported. The current speeds are somewhat larger than observed in the OTE, although water depths are similar to those on Long Sands and Kentish Knock. The plotted S/D values are believed to have been acquired from a survey taken approximately 12 months after monopile installation, thus might not have quite reached "final" depth as suggested by the analysis of time-evolution in section 3.4.6. Similarly, Scroby Sands is a sand bank off coastal Norfolk made up of fine to medium sands and underlain by clay; the thickness of the sediment layer is not mentioned in Whitehouse et al. (2011). However the scour is understood to have developed without any influence from the underlying cohesive substrate. Again, while water depths and wave conditions are similar, current speeds are greater. At Scroby Sands the elapsed time T between installation and survey was circa 1-5 months, thus it is likely that the recorded S/D does not represent the fully developed scour, possibly explaining the somewhat lower scour depths relative to Robin Rigg, London Array and Gunfleet Sands. Scour protection was placed here in the meantime. Similarly, T is likely to play a role for other locations in sandy sediments. As shown in Figure 3.50, Destin pier and Scarweather Sands met mast were surveyed soon after installation, thus are probably not fully developed. At Arklow Bank, the foundation scoured rapidly to a depth of $0.8D$ over a relatively short, but unknown, time-period (Whitehouse et al., 2011) before scour protection was installed, thus is also not representative of uninhibited scour in sandy sediment. Judging from scour time development in sandy sediments at London Array (Sections 3.4.6 and 3.4.7), the recorded scour at Otzumer Balje ($T = 5 - 6$ months) is also still progressing. Previously, the greatest observed scour depth was $1.77D$ located at Robin Rigg wind farm. This value has been exceeded by a number of scour pits at London Array and the new deepest scour hole ($2.02D$) is just under 2m deeper in absolute terms. This difference is likely to be a result of the timing of the survey, since the largest scour at London Array at $T \approx 1$ year is $1.79D$ which is very close to the greatest scour observed at Robin Rigg at the same T. The range of scour values shows very good agreement between the 4 wind farm sites.

In Section 5.1.1.2 the effect of water depth on scour was examined and based on a best-fit polynomial trend scour was found to diminish in shallow water less than $1.66D$ deep. While this explains the general distribution of the data it does not necessarily identify the limiting water depth which controls the greatest scour values observed in shallow water. In Figure 5.48 the limiting depth was given as $S_{max}/D \tanh(K_2 h/D)$, where $S_{max}/D = 1.75$ after den Boon et al. (2004) and $K_2 = 1$. This assumes a water depth effect from $h/D \leq 2.7$. Considering the London Array data which exceeds the suggested boundary, a revised limiting depth is given that better describes the data distribution. The proposed scour depth limit is calculated with $S_{max}/D = 2.02$ and $K_2 = 1.2$. Increasing K_2 shifts the water depth influence to shallower water depths and for $K_2 = 1.2$ scour depth reduction begins at approximately $h/D \leq 2.4$. This revised ceiling captures the majority of the large scour values in shallow water.

The statistics for foundations in sandy sediments from the OTE are given in Table 5.8. The average S/D is calculated as $0.98D$ with a standard deviation $\sigma_{S/D} = 0.5$. This suggests shallower scour and less scatter than $1.3D$ and $\sigma_{S/D} = 0.7$ (Det Norske Veritas, 2013). The expected maximum scour depth, based on statistical considerations is thus

Table 5.8: Statistics for S/D (top) and S [m] (bottom) for substrates encountered in the Outer Thames Estuary. Substrate classification after Whitehouse (2006).

S/D	sandy sediments		cohesive/consolidated sediments				
	muddy sand	sand	sandy mud	stiff clay	clay	chalk	gravel
Min	0.12	0.21	0.29	0.00	0.10	0.12	0.13
Max	1.61	2.02	0.42	0.23	0.55	0.42	0.39
Mean	0.54	1.12	0.36	0.11	0.25	0.24	0.23
σ	0.31	0.47	0.07	0.08	0.13	0.09	0.09
Mean	0.98			0.21			
σ	0.50			0.12			

S [m]	sandy sediments		cohesive/consolidated sediments				
	muddy sand	sand	sandy mud	stiff clay	clay	chalk	gravel
Min	0.53	0.86	1.36	0.0	0.43	0.56	0.57
Max	7.54	9.50	1.89	1.01	2.57	1.89	1.84
Mean	2.67	5.63	1.63	0.52	1.14	1.06	1.03
σ	1.56	2.15	0.26	0.35	0.62	0.39	0.40
Mean	4.93			0.95			
σ	2.38			0.55			

given as $S_{max} = 0.98D + 2\sigma_{S/D} = 1.98$, which is just below the observed maximum of $2.02D$.

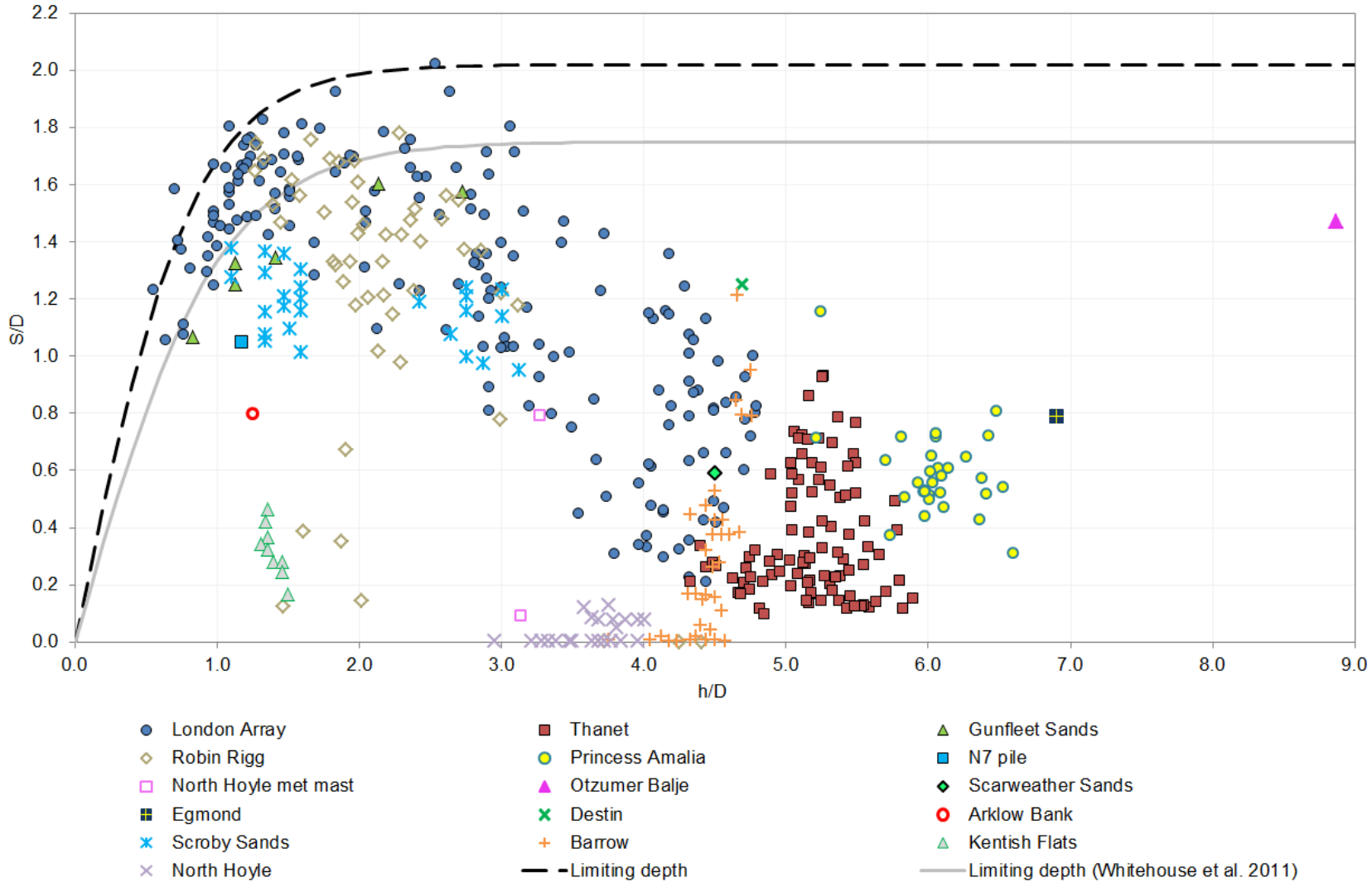

Figure 5.48: Relationship between and relative water depth h/D and S/D for collated marine monopile scour data. Previously existing data taken from COWRIE (2010) and Whitehouse et al. (2011).

5.2.2 Scour in complex substrates

Scour depths at Thanet wind farm are in a similar range to Princess Amalia and Barrow wind farm. Whitehouse et al. (2011) describe these sites as clay-influenced. Barrow is stratigraphically, albeit not lithologically, quite similar to Thanet. The area is underlain by relatively erosion resistant glacial till with a surface sediment veneer varying from $0-10$m and a clear sediment depth control was identified at Barrow wind farm. The first scour depths were measured 9 weeks after installation and very small scour of $S/D \leq 0.04$ was observed in the clay-rich glacial till deposit, while the greatest scour depth in sandy sediments was $0.44D$. Resurveying after 16 months revealed up to $0.1D$ in the glacial deposit, whereas in sandy areas of the site a scour of $1.21D$ had developed. Barrow is an important site since scour in sandy sediments and glacial till occur in very similar hydrodynamic conditions, thus the effect of geotechnics on scour development can be isolated. Based on the scour values, the approximate average rate of scour in glacial till is 3.2mm/day before the first survey and 0.7mm/day in the period between first and second survey, which is 11-13 times slower than scour in non-cohesive granular sediments at Barrow. The rates of change compare favourably with the scour progression rates in cohesive substrates at Thanet of between 0.4-2.6mm/day (see Table 4.3). At Princess Amalia wind farm, a surface veneer of fine to medium sands of up to 3m ($0.75D$) thickness covers soft to firm clay. As demonstrated in Figure 5.48, all but 2 data points are less than $0.75D$ suggesting the scour depth is controlled by the thickness of sediment however it was not reported whether any scour occurred in the underlying clay layer. Figure 5.49 shows the scour depths in consolidated and cohesive substrates with time from Thanet, Barrow, Kentish Flats and North Hoyle wind farms. The smallest scour is observed in stiff clays and glacial till with $S/D < 0.22$. Chalk and clay show a larger range of scour depths, with the greatest depth in chalk measuring $0.42D$ and $0.55D$ in soft clay. The effect of substrate will be investigated more closely in Section 5.1.4.2.

The statistics for foundations in cohesive or consolidated sediments from the OTE are given in Table 5.8. The average S/D is calculated as $0.21D$ with a standard deviation $\sigma_{S/D} = 0.12$.

5.3 Scour Predictions

Using the empirical methods outlined in Chapter 1, scour predictions were undertaken for monopiles at London Array and Thanet wind farms. The data sets are treated separately in order to evaluate the performance of the prediction equations in different geotechnical environments. The forecast scour values will be compared to the prototype data and discussed. An evaluation of individual methods will be given based on statistical measures of model performance (outlined in section 2.4.3).

5.3.1 London Array

At London Array, the uniformity of cohesionless sediment, particularly on the sand banks, and the dominance of uni-directional flow in certain locations, most closely replicates the

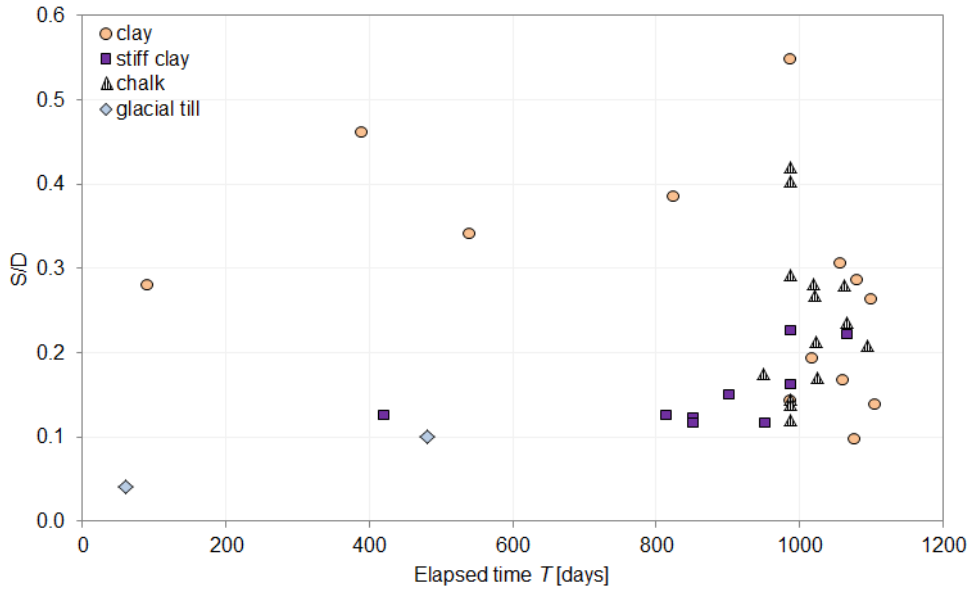

Figure 5.49: Range of S/D by substrate with elapsed time T from wind farms with cohesive/consolidated substrates.

experimental conditions that were used to determine the prediction equations (introduced in Section 1.3.1). Thus, it is expected that the semi-empirical equations should perform reasonably well.

Sumer et al. (1992b) This method (Equations 1.3 and 1.4) has been adopted as the industry standard for design of wind turbine structures as set out by Det Norske Veritas. Figure 5.50 shows the observed scour depths against the suggested value of $S/D = 1.3$ and design value $S/D + \sigma_{S/D} = 2.0$. While the distribution of points is not accounted for in this very simple equation, $1.3D$ is close to the overall mean scour depth of $S/D = 1.22$ at London Array. However, it is clear that scour varies by topography, with the highest scour on Long Sands and smallest scour in Knock Deep, thus the variance from $1.3D$ can be significant around the site. The design value of $2D$ is appropriate as a limiting value, as only a single data point exceeds this value by a very small margin. The $RMSE$ and efficiency parameter E are determined as $0.45S/D$ and -0.03, respectively, the latter indicating the predictive capacity of the population mean.

Breusers et al. (1977) The formula suggested by Breusers et al. (Equation 1.5) was tested with a number of values for constant α, which controls the maximum scour value in deep water. Figure 5.51 (left) shows the observed scour depths against predicted depths using $\alpha = 1.3$ and Figure 5.51 (right) with $\alpha = 1.75$. Both values produce over- and under-predictions. Based on the RMSE of $0.51S/D$ and $0.68S/D$ and E of -0.33 and -1.38, respectively, the lower constant ($\alpha = 1.3$) produces an overall closer fit. However, in shallow water at Long Sands, the calculation with $\alpha = 1.75$ produces better agreement with field observations, reflecting the fact that the greatest scour is found on the topographical highs of the sand banks.

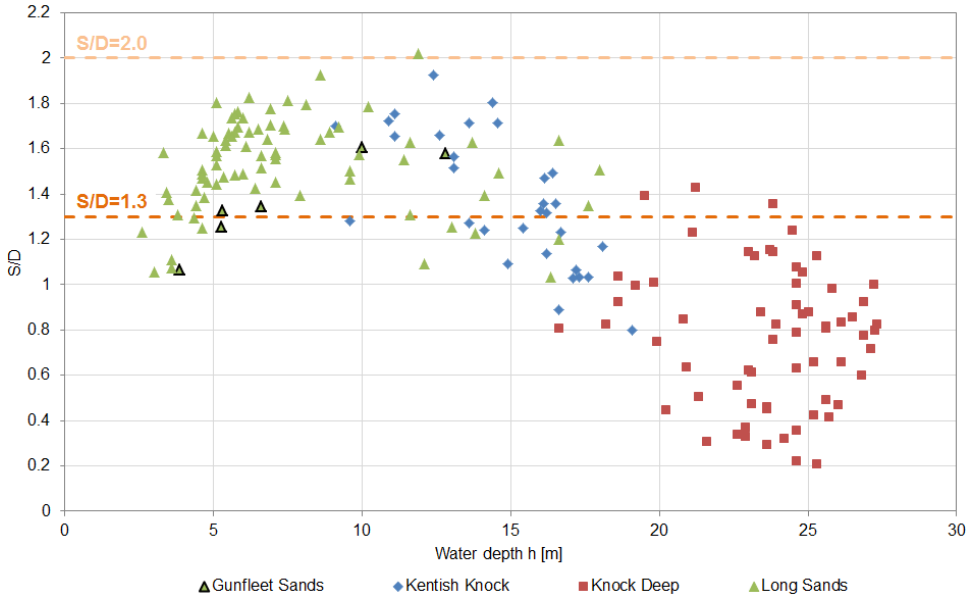

Figure 5.50: Prototype scour from London Array and Gunfleet Sands compared with prediction after Sumer et al. (1992b).

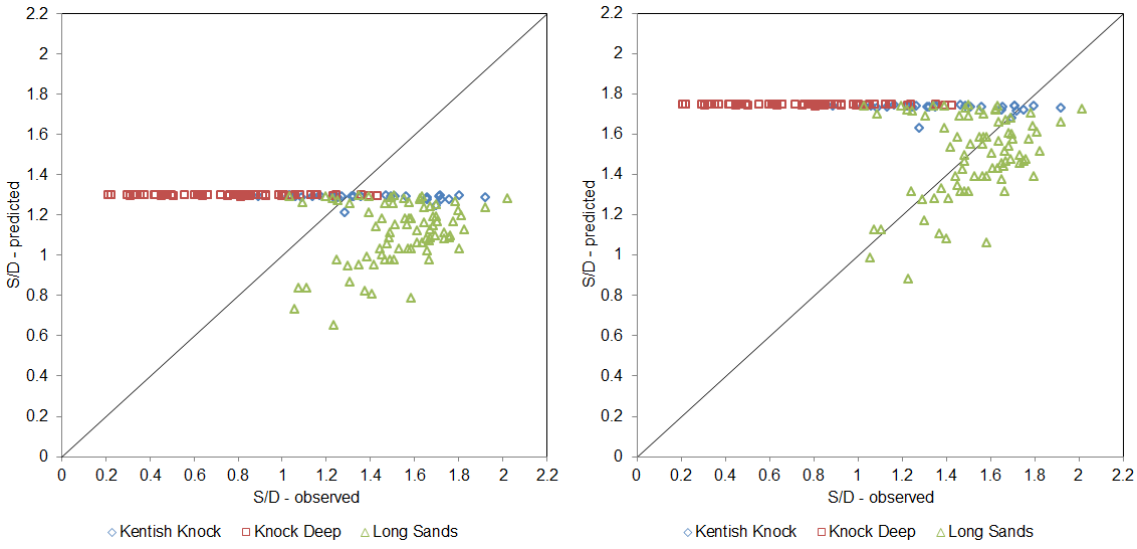

Figure 5.51: Observed vs predicted scour after Breusers et al. (1977) with $\alpha = 1.3$ (left) and $\alpha = 1.75$ (right).

Melville (1997) Melville's formula, given in Equation 1.8, for scour in rivers shows wholesale over-prediction of scour (Figure 5.52). In deep water, the maximum expected scour value of $S/D = 2.4$ is forecast which is much greater than the observed scour, thus resulting in large errors. Generally, the equation appears to be very conservative for marine monopile scour. The RMSE is $1.01S/D$ and $E = -4.30$.

Richardson et al. (2001) This method requires an estimation of flow speed to determine scour depth (see Equation 1.6). From Table 3.1 three different values for U_c were taken for each of the three main areas to represent minimum, mean and maximum current in the calculation. The result can be found in Figure 5.53. Predicted values are mostly lower than observed values other than for deep water points, where scour is overestimated. The lowest RMSE is achieved with $U_{c,max}$ at $0.48S/D$ and $E = -0.2$. The value for E indicates that, overall, the prediction is close to the mean of the observations.

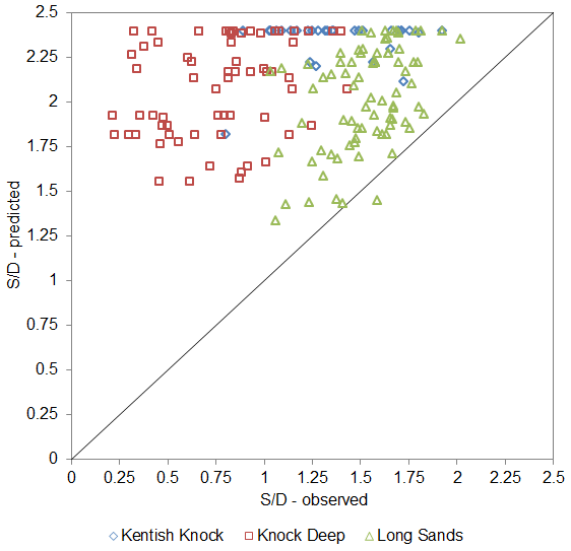

Figure 5.52: Observed vs predicted scour after Melville (1997).

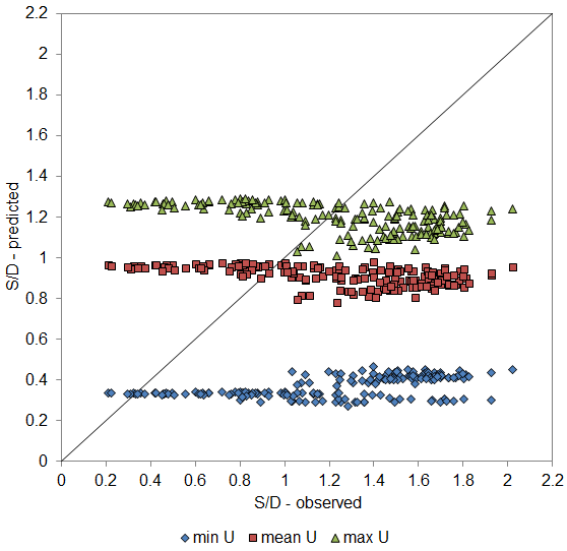

Figure 5.53: Observed vs predicted scour after Richardson et al. (2001).

Escarameia and May (1999) Using Escarameia and May's equation for scour in tidal flow (Equation 1.16), the results of the prediction can be found in Figure 5.54. Although some scatter is seen, the prediction generally is within $\pm 0.5S/D$ for Long Sands. Scour in Kentish Knock is somewhat over-estimated. The method performs worst for scour in Knock Deep; here the scatter from the line of equality is greatest. The $RMSE$ of the prediction is $0.65S/D$ and $E = -1.21$.

May and Willoughby (1990) A similar pattern is observed using May and Willoughby's equation 1.20. Scour in Knock Deep is not well predicted with points scattered either side of the equality line. Again, the method shows the best fit with data from Long Sands, while on Kentish Knock scour is over-predicted. Overall, the fit is poor with an $RMSE = 0.81S/D$ model efficiency of -2.42.

Sumer and Fredsoe (2002) This method was employed to determine the effect of waves on scour (Equation 1.18) and scour under combined flow (Equation 1.19). However, due to the limited wave energy at this site, the threshold number $KC > 6$ is not exceeded under average wave conditions. Even under the mean conditions for the 10% largest waves on record at this site, no wave scour was forecast, resulting in the current-only scour value of $S/D = 1.3$ being given. However, were the threshold of wave scour to be exceeded, the method predicts a reduction in scour due to waves. Under combined flow in the shallowest water depths, the method gives a maximum value of $S = 0.2$m or $0.04D$ under average flow conditions, which is unrealistic. For this reason, no goodness-of-fit statistics are calculated.

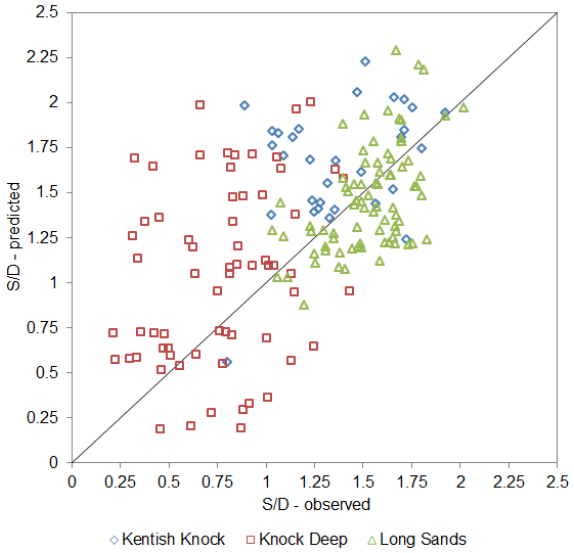

Figure 5.54: Observed vs predicted scour after Escarameia and May (1999).

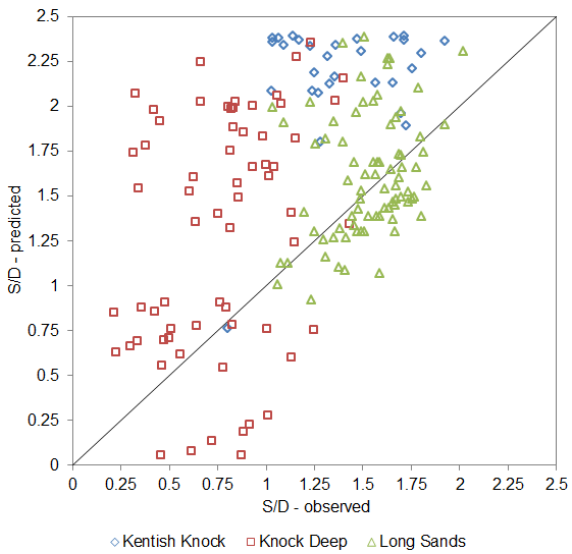

Figure 5.55: Observed vs predicted scour after May and Willoughby (1990).

Summary It has been shown that none of the tested equations can accurately describe the distribution of scour depths observed at London Array wind farm. There is a determining influence on scour that is not captured by the available methods. While the equations include simplified parameters to account for hydrodynamics (eg. h, U, Fr) and sediment (eg. d_{50}, U_{cr}), from the model performance, it appears that these are insufficient to accurately describe the scour depth in the prototype situation. Furthermore, at London Array the actual distribution of scour depths is opposite to predictions as the shallowest areas show on average the deepest scour.

Table 5.9 offers a summary of the performance of individual empirical equations, giving the $RMSE$ and efficiency parameter E. Interestingly, it is suggested, according to the statistical measures, the simplest method by Sumer et al. (1992b) still provides the best fit. It achieves the lowest $RMSE$ and the efficiency E is very close to 0, indicating that the model has predicted well the mean of all observations. This implies that although the exact scour at an individual location cannot necessarily be forecast correctly, the expected scour of $1.3D$ agrees well with average observations from prototypes at this particular site. While this is not overly useful for any scour-related design purposes, it does show that the mean trend is captured, and that, in its simplicity, still performs better than

more intricate equations. The scour in deep water is typically overestimated by the fluvial scour methods (Breusers et al., 1977; Melville, 1997; Richardson et al., 2001) equations since they have been developed for uni-directional flows at bridge piers where deepest scour is expected in high flow conditions. Nevertheless, the next best fit is achieved by the Richardson et al. method, when tweaked with parameter choice of $U_{c,max}$, followed by Breusers et al. equation with $\alpha = 1.3$; again this reflects the mean of the prototype observations at the site. Interestingly, the equation for tidal flow by Escarameia and May (1999) does not appear to offer an improvement over most of the river scour equations. The least agreement between model and reality is achieved with Melville's equation.

Table 5.9: Scour predictions using empirical formulae from various authors.

Method		$RMSE[S/D]$	E
Sumer et al. (1992b)	$S/D = 1.3$	0.45	-0.03
	$S/D = 2.0$	0.89	-3.18
Breusers et al. (1977)	$a = 1.3$	0.51	-0.33
	$a = 1.75$	0.68	-1.38
Melville (1997)		1.01	-4.30
Richardson et al. (2001)	$U_{c,min}$	0.95	-3.69
	$U_{c,av}$	0.55	-0.60
	$U_{c,max}$	0.48	-0.20
Escarameia and May (1999)	$U_{c,av}$	0.65	-1.21
May and Willoughby (1990)	$U_{c,av}$	0.81	-2.42

5.3.2 Thanet

Across the Thanet wind farm site the substrate is very diverse, including a large number of turbine foundations in cohesive and consolidated sea bed material. For this reason, a considerable discrepancy between prediction and observation is expected here as the methods are not designed to account for these differences in sediment properties. Where appropriate, a prediction equation for scour in cohesive substrate (Equation 1.24) is also employed.

Sumer et al. (1992b) and Breusers et al. (1977) The scour depth of $S/D = 1.3$ as suggested by Sumer et al. (1992b) is plotted against the observed scour depths at Thanet wind farm in Figure 5.56. The observed scour is significantly less than the prediction. In deep water, the Breusers et al. equation becomes equal to Sumer et al.'s relationship if a constant of $\alpha = 1.3$ is applied. Larger values for α are not discussed since these only enhance the scour depths predicted by the equation. The $RMSE$ of this prediction is 0.98 and the model efficiency is -18.54 indicating very poor fit.

Melville (1997) The results of the scour depth prediction using this method (Equation 1.8) is shown in Figure 5.57. The values were calculated with the minimum and average current speed of $U_{c,av} = 1.0\text{ms}^{-1}$. However, in this method the current speed only affects the results when $U_c < U_{cr}$. Here, even $U_{c,min} = 0.6\text{ms}^{-}1$ creates live-bed conditions,

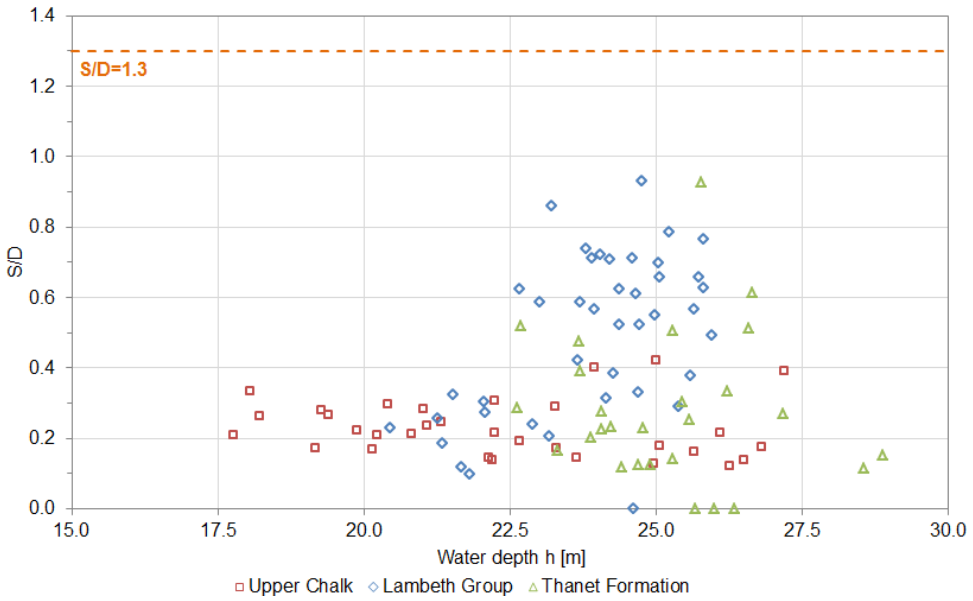

Figure 5.56: Prototype scour compared with prediction after Sumer et al. (1992b).

thus the results are independent of the actual current speed value. The $RMSE = 1.95$ and $E = -77.02$ as the method results is very large over-predictions.

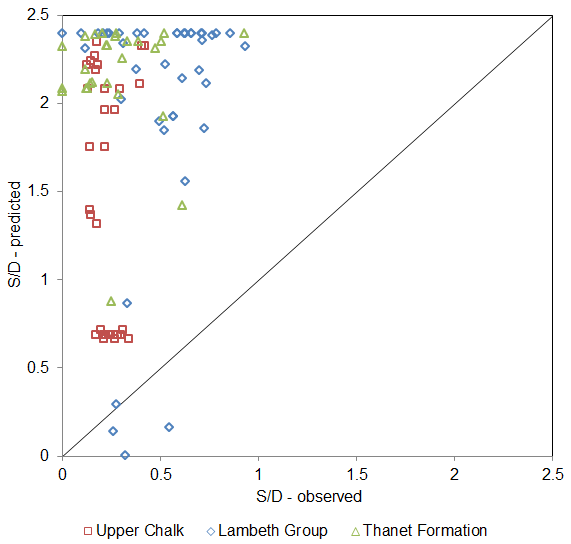

Figure 5.57: Observed vs predicted scour after Melville (1997).

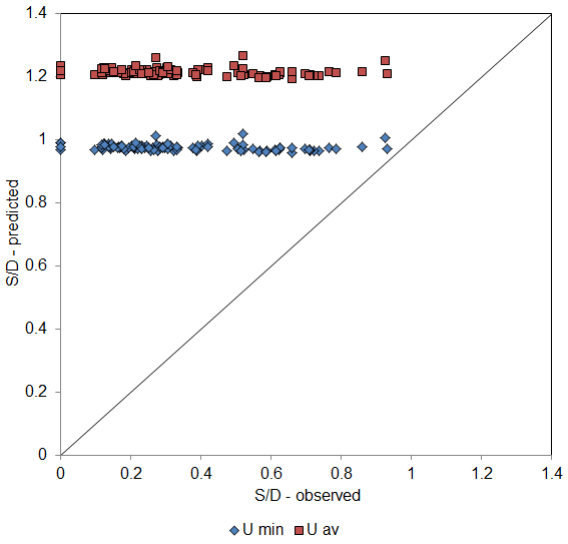

Figure 5.58: Observed vs predicted scour after Richardson et al. (2001).

Richardson et al. (2001) Using the average $U_{c,av} = 1.0\text{ms}^{-1}$ and minimum current speed $U_{c,min} = 0.6\text{ms}^{-1}$, the predicted scour depths, using Equation 1.6, are plotted in Figure 5.58. Although the scour is generally overestimated, the agreement between the largest observed and predicted scour is good, especially for $U_{c,min}$. Overall, better fit is achieved with $U_{c,min}$ giving a root mean square error $RMSE = 0.66$ and model efficiency E of -8.1.

Escarameia and May (1999) Using Escarameia and May's equation for scour in tidal flow (Equation 1.16), the results of the prediction can be found in Figure 5.59. The root mean square error is 2.63 and the model efficiency is $E = -134.9$, indicating very little

agreement between the prediction and observations. The formula predicts very high S/D values for live-bed scour with small d_{50} and high U_c.

May and Willoughby (1990) Equation 1.20 is not defined for live-bed scour in deep water. Thus, scour could only be calculated for just over half of the locations. These results are presented in Figure 5.60. The maximum predicted scour is $S/D = 2.4$ and in general scour is over-estimated giving a goodness of fit of $RMSE = 1.70$ and $E = -32.86$.

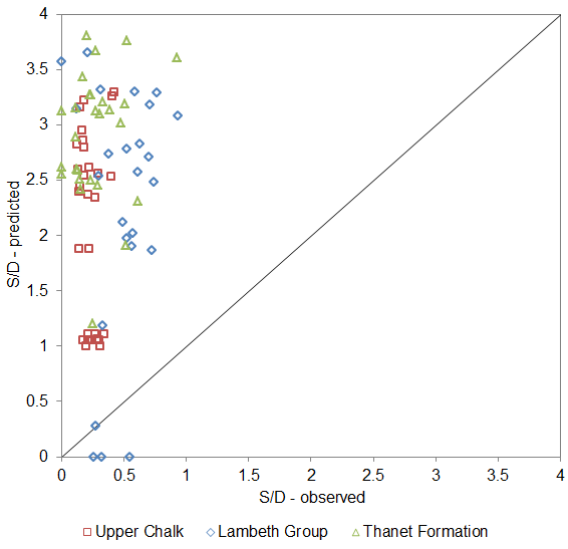

Figure 5.59: Observed vs predicted scour after Escarameia and May (1999).

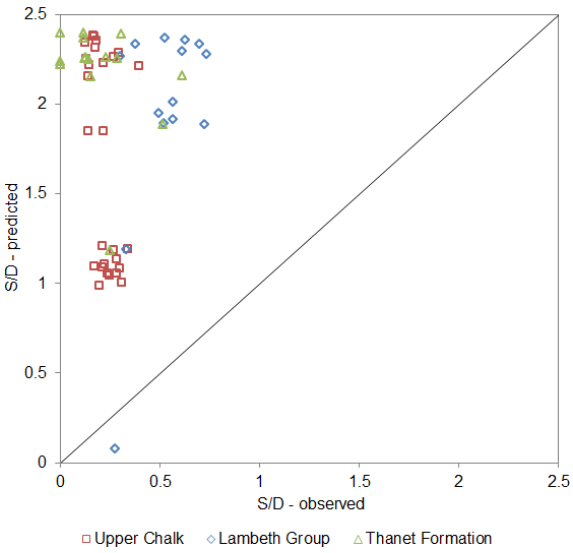

Figure 5.60: Observed vs predicted scour after May and Willoughby (1990).

Briaud et al. (1999) The SRICOS method of Briaud et al. (1999) is employed to estimate maximum scour in the cohesive and consolidated substrates at Thanet wind farm (see Figure 5.61). According to the CPT records, the Upper Chalk bed rock behaves like a clay substrate, varying in strength from soft to very stiff, thus the same method can be used here. The results from $U_{c,min}$ are closer to the equality line and the larger observed scour is captured well by this equation, suggesting these have reached the maximum value. However most of the data points are overestimated; this indicates that either scour has not yet reached the maximum value, or the method is overconservative. Another survey is required to determine whether the scour in these substrates is still developing. The $RMSE$ for the low-velocity prediction is 0.22 and $E = -2.50$ indicating that the prediction performs worse than simply using the mean of the population.

Summary The prediction equations have been shown to be mostly unsuitable for the physical conditions encountered at Thanet. It seems clear that the geotechnical complexity of the seabed, which has been discussed in Section 4.2, is influencing the erodibility of the sediment in a way that cannot be captured accurately by these methods, thus over-predictions are common. In this particular case the discrepancy between the models and the observations can be severe, although Richardson et al.'s equation successfully predicted the very largest scour depths, which conform closer to the conditions the method was developed for. The equation offered by Briaud et al. (1999) for cohesive substrates

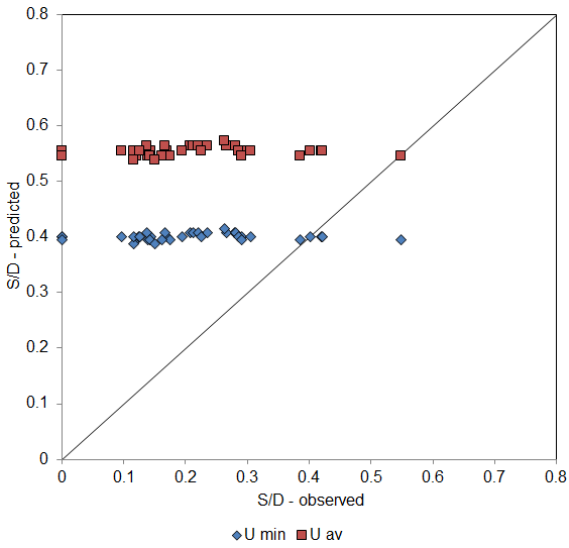

Figure 5.61: Prototype scour compared with prediction after Briaud et al. (1999).

achieves good fit for the larger observed scour values but generally produces overpredictions. Table 5.10 offers a summary of the performance of individual empirical equations, giving the $RMSE$ and efficiency parameter E. For the entire data set, the best fit is achieved with Richardson et al.'s equation followed by Sumer et al.'s rule of thumb. The other equations show very high deviations from reality.

Table 5.10: Scour predictions using empirical formulae, from HR Wallingford (2008).

Method		$RMSE[S/D]$	E
Sumer et al. (1992b)	$S/D = 1.3$	0.98	-18.54
Breusers et al. (1977)	$a = 1.3$	0.98	-18.54
Melville (1997)		1.95	-77.02
Richardson et al. (2001)	$U_{c,min}$	0.66	-8.07
	$U_{c,av}$	0.89	-15.42
Escarameia and May (1999)	$U_{c,av}$	2.63	-134.9
May and Willoughby (1990)	$U_{c,av}$	1.70	-32.86
Briaud et al. (1999)	$U_{c,min}$	0.22	-2.50
	$U_{c,av}$	0.36	-8.21

5.4 Summary

Pulling together data from all wind farm sites in the Outer Thames Estuary, the wide range of scour dimensions and morphologies has been demonstrated. The data were examined with the aim of deriving generalised statements on the scour development around marine monopiles. Based on trends in the data distributions, relationships are suggested for scour area, volume, width and length based on scour depth S/D. Previous predictors for width, length and slope angles in the scour pit were based on the internal friction angle of sediment ϕ; however it has been concluded, based on statistical model fit measures, that this factor does not allow accurate predictions when compared to prototype data. Analysis of the effect of the foundation diameter on scour demonstrated that D does not have a significant impact on the dimensions of scour at prototypes (unlike in physical tests).

This contradicts the expectations from experimental knowledge and brings into question the basis for non-dimensionalisation over D and the basic premise of the empirical prediction equations that are derived from this assumption. The effect of water depth was investigated, showing that a strong relationship exists between observed scour depths in the OTE and the relative water depth, which can explain the majority of variability over the sites. The relationship remains significant when existing prototype data are added and has also been demonstrated in experimentally derived data. The analysis has shown that the influence of water depth is strongest for scour in granular sediments and its significance diminishes for complex substrates such as cohesive and consolidated materials, highlighting the importance of understanding geotechnical effects in order to accurately predict scour in such materials. Nevertheless, based on the findings, new prediction models have been put forward, that allow scour S and maximum scour S_{max} to be estimated, requiring knowledge of structure diameter D and mean water depth h only. The statistical evaluation of the model performance shows high predictive accuracy, particularly in sandy sediments, that is greater than any of the existing models discussed in this chapter. Geotechnical effects were investigated in both granular and cohesive/consolidated materials. The thickness of granular sediment can act as a predictor of limited scour depth, depending on the erosion resistance of the underlying substrate. The scour depth data seemed to suggest variability of erosion within packages of granular sediments; however it was found that most of those can be explained by the age of the scour hole and water depth effects. There are certainly subtle geotechnical effects; however the data configuration made it difficult to extract these. Grain-size effects were investigated but no clear influence of grain size on scour depth could be established. When scour depths are analysed in the context of the characteristics of the sea bed, it has been demonstrated that scour is significantly reduced in cohesive and consolidated substrates (up to a factor of 5 on average). Scour areas and volumes are also smaller by factors of 7.5 and 28.7, respectively. Based on the statistical properties of the scour dimensions in different materials, some modifications to the conceptual scour model by Whitehouse (2006) are put forward. The influence of natural bed mobility was found to depend on two factors, the distinction between live-bed and clear-water regime, which affects the capability for backfilling, and the level and nature of sediment availability, the configuration of which can affect scour dimensions. It is believed that these two considerations can explain the opposing trends in the scour dimension development with increasing bed mobility observed at London Array and Thanet. The temporal examination of the prototype data has confirmed an envelope of time-related scour development for locations in granular sediments. Scour in complex sediments displays much slower progression; however not enough data are available to develop a relationship. The analysis demonstrated that little is known for the initial rapid phase of scour growth and for the very long term scour development, past approximately 3 years. The timing of surveys has been shown to have an influence on the interpretation of the data set and survey design can be optimised to increase the usefulness of post-installation surveys. All previously collated monopile scour observations from COWRIE (2010) and Whitehouse et al. (2011) are included in the analysis and contrasted with the study data to inform on water depth and substrate effects. It was found that scour depths in similar substrates agree well between different geographic locations, although

the previously largest scour observed at a marine monopile from Robin Rigg wind farm has been exceeded at a number of foundation locations at London Array. In sandy sediments, all prototypes seem to show a strong influence of water depth on scour, insinuating that geotechnical factors are less influential in granular deposits. Descriptive statistics were calculated for scour dimensions in various substrates; these can be consulted for first order estimates of expected scour in different materials.

Chapter 6

Conclusions

This study has shown how routinely collected data in the planning and design phase of wind farms can be used to facilitate a full characterisation of scour, including dimensional and shape characteristics. A large volume and variety of high quality data were available which includes bathymetric, geotechnical, seismic and hydrodynamic information, as well as (in places) multiple post-installation scour surveys allowing access to the temporal dimension. The analysis exploited the properties of the outdoor laboratory to maximise the amount of causal interpretation with geotechnical and hydrodynamic factors. The basis of the interpretation of prototype scour was provided by scour assessment at 281 turbine foundations, in the relatively well-constrained hydrodynamic regime of the Outer Thames Estuary, but which displays strongly varying topography, sea bed stratigraphy and material composition, providing enough variability to examine geotechnical effects on scour.

The results have been used to test existing scour knowledge, fill gaps in the current understanding and identify, describe and account for hitherto unreported characteristics of scour. A number of research questions were developed in Chapter 1 out of the review of the current state of the art in scour research which have guided the subsequent analysis in Chapters 3 to 5. The relevant findings to each of the research questions will be summarised below, alongside a discussion of other important findings and their implication for future scour research and the optimisation of data collection for scour purposes.

Scour dimensions:

1. ***What is the range and statistical characteristics of observed prototype scour dimensions and how do they compare to existing field data and literature?***

   The statistics for the scour analysis of the available data from the Outer Thames Estuary is given in Table 5.2. The scour depth varies from no scour to $2.02D$ with an average depth of $0.93D$. This study is first in calculating and reported the areal and volumetric dimensions, which has its relevance with respect to the exposure of inter-array cables and the estimation of required scour protection. The dimensionless scoured areas and volumes are reported to

be between $2.9 - 411.6D^2$ and $0.1 - 77.7D^3$, respectively. Although the range is significant, the distribution is skewed towards the small values as indicated by an average area and volume of $37.7D^2$ and $8.9D^3$, respectively. The observed scour depths ($N = 281$) were compared to existing prototype data ($N = 183$) and it was found that they agree well with scour depths from other geographic locations if the sea bed substrate is similar. At London Array, the hitherto greatest scour reported from an offshore monopile has been exceeded in several locations.

2. ***What is controlling the observed pattern of scour dimensions? Does the data distribution reflect:***

   - ***differences in flow type (symmetric, uni-directional, combined wave and currents)?***

     The general flow regime is relatively homogeneous in terms of current dominance and magnitudes of flow and the negligible effect of waves. As such, the scour in the Outer Thames is deemed, for all intents and purposes, to be a result of erosive action by currents alone. Local variations in the tidal current symmetry allowed the effect of directionality of flow on scour depths to be investigated. However, no significant relationship between flow type and scour depths could be established. The effect of waves in combined flow was evaluated by means of empirical formulae and due to the benign conditions no scour is forecast. Even scour holes in shallow water display morphological features that are consistent with current scour.

   - ***scaling of scour with diameter D? How sound is the scientific basis for non-dimensionalisation of scour depths as S/D?***

     It was found that a wide range of scour depths were observed for individual pile diameters implying there is no significant correlation between those two parameters. This observation questions the basis on which the experimentally-derived prediction methods have been developed and implies that they cannot, by design, perform satisfactorily. It also calls into question the practice of reporting scour as dimensionless magnitudes, at least for prototype data. Nevertheless, it has also been shown that the currently existing scour design value of $2D$ appears to be appropriate to capture the largest scour.

   - ***scaling of scour with water depth h? Are scour depths in shallow water influenced by the proposed depth threshold of $h/D < 2$?***

     Scour depths do display a relationship with water depth. First, it was noted that scour in deeper water is considerably less than in shallow water. In very shallow water scour was found to be limited by water depth. The critical threshold at which a scour depth reduction is observed was found to be $h/D < 1.66$. When the scour depth is normalised over h, a strong relationship between S/h and h/D is found. This trend is particularly strong in granular sediments, suggesting that most the variability in scour from prototypes (and physical

tests) can be explained by water depth, which is acting as a proxy for the scour process, and sea bed properties are subordinate factors for scour in these sediments. Further investigation is required to fully understand the mechanics of this link although it is believed that enough evidence has been provided to prove the significance of the relationship, which is also found in experimental data. Based on the water depth control, the following equation, derived from prototype observations is suggested as an improved predictor of scour depths, valid for h from $0.5D$ to approximately $5-6D$, and scour in granular sediments:

$$\frac{S}{h} = 3.440e^{-0.757h/D} \tag{6.1}$$

It is known that the proposed equation, due to the exponential nature, breaks down in deep water as it predicts very low scour values for $h > 5-6D$. Due to the configuration of the Outer Thames data set used to develop the equation the confidence is greatest in depths between $0.5-3D$. When this equation is applied to the existing prototype observations in granular sediments the equation shows very high model accuracy with $RMSE = 0.18$ and $E = 0.80$. Nevertheless, it is recommended that the water depth control and the suggested relationships are validated against further prototype data to increase the confidence in the model. Additionally, more detailed information on local flows are required to enhance the understanding of how the scour-relevant flow components are captured or controlled by water depth. Complementary lab experiments should be undertaken which are designed to specifically address this issue. If the strong water depth control for marine scour in granular sediments is indeed confirmed, then this will have implications for the future of scour research, such as the design of physical tests or field data collection campaigns. Conversely to scour in particulate materials, in consolidated and cohesive substrates, geotechnical considerations have been demonstrated to be paramount and the water depth control is visibly diminished, as demonstrated by prototype observations in shallow water that do not follow the proposed equation.

3. ***How does natural morphological activity affect the observed scour dimensions? Is scour greater in areas of high bed mobility as suggested by current knowledge?***

   The evidence concerning the effect of natural bed mobility on scour is contradictory. Bed mobility can encompass multiple dimensions from large-scale changes such as growth and decay of entire bank margins, medium scale changes such as migrating sand waves and larger bed features to small scale fluctuations caused by megaripples or in areas of mobile beds. At London Array, the range and median scour dimensions are very similar for morphological activity limited to within $\pm$1m since installation and survey. Counter to current knowledge, larger bed mobility appeared to produce a reduction in scour; however the significance of this trend is uncertain due to the small number of data points in the higher mobility range. Proposed mechanisms for scour reduction in active beds are backfilling or modification of hydrodynamics by the presence of bed

forms in the vicinity of the foundation. At Thanet, increased mobility seems to cause an increase in scour. This observation is believed to be explained by the availability of sediment as the layer of granular material at Thanet is typically small, thus scour depths tend to be limited by the influence of the underlying strata. Larger thickness of mobile sediment is available in areas of large migratory bed forms. These areas allow greater scour to form, but due to the transient nature of the sediment supply these areas show higher bed level fluctuations, thus a relationship between these parameters appears plausible. In areas of large morphological change, the evidence suggests that this might affect the long-term development of scour and this notion should be revisited with additional data in the future.

Scour morphology:

1. ***What is the range and statistical characteristics of prototype scour horizontal extents and slope angles and how do they compare to existing field data and literature? Are these measures controlled by the internal friction angle of the sediment?***

   The lateral extents of scour have shown considerable variability in all sites over the OTE. The observed range of scour widths W spans from $2.1 - 18.6D$, while lengths show an even greater range from $2.4 - 39.9D$. The average width and length of $5.4D$ and $7.4D$, respectively, reveal however that the mean horizontal growth compares favourably with the expected range from previous observations and current theory, which suggests the lateral dimensions are controlled by the internal friction angle of sediments. Although the latter relationship has been found to be insufficient to explain or predict the extents at individual scour holes, the range determined from the predictions gives appropriate approximations of the observation mean. The slope angles show a large range from $1.3 - 74.6°$, although the distribution is very heavily skewed towards low values with over 50% of recorded angles in scour pits measuring less than $10°$. No comparable data have been compiled previously, thus there is no data to validate the observations against. However, this does confirm that a single slope angle based on the sediment friction angle ϕ, as currently suggested, is not an adequate representation or predictor of the large variability of angles in scour holes and it shows that much greater slope angles are possible, even in unconsolidated granular materials, than previously assumed on the basis of ϕ. The difference between upstream and downstream slope angles is found to be controlled by the asymmetry of the scour hole. The more pronounced an extension in a particular direction, ie. the greater the directionality of flow, the greater the ratio of upstream to downstream angle. Directionally-dominated scour pits exhibit ratios $2 - 6$, whereas symmetric scour holes show smaller ratio of $1 - 1.5$. In the Outer Thames the mean ratio is 1.41. The analysis emphasises the need for high-quality high-resolution bathymetric surveys to capture the subtleties of slope changes within scour holes.

2. ***What range of scour hole morphologies are observed? Is the scour shape controlled by differences in flow type such as symmetric tidal, uni-directional, and combined flow?***

   Scour hole shapes are evaluated in a categorisation system developed from the pit morphologies observed in the OTE. The classification is based on two shape parameters, the isoperimetric quotient IQ, essentially a measure for "circularity" of the scour pit and the long-short-axis ratio L/W which represents a measure of lateral elongation. Based on these factors the gross morphology of the scour pit can be described. The range of IQ is given as $0.43 - 0.98$ and that of L/W is between $1.02 - 3.36$. Despite this large variability, it was found that the majority of scour pits shows one of three circle-type shapes ("circular", "near-circular" and "modified circle") which are characterised by less than 20% deviation from a perfect circle ($IQ > 0.8$) and relatively equitable length and width ($L/W < 1.4$). Symmetric flow has been shown to produce scour pits that are on average closer to unity for both IQ and L/W; the more asymmetric the flow, the greater the deviation from unity. The relative effect of waves in combined flow is too small to have registered as a significant change in shape, as the range of shape parameters is similarly large in deep and shallow water. The applicability and validity of the shape classification system should be tested in future scour studies.

3. ***How does natural morphological activity affect scour hole slopes?***

   At London Array, the average slope angle per scour hole shows a slight trend towards becoming steeper with increased bed mobility, which is the opposite to previous observations in literature. The same trend is observed for upstream and downstream angles. At Thanet, the gross trend is towards a small decrease in slope angles, although some fluctuation is observed. It is not clear whether the weak trend is a results of small N rather than physical change.

Scour time development:

1. ***What is the nature of the scour time development at prototype monopiles? Does it follow the suggested exponential relationship?***

   The investigation of scour time evolution has shed some light on the question of the timing of the hydrographic scour survey. To establish accurate rates of change in various phases of scour development, the frequency of surveying must reflect the time-scale at which the scour process is operating. This means that very little is known about the exponential growth phase in sandy sediments that commences immediately after installation, since the change is so rapid that surveys need to be carried with a delay on the order of hours to accurately capture the scour development in respect to time. Where surveys are delayed for long time periods after installation, as appears to be typical for offshore wind farm developments, only average rates of change can be calculated that

are not necessarily representative of the dynamics of the scour process. From the little data that were taken within a number of days of the scour survey, it does confirm the initial exponential growth of scour with up to 0.7m of erosion in a day. After approximately 100 days scour rates are much reduced, in a range of circa 1-2cm/day, and begin approaching zero asymptotically. The evolution of scour dimensions with time can have implications for the post-installation survey strategy. The investigation into the time evolution of scour showed that, in granular material, the full scour depth is reached approximately between 400-500 days after installation at London Array, suggesting for engineering purposes a single survey after 1.5-2 years should record most of the sea bed change. However, the currently available prototype data confirm a lack of observations of scour development in the initial rapid scour phase, and similarly for the long-term, past circa 3 years. Initial evidence suggests that the long-term development can be significant in areas of high net morphological activity. The initial scour phase is interesting from a process perspective but can also inform on the implication of timing of scour protection, in terms of area and volume required. For the early stage of scour, a dedicated prototype study is proposed that involves high-frequency surveying of a number of turbines to record the initial growth phase and determine accurate rates for vertical and horizontal scour progression in various sediment types.

2. ***Is there a relationship between scour dimensions and scour hole age?***

   Whether this relationship is captured depends again on the survey timing and the erosion rate in the respective substrate. In sandy sediments, the trend can be obfuscated by long survey delays, since the differences in scour development are likely to be greatest in the first 100 days of scour development. Nevertheless, scour hole age was found to explain some of the discrepancies in scour depths observed in the deep channel at London Array. In cohesive and consolidated substrates, where the rate of scour is much slower than in mobile granular sediments even widely spaced surveys can show slow increases in scour depth over large time periods.

Substrate:

1. ***How does prototype scour in various substrates compare to the conceptual scour model by Whitehouse (2006)?***

   Based on the field data analysis, some modifications to the model are proposed. The prototype observations suggest a greater range of scour dimensions observed in sandy sediments and smaller range in clays than proposed in the model. Additionally, a range for scour in chalk is added. This analysis can be used to determine first-order estimates for typical scour dimensions in various substrates. However, it also demonstrates the need to collate further scour data in various substrates to increase the confidence in suggested ranges.

2. ***Does the thickness of surface sediment control the observed scour depths?***

The thickness of granular sediment is found to have a bearing on observed scour depths in the Outer Thames. However, the degree of control is influenced by the erodibility of the more resistant layer beneath. At London Array, the proximity of the London Clay bed rock is an effective limiter of scour depths. At Thanet, some degree of erosion in bed rock is observed thus, the significance of the relationship between these two parameters is reduced. The implications of these findings is that to successfully predict scour depths, it is important to understand the erodibility of the underlying substrate and what geotechnical parameters affect it. For cohesive and consolidated sediments, in this study the erodibility has been quantified based on the undrained shear strength as will be shown below. For granular materials, neither the cone resistance nor the relative density, both proxies for compaction and granular material strength, were found to be capable of explaining the erosion resistance in particulate material. It has been demonstrated with data from Gunfleet Sands and Thanet that compaction and (partial) lithification of non-cohesive granular sediments does not necessarily prevent scour.

3. ***Do geotechnical properties of the sea bed control the pattern of observed scour depths?***

   - ***What is the nature of prototype scour in cohesive and consolidated substrates and is it less than, equal to, or larger than in unconsolidated sediment?***

     Scour in cohesive and consolidated substrates in the Outer Thames is on average 5 times shallower and areas are more confined by a factor of 7.5 than in sandy sediments. Volumes are considerably smaller by a factor of 28.7. In these substrates the scour depth range is found to be between $0 - 0.55D$ with a mean of $0.21D$. The smallest mean scour depth is found in stiff clay ($0.11D$), while sandy muds shows the largest average scour; the largest range of S/D is found in clay. This confirms that scour in complex substrates is typically benign from an engineering point of view. The rates of change and absolute scour dimensions are considerably greater in unconsolidated sediments; these locations are more challenging in terms of accounting for vertical erosion, reduced lateral loads on the monopile and excavation and free-spanning of inter-array cables. There is evidence to suggest that the depressions found in plastic substrates (e.g clays) are potentially the result of downward pressure during piling of the foundation rather than hydraulic erosion processes. To confirm this notion, a dedicated study is suggested, which will be outlined at the end of this section.

   - ***What is the nature of prototype scour in bed rock?***

     At Thanet, scour in Upper Chalk and Thanet Sand Formation bed rock is limited to less than $0.35D$, while up to $0.57D$ of scour was observed in the less erosion resistant Lambeth Group bed rock. At London Array, scour in London Clay appears to be limited to less than $0.1D$.

- ***Which engineering properties of cohesive or consolidated substrates can be identified that influence observed scour depths?***

  Previous studies have indicated that the undrained shear strength c_u can be related to scour depth in experiments, and thus potentially exerts some control on the erodibility of these substrate types. This parameter can also be derived from CPT measurements and, hence, a continuous record of c_u is available along the vertical profile. Based on this data, two relationships were devevloped that allow the required material strength (as $c_{u,max}$ or $c_{u,med}$) capable of inhibiting scour at a given depth (up to $1D$) below the soil surface to be estimated, allowing potential scour depths to be determined:

  $$S_{max}/D = 7.71 c_{u,med}^{-0.54} \qquad (6.2) \qquad S_{max}/D = 6.53 c_{u,max}^{-0.49} \qquad (6.3)$$

  The exponential equations account for the reduction of the critical c_u depth, which reflects the reduced hydraulic forcing inside the scour hole. Only a limited number of data points were available for this analysis, thus it is recommended that the validity of the proposed relationships be evaluated and improved with additional data in future.

- ***Is there an effect of relative grain size D/d_{50} on scour?***

  The analysis suggests the effect of grain size on scour is limited and no influence of the ratio D/d_{50} was found. Erosion depths were greatest in sediments with d_{50} in the range of fine and medium sands; however this was also by far the largest data population, and those sediments also display a wide range of scour depths. In coarser and finer sediments, scour depth are less in the prototype data set. However, it has been demonstrated on a experimental data set purporting to show the effect of D/d_{50} on scour that nearly all of the variability could be explained by water depth consideration. Similarly, it is believed, relating to the discussion of the water depth control in granular sediments, that most of this variability is believed to be attributed to water depth effects rather than grain size.

4. ***Does the nature of the sea bed substrate affect the observed scour hole morphologies or slope angles?***

   The largest variability in scour morphological parameters is observed in sandy sediments (muddy sand, sand). On average, the IQ, L/W and the average slope angles are greater in these sediments than in cohesive/consolidated substrates.

5. ***How does the prototype data compare to the scour equation for cohesive substrates?***

   The equation for maximum scour depth in cohesive substrates shows good agreement with largest observed scour. Overall the equation is generally conservative. The equation only includes hydrodynamic parameters and is calibrated against experimental data. This study has demonstrated the strong influence

of geotechnical parameters in complex substrates, thus it is unlikely that an equation based solely on Re number will provide very accurate predictions.

Field data requirements: During the analysis some shortcomings in the field data were noted that could be improved for scour analysis purposes. Firstly, the scour surveys should be undertaken at sufficient coverage and resolution. The latter is important in order for the detailed scour features to be captured. This is particularly relevant in erosion-resistant materials where little scour is expected; here higher resolutions are required so that details are adequately recorded and derived parameters such as slope angles can be determined with confidence from the survey. In this study it was found that a minimum resolution of 0.5m should be used in order to enable scour analysis. Also, it is imperative that the exact date of surveying is recorded to have a confidence in the elapsed time. The geotechnical data collection could be optimised by increasing the number of boreholes. From these a better record of down-hole grain size changes could be gained, at least in the scour-relevant depth range. Along with this, more surface sediment grab samples could be collected to have a greater spatial density of grain size information. Although this is probably not possible in practice, the timing of the intrusive ground investigations should be closer to the installation date, to remove some of the effects of natural bed level changes and sediment volume fluctuations. Furthermore, more detailed hydrodynamic data are required; even within the natural laboratory where the overriding hydrodynamic regime is similar, there are local variations due to topography or external forcings, the understanding of which would have been beneficial in the data analysis. The mentioned improvements to the data collection would help increase confidence in the notion that water depth is the main control in granular materials. For cohesive sediments,

Future work: One of the main questions that developed from the geotechnical data interpretation is the question of how representative the pre-installation ground investigations are of those after the piling of the foundation has been carried out. This notion was put forward due to observed incongruence with respect to measured engineering properties and recorded scour depths. A dedicated study is suggested to investigate the change in material properties after the piling operation to determine whether any significant deviation from pre-installation measurements can be established. In consolidated materials any structural change such as fracturing could be investigated. In plastic cohesive materials, it could help determine whether the downward pressure and pile skin friction are sufficient to cause depressions around the foundation.

It is believed that to improve scour knowledge in the future, the access to and interpretation of prototype observations is paramount. For this reason, it is recommended that future data is used to further populate the prototype knowledge base which can be used to further validate existing and develop new methods. In respect to this study, additional data are required to develop further the predictive relationships for scour in unconsolidated and complex materials suggested.

In Round 3 wind farm developments, it appears likely that foundation types different from monopiles will be employed, e.g. jacket structures, gravity bases or floating variants.

So far, due to limited proliferation, a paucity of information or design guidance is available regarding scour around these more complex foundations. At present, typically design guidance for monopiles is extrapolated to these new structure types and observed scour can behave similarly to that of monopiles or monopile groups (e.g. Bolle et al., 2012). Thus, the large amount of monopile prototype analysis provided here can be valuable to guide scour predictions and assessments around these foundations. Conversely, scour data collected at these deep water foundations should be recycled back into the knowledge framework; by providing additional data points for larger h, the validity and application range of prediction methods based on the water depth parameter can be tested and improved.

This study has also shown that more work is needed in the future to understand the nature of substrate controls in shelf sea sediments to improve scour depth predictions in complex and cohesive soils. It is believed that recording undrained shear strength at scour depth can be a successful method, however more geotechnical validation data from future offshore structures is required to increase the confidence in this relationship at prototypes.

Bibliography

Abou-Seida, M. M. (1963). *Sediment scour at structures*, Technical Report HEL-4-2, University of California, Berkeley.

ABPmer (2004). Gunfleet Sands Metocean Assessment, R/3412, R.1089.

ABPmer (2005). London Array Offshore Wind Farm, Coastal Process Investigation, R.1179, *Technical report*, ABPmer.

ABPmer (2007). London Array: Assessment of Future Morphology, R.1405, *Technical report*, ABPmer.

ABPmer (2008). Atlas of UK Marine Renewable Energy Resources, *Technical report*, ABPmer.

Abu-Farsakh, M. Y., Zhang, Z., Tumay, M. T. and Morvant, M. (2008). Development of MS-Windows CPT Soil Classification Software, *87th Transportation Research Board Annual Meeting*, Washington D.C., p. 25.

Ali, K. and Karim, O. (2002). Simulation of flow around piers, *Journal of Hydraulic Research* **40**(2): 161–174.

Annandale, G. W. (2006). *Scour Technology*, McGraw-Hill Civil Engineering Series, New York.

Ansari, S. a., Kothyari, U. C. and Ranga Raju, K. G. (2002). Influence of cohesion on scour around bridge piers, *Journal of Hydraulic Research* **40**(6): 717–729.

Armbrust, S. F. (1982). *Scour about a cylindrical pile due to steady and oscillatory motion, MSc Thesis*, PhD thesis, Texas A&M University.

Ashley, G. M. (1990). Classification of Large-Scale Subaqueous Bedforms: A New Look at an Old Problem-SEPM Bedforms and Bedding Structures, *Journal of Sedimentay Research* **60**(1): 160–172.

Astley, A. J., Dix, J. K., Thompson, C. E. and Sturt, F. (2014). A seventeen year, near-annual, bathymetric time-series of a marine structure (SS Richard Montgomery), *Proceedings of the 7th International Conference on Scour and Erosion*, Perth, Australia, p. in press.

Baker, C. J. (1979). The laminar horseshoe vortex, *Journal of Fluid Mechanics* **95**: 347–367.

Baker, C. J. (1980). The turbulent horseshoe vortex, *Journal of Wind Engineering and Industrial Aerodynamics* **6**(1): 9–23.

Barata, T., Alves, E. I., Saraiva, J. and Pina, P. (2004). Automatic Recognition of Impact Craters on the Surface of Mars, *International Conference on Image Analysis and Recognition*, Porto, Portugal, pp. 489–496.

Bijker, E. W. and de Bruyn, C. A. (1988). Erosion around a pile due to current and breaking waves, *Proceedings of the 21st International Conference on Coastal Engineering*, Malaga, Spain, pp. 1368–1381.

Bishop, J. R. (1980). Experience with scour at the Christchurch Bay tower, *Proceedings of the one day Society of Underwater Technology seminar on scour prevention techniques around offshore structures*, pp. 11–22.

Black, K. (2013). Scour Prediction at Offshore Structures: Utility of the DNV (2013) Guidance and the Way forward for Scour Prediction, *All-Energy Conference*.

Bolle, A., Winter, J. D. E., Goossens, W., Haerens, P. and Dewaele, G. (2012). Scour monitoring around offshore jackets and gravity based foundations, *Proceedings of the 6th International Conference of Scour and Erosion*, Paris, France, pp. ICSE–000065.

Bomel (2006). *Geological Study of Chalk at Thanet Offshore Wind Farm. C1179\04\347R*, Bomel Ltd.

Breusers, H. N. C. (1972). *Local scour near offshore structures*, Delft Hydraulics Publication 105, Delft, Netherlands.

Breusers, H. N. C. and Raudkivi, A. J. (1991). *Scouring*, Balkema, Rotterdam.

Breusers, H. N. C., Nicollet, G. and Shen, H. W. (1977). Local Scour Around Cylindrical Piers, *Journal of Hydraulic Research* **15**(3): 211–252.

Briaud, J.-L., Ting, F. C. K., Chen, H. C., Cao, Y., Han, S. W. and Kwak, K. W. (2001). Erosion function apparatus for scour rate predictions, *Journal of Geotechnical and Geoenvironmental Engineering* **127**(February): 105–113.

Briaud, J.-L., Ting, F., Chen, H. C., Gudavalli, R., Perugu, S. and Wei, G. (1999). SRICOS: Prediction of scour rate in cohesive soils at bridge piers, *Journal of Geotechnical and Geoenvironmental Engineering* **125**(4): 237–246.

British Geological Survey (2002). Gunfleet Sand Offshore Wind Farm Study: A Geological Review. CR/02/162.

British Standard (2010). *BS 5930:1999+A2:2010, Code of practice for site investigations*, British Standards Institution.

Burningham, H. and French, J. (2011). Seabed dynamics in a lage coastal embayment: 180years of morphological change in the outer Thames estuary, *Hydrobiologia* **672**(1): 105–119.

Byrne, B. and Houlsby, G. (2003). Foundations for offshore wind turbines, *Philosophical Transactions of the Royal Society of London, Series A, Mathematical and Physical Sciences* **361**: 2909–2930.

Cameron, T., Crosby, A., Balson, P., Jeffery, D., Lott, G., Bulat, J. and Harrison, D. (1992). *United Kingdom offshore regional report: the geology of the southern North Sea*, HMSO for the British Geological Survey, London.

Cantwell, B. and Coles, D. (1983). An experimental study of entrainment and transport in the turbulent near wake of a circular cylinder, *Journal of Fluid Mechanics* **136**: 321–374.

Carrizales, A. (2010). *Development and refinement of regional sediment mobility models: Implications for coastal evolution, preservation of archaeological potential, and commercial development*, Msc, University of Southampton.

Carstens, M. R. (1966). Similarity laws for localised scour, *Journal of Hydraulics Division, Proceedings of the ASCE* **92**(3): 13–36.

Carter, M. and Bentley, S. (1991). *Correlations of soil properties*, Penetech Press Publishers, London.

Cazenave, P. W., Dix, J. K., Lambkin, D. O. and McNeill, L. C. (2013). A method for semi-automated objective quantification of linear bedforms from multi-scale digital elevation models, *Earth Surface Processes and Landforms* **38**(3): 221–236.

Challis, K., Forlin, P. and Kincey, M. (2011). A Generic Toolkit for the Visualization of Archaeological Features on Airborne LiDAR Elevation Data, *Archaeological Prospection* **18**: 279–289.

Cheng, L., Yeow, K., Zhang, Z. and Teng, B. (2009). Three-dimensional scour below offshore pipelines in steady currents, *Coastal Engineering* **56**(5-6): 577–590.

Chiew, Y. M. and Melville, B. W. (1987). Local Scour around bridge piers, *Journal of Hydraulic Research* **25**(1): 15–26.

Chiew, Y. M. and Melville, B. W. (1989). Local scour at bridge piers with non-uniform sediments, *Proceedings of the Institution of Civil Engineers* **87**(2): 215–224.

Chow, W.-Y. and Herbich, J. B. (1978). Scour around a group of piles, *Offshore Technology Conference*, Paper OTC 3308, Houston.

CIGRE (2009). Third-party damage to underground submarine cables. CIGRE publication 398.

Clark, A. (1982). Modelling of local scour with particular reference to offshore structures, *Proceedings BHRA International Conference on Hydraulic Modelling of Civil Engineering Structures*, Coventry, UK, pp. 411–422.

Clark, A. and Novak, P. (1984). Local Erosion at vertical piles by waves and currents, *in* B. Dennes (ed.), *Sea Bed Mechanics, Proceedings of the IUTAM-IUGG Symposium*, Graham and Trotman, London, pp. 243–249.

Coppens, A. B. (1981). Simple equations for the speed of sound in Neptunian waters, *Journal of the Acoustic Society of America* **69**(3): 862–863.

COWRIE (2010). *A Further Review of Sediment Monitoring Data*, Cowrie Ltd., Project reference ScourSed-09.

Dargahi, B. (1989). The turbulent flow field around a circular cylinder, *Experiments in Fluids* **8**(1): 1–12.

Dargahi, B. (1990). Controlling mechanism of local scouring, *Journal of Hydraulic Engineering* **116**(10): 1197.

De Vos, L. (2008). *Optimisation of Scour Protection Design for Monopiles and Quantification of Wave Run-Up*, Phd, University of Gent.

Debnath, K. and Chaudhuri, S. (2010). Laboratory experiments on local scour around cylinder for clay and claysand mixed beds, *Engineering Geology* **111**(1): 51–61.

DECC (2008). *Dynamics of scour pits and scour protection - Synthesis report and recommendations (Milestones 2 and 3)*, Department for Energy and Climate Change, Final Report.

den Boon, H., Sutherland, J., Whitehouse, R. J. S., Soulsby, R., Stam, C.-J., Verhoeven, K., Hoegedal, M. and Hald, T. (2004). Scour Behaviour and Scour Protection for Monopile Foundations of Offshore Wind Turbines, *Proceedings of the European Wind Energy Conference*, London, p. 14.

Det Norske Veritas (2007). Design of Offshore Wind Turbine Structures, Offshore Standard DNV-OS-J101.

Det Norske Veritas (2010). Design of Offshore Wind Turbine Structures, Offshore Standard, DNV-OS-J101.

Det Norske Veritas (2013). Design of Offshore Wind Turbine Structures, Offshore Standard DNV-OS-J101.

Devereux, B. J., Amable, G. S. and Crow, P. (2008). Visualisation of LiDAR terrain models for archaeological feature detection, *Antiquity* **82**: 470–479.

Dey, S., Helkjæ r, A., Sumer, B. M. and Fredsoe, J. (2011). Scour at Vertical Piles in Sand-Clay Mixtures under Waves, *Journal of Waterway, Port, Coastal and Ocean Engineering* **137**(December): 324–331.

D'Olier, B. (1972). Subsidence and sea-level rise in the Thames Estuary, *Philosophical Transactions of the Royal Society of London, Series A, Mathematical and Physical Sciences* **272**(1221): 121–130.

Dubayah, R. and Rich, P. M. (1995). Topographic solar radiation models for GIS, *International Journal of Geographical Information Systems* **9**(4): 405–419.

Einstein, H. and Li, H. (1956). The viscous sub-layer along a smooth boundary, *Journal of Engineering Mechanics Division, Proceedings of ASCE* **82**(EM2): 27.

Emeis, S. (2010). Meteorological Explanation of Wake Clouds at Horns Rev Wind Farm, *DEWI Magazin* **37**(August): 52–55.

Entwisle, D. C., Hobbs, P. R. N., Northmore, K. J., Skipper, J., Raines, M. R., Self, S. J., Ellison, R. A. and Jones, L. D. (2013). Engineering Geology of British Rocks and Soils - Lambeth Group - OR/13/006, *Technical report*, British Geological Survey, Keyworth, Nottingham.

Escarameia, M. (1998). Laboratory investigation of scour around large structures in tidal waters, *Proceedings of the Conference on Basics of Sediment Transport and Scouring*, pp. 1–15.

Escarameia, M. and May, R. P. (1999). *Scour around structures in tidal flows - SR521*, HR Wallingford.

Escauriaza, C. and Sotiropoulos, F. (2011). Initial stages of erosion and bed form development in a turbulent flow around a cylindrical pier, *Journal of Geophysical Research* **116**(F3): 1–24.

Ettema, R. (1976). *Influence of bed material gradation on local scour*, Meng, University of Auckland.

Ettema, R., Kirkil, G. and Muste, M. (2006). Similitude of Large-Scale Turbulence in Experiments on Local Scour at Cylinders, *Journal of Hydraulic Engineering* **132**(1): 33.

Fredsoe, J. (1990). *Hydrodynamik*, Danmarks Tekniske Universitet.

Freeze, R. A. and Cherry, J. A. (1979). *Groundwater*, Prentice Hall, Englewood Cliffs, NJ.

Fugro Engineering Services (2004). *Cone Penetration Testing (CPT), Simplified Description of the Use and Design Methods for CPTs in Ground Engineering*, Fugro Engineering Services.

Gardline Lankelma (2008). Thanet Offshore Windfarm, Geotechnical Investigation, Report 7422.

GE Gunfleet (2002). Gunfleet Sands Offshore Wind Farm Environmental Statement.

Hancu, S. (1971). Sur le calcul des affouillements locaux dans la zone des piles de ponts, *Proceedings of the 14th IAHR Congress*, pp. 299–313.

Hardy, R. J., Best, J. L., Lane, S. N. and Carbonneau, P. E. (2010). Coherent flow structures in a depth-limited flow over a gravel surface: The influence of surface roughness, *Journal of Geophysical Research* **115**(F3): F03006.

Harris, J. M. and Whitehouse, R. J. S. (2012). Scour Management A Risk Based Approach Key words, *Proceedings of the 6th International Conference of Scour and Erosion*, Paris, France, pp. ICSE–000246.

Harris, J. M., Herman, W. M. and Cooper, B. S. (2004). Offshore windfarms an approach to scour assessment, *in* Y. M. Chiew, S.-Y. Lim and N.-S. Cheng (eds), *Proceedings*

of the 2nd International Conference on Scour and Erosion, Stallion Press, Singapore, pp. 283–291.

Harris, J. M., Whitehouse, R. J. S. and Benson, T. (2010a). The time evolution of scour around offshore structures, *Proceedings of the Institution of Civil Engineers, Marine Engineering* **163**(MA1): 3–17.

Harris, J. M., Whitehouse, R. J. S. and Sutherland, J. (2010b). Scour Assessment in Complex Soils - An Evaluation through Case Examples, *Proceedings of the 5th International Conference on Scour and Erosion, San Francisco, California*, pp. 450–459.

Harris, J. M., Whitehouse, R. J. S. and Sutherland, J. (2011). Marine scour and offshore wind - lessons learnt and future challenges, *Proceedings of the ASME 2011 30th International Conference on Ocean, Offshore and Arctic Engineering*, ASME, Rotterdam, Netherlands, pp. 1–10.

Harris, P. T. (1988). Large-scale bedforms as indicators of mutually evasive sand transport and the sequential infilling of wide-mouthed estuaries, *Sedimentary Geology* **57**: 273–298.

Heathershaw, A. D. (1988). Sediment transport in the sea, on beaches and rivers: part 1 -fundamental principles, *Journal of Naval Science* **14**: 154–170.

Herbich, J. B., Schiller, R. E., Watanabe, R. K. and Dunlap, W. A. (1984). *Seafloor scour. Design Guidelines for Ocean-founded Structures*, Marcell Dekker, New York.

Hesse, R. (2010). LiDAR-derived Local Relief Models - a new tool for archaeological prospection, *Archaeological Prospection* **17**: 67–72.

Hjorth, P. (1975). Studies on the nature of local scour, *Bulletin Series A*, Vol. 46, Department of Water Resources Engineering, Lund Institute of Technology, Department of Water Resources Engineering, Lund Institute of Technology, Lund.

Hoffmans, G. J. C. M. and Verheij, H. J. (1997). *Scour Manual*, A.A. Balkema, Rotterdam.

Hosny, M. M. (1995). *Experimental study of local scour around circular piers in cohesive soils*, Phd, Colorado State University.

HR Wallingford (1992). *Port Ramsgate: Physical and numerical model studies*, HR Wallingford Report EX2598.

HR Wallingford (2002a). *Southern North Sea Sediment Transport Study, Phase 2*, HR Wallingford Report EX 4526.

HR Wallingford (2002b). *Turner Centre, Margate: Wave climate and overtopping predictions*, HR Wallingford Report EX4602.

HR Wallingford (2008). *London Array Windfarm, Scour Protection Assessment*, HR Wallingford Report EX5745.

HydroSoil Services (2005). London Array, Offshore Ground Investigation, Interpretative Report, Part B. 3690-FRP-002, *Technical report*, HydroSoil Services.

Inman, D. L. and Jenkins, S. A. (2002). *Scour and burial of bottom mines. A primer for fleet use*, Scripps Institution of Oceanography, La Jolla, California.

Jiang, J., Ganju, N. K. and Mehta, A. J. (2004). Estimation of Contraction Scour in Riverbed Using SERF, *Journal of Waterway, Port, Coastal and Ocean Engineering* **130**(4): 215–218.

Kaminsky, F. C., Kirchhoff, R. H. and Sheu, L.-J. (1987). Optimal Spacing of Wind Turbines in a Wind Energy Power Plant, *Solar Energy* **39**(6): 467–471.

Karlsdottir, S. H. (2013). *Experience in transporting energy through subsea power cables : The case of Iceland*, Msc, University of Iceland.

Kennelly, P. J. (2008). Terrain maps displaying hill-shading with curvature, *Geomorphology* **102**(3-4): 567–577.

Kenyon, N. and Cooper, B. (2005). *Sand banks , sand transport and offshore wind farms*, Gov.uk.

Kirkil, G., Constantinescu, G. and Ettema, R. (2009). Detached Eddy Simulation Investigation of Turbulence at a Circular Pier with Scour Hole, *Journal of Hydraulic Engineering* **135**(11): 888.

Kokalj, v., Zakšek, K. and Oštir, K. (2011). Application of sky-view factor for the visualisation of historic landscape features in lidar-derived relief models, *Antiquity* **85**: 263–273.

Komar, P. (1977). Boundary Layer Flow Under Steady Unidirectional Currents, *in* D. Stanley and D. Swift (eds), *Marine Sediment Transport and Environmental Management*, John Wiley & Sons, New York, chapter 7, pp. 91–106.

Kroezen, N. C., Vellinga, P., Lindenberg, J. and Burger, A. M. (1982). *Geotechnical and hydraulic aspects with regard to sea bed and slope stability*, Delft Hydraulics Laboratory, Publication 272, Delft, Netherlands.

Laursen, E. M. (1963). An analysis of relief bridge scour, *Journal of Hydraulics Division, Proceedings of the ASCE* **89**(HY3): 93–118.

Link, O., Klischies, K., Montalva, G. and Dey, S. (2013). Effects of Bed Compaction on Scour at Piers in Sand-Clay Mixtures, *Journal of Hydraulic Engineering* **139**(9): 1013–1019.

Liu, X. and García, M. H. (2008). Three-Dimensional Numerical Model with Free Water Surface and Mesh Deformation for Local Sediment Scour, *Journal of Waterway, Port, Coastal, and Ocean Engineering* **134**(4): 203–217.

London Array Ltd (2005). Environmental Statement Volume 1: Offshore Works, *Technical report*, London Array Ltd.

Louwersheimer, W. F., Verhagen, H. J. and Olthof, J. (2009). Scour around an offshore windturbine, *Coastal Structures 2007 - Proceedings of the 5th Coastal Structures International Conference, CST07*, Venice, Italy, pp. 1903–1912.

Lunne, T., Robertson, P. K. and Powell, J. J. M. (1997). *Cone Penetration Testing in Geotechnical Practice*, Blackie Academic and Professional, New York.

Machemel, J. L. and Abad, G. (1975). Scour around marine foundations, *Offshore Technology Conference*, Paper OTC 2313, Dallas.

Mackenzie, K. V. (1981). Nine-term equation for the sound speed in the oceans, *Journal of the Acoustic Society of America* **70**(3): 807–812.

Matutano, C., Negro, V., López-Gutiérrez, J.-S. and Esteban, M. D. (2013). Scour prediction and scour protections in offshore wind farms, *Renewable Energy* **57**: 358–365.

May, R. P. and Escarameia, M. (2002). Local Scour Around Structures in Tidal Flows, *Proceedings of the 1st International Conference on Scour of Foundations, Texas A&M University, College Station, Texas*, pp. 320–331.

May, R. P. and Willoughby, I. R. (1990). *Local scour around large obstructions*, HR Wallingford Report SR240.

McGovern, D. and Ilic, S. (2014). Time Development of Scour around a Cylinder in Simulated Tidal Currents, *Journal of Hydraulic Engineering* **140**(6): 04014014.

McNinch, J. E., Wells, J. T. and Drake, T. G. (2001). The fate of artifacts in an energetic, shallow-water environment: scour and burial at the wreck site of Queen Annes Revenge, *Southeastern Geology* **40**(1): 19–27.

Melville, B. (2008). The physics of local scour at bridge piers, *Proceedings of the 4th International Conference on Scour and Erosion*, ISSMGE, Tokyo, Japan, pp. 28–40.

Melville, B. W. (1997). Pier and Abutment Scour: Integrated Approach, *Journal of Hydraulic Engineering* pp. 125–136.

Melville, B. W. and Chiew, Y. M. (1999). Time scale for local scour at bridge piers, *Journal of Geophysical Research* **125**(1): 59–65.

Melville, B. W. and Coleman, S. (2000). *Bridge Scour*, Water Resources Publications, LLC, Colorado.

Melville, B. W. and Sutherland, J. (1988). Design method for local scour at bridge piers, *Journal of Hydraulic Engineering* **114**(10): 1210–1226.

Molinas, A. (2003). *Bridge scour in nonuniform sediment mixtures and in cohesive materials: Synthesis Report, FHWA-RD-03-083*, United States Department of Transportation - Federal Highway Administration.

Molinas, A. and Hosny, M. M. (1999). *Experimental study on scour around circular pier in cohesive soil, FHWA-RD-99-186*, United States Department of Transportation - Federal Highway Administration.

Muzzammil, M. and Gangadhariah, T. (2003). The mean characteristics of horseshoe vortex at a cylindrical pier, *Journal of Hydraulic Research* **41**(3): 285–297.

Nash, J. E. and Sutcliffe, J. V. (1970). River flow forecasting through conceptual models. Part I - a discussion of principles, *Journal of Hydrology* **10**(3): 282–290.

Nicollet, G. and Ramette, M. (1971). Affouillements au voisinage de piles de ponts cylindriques circulaires, *Proceedings fo the 14th IAHR Congress*, Paris, France, pp. 315–322.

Niedoroda, A. W. and Dalton, C. (1982). A review of the fluid mechanics of ocean scour, *Ocean Engineering* **9**(2): 59–170.

Noormets, R., Ernstsen, V., Bartholoma, A., Flemming, B. and Hebbeln, D. (2003). *Local scour in a tidal environment: a case study from the Otzumer Balje tidal inlet, southern North Sea*, Poster reproduced in Appendix A of Offshore Center Danmark (2006).

Offen, G. and Kline, S. (1975). A proposed model of the bursting processes in turbulent boundary layers, *Journal of Fluid Mechanics* **70**(2): 209–228.

Offshore Center Danmark (2006). *Offshore Wind Turbines situated in Areas with Strong Currents, Doc No 6004RE01ER1*, Offshore Center Danmark, Esbjerg.

Oldfield, D. G. (1980). *Appraisal on Marine Fouling on Offshore Structures. Offshore Technology Paper 6*, Offshore Energy Technology Board, Department of Energy.

Olsen, N. and Melaaen, M. C. (1993). Three-Dimensional Calculation of Scour Around Cylinders, *Journal of Hydraulic Engineering* **119**(9): 1048–1054.

Pasiok, R. and Stilger-Szydlo, E. (2010). Sediment particles and turbulent flow simulation around bridge piers, *Archives of Civil and Mechanical Engineering* **X**(2): 67–79.

Peck, R., Hanson, W. and Thornburn, T. (1974). *Foundation Engineering Handbook*, Wiley, London.

Porter, K., Simons, R. and Harris, J. M. (2012a). Scour Development in Layered Sediments A Laboratory Study, *Proceedings of the 6th International Conference of Scour and Erosion*, Paris, France, pp. ICSE–000067.

Porter, K., Simons, R., Harris, J. M. and Ferradosa, T. (2012b). Scour development in complex sediment beds, *Coastal Engineering Proceedings, 33*, p. sediment.3.

Quinn, R. (2006). The role of scour in shipwreck site formation processes and the preservation of wreck-associated scour signatures in the sedimentary record evidence from seabed and sub-surface data, *Journal of Archaeological Science* **33**(10): 1419–1432.

Rambabu, M. (2003). Current-induced scour around a vertical pile in cohesive soil, *Ocean Engineering* **30**(7): 893–920.

Ramboll (2009). *Thanet Offshore Wind Farm, Design Report - Scour Assessment*, Ramboll Report Ref. 853452/340_0008(0).

Rance, P. J. (1980). The potential for scour around large objects, *Scour Prevention Techniques around Offshore Structures, Proceedings of a one day seminar, 16 December 1980, Society for Underwater Technology, London*, pp. 41–53.

Raudkivi, A. J. and Ettema, R. (1977). Effect of sediment gradation on clear water scour, *Journal of the Hydraulics Division, ASCE* **103**(10): 1209–1213.

Raudkivi, A. J. and Ettema, R. (1985). Scour at cylindrical bridge piers in armored beds, *Journal of Hydraulic Engineering* **111**: 713–731.

Richardson, E. V. and Davis, S. R. (1995). *Evaluating scour at bridges*, 4th edn, Federal Highway Administration.

Richardson, M. D. and Briggs, K. (1993). On the use of acoustic impedance values to determine sediment properties, *in* N. G. Pace and D. N. Langhorne (eds), *Acoustic Classification and Mapping of the Seabed, Underwater Acoustics Group Conference. Proceedings of the Institute of Acoustics*, University of Bath, Bath, UK, pp. 15–24.

Richardson, M. D., Valent, P., Briggs, K., Bradley, J. and Griffin, S. (2001). NRL mine burial experiments, *Proceedings of the 2nd Australian-American Joint Conference on the Technologies of Mines and Mine Countermeasures, Sydney, Australia*, pp. 1–23.

Robb, G. (2004). *The in situ compressional wave properties of marine sediments*, Phd, University of Southampton.

Robertson, P. K. and Cabal, K. L. (2010). *Guide to Cone Penetration Testing for Geotechnical Engineering*, 4th edn, Gregg Drilling, Signal Hill, California.

Robertson, P. K., Campanella, R. G., Gillespie, D. and Greig, J. (1986). Use of piezometer cone data, *Proceedings of the ASCE Specialty Conference In Situ '86*, American Society of Civil Engineers, Blacksburg, pp. 1263–1280.

Roulund, A., Sumer, B. M., Fredsoe, J. and Michelsen, J. (2005). Numerical and experimental investigation of flow and scour around a circular pile, *Journal of Fluid Mechanics* **534**: 351–401.

Royal Haskoning (2005). Thanet offshore wind farm, Environmental Statement.

RPS Hydrosearch (2004). Gunfleet Sands offshore wind farm, Summary of oceanographic data acquired between January 2002 and February 2003, Report 01-306.14.

Rudolph, D., Bos, K. J., Luijendijk, A. P., Rietema, K. and Out, J. M. M. (2004). Scour around offshore structures - Analysis of field measurements, *in* Y. M. Chiew, S.-Y. Lim and N.-S. Cheng (eds), *Proceedings of the 2nd International Conference on Scour and Erosion*, Stallion Press, Singapore, pp. 400–407.

Saravanan, J., Karthikeyan, C. and Samuel, A. (2011). Exergy Analysis of Single Array Wind Farm Using Wake Effects, *Engineering* **3**(9): 949–958.

Schmertmann, J. H. (1978). Guidelines for Cone Penetration Test, Performance and Design, *Technical report*, U.S. Department of Transportation, Report No. FHWA-TS-78-209.

Shen, H. W., Ogawa, Y. and Karaki, S. S. (1965). Time variation of bed deformation near bridge piers, *Proceedings of the 11th IAHR Congress, Vol. 3*, Leningrad, USSR, pp. 1–9.

Shen, H. W., Schneider, V. R. and Karaki, S. S. (1966). Mechanisms of local scour, Report CER66HWS22, *Technical report*, Engineering Resources Centre, Colorado State University.

Sheppard, D. M., Odeh, M. and Glasser, T. (2004). Large Scale Clear-Water Local Pier Scour Experiments, *Journal of Hydraulic Engineering* **130**(10): 957–963.

Soulsby, R. (1983). The bottom boundary layer of shelf seas, *in* B. Johns (ed.), *Physical oceanography of coastal and shelf seas*, Elsevier, p. 470.

Soulsby, R. (1997). *Dynamics of Marine Sands*, Thomas Telford Ltd.

Stahlmann, A. and Schlurmann, T. (2012). Kolkbildung an komplexen Gründungsstrukturen für Offshore-Windenergieanlagen, *Bautechnik* **89**(5): 293–300.

Stride, A. H. (1963). Current-swept sea floors near the southern half of Great Britain, *Quarterly Journal of the Geological Society of London* **119**: 175–199.

Sturt, F., Dix, J. K. and EMU Ltd (2009). The Outer Thames Estuary Regional Environmental Characterisation, Marine Aggregate Levy Sustainability Fund, 09/J/1/06/1305/0870, *Technical report*, Marine Aggregate Levy Sustainability Fund.

Sumer, B. M. (2007). Mathematical modelling of scour: A review, *Journal of Hydraulic Research* **45**(6): 723–735.

Sumer, B. M. and Fredsoe, J. (1992). A Review of wave/current-induced scour around pipelines, *Proceedings of the 23rd International Conference on Coastal Engineering, Venice, Italy*, pp. 2839–2852.

Sumer, B. M. and Fredsoe, J. (2001). Wave scour around a large vertical circular cylinder, *Journal of Waterway, Port, Coastal, and Ocean Engineering* **127**(3): 125–134.

Sumer, B. M. and Fredsoe, J. (2002). *The Mechanics Of Scour In The Marine Environment*, World Scientific.

Sumer, B. M., Christiansen, N. and Fredsoe, J. (1992a). Time scale of scour around a vertical pile, *Proceedings of the 2nd International Offshore and Polar Engineering Conference*, San Francisco, pp. 308–315.

Sumer, B. M., Christiansen, N. and Fredsoe, J. (1993). Influence of cross section on wave scour around piles, *Journal of Waterway, Port, Coastal and Ocean Engineering* **119**(5): 477.

Sumer, B. M., Christiansen, N. and Fredsoe, J. (1997). The horseshoe vortex and vortex shedding around a vertical wall-mounted cylinder exposed to waves, *Journal of Fluid Mechanics* **332**: 41–70.

Sumer, B. M., Chua, L. H. C., Cheng, N.-S. and Fredsoe, J. (2003). Influence of Turbulence on Bed Load Sediment Transport, *Journal of Hydraulic Engineering* **129**(8): 585.

Sumer, B. M., Fredsoe, J. and Christiansen, N. (1992b). Scour around vertical pile in waves, *Journal of Waterway, Port, Coastal and Ocean Engineering* **118**: 15.

Tempel, J. V. D., Zaaijer, M. B. and Subroto, H. (2004). The effects of Scour on the design of offshore wind turbines, *Proceedings of the 3rd International Conference on Marine Renewable Energy*, IMarEST, Blyth, UK, pp. 27–35.

Thales (2002). Current, wave and turbidity measurements in the Thames Estuary, Data Report 1, Ref. 5914.

Ting, F. C. K., Briaud, J.-L., Chen, H. C., Gudavalli, R., Perugu, S. and Wei, G. (2001). Flume tests for scour in clay at circular piers, *Journal of Hydraulic Engineering* **127**(11): 969–978.

Torsethaugen, K. (1975). *Lokalerosjon ved store konstruksjoner. Modellforsok*, SINTEF Report STF60 A75055, Norwegian Hydrotechnical Laboratory, Trondheim, Norway.

Trembanis, A. C. and McNinch, J. E. (2003). Predicting scour and maximum settling depths of shipwrecks: a numeric simulation of the fate of Queen Annes revenge, *Proceedings of the International Conference on Coastal Sediments*, pp. 1–13.

Trembanis, A. C., Friedrichs, C. T., Richardson, M. D., Traykovski, P., Howd, P. a., Elmore, P. a. and Wever, T. F. (2007). Predicting Seabed Burial of Cylinders by Wave-Induced Scour: Application to the Sandy Inner Shelf Off Florida and Massachusetts, *IEEE Journal of Oceanic Engineering* **32**(1): 167–183.

Tseng, M.-H., Yen, C.-L. and Song, C. C. S. (2000). Computation of three-dimensional flow around square and circular piers, *International Journal for Numerical Methods in Fluids* **34**(3): 207–227.

Tumay, M. T. (1985). Field Calibration of Electric Cone Penetrometers in Soft Soils Executive Summary, *Technical report*, U.S. Department of Transportation, Report No. FHWA/LA/LSU-GE-85/2.

Vallejo, L. E. and Mawby, R. (2000). Porosity influence on the shear strength of granular materialclay mixtures, *Engineering Geology* **58**(2): 125–136.

Van Landeghem, K. J., Baas, J. H., Mitchell, N. C., Wilcockson, D. and Wheeler, A. J. (2012). Reversed sediment wave migration in the Irish Sea, NW Europe: A reappraisal of the validity of geometry-based predictive modelling and assumptions, *Marine Geology* **295-298**: 95–112.

Walker, W. (1995). *Field measurements of local pier scour in a tidal inlet*, Msc, University of Florida.

Whitehouse, R. J. S. (1998). *Scour at marine structures: a manual for practical applications*, Thomas Telford.

Whitehouse, R. J. S. (2004). Marine scour at large foundations, *Proceedings of the 2nd International Conference on Scour and Erosion, Singapore* **2**: 455–460.

Whitehouse, R. J. S. (2006). Scour at Coastal Structures, *3rd International Conference on Scour and Erosion*, Amsterdam, Netherlands.

Whitehouse, R. J. S., Harris, J. M., Mundon, T. R. and Sutherland, J. (2010). Scour at Offshore Structures, *Proceedings of the 5th International Conference on Scour and Erosion*, San Francisco, pp. 11–20.

Whitehouse, R. J. S., Harris, J. M., Sutherland, J. and Rees, J. (2011). The nature of scour development and scour protection at offshore windfarm foundations., *Marine Pollution Bulletin* **62**(1): 73–88.

Whitehouse, R. J. S., Sutherland, J. and O'Brien, D. (2006). Seabed scour assessment for offshore windfarm, *Proceedings of the 3rd International Conference on Scour and Erosion*, Gouda, Netherlands.

Williamson, C. H. K. (1996). Vortex dynamics in the cylinder wake, *Annual Review of Fluid Mechanics* **28**(1): 477–539.

Wohl, E. (2014). *Rivers in the landscape, Science and Management*, Wiley Blackwell.

Worzyk, T. (2009). Damages and repair, *Submarine Power Cables: Design, installation, repair, environmental aspects*, Springer, Berlin, chapter 8, pp. 211–236.

Yanmaz, A. M. (1991). Study of Time-Dependent Local Scour around Bridge Piers, *Journal of Hydraulic Engineering* **117**(10): 1247.

Zakšek, K., Oštir, K. and Kokalj, v. (2011). Sky-View Factor as a Relief Visualization Technique, *Remote Sensing* **3**(12): 398–415.

Zanke, U., Hsu, T.-W., Roland, A., Link, O. and Diab, R. (2011). Equilibrium scour depths around piles in noncohesive sediments under currents and waves, *Coastal Engineering* **58**(10): 986–991.

Zdravkovich, M. M. (1997). *Flow around circular cylinders : a comprehensive guide through flow phenomena, experiments, applications, mathematical models, and computer simulations. Vol 1: Fundamentals*, Oxford University Press, Oxford.

Zhao, Z. and Fernando, H. J. S. (2007). Numerical simulation of scour around pipelines using an EulerEuler coupled two-phase model, *Environmental Fluid Mechanics* **7**(2): 121–142.